Modelling of fluidized bed gasification for hydrogen production from waste

Alex Sebastiani

Department of Chemical Engineering

University College London

A Thesis submitted for the degree of

Doctor of Philosophy of University College London

January 2025

I, Alex Sebastiani, confirm that the work presented in this Thesis is my own.

Where information has been derived from other sources, I confirm that this has been indicated in the Thesis.

Abstract

The need for sustainable waste management and the requirement for a reliable and constant source of renewable energy are the pillars of the current environmental agendas of many developing and developed countries. On a global level, bioenergy systems, and advanced thermochemical technologies, gasification in particular, are deemed to play a pivotal role in the quest for decarbonization of the energy sector, representing a strategic pathway towards reducing dependency on fossil fuel resources. This is especially true when waste feedstock is used, often favoured over other biomass-based fuels due to its low cost and abundance. Fluidized bed gasifiers offer the best opportunity for large-scale deployment of advanced thermochemical technologies due to the higher flexibility and application potential in comparison to other alternatives.

However, despite gasification being a rather mature process, challenges still persist when dealing with unconventional solid feedstock such as waste-derived biomass and plastics. These heterogeneous materials, often containing high ash and moisture fractions, are highly volatile and can hinder the renowned features of fluidized bed reactors in terms of mixing and thermal stability.

Additional challenges for the new-generation gasification systems arise from the choice of the most suited gasification agent for applications like hydrogen and low-carbon fuels production, where air is ruled out to avoid nitrogen dilution. Most of the industrial waste-fuelled gasifiers were developed as air-blown systems, and only a very limited experience exists in steam-oxygen operations, particularly on large (pilot and demonstrative scale) plants.

For these reasons, the existence of a valid modelling tool is deemed essential for understanding the complexity of simultaneous phenomena occurring, as well as better predicting the system behaviour upon variation of process inputs and improving the design for future commercial plants.

The current work aims at filling the gaps in existing kinetic models to accurately predict the performance of large-scale gasifiers, such as syngas composition and temperature profile, while maintaining low computational requirements and the inherent simplicity of 1D models. Particular focus is given to the main bottleneck of this technology represented by the prediction of light hydrocarbons, tars composition and gas energy throughput, investigating means of bolstering the performance within feasible operating conditions and technological constraints.

A holistic approach is then adopted to investigate the potential of waste gasification in fluidized bed reactors as part of a waste-to-H_2 plant, addressing technical challenges, environmental opportunities and the related strategies for large-scale deployment to support the transition to Net-zero.

Impact statement

This work focuses on hydrogen production from waste, with particular emphasis on the operations of fluidized bed reactors for advanced thermochemical conversions of various feedstocks, including biomass and plastics, and waste-derived fuels. The following key impacts emerge from this research:

1. **Enhancing Reactor Design and Operation:** the developed fast, easy to operate and accurate kinetic model presented in this work represents a valuable tool for technology developers and plant operators, as it can serve the design and operations of large-scale reactors, whilst offering crucial insights regarding common operational challenges. The findings around the impact of the main operating parameters on process performance offer a foundation for optimizing fluidized bed reactor configurations and operational procedures based on the specific nature of the feedstock being processed, leading to more effective and sustainable processes.
2. **Modelling Approach:** This research advances fluidized bed reactor modelling by addressing the major issues of this type of reactor, such as devolatilization and reactor fluid dynamic, and overcoming limitations of existing models, including poor predictive capabilities of tars and complexity and computational costs. The developed framework enables fundamental analysis of reaction pathways and heavy hydrocarbon behaviour, representing an important contribution to the field. The predictive capabilities of the model support reactor design and process optimization across diverse feedstocks
3. **Full-plant assessment:** While bioenergy systems are crucial for achieving Net-Zero targets, their technical viability remains uncertain. This research evaluates waste gasification for pure hydrogen production with carbon dioxide removal, analyzing associated challenges and opportunities. The study examines how different waste feedstocks affect technical performance, investigates hydrogen purity requirements and carbon dioxide separation methods, and identifies integration opportunities and development priorities. These insights support the successful deployment of waste-to-fuel technologies at an industrial scale.
4. **Future Research:** The findings presented in this Thesis serve as a foundation for future research, especially for tackling more complex feedstocks, and addressing other common operational challenges, related to ashes and corrosive elements. The knowledge gained with this work can be extended to develop alternative methodologies and solutions for process optimization.

Acknowledgements

I would like to express my deepest gratitude to Professor Massimiliano Materazzi, someone who went beyond the simple role of supervisor for me, with solid guidance, insightful inspiration and growth together. Thank you for making me feel part of something bigger, something worthy and exciting. Thank you for making me believe in someone with creative and extravagant thinking like you, which helped me believe a little more in myself.

I am grateful to the second supervisor during this journey, Professor Paola Lettieri, and to the academics who were part of my PhD journey: Professor Umberto Arena and Dr Francesco Parrillo. Collaborating with them has expanded my horizons and contributed significantly to my growth as a researcher.

Heartfelt thanks to Stefano, the person who's been the most by my side, in light and shadow. You're the purest example of strength and kindness, like our Abruzzo. There is so much admiration in you, in your innocence and resilience. You have always set the example of how self-improvement and hard work can lead to success. Same special thanks also to the missing two of the quartet, Matteo and Suvi. We all walked together through the aspera of this journey, but you always brought laughter and light even to the darkest of nights and crises. Watching you blossom through your journey, owning your insecurities and nurturing your strengths and independence has been a bliss. I am happy to say I'm proud of who you have grown into, well done. Now waiting for the astra, or ready together to fight more aspera. Thank you for the ride, for the love, for the diagio, for becoming so important that the future looks painful.

Thanks to Aurora, you entered my life during one of the least stable times, almost like an intrusive thought, but you ended up being essential. Thank you for your energy, your neapolitan attitude and your caring instinct. As you often say, you're stronger than what brings you down, now let's try and live by it. Thank you Ishaa, for being there when you didn’t need to, or probably want to, in times when you didn’t have enough for yourself, but still giving everything you had. Thank you for being an almost baby version of me, enough to be worried about but not to feel alone.

Thanks to all the friends who enriched this journey, and probably you did too good of a job and that is why I did not want to finish. Your constant presence and support felt like a safe haven. Thank you, Elan, Mina, Andrea, Barbara, Qiang, Prince, Klara, Andrea P., Enrico, Maryam, Nena, Lucy, Claude. Thanks to everyone else who I may have forgotten. Thank you for letting me complain. Thank you,

Domenico, Fabio, Roberta, Luca, Unkha, Giovanni, Simona, Martina, Victoria and Chiara. CheERS to everyone!

I wish to also thank the CENG0016 Design Team, for welcoming me as part of their group, supporting my educational growth, expanding my interests and challenging my skills with open-ended ever-changing design projects. Thank you for trusting me.

I wish to thank also my precious friends who have always represented a solid base for me to go back to in Italy, the family I'd choose all over again. Thank you, Gina, Pietro, Chiara, Francesco, Jacopo, Francesca, Matteo and Luigi. Thank you, Giorgia, Michela, Mariateresa e Samuele. And all who I've left out.

The greatest of thank you goes to my family, the foundation of who I am, and who they made me become. Thank you for always being there even when I didn't know how much I needed you there.

Finally, thanks to me, and to my demons, always by my side. I thank myself for always choosing the challenge, for all the effort and the struggles, for believing in altruism and for finding in myself the reason to believe in. After reaching so many achievements for the sake and pride of others, for what was expected and putting everyone else's first, I offer this work to me, for all the imperfect satisfaction I have been longing for. The least Alex thing.

UCL Research Paper Declaration Form

referencing the doctoral candidate's own published work(s)

1. **For a research manuscript that has already been published** (if not yet published, please skip to section 2)**:**

(a) **What is the title of the manuscript?**

Steam - oxygen gasification of refuse derived fuel in fluidized beds: Modelling and pilot plant testing

(b) **Please include a link to or doi for the work:**

https://doi.org/10.1016/j.fuproc.2021.106783

(c) **Where was the work published?**

Fuel Processing Technology

(d) **Who published the work?**

Elsevier

(e) **When was the work published?**

2021

(f) **List the manuscript's authors in the order they appear in the publication:**

Sebastiani Alex, Macrì Domenico, Gallucci Katia, Materazzi Massimiliano

(g) **Was the work peer reviewed?**

Yes

(h) **Have you retained the copyright?**

Yes

(i) **Was an earlier form of the manuscript uploaded to a reprint server (e.g. medRxiv)?** If 'Yes', please give a link or doi.

No

If 'No', please seek permission from the relevant publisher and check the box next to the below statement:

☒ *I acknowledge permission of the publisher named under 1d to include in this thesis portions of the publication named as included in 1c.*

2. **For a research manuscript prepared for publication but that has not yet been published** (if already published, please skip to section 3)**:**

   (a) **What is the current title of the manuscript?**

   (b) **Has the manuscript been uploaded to a preprint server e.g. medRxiv' ?** If 'Yes', please please give a link or doi:

   (c) **Where is the work intended to be published?**

   (d) **List the manuscript's authors in the intended authorship order:**

   (e) **Stage of publication** (e.g. in submission)

3. **For multi-authored work, please give a statement of contribution covering all authors** (if single-author, please skip to section 4)**:**
   Alex Sebastiani: Writing – original draft, Writing – review & editing, Visualization, Validation, Software, Methodology, Investigation, Formal analysis, Data curation, Conceptualization. Domenico Macrì: Writing – review & editing, Methodology, Investigation. Katia Gallucci: Writing – review & editing. Massimiliano Materazzi: Writing – original draft, Writing – review & editing, Validation, Supervision, Investigation, Conceptualization.

4. **In which chapter(s) of your thesis can this material be found?**
   Chapter 2 and Chapter 3

5. **e-Signatures confirming that the information above is accurate** (this form should be co-signed by the supervisor/ senior author unless this is not appropriate, e.g. if the paper was a single-author work)**:**

Candidate: Alex Sebastiani

Date: 17/06/2025

Supervisor: Massimiliano Materazzi

Date: 17/06/2025

UCL Research Paper Declaration Form

referencing the doctoral candidate's own published work(s)

1. **For a research manuscript that has already been published** (if not yet published, please skip to section 2)**:**

   (a) **What is the title of the manuscript?**

   Plastic waste gasification using oxygen-enriched air and steam: Experimental and model results from a large pilot-scale reactor.

   (b) **Please include a link to or doi for the work:**

   https://doi.org/10.1016/J.WASMAN.2024.04.045

   (c) **Where was the work published?**

   Waste Management

   (d) **Who published the work?**

   Elsevier

   (e) **When was the work published?**

   2024

   (f) **List the manuscript's authors in the order they appear in the publication:**

   Parrillo Francesco, Calì Gabriele, Pettinau Alberto, Materazzi Massimiliano, Sebastiani Alex*, Arena Umberto

   (g) **Was the work peer reviewed?**

   Yes

   (h) **Have you retained the copyright?**

   Yes

   (i) **Was an earlier form of the manuscript uploaded to a reprint server (e.g. medRxiv)?** If 'Yes', please give a link or doi.

   No

   If 'No', please seek permission from the relevant publisher and check the box next to the below statement:

   ☒ *I acknowledge permission of the publisher named under 1d to include*

in this thesis portions of the publication named as included in 1c.

2. **For a research manuscript prepared for publication but that has not yet been published** (if already published, please skip to section 3)**:**

   (a) **What is the current title of the manuscript?**

   (b) **Has the manuscript been uploaded to a preprint server e.g. medRxiv'?** If 'Yes', please please give a link or doi:

   (c) **Where is the work intended to be published?**

   (d) **List the manuscript's authors in the intended authorship order:**

   (e) **Stage of publication** (e.g. in submission)

3. **For multi-authored work, please give a statement of contribution covering all authors** (if single-author, please skip to section 4)**:**

   Francesco Parrillo: Methodology, Investigation, Data curation, Visualization, Writing – original draft, Writing – review & editing. Filomena Ardolino: Investigation, Writing – review & editing. Gabriele Calì: Methodology, Investigation, Writing – review & editing. Alberto Pettinau: Writing – review & editing, Project administration, Supervision. Massimiliano Materazzi: Methodology, Writing – original draft, Writing – review & editing. Alex Sebastiani: Methodology, Software, Data curation, Visualization, Writing – review & editing. Umberto Arena: Conceptualization, Investigation, Methodology, Writing – original draft, Writing – review & editing, Supervision.

4. **In which chapter(s) of your thesis can this material be found?**
   Chapter 5

5. **e-Signatures confirming that the information above is accurate** (this form should be co-signed by the supervisor/ senior author unless this is not appropriate, e.g. if the paper was a single-author work)**:**

Candidate: Alex Sebastiani

Date: 17/06/2025

Supervisor: Massimiliano Materazzi

Date: 17/06/2025

UCL Research Paper Declaration Form

referencing the doctoral candidate's own published work(s)

1. **For a research manuscript that has already been published** (if not yet published, please skip to section 2)**:**

   (a) **What is the title of the manuscript?**

   Modelling of Oxygen-Steam Gasification of Waste Feedstock in Industrial Fluidized Bed Reactors.

   (b) **Please include a link to or doi for the work:**

   https://doi.org/10.1016/J.CEJ.2025.159763

   (c) **Where was the work published?**

   Chemical Engineering Journal

   (d) **Who published the work?**

   Elsevier

   (e) **When was the work published?**

   2025

   (f) **List the manuscript's authors in the order they appear in the publication:**

   Sebastiani Alex, Parrillo Francesco, Ardolino Filomena, Arena Umberto, Iannello Stefano, Materazzi Massimiliano

   (g) **Was the work peer reviewed?**
   Yes

   (h) **Have you retained the copyright?**

   Yes

   (i) **Was an earlier form of the manuscript uploaded to a reprint server (e.g. medRxiv)?** If 'Yes', please give a link or doi.

   No

   If 'No', please seek permission from the relevant publisher and check the box next to the below statement:

   ☒ *I acknowledge permission of the publisher named under 1d to include in this thesis portions of the publication named as included in 1c.*

2. **For a research manuscript prepared for publication but that has not yet been published** (if already published, please skip to section 3)**:**

   (a) **What is the current title of the manuscript?**

   (b) **Has the manuscript been uploaded to a preprint server e.g. medRxiv'?** If 'Yes', please please give a link or doi:

   (c) **Where is the work intended to be published?**

   (d) **List the manuscript's authors in the intended authorship order:**

   (e) **Stage of publication** (e.g. in submission)

3. **For multi-authored work, please give a statement of contribution covering all authors** (if single-author, please skip to section 4)**:**

   Alex Sebastiani: Writing – original draft, Writing – review & editing, Visualization, Validation, Software, Methodology, Investigation, Formal analysis, Data curation, Conceptualization. Francesco Parrillo: Writing – original draft, Writing – review & editing, Visualization, Validation, Methodology, Investigation, Funding acquisition, Formal analysis, Data curation. Filomena Ardolino: Writing – original draft, Investigation, Conceptualization. Umberto Arena: Writing – original draft, Visualization, Validation, Project administration, Methodology, Investigation, Funding acquisition, Formal analysis, Data curation, Conceptualization. Stefano Iannello: Writing – original draft, Visualization, Investigation, Formal analysis, Data curation, Conceptualization. Massimiliano Materazzi: Writing – original draft, Writing – review & editing, Visualization, Validation, Supervision, Software, Project administration, Methodology, Investigation, Conceptualization.

4. **In which chapter(s) of your thesis can this material be found?**
   Chapter 3 and Chapter 5

5. **e-Signatures confirming that the information above is accurate** (this form should be co-signed by the supervisor/ senior author unless this is not appropriate, e.g. if the paper was a single-author work)**:**

Candidate: Alex Sebastiani

Date: 17/06/2025

Supervisor: Massimiliano Materazzi

Date: 17/06/2025

UCL Research Paper Declaration Form

referencing the doctoral candidate's own published work(s)

1. **For a research manuscript that has already been published** (if not yet published, please skip to section 2)**:**

   (a) **What is the title of the manuscript?**

   Biohydrogen: A life cycle assessment and comparison with alternative low-carbon production routes in the UK.

   (b) **Please include a link to or doi for the work:**

   https://doi.org/10.1016/j.jclepro.2021.128886

   (c) **Where was the work published?**

   Journal of Cleaner Production

   (d) **Who published the work?**

   Elsevier

   (e) **When was the work published?**

   2021

   (f) **List the manuscript's authors in the order they appear in the publication:**

   Chari Suviti, Amaya-Santos Gema, Sebastiani Alex, Grimaldi Fabio, Lettieri Paola, Materazzi Massimiliano

   (g) **Was the work peer reviewed?**

   Yes

   (h) **Have you retained the copyright?**

   Yes

   (i) **Was an earlier form of the manuscript uploaded to a reprint server (e.g. medRxiv)?** If 'Yes', please give a link or doi.

   No

   If 'No', please seek permission from the relevant publisher and check the box next to the below statement:

   ☒ *I acknowledge permission of the publisher named under 1d to include in this thesis portions of the publication named as included in 1c.*

2. **For a research manuscript prepared for publication but that has not yet been published** (if already published, please skip to section 3)**:**

   (a) **What is the current title of the manuscript?**

   (b) **Has the manuscript been uploaded to a preprint server e.g. medRxiv'?** If 'Yes', please please give a link or doi:

   (c) **Where is the work intended to be published?**

   (d) **List the manuscript's authors in the intended authorship order:**

   (e) **Stage of publication** (e.g. in submission)

3. **For multi-authored work, please give a statement of contribution covering all authors** (if single-author, please skip to section 4)**:**

   Gema Amaya-Santos and Suviti Chari equally contributed to Investigation, model development, Formal analysis, Writing – original draft, Writing – review & editing. Alex Sebastiani: Data curation, Investigation, Writing – review & editing. Fabio Grimaldi: Support in. Paola Lettieri: LCA, Supervision. Massimiliano Materazzi: Conceptualization, Supervision, Writing – review & editing, Funding acquisition.

4. **In which chapter(s) of your thesis can this material be found?**
   Chapter 6

5. **e-Signatures confirming that the information above is accurate** (this form should be co-signed by the supervisor/ senior author unless this is not appropriate, e.g. if the paper was a single-author work)**:**

Candidate: Alex Sebastiani

Date: 17/06/2025

Supervisor: Massimiliano Materazzi

Date: 17/06/2025

UCL Research Paper Declaration Form

referencing the doctoral candidate's own published work(s)

1. **For a research manuscript that has already been published** (if not yet published, please skip to section 2)**:**

   (a) **What is the title of the manuscript?**

   Retrofitting Waste-to-Energy with carbon Capture and Storage in the UK: a Techno-economic and Environmental Assessment.

   (b) **Please include a link to or doi for the work:**

   https://doi.org/10.5071/31stEUBCE2023-4CO.3.2

   (c) **Where was the work published?**

   31st European Biomass Conference and Exhibition

   (d) **Who published the work?**

   Etaflorence

   (e) **When was the work published?**

   2023

   (f) **List the manuscript's authors in the order they appear in the publication:**

   Sebastiani Alex, Paulillo Andrea, Lettieri Paola, Materazzi Massimiliano

   (g) **Was the work peer reviewed?**

   Yes

   (h) **Have you retained the copyright?**

   Yes

   (i) **Was an earlier form of the manuscript uploaded to a reprint server (e.g. medRxiv)?** If 'Yes', please give a link or doi.

   No

   If 'No', please seek permission from the relevant publisher and check the box next to the below statement:

   ☒ *I acknowledge permission of the publisher named under 1d to include in this thesis portions of the publication named as included in 1c.*

2. **For a research manuscript prepared for publication but that has not yet been published** (if already published, please skip to section 3)**:**

   (a) **What is the current title of the manuscript?**

   (b) **Has the manuscript been uploaded to a preprint server e.g. medRxiv'?** If 'Yes', please please give a link or doi:

   (c) **Where is the work intended to be published?**

   (d) **List the manuscript's authors in the intended authorship order:**

   (e) **Stage of publication** (e.g. in submission)

3. **For multi-authored work, please give a statement of contribution covering all authors** (if single-author, please skip to section 4)**:**

   Alex Sebastiani: Writing – original draft, Writing – review & editing, Visualization, Validation, Software, Methodology, Investigation, Formal analysis, Data curation. Andrea Paulillo: Writing – review & editing, Methodology, Investigation. Paola Lettieri: Writing – review & editing, Supervision. Massimiliano Materazzi: Conceptualization, Supervision, Writing – review & editing, Funding acquisition.

4. **In which chapter(s) of your thesis can this material be found?**
   Appendix E

5. **e-Signatures confirming that the information above is accurate** (this form should be co-signed by the supervisor/ senior author unless this is not appropriate, e.g. if the paper was a single-author work)**:**

Candidate: Alex Sebastiani

Date: 17/06/2025

Supervisor: Massimiliano Materazzi

Date: 17/06/2025

Table of Contents

Nomenclature

Acronyms	
1D	One dimensional
2PT	Two-phase the
AGT	Advanced Gasification Technologies
APS	Announced Pledges Scenario
ATR	and Autothermal Reforming
ATT	Advanced thermochemical technologies
BBM	Black box model
BECCS	Bioenergy with Carbon Capture and Storage
BFB	Bubbling fluidized bd
BFBG	Bubbling fluidized bed gasifier
CCC	Committee on Climate Change
CCE	Carbon conversion efficiency
CCS	Carbon Capture and Storage
CCUS	Carbon Capture, Utilization and Storage
CFB	Circulating fluidized bed
CFD	Computational Fluid Dynamics
CFDM	Computational Fluid Dynamics Model
CGE	Cold gas efficiency
DCFB	Dual Circulating fluidized bed
DM	Design model
EEM	Eulerian-Eulerian Model
EF	Entrained flow
ELM	Eulerian-Lagrangian Model
EM	Equilibrum model
ER	Equivalence Ratio
FC	Fixed carbon
FB	Fluidized bed
FBG	Fluidized bed gasifier
FBR	Fluidized bed reactor
FI	Fluidization Index
FM	Fluidization model
GHG	Greenhouse gas
GHV	Gross heating value
HDPE	High-density polyethylene
LCA	Life cycle assessment
LDPE	Low-density polyethylene
LHV	Low heating value
LM	Learning model
MDEA	methyldiethanolamine

MEA	Mono-ethanolamine
MSW	Municipal Solid Waste
NEE	Net energy efficiency
NMP	N-methyl-2-pyrrolidone
NZE	Net-Zero emissions
PAH	Polyaromatic hydrocarbons
PC	Particle conversion
PE	Polyethylene
PEM	Proton-exchange membrane
PFR	Plug flow reactor
PHA	Polyhydroxyalkanoate
PLIF	Planar laser induced fluorescence
PLLS	Planar laser light scattering
PP	Polypropylene
PSA	Pressure-swing adsorption
RDF	Refuse Derived Fuel
RMSE	Root mean square error
SEWGS	Sorption enhanced water gas shift
SMR	Steam Methane Reforming
SS	Steady state
STEPS	Stated Policies Scenario
StC	Steam-to-Carbon molar ratio
StO_2	Steam-to-Oxygen molar ratio
TDH	Transport disengagement height
TEA	Triethanolamine
TGA	Thermogravimetric analysis
TM	Transient model
TRL	Technology readiness level
US	Unsteady state
VM	Volatile matter
WGS	Water gas shift
WtE	Waste-to-Energy
WtH_2	Waste-to-Hydrogen
x_{O2}	Oxygen molar fraction in the enriched air

Symbols	
A	Pre-exponential factor
A_{bed} [m^3]	Cross-sectional area
Ar	Archimedes number
AW [g/mol]	Atomic molar mass
c [mol/m^3]	Concentration
c_p [J/mol K]	Heat capacity
d/D [cm]	diameter

Da	Damköhler number
$\mathcal{D}_{ij}$ [cm^2/s]	Gas phase diffusivities
Ea [J/mol]	Activation energy
$F\ [kg\ h^{-1}]$	Fuel feeding rate
g [m/s^2]	Gravity acceleration
$\mathcal{H}$ [W/m^3 K]	Heat transfer coefficient
h [cm]	Axial position
H	Height
ΔH^r [J/mol]	Reaction enthalpy change
$\mathcal{J}\ kg\ m^{-2}s^{-1}$	Solids circulation rate
k	Kinetic coefficient
K [s^{-1}]	Mass interchange coefficient
M [kg]	Mass
MW [g/mol]	Molecular weight
N_{or}	Number of orifices
N	Number of compartment
$\dot{n}_i^{in/out}\ [kmol\ h^{-1}]$	Inlet or outlet molar flowrate of species *i*
p [bar]	Pressure
$\dot{Q}$	Flowrate
R [J/mol K]	Universal gas constant
R_{tot} [Km^3/W]	Total thermal resistance
r [mol/m^{3}s]	Reaction rate
T [K]	Temperature
t [s]	Time
u [cm/s]	Velocity
u_0 [cm/s]	Superficial gas velocity
u_{br} [cm/s]	Rise velocity of a single bubble
$\dot{V}$ [mol/s]	Splashing zone mixing rate
$\dot{\mathcal{V}}^{out}\ [Nm^3\ h^{-1}]$	Outlet volumetric flowrate
v	Diffusion volume
x	Molar fraction
z	Axial direction

Greek Letters	
δ [m^3_b/m$^3_{bed}$]	Fraction of bed in bubbles
ε	Void fraction
ν	Stoichiometric ratio
μ [Pa s]	Gas viscosity
η [%]	Efficiency
ρ [kg/m^3]	Density

$\sum$	Summation
χ	Conversion

Subscripts and superscripts	
0	Initial
a	Ambient
AS	Axial segregation
b	Bubble phase
char	Char particles
cyl	Cylinder
D	Devolatilization
e	Emulsion phase
eb	Endogenous bubble
ff	Formation
f	Freeboard
g	Gas phase
gb	Ghost bubble
i	Number of species
j	Reaction number
m	mainstream
mf	Minimum fluidization
mb	Minimum bubbling
p	Particle
sz	Splashing zone
ter	Terminal

List of tables

List of figures

Publications

- **Sebastiani, A.**, Parrillo, F., Ardolino, F., Arena, U., Iannello, S., Materazzi, M. (2025). Modelling of Oxygen-Steam Gasification of Waste Feedstock in Industrial Fluidized Bed Reactors. *Chemical Engineering Journal*, *506*, 159763. https://doi.org/10.1016/J.CEJ.2025.159763
- Paulillo, A., **Sebastiani, A**., Lettieri, P., & Materazzi, M. (2024). Decarbonising waste-to-energy: A life cycle assessment study. *Resources, Conservation and Recycling*, *209*, 107812. https://doi.org/10.1016/j.resconrec.2024.107812
- Parrillo, F., Ardolino, F., Calì, G., Pettinau, A., Materazzi, M., **Sebastiani, A.***, & Arena, U. (2024). Plastic waste gasification using oxygen-enriched air and steam: Experimental and model results from a large pilot-scale reactor. *Waste Management*, *183*, 53–62. https://doi.org/10.1016/J.WASMAN.2024.04.045
- Iannello, S., **Sebastiani, A.**, Errigo, M., & Materazzi, M. (2024). The behaviour of plastic particles during pyrolysis in bubbling fluidized bed reactors: Incipient agglomeration and axial segregation. *Powder Technology*, *441*, 119846. https://doi.org/10.1016/J.POWTEC.2024.119846
- Malsegna, B., **Sebastiani, A.**, da Gama Paz-Dias, J. G., Di Luca, F., Di Giuliano, A., Gallucci, K., & Materazzi, M. (2024). Simulation of a sorption-enhanced water gas-shift pilot technology for pure hydrogen production from a waste gasification plant. *Fuel Processing Technology*, *254*, 108032. https://doi.org/10.1016/J.FUPROC.2024.108032
- Materazzi, M., Chari, S., **Sebastiani, A.**, Lettieri, P., & Paulillo, A. (2024). Waste-to-energy and waste-to-hydrogen with CCS: Methodological assessment of pathways to carbon-negative waste treatment from an LCA perspective. *Waste Management*, *173*, 184–199. https://doi.org/10.1016/J.WASMAN.2023.11.020
- Errigo, M., **Sebastiani, A.**, Iannello, S., Materazzi, M., & Lettieri, P. (2023). Application of imaging techniques for the characterization of lumps behaviour in gas–solid fluidized-bed reactors. *Fuel*, *349*, 128634. https://doi.org/10.1016/j.fuel.2023.128634
- Materazzi, M., Chari, S., Bajwa, S., & **Sebastiani, A.** (2023). Waste-To-Hydrogen: Challenges and Opportunities in the Uk Scenario. *Detritus*, *23*(23), 65–75. https://doi.org/10.31025/2611-4135/2023.18274
- Iannello, S., Bond, Z., **Sebastiani, A.**, Errigo, M., & Materazzi, M. (2023). Axial segregation behaviour of a reacting biomass particle in fluidized bed reactors: experimental results and model validation. *Fuel*, *338*, 127234. https://doi.org/10.1016/J.FUEL.2022.127234

- **Sebastiani, A.**, Paulillo, A., Lettieri, P., & Materazzi, M. (2023). Retrofitting waste-to-energy with Carbon Capture and Storage in the UK: a techno-economic and environmental assessment. *European Biomass Conference and Exhibition Proceedings*, 628–634.
- Chari, S., **Sebastiani, A.**, Paulillo, A., & Materazzi, M. (2023). The Environmental Performance of Mixed Plastic Waste Gasification with Carbon Capture and Storage to Produce Hydrogen in the U.K. *ACS Sustainable Chemistry and Engineering*. https://doi.org/10.1021/acssuschemeng.2c05978
- **Sebastiani A.**, Iannello S., Chari S., Macri' D., Materazzi M. (2022) Steam-CO_2/Oxygen gasification of biomass waste in lab-scale fluidized bed. Fluidized bed conversion conference. The 24th fluidized bed conversion conference.
- Amaya-Santos, G., Chari, S., **Sebastiani, A.**, Grimaldi, F., Lettieri, P., & Materazzi, M. (2021). Biohydrogen: A life cycle assessment and comparison with alternative low-carbon production routes in UK. *Journal of Cleaner Production*, *319*, 128886. https://doi.org/10.1016/j.jclepro.2021.128886
- **Sebastiani, A.**, Macrì, D., Gallucci, K., & Materazzi, M. (2021). Steam - oxygen gasification of refuse derived fuel in fluidized beds: Modelling and pilot plant testing. *Fuel Processing Technology*, *216*(October 2020), 106783. https://doi.org/10.1016/j.fuproc.2021.106783

Conference presentations

- **Sebastiani A.**, Paulillo A., Lettieri P., Materazzi M. *Decarbonising Energy-from-Waste in the UK: a techno-economic and environmental assessment of capturing carbon emissions*. The 31st European Biomass Conference & Exhibition (2023), Bologna, Italy, (Oral presentation).
- **Sebastiani A.**, Iannello S., Errigo M., Materazzi M. *Gasification of Refuse Derived Fuels in Fluidized Bed Reactors: Bed-Freeboard Coupled Models, Results and Validation*. Fluidization XVII (2023), Edinburgh, UK (Oral presentation).
- **Sebastiani A.**, Iannello S., Chari S., Amaya-Santos G., Paulillo A., Lettieri P., Materazzi M. *Techno-Environmental Analysis of Different Pre-Combustion Carbon Capture Technologies for Hydrogen Production from Waste*. AIChE Annual Meeting (2022), Phoenix, AZ, (Oral presentation).
- **Sebastiani A.**, Iannello S., Chari S., Errigo M., Materazzi M. *Fluidized bed technologies for intensified hydrogen production from waste*. Particle Technology Forum (2022), London (virtual), UK, (Poster presentation)
- **Sebastiani A.**, Chari S., Amaya-Santos G., Paulillo A., Lettieri P., Materazzi M. *Techno-environmental analysis of different pre-combustion carbon capture technologies for hydrogen production from waste*. ChemEngDayUK (2022), London, UK, (Oral presentation)
- **Sebastiani A.**, Iannello S., Chari S., Macri' D., Materazzi M. *Steam-CO_2/Oxygen gasification of biomass waste in lab-scale fluidized bed. Fluidized bed conversion conference*. The 24th fluidized bed conversion conference (2022), Chalmers University of Technology, Gothenburg, Sweden (Oral presentation).
- **Sebastiani A.**, Chari S., Bethapudi S., Materazzi M., *Biohydrogen production from waste: experimental investigation and deployment prospect for transportation*. 29th European Biomass Conference & Exhibition (2021), Nice (virtual), France, (Oral presentation).
- **Sebastiani A.**, Macri' D., Galluci K, Materazzi M., *Steam-Oxygen Gasification of Refuse-Derived Fuel in Fluidized Beds: Modelling and Data validation*. 7th International Symposium on Gasification and its Applications (2021), Nancy (virtual), France, (Oral presentation).
- **Sebastiani A.**, Macri' D., Galluci K, Materazzi M., *Steam-Oxygen Gasification of Refuse-Derived Fuel in Fluidized Beds*. The 15th International Conference on Chemical and Process Engineering ICheaP15 (2021), Naples (virtual), (Poster presentation).
- **Sebastiani A.**, Macri' D., Galluci K, Materazzi M.*, Steam-O_2 Gasification of Refuse-Derived Fuel in Fluidized Beds: Modelling and Pilot plant testing*. ChemEngDayUK (2021), Bradford (virtual), UK, (Oral and Poster presentations).

Chapter 1. Introduction

Global population growth and economic expansion have intensified resource depletion and waste generation, creating pressing environmental challenges across all governance levels. These challenges encompass deteriorating air quality, resource limitations, waste management issues and climate change. This context has driven the search for alternatives to fossil fuel usage and landfill disposal, with an increasing focus on converting biomass and waste materials into valuable chemicals and sustainable fuels.

Although the concept of waste conversion is established, recent years have seen renewed interest in advanced thermochemical processes, notably pyrolysis and gasification, as pathways to transform waste materials into high-value fuel and chemical products. This thesis focuses on understanding the impact of operating parameters and engineering design solutions on the overall process of waste gasification. The main objective is the development of an accurate and easy-to-operate model that can provide crucial insights for improving system design and operational decisions. This chapter outlines the research motivation, objectives, and thesis structure.

1.1 World energy outlook

Fossil fuels (coal, oil, and natural gas) have served as cheap and convenient energy sources for the past 200 years. However, their extensive use has resulted in severe environmental consequences, including pollution, ozone depletion, and global warming, through harmful emissions to land, water, and air. Since the industrial revolution began, the increasing dominance of fossil fuels in the global energy supply has led to rapid, uncontrolled growth in air-polluting emissions, specifically carbon monoxide, nitrogen oxides, sulfur oxides, and particulate matter. Moreover, energy production systems based on fossil sources contribute significantly to atmospheric greenhouse gas (GHG) emissions. Public awareness about the detrimental effects of these emissions on human health and the environment has increased substantially in recent years.

Addressing the impacts of anthropogenic global warming represents the most significant challenge facing the global community in the 21st century, requiring coordinated action on multiple fronts. A fundamental transformation of energy supply structures must occur to meet growing energy demands while reducing environmental impact. With continuing population growth and economic expansion, global energy consumption is rising rapidly, making an energy economy based solely on fossil fuels increasingly unsustainable at both global and national levels. The International Energy Outlook (IEO)

[1] projects that world energy consumption will increase by 50% between 2018 and 2050. Countries outside the Organization for Economic Cooperation and Development (non-OECD) will account for approximately 70% of this growth, compared to a 17% increase in OECD countries [2].

Figure 1.1 shows the global energy mix scenario as developed by the International Energy Agency [3], highlighting primary energy consumption patterns from various fuel sources with projections to 2050. Fossil fuels continue to dominate, comprising a large fraction of the global energy consumption. While liquid fuels consumption increases in absolute terms due to demand from industrial, commercial, and transportation sectors, their overall share is projected to decline from 32% in 2018 to 27% in 2050.

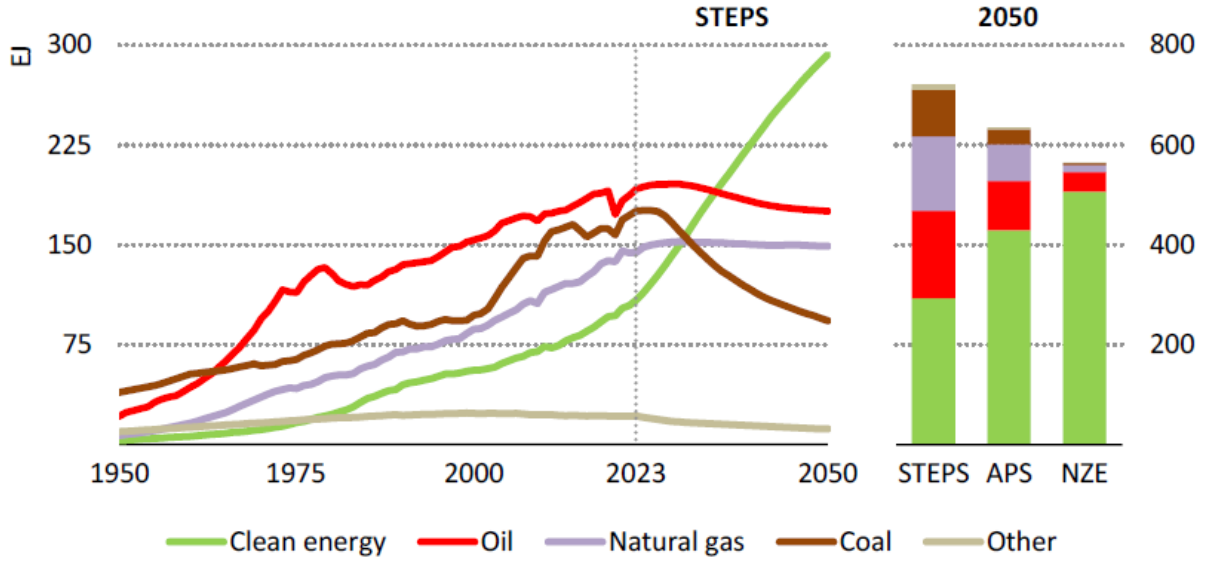

Figure 1.1 – Global energy mix by scenario to 2050. Stated Policies Scenario (STEPS), Announced Pledges Scenario (APS) and Net Zero Emissions by 2050 Scenario (NZE), from [3].

Current energy policy projections, as outlined in the Stated Policies Scenario (STEPS), indicate significant shifts in the global energy landscape. Analysis suggests that all fossil fuel consumption will reach its peak before 2030, coinciding with accelerated clean energy adoption and moderating energy demand growth. A notable transition occurs as natural gas consumption surpasses coal utilization in the global energy portfolio by 2030. The period from 2023 to 2035 marks a critical phase where clean energy expansion outpaces overall energy demand growth. This transformation is primarily driven by expansions in wind power generation and solar photovoltaic installations, positioning clean energy as the primary energy source during the mid-2030s. Despite projections showing renewable energy capacity tripling and reducing fossil fuel utilization from 80% (2023) to 58% (2050) of total energy demand, these changes remain insufficient compared to more ambitious scenarios [3].

The Announced Pledges Scenario (APS) and Net Zero Emissions by 2050 (NZE) Scenario present more dramatic transformations in the energy sector. These frameworks project renewable energy sources rapidly gaining market dominance over conventional fossil fuels. Under the APS framework,

clean energy sources are projected to fulfil 40% of global energy requirements by 2035, expanding to approximately 75% by 2050. The NZE Scenario presents an even more ambitious outlook, with clean energy technologies meeting 90% of global energy needs by 2050. Within this scenario, the limited remaining fossil fuel consumption follows specific pathways: fully abated processes account for one-third, while feedstock and non-energy applications comprise roughly half. The remaining portion requires carbon offset mechanisms, including direct air capture technology, bioenergy-based negative emissions, and various carbon removal strategies.

The landmark 2015 Paris Agreement agreed to hold the increase in the global average temperature to well below 2°C above pre-industrial levels and to pursue efforts to limit it to 1.5°C. To keep global warming well below 2 °C, current greenhouse gas (GHG) emissions must be halved by mid-century and must then continue to decline [4]. This will require rapid changes in energy systems and land-use practices.

The pathway to Net Zero (Figure 1.2) published by the International Energy Agency outlines critical transitions in transforming the global energy sector [5]. By 2050, renewable sources including wind, solar, bioenergy, geothermal, and hydropower are projected to provide two-thirds of the total energy supply. Residual fossil fuel usage in 2050 will be limited to specific applications: carbon-embedded products such as plastics, facilities equipped with Carbon Capture, Utilization and Storage (CCUS) systems, and sectors with limited low-emission alternatives, particularly heavy transportation including trucks, buses, and aviation.

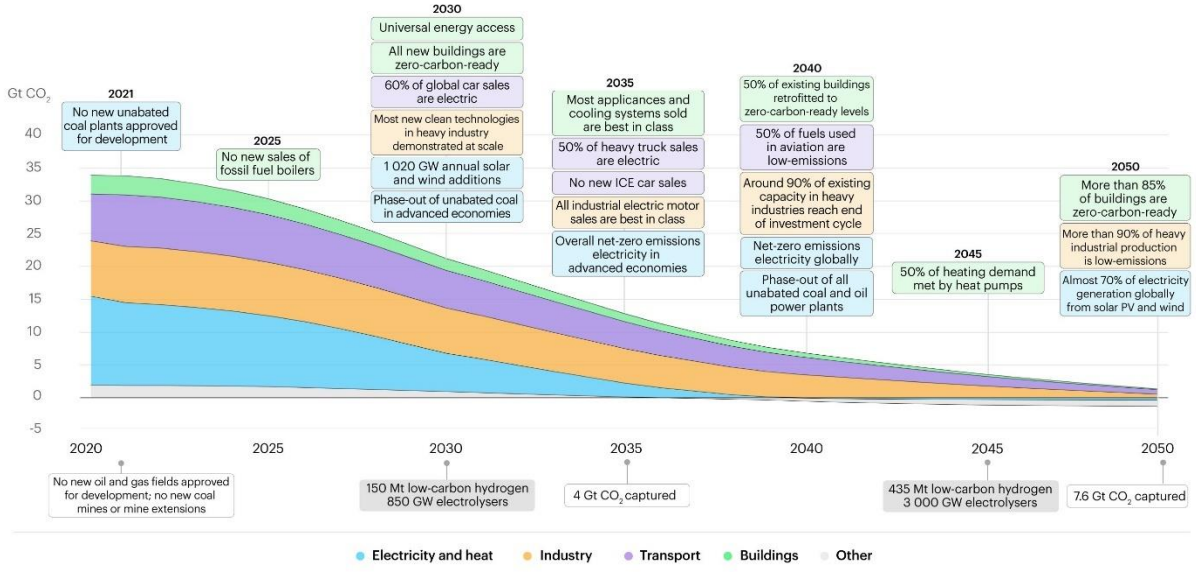

Figure 1.2 – Key milestones in the pathway to Net-Zero, from[5].

Achieving the 2050 net-zero target demands both rapid implementation of existing technologies and continued advancement of emerging solutions. Carbon-negative technologies play a vital role in offsetting residual fossil CO_2 emissions. Major technological innovation priorities include advanced

energy storage systems, low-carbon hydrogen production through electrolysis and bio-based methods, and enhanced carbon capture and storage technologies.

Meeting substantial emissions reduction targets in coming decades, while progressing toward near-zero emissions of CO_2 and other persistent greenhouse gases, requires coordinated global action. The scale of technological, economic, and social challenges intensifies with delayed implementation of mitigation strategies and limited access to proven technologies. These challenges remain consistent whether targeting higher or lower warming thresholds, though their urgency varies [4]. Within all mitigation approaches, bioenergy and carbon capture and storage technologies, particularly their integration through Bioenergy with Carbon Capture and Storage (BECCS), serve as fundamental components, offering both low-carbon energy generation and potential negative emissions capabilities.

1.2 Resourceful nature of waste

Society faces two interconnected challenges: addressing anthropogenic global warming and developing sustainable solutions for managing escalating global waste volumes.

Municipal Solid Waste (MSW) generation presents a significant environmental challenge, with volumes projected to increase (Figure 1.3). Contemporary waste management hierarchies prioritize reduction, recycling, and reuse strategies, positioning landfill disposal as the least favourable option. Despite this approach, landfills remain the predominant disposal method in the EU-27, handling approximately 41% of waste. Although projections indicate a decrease to 35% by 2020, rising MSW generation suggests absolute landfill volumes may remain relatively stable. While recycling initiatives play an essential role in waste reduction, opportunities exist for innovative energy recovery from materials traditionally destined for landfill disposal. The concept of Waste-to-Energy (WtE) has emerged as a viable strategy, combining waste management with energy generation through electricity and heat production.

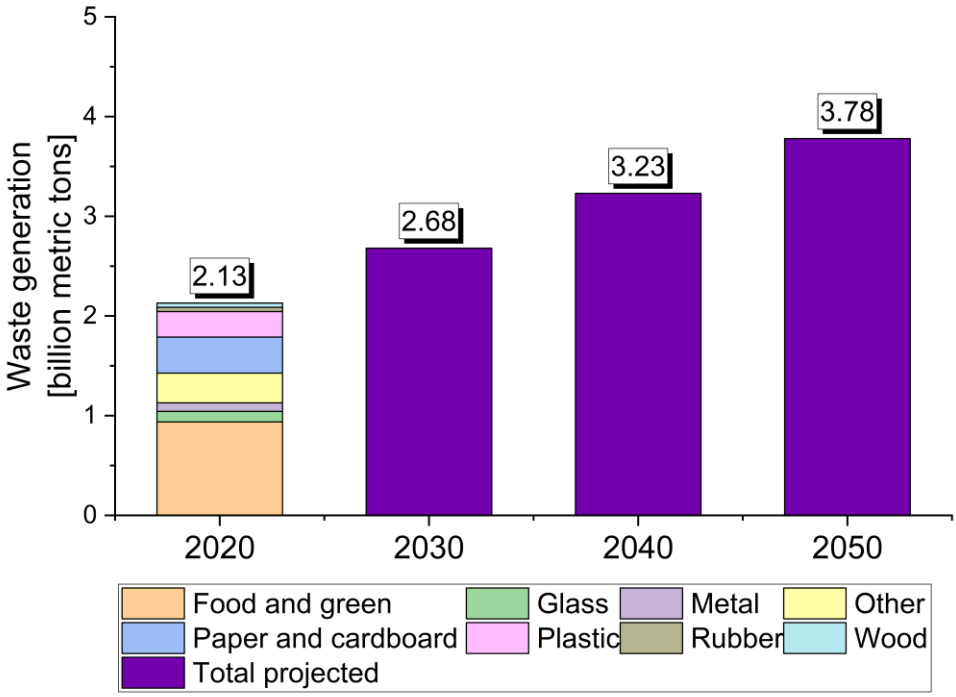

Figure 1.3 – Municipal solid waste generation worldwide in 2020, and projection from 2030 to 2050. Form [6]. Waste composition adapted from [7].

The total volume of Municipal Solid Waste (MSW) waste produced annually is very considerable and is anticipated to grow in the future. The modern waste management strategy promotes minimisation, recycling and reuse of waste, with disposal to landfill being considered as the least desirable option. However, landfill remains the main method of waste disposal, currently accounting for around 41 % within the EU 27, and although this figure is anticipated to fall to around 35 % by 2020, the increasing levels of MSW generated means that the total amount of waste sent to landfill is unlikely to reduce markedly over this period. Whilst recycling clearly has a critical role to play in reducing the 'waste mountain', there is further opportunity, innovation and environmental benefit in recovering energy from what might previously have been seen as residual waste destined for landfill. Waste-to-Energy (WtE), i.e., the production of electricity and heat from waste feedstocks, has been one of the most promising pathways for managing the ever-increasing amount of waste generated combined with energy recovery.

New technologies are being developed which can fully exploit the inherent value of waste by transforming it into an energy source in its own right. Advanced conversion technologies in particular have an important role to play in converting waste into energy and can be completely complementary to recycling, maximising the value extracted out of municipal and commercial waste. Besides a substantial reduction in the overall waste quantities requiring final disposal, these technologies can also play a vital role in mitigating energy problems.

Waste composition differs across income levels, reflecting varied patterns of consumption. High-income countries generate relatively less food and green waste, at 32% of total waste, and generate more dry waste that could be recycled, including plastic, paper, cardboard, metal, and glass, which account for 51% of waste. Middle- and low-income countries generate 53% and 57% of food and green waste, respectively, with the fraction of organic waste increasing as economic development levels decrease. In low-income countries, materials that could be recycled account for only 20% of the waste stream. Across regions, there is not much variety within waste streams beyond those aligned with income.

Analysis by the Committee on Climate Change (CCC) regarding long-term bioenergy integration reveals that household waste constitutes the primary biomass resource in the United Kingdom. This dominance persists even in scenarios incorporating expanded land allocation for energy crop cultivation [8]. According to these projections, domestic waste will continue to serve as the principal contributor to UK bioenergy resources, maintaining its significance among local bioenergy feedstocks.

1.3 Overview of thermochemical technologies for waste conversion

Thermochemical conversion technologies are used to transform waste and biomass feedstock into commercial fuels and energy by employing processes at high temperatures. These include combustion, pyrolysis, and gasification, often coupled with additional chemical processes for the upgrading of the final product. Gasification and pyrolysis, in particular, are often employed to produce syngas (a fuel gas mixture constituted mainly by hydrogen and carbon monoxide) for use in the production of modern synthetic fuels (e.g. biodiesel, ethanol, bio-syngas, or bio-hydrogen). This allows for the substitution of considerable quantities of fossil-based fuels in the energy market.

The thermochemical routes differ according to the operating temperature, amount of oxygen required, and reactor design. These processes generate CO_2 and water as products of oxidative reactions, together with intermediate valuable products depending on the operating conditions. By increasing the amount of oxygen employed, a higher amount of thermal energy can be recovered. However, this entails lowering the chemical energy that ends up in the product gas. The increase in recoverable thermal energy reaches the maximum in the case of complete combustion, where the chemical energy of the feedstock is completely transformed into heat and mainly steam and CO_2. On the other hand, pyrolysis and gasification make use of sub-stoichiometric quantities of oxygen. This allows for sufficiently high temperatures to take place, and the partially-oxidative atmosphere permits the thermal degradation of the carbonaceous material. The valuable products are released in gas or liquid form, mostly hydrocarbons, and syngas. Thermochemical conversions have potential benefits over other technologies, including enhanced efficiency, but also flexibility in the way the product

energy is utilized having a much wider spectrum of applications. Therefore, this work will be focusing on these technologies.

1.3.1 Combustion

Combustion represents perhaps the oldest utilization of solid fuels in thermochemical processes. Chemically, combustion is the complete oxidation of the hydrocarbon species in biomass or wastes, and conversion into mainly H_2O and CO_2. Combustion involves several processes which occur simultaneously. Initially, the moisture content is driven off by the heat in the combustion chamber (or boiler), followed by the release of its volatile content (referred to as devolatilization). Actual combustion only commences once the volatiles are ignited in the presence of air. The heat released is used to produce high-pressure steam for electricity generation in steam turbines, and low-pressure steam for internal use. Although bottom and fly ashes (derived from the inorganic content of the waste) play a small role in the overall process, they have a significant effect on the energy balance, by reducing the heat capacity of the feedstock [9]. Incidentally, ferrous and non-ferrous metals may also be recovered depending on the bottom ash treatment options. Furthermore, the residual ash can be upgraded, enabling its use as a construction material [10].

1.3.2 Pyrolysis

Pyrolysis takes place in the total absence of oxygen, except in cases where partial combustion is needed to provide the heat for the process itself. During the pyrolysis of solid waste fuel, decomposition occurs at relatively low temperatures (approx. 300°C – 600°C) [11]. The biomass or waste feedstock is converted into gaseous (syngas), solid (char), and liquid (tar) products. The net calorific value of the syngas is typically in the range of 10 – 20 MJ/Nm^3. The condensable fraction is recovered by cooling the syngas for use as liquid fuel. The rate of heating and the pyrolysis temperature affect the proportion of useful products generated from the process (namely H_2, CO, CH_4, and other hydrocarbons) [12]. The liquid product is referred to as bio-oil and can be used as alternative fuel oil in power and heat applications or as feedstock in the production of various commodity chemicals. The major drawback concerning bio-oil is its high oxygen content (35- 60 wt%) [13,14], which results in a low calorific value, instability, and corrosiveness of the fuel [15]. The lower heating value (LHV) is usually between 18 MJ/kg and 20 MJ/kg, which is lower than the LHV of conventional liquid fuels such as diesel (42 MJ/kg) and gasoline (44 MJ/kg) [16]. Recently, different studies to solve this issue have been conducted on the co-pyrolysis of biomass and waste plastics. These substances are particularly attractive for their high hydrogen contents of about 14 wt% (e.g. polyethylene,

polypropylene, polystyrene), hence they could donate hydrogen during the process with biomass and improve the bio-oil quality [14].

1.3.3 Gasification

Gasification is an intermediate between combustion and pyrolysis, involving partial oxidation of the fuel. In particular, the oxygen can be added in a sub-stoichiometric amount to allow high temperatures to take place, temperatures typically above 700°C, without the complete oxidation of the fuel [49]. The products of gasification consist of partially oxidised compounds – mainly H_2, CO, and CO_2. Partial combustion or external heat supply is necessary to sustain the gasification process. The main product is syngas that contains hydrogen, carbon monoxide, and methane with a net calorific value of 4-10 MJ/Nm^3 [17]. This high calorific value means that the gases from gasification can be used in gas turbines and/or internal combustion engines, or burned in conventional boilers connected to steam turbines. Concerning energy production, gasification has many advantages over combustion. For instance, the syngas product may be more valuable as it can be combusted at higher temperatures or used in fuel cells [18,19]. It also produces a solid ash product, low in carbon (i.e. char) and other inorganic contaminants (for example, chlorides, sulfides, heavy metals, etc.). The biggest potential of waste and biomass gasification, however, is still not fully realized. Once the syngas is cleaned and all impurities removed, it can be used to generate hydrogen, chemicals, or high-quality fuels via catalytic stages (e.g. Fischer-Tropsch, methanation, etc.) [20], while at the same time producing varying quantities of CO2 ready for storage. This opens the door to a new and potentially outstanding biorefinery industry that sees gasification as one of the most promising thermochemical technologies in the future for the production of sustainable fuels and greenhouse gas removal [21].

1.3.3.1 Note on types of gasification reactors

The most commonly used gasification technologies for single-stage processes are fixed bed (up-draft, down-draft, side-draft), entrained bed, and fluidized bed reactors (bubbling bed, circulating fluidized bed, spout fluid bed) [22]. The main reactor configurations for gasification are reported in Figure 1.4.

Fixed bed gasifiers can be classified according to how the gasifying agent enters the gasifier. The main configurations are updraft and downdraft. Fixed bed gasifiers use a bed of solid fuel particles through which oxidants (air, steam, oxygen or a mixture) and gas pass either up or down. They are the simplest type of gasifiers and generally operate with high carbon conversion and long solid residence time. Fixed beds in single-stage mode are usually limited to high-grade fuels gasification, and mainly used in small-scale plants, and the produced gas is typically used in thermal (heat gasifiers) or engine (power gasifiers) applications [23].

Entrained-flow gasifiers are all oxygen-blown, slagging gasifiers producing medium heating value syngas. In an entrained flow gasifier, fine fuel particles are added to water to produce the slurry. Water serves as a transport medium, temperature moderator and reactant. A turbulent flame at the top of the gasifier burns some of the fuel, providing heat at high temperatures (1200–1500 °C, anyway above the ash melting temperature). However, even after several decades of development and commercialization of coal treatment, the availability of entrained flow gasifiers is still limited for waste treatment applications. The typically short residence time requires the feedstock to be pulverized, which makes this technology very unsuitable for general waste processing.

Fluidized-bed gasifiers can be divided into two classes: bubbling and circulating. In fluidized beds, the flow of gaseous oxidant (air, oxygen, or oxygen-enriched air) is blown upwards through a distributor plate and fluidizes a bed of inert material at the bottom of the gasifier, where the waste to be treated is fed. The fluid-like state results in intense mixing and gas-solid contact that allows very high heat and mass transfers. This type of gasifier operates at temperatures below 800-900 ºC to avoid ash melting and sintering that can determine a worsening of the fluidization quality and defluidization. Fluid bed systems allow for more efficient gasification due to homogeneous temperature, good flow mixing inside the reactor, rapid heating of the feedstock, and the possibility of including catalysts in the bed inventory to enhance the reactions. They are suitable for various types of feedstock and can be scaled up to relatively large plant sizes [24,25]. Fluidized bed gasifiers are the preferred type of reactor for large plant operations.

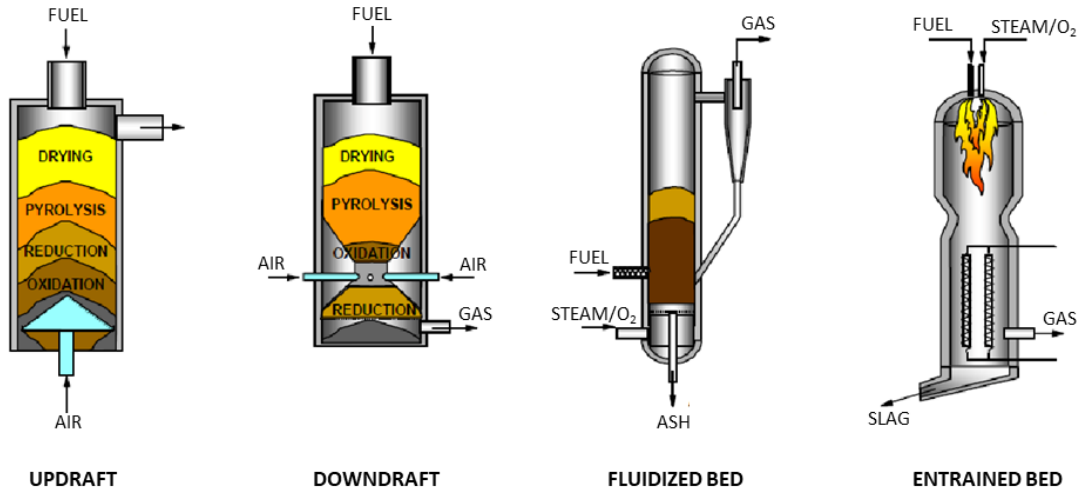

Figure 1.4 – Schematic representation of different types of gasifiers. Adapted from [26].

1.3.3.2 Note on waste gasification for low-carbon fuels production

Gasification is one of the most versatile thermochemical processes for biomass conversion, and according to many, the basis of most of the future BECCS systems. Although gasification is not a new

concept, it is only in recent years that it has been commercially used to treat low-quality feedstock, like waste-derived materials, due to the non-trivial adaptation of process conditions to non-conventional feedstock and the economic interests of stakeholders.

In the UK, advanced gasification technologies are recognised as key enabling solutions in the transition to a net-zero carbon economy. These technologies can be used to produce a variety of energy products including methane, hydrogen, and drop-in fuels that can be used to substitute fossil fuels (e.g. diesel, gasoline, and aviation fuel) without infrastructural or vehicle changes. Therefore, these technologies are considered to be effective low-carbon routes for sectors that may otherwise be difficult or expensive to decarbonise (e.g. aviation). Whilst these technologies are integral to achieving the UK's net-zero carbon emissions target, the UK government pursues its commitment to developing policies and innovation spending initiatives to incentivise investment and promote wide-scale deployment of gasification technologies by 2030 [27,28].

Despite the great potential held by advanced gasification technologies when using sustainable feedstock, the technical challenges, combined with the lack of operational experience, inhibit the deployment of the technology.

1.4 Waste-to-Hydrogen: a pathway towards circular economy and Net-Zero

In recent years, low-carbon hydrogen has received increasing attention as a high-efficiency energy vector that could be produced from both fossil and non-fossil sources, with low greenhouse gas (GHG) emissions associated with production, and no emissions at the point of use. Globally, hydrogen is being promoted as an ideal energy/fuel source for heating and transport, particularly on bus, shipping, and train routes that are not suitable for electrification [29]. For these reasons, hydrogen is recognised to have an important role in industrial transformation and therefore has a major role in the UK and European industrial strategies. For example, for the UK to deliver a net-zero carbon energy system, it has explicitly identified the requirement for 225 TWh/year of low-carbon hydrogen production [30].

Hydrogen offers a unique cross-system opportunity for fundamental change in the energy landscape, helping to reduce the carbon intensity of potentially all energy sectors, particularly in sectors hard to electrify (i.e. heat, power, and transport). Therefore, low-carbon hydrogen will be critical for meeting the Paris Agreement goal, because it generates no GHG emissions at the point of use and can displace large volumes of conventional fuels from an energy standpoint. As part of a deeply decarbonised and renewable energy system, low-carbon hydrogen could be a versatile replacement for high-carbon fuels, helping to bring down emissions in other industrial sectors and providing flexible energy for power, heat, and transport. There are no abundant natural sources of pure hydrogen, which means that it has to be obtained by converting a different feedstock.

Nowadays, there are a number of existing technologies that produce hydrogen using different pathways and feedstock. The conversion of natural gas is the most widely deployed, as it offers the potential for bulk low-carbon hydrogen production, at a relatively low cost [31,32]. For the carbon benefit to be real, CO_2 must not be released into the atmosphere, therefore the process would need to be coupled with a CCS system, to produce the so-called Blue Hydrogen (Blue-H_2) [33]. Two principal technologies are available for Blue-H_2 production: Steam Methane Reforming (SMR) and Autothermal Reforming (ATR) [32]. However, none of these technologies use renewable or bioenergy, so they will not be sustainable in the long term.

The production of hydrogen via water electrolysis is also garnering attention. This technology, also known as Green-H_2 uses renewable electricity to split water and produce hydrogen and oxygen [32]. This technology has seen limited commercial-scale usage for hydrogen production until recently, due to high capital costs and moderate efficiencies, strictly related to the electrolysis system [34,35]. Electrolysis is a clean process, nonetheless, for the process to be considered 'green', the electricity input required must come from renewable resources such as solar and wind [36,37]. The intermittency of renewable electricity poses another barrier to the large-scale utilization of Green-H_2.

In recent years, the research focused on the development of different Waste-to-Hydrogen (WtH_2) processes as key enablers solutions of effective BECCS [37–41]. Hydrogen generated by gasification of biogenic feedstock is defined as Biohydrogen. This is one of the most innovative technologies that has one of the lowest environmental impacts among other technologies [42], and when coupled with a CCS facility has the highest potential of delivering a negative impact to climate change removing all the carbon contained in the biogenic feedstock, by sequestering and permanently CO_2 from the natural carbon cycle. As such, biohydrogen with CCS is recognised to be among the most effective form of BECCS in the future. The process steps for Biohydrogen are shown in Figure 1.5. These can be summarised as follows:

- Production of syngas, a mixture of mainly hydrogen, carbon monoxide and carbon dioxide, through gasification of wastes or biomass.
- Syngas cleaning from impurities and harmful compounds (e.g. fly ashes, tars and heavy hydrocarbons, heavy metals, acid and sulfur compounds).
- Increasing the hydrogen content in water gas shift reactors with steam injection to enhance hydrogen bulk production. In this stage, carbon monoxide is converted into carbon dioxide.
- Refining the hydrogen by removing and storing carbon dioxide with appropriate CCS technologies.
- Removal of residual traces of impurities to achieve the required design H_2 purity.

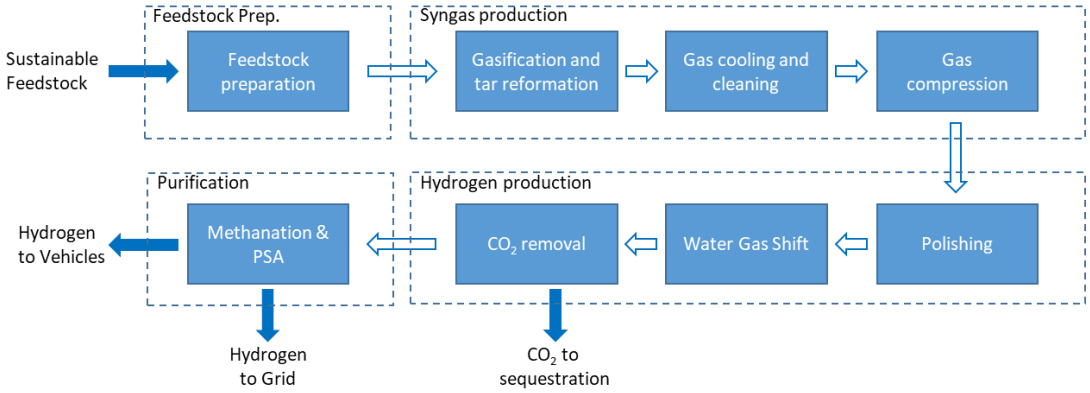

Figure 1.5 – Block flow diagram of the WtH_2 process.

1.5 Main challenges in WtH_2 plant deployment

Waste-to-H_2 technologies offer a dual environmental benefit: they simultaneously reduce issues associated with conventional waste management, including land use and pollution, while decreasing reliance on fossil fuels and their associated environmental consequences.

The development of thermochemical waste-to-H_2 systems, however, faces ongoing technical and economic challenges, with the gasification stage representing the major bottleneck of the overall process. These systems currently demonstrate limited waste processing capabilities, with economic viability achieved only in specific applications. Technology developers have attempted to adapt conventional technologies for processing solid waste, including fluidized bed reactors, entrained flow systems, and plasma furnaces. This development path has led to numerous processes and large-scale facilities aimed at converting waste into clean synthesis gas. The intended applications include power generation through gas engines or turbines, potentially offering higher efficiency than traditional incineration methods. Despite these efforts and the construction of demonstration facilities, widespread commercial implementation remains limited.

The greatest technical challenge to overcome for the successful growth of gasification technologies treating low-quality feedstock is that of achieving a quality of syngas that is good enough to sustain a stable and long-term operation of high-efficiency energy devices (e.g. fuel cells) or catalytic reactors for synthetic fuels [43–45]. All of these syngas end-use technologies require a suitable gas composition and the absolute absence of tar species and other catalyst polluters, such as sulphur and chlorine [46–48]. In many cases, nitrogen dilution in the syngas should also be avoided to reduce the cost of compression and simplify the gas separation downstream. This is particularly true in new bioenergy applications like Biohydrogen and biogas production [31,49,50], which are gaining great attention in Europe [51]. Additional challenges are related to process scalability and flexibility, both necessary conditions for operation on waste-derived feedstock. Moreover, the integration of

these gasification technologies with CCS facilities is essential to provide significant CO_2 emission reductions. However, the infrastructures to support this are currently unavailable.

The widespread adoption of waste-to-hydrogen facilities faces several significant technical challenges, primarily centred on the gasification process. The main reasons for this slowdown can be summarized in the following points:

- Traditional gasification systems, while proven for conventional feedstocks, exhibit inherent stability issues when processing waste materials. The heterogeneous nature of waste streams creates unique operational challenges, particularly in fluidized bed systems. The current understanding of waste fuel behaviour and its interactions within the gasification process lacks the depth and certainty required for confident commercial deployment.
- Scale-up challenges represent another critical barrier. While lab and pilot-scale experiments have demonstrated promising results, translating these successes to larger scales has proven problematic due to non-linear phenomena involved and differences in process dynamics. The limited insights from pilot-scale operations hamper technology development, as comprehensive testing at pilot and demonstration scales requires substantial financial investment, often exceeding available research and development budgets.
- Even assuming the successful resolution of gasifier reliability and operational issues, significant uncertainties persist regarding the overall performance of waste-to-hydrogen plants. These concerns encompass both process efficiency and environmental benefits. The substantial energy requirements of these facilities raise questions about their net environmental impact and overall efficiency. A comprehensive evaluation of the energy balance and environmental benefits remains necessary to validate the viability of the technology as a sustainable waste management and hydrogen production solution.

The historical challenges in waste gasification explain the limited commercial adoption of these technologies for producing high-quality synthesis gas suitable for fuel applications [28,52]. These setbacks have driven intensive research toward innovative technological solutions that optimize syngas quality while reducing operational costs and minimizing residual waste. Although outcomes have varied, several promising approaches have emerged, particularly those utilizing dual-stage reactor configurations.

A notable advancement involves the integration of two stages: a primary waste gasification unit, typically employing bubbling fluidized bed technology, followed by a high-temperature refining stage. This secondary stage might incorporate either an ash-melting furnace or a plasma converter,

enhancing the overall process efficiency and product quality. This dual-stage approach addresses many limitations encountered in conventional single-stage systems.

The development and operation of these advanced waste treatment technologies remain constrained by limited technical expertise and operational experience. The current understanding of system behaviour lacks sufficient depth to enable reliable performance prediction, while simulation and modelling capabilities require further refinement. These knowledge gaps impede both the optimization of existing systems and the development of improved designs.

1.6 Aims of the thesis

Thermochemical conversions in fluidized bed reactors represent one of the most intense topics of ongoing scientific investigation. Numerous aspects within this domain remain uncertain, necessitating further clarification to favour the effective exploitation of these technologies on a commercial scale, mainly when operating with highly heterogeneous and volatile feedstocks. In this context, the aims of this Thesis are delineated as follows:

- To gain a deeper understanding of thermochemical processes in large-scale fluidized bed reactors. With the main focus on gasification as the key process for waste conversion, understand the influence of key operating variables, such as gasification agents and their relative amount to the feedstock, and engineering choices (e.g. related to reactor design and operations) and how these impact the final quality of the syngas and suitability of different waste materials.
- To develop a fundamental understanding of how different waste feedstock constituents, particularly biomass and plastic materials, behave during thermochemical conversion processes. The investigation focuses on characterizing key distinctions, with the starting point being devolatilization patterns and segregation behaviour, analysing their impact on syngas composition and overall gasifier performance metrics.
- To investigate the feasibility and integration opportunities of novel intensified technologies for hydrogen production from waste feedstock. The aim is to understand the technical challenges and opportunities of a fully integrated Waste-to-H_2 plant, with unit requirements, plant productivity and test the environmental benefits.

The main objective of this work is to develop an accurate, fast and easy-to-operate model for the gasification of different feedstock in fluidized beds. This model can serve as a tool to address the general aims outlined above. A more detailed and refined list of objectives is reported in Section 2.5.

1.7 Thesis outline

- **Chapter 1** provides the background and motivations of this Thesis, along with the main challenges and objectives driving this research study.
- **Chapter 2** provides a literature review focused on modelling approaches of the gasification of highly volatile feedstocks, as well as an overview of bubbling fluidized bed reactors hydrodynamics. Further emphasis is placed on the key challenges related to thermochemical conversions in bubbling fluidized bed reactors, informed by preliminary modelling endeavours and findings from literature review. The refined objectives of the Thesis are then provided.
- **Chapter 3** describes the methodology used to develop the fluidized bed gasifier model, with particular emphasis on the novel distribution of the products of devolatilization, informed by advanced X-ray imaging technique, and the detailed reaction kinetic pathway developed.
- **Chapter 4** reports an investigation on the gasification of different feedstocks using air in large-scale fluidized bed reactors. Extensive validation over several experimental tests at different conditions is reported. This serves as a foundation for the following systematic investigation of operating parameters on syngas quality and performance metrics.
- **Chapter 5** presents a comprehensive investigation of the sensitivity of fluidized bed gasifiers to the gasification agent, with a particular focus on the role of steam replacing air as a gasification agent. The rather limited operational experience on steam-oxygen gasification systems, as confirmed by the rather restricted availability of literature data, highly benefits from the systematic study of the most relevant operating parameters. The investigation is conducted running the validated model to explore the space of operating conditions in order to identify trade-offs and optima.
- **Chapter 6** links the findings from Chapters 4 and 5 to build a comprehensive waste-to-H_2 process simulation. This overall process simulation is directly informed by the gasifier kinetic model, and it extends the focus to the whole plant, including all the process units required to deliver pure H_2. The investigation is then directed towards the effect of different waste feedstocks towards the plant efficiency, as well as the impact of different H_2 purity requirements and carbon capture technologies on the environmental performance of the process.
- **Chapter 7** summarizes the conclusions of the Thesis and delineates potential future endeavours supported by the findings presented in this research study.

Chapter 2. Literature review

This Chapter provides an overview of the current state of research and development regarding critical aspects in the field of fluidized bed systems for the treatment of non-conventional feedstocks. The review begins by introducing some concepts regarding the classification of the feedstocks, to better understand the challenges and opportunities arising from this type of fuels in gasification processes. The survey will then address an overview of fluidized bed technologies, with a focus on mixing and segregation patterns of both feedstocks and gas phases. The review then delves into the realm of modelling approaches of fluidized bed reactors, reviewing the three main categories. Particular emphasis is then given to Fluidization models, deemed as the most suitable for process modelling and reactor design with accurate and fast results. The review analyses common practices and pitfalls in the literature available, to identify areas where to focus the modelling efforts that would produce a powerful and insightful tool for technology developers. The Chapter concludes with an update of the key research questions and objectives of the Thesis in light of the information provided by the literature review.

Parts of this chapter have been published in:

Sebastiani, D. Macrì, K. Gallucci, M. Materazzi, Steam - oxygen gasification of refuse derived fuel in fluidized beds : Modelling and pilot plant testing, Fuel Process. Technol. 216 (2021) 106783. https://doi.org/10.1016/j.fuproc.2021.106783

2.1 Fuel characterisation

This section examines the key characteristics of various waste feedstocks, including biomass, refuse-derived fuels (RDF), and plastics. While direct characterization of the feedstocks used in this research was not conducted, understanding these fundamental properties remains essential for the concepts explored later in this thesis, particularly volatile matter content, ash composition, and char formation.

A significant contrast exists between synthetic polymers commonly found in waste streams and biomass materials. Polymers such as polypropylene (PP) and polyethylene variants (PE, HDPE, LDPE)

feature simple, linear molecular structures. In contrast, biomass comprises a complex mixture of organic compounds including fats, carbohydrates, and proteins, along with trace minerals such as iron, potassium, sodium, calcium, and phosphorus. As illustrated in the Van Krevelen diagram (Figure 2.1), biomass demonstrates higher hydrogen-to-carbon ratios compared to coal, correlating with its elevated volatile and moisture content, though this results in lower heating values [53,54].

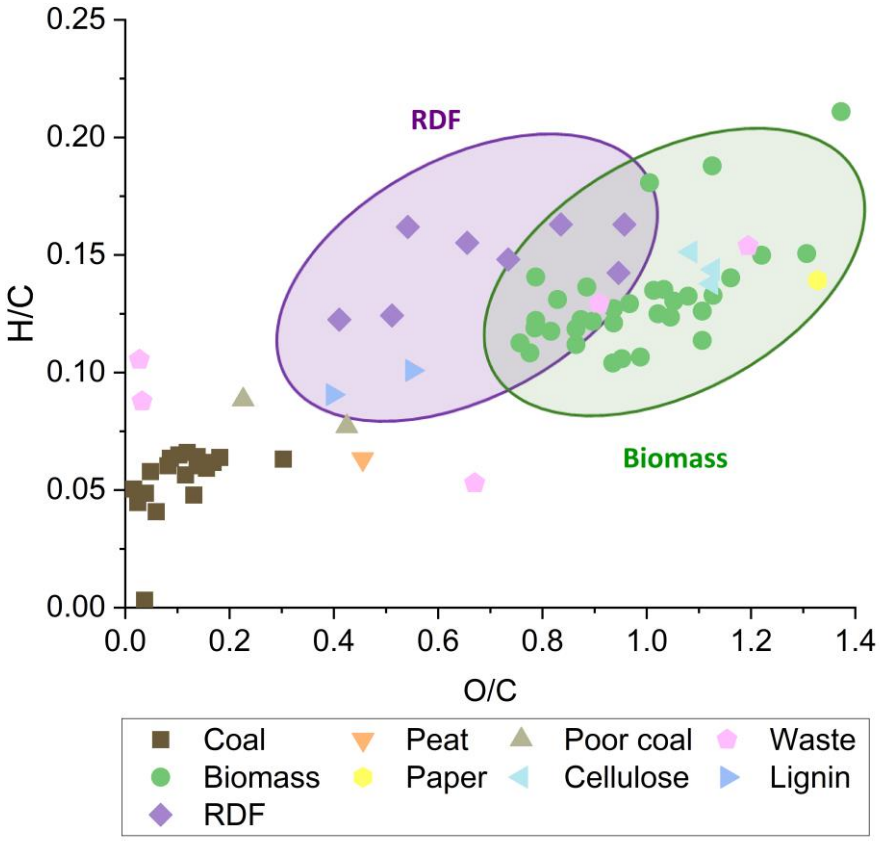

Figure 2.1 – Van Krevelen diagram for different feedstocks. Adapted from [53].

Biomass originates from biological or botanical sources, encompassing diverse materials such as forestry residues, agricultural byproducts, purpose-grown energy crops, and various biological or municipal wastes. Secondary biomass, which includes waste materials, derives from the processing or utilization of primary biomass sources like trees and vegetables.

Municipal Solid Waste (MSW) represents a significant secondary biomass source, containing renewable components such as food waste, yard trimmings, paper products, and organic materials. However, MSW also includes non-biomass materials like plastics, metals, and glass. In the plastic waste stream, approximately two-thirds consists of short-lifecycle products - primarily packaging materials, consumer goods, and textiles [55]. Among these, polypropylene and polyethylene variants constitute the predominant plastic types [55–57].

The three feedstocks modelled in the study, waste woody-biomass, plastic waste and RDF obtained from treating MSW, their respective compositions are reported in Table 2.1.

Table 2.1 – Waste compositions, adapted from[42].

Waste fractions [wt% as received]	MSW	Waste wood	Plastic waste
Paper and cardboard	22.7	0.8	-
Wood	3.7	93.4	-
Metals	4.3	1.7	-
Glass	6.6	-	-
Textile	2.8	-	-
WEEE	2.2	-	-
Plastics	10	0.5	>95
Inert/aggregates/solid	5.3	2.5	-
Organic fines	35.5	1.1	<5
Miscellaneous	7.1	-	-

2.1.1 Proximate and ultimate analyses of different feedstocks

The ultimate analysis quantifies the elemental composition of feedstocks by measuring carbon (C), hydrogen (H), oxygen (O), nitrogen (N), and sulphur (S) content, along with ash and moisture levels. The hydrogen and oxygen measurements specifically reflect organic components within the feedstock. The combination of carbon, oxygen, and hydrogen content largely determines the heating value of the feedstock.

Proximate analysis examines four main feedstock components: moisture, volatile matter (VM), ash, and fixed carbon (FC). While moisture and ash measurements align between ultimate and proximate analyses, the fixed carbon determination differs significantly from elemental carbon content. In proximate analysis, fixed carbon represents the char remaining after volatile matter release, excluding carbon present in volatiles. Ash content indicates the inorganic residue remaining after complete feedstock combustion.

Typical values of proximate and ultimate analyses of the types of feedstocks considered in this work are reported in Table 2.2.

Table 2.2 – Proximate and ultimate analysis of different waste materials. Adapted from [42].

Proximate analysis [wt%, as received]	RDF	Waste wood	Plastic waste
Fixed Carbon	8.9	10.75	1.71
Volatile matter	64.7	64.24	95.44
Ash	11.8	0.41	1.9
Moisture	14.6	24.6	0.95
Ultimate analysis [wt%, dry ash free (DAF)]	**RDF**	**Waste wood**	**Plastic waste**
Fossil Carbon	20.51	0.8	73.728
Biogenic Carbon	36.23	50.13	8.192
Hydrogen	6.86	5.76	11.89
Oxygen	31.78	43.01	0.36
Nitrogen	4.1	0.28	0.06
Sulphur	0.18	0.01	5.21
Chlorine	0.34	0.01	0.57
Energy content [MJ/kg DAF]	**RDF**	**Waste wood**	**Plastic waste**
Gross calorific value (HHV)	20.51	19.08	41.11

2.2 Fluidized bed gasification: Technology Overview

Fluidized bed reactors (FBR) have a long record of success in the field of thermochemical conversion due to their favourable mixing features, near-constant temperatures, and good operating flexibility [61]. These features make fluidized beds particularly suitable for the application with heterogeneous feedstock, including biomass and RDF [62]. In a fluidized bed, the fuel is suspended in a swirling mass of hot particles (such as sand), fluidized by an updraft of hot gases. This system facilitates thorough mixing, and therefore good mass and heat transfer. These are the main reasons why fluidized beds are best suited to transform heterogeneous materials via thermochemical processes. The exit gases carry off some particulates of ash, fines and bed material. Heavier bed particles and ash are decanted from the base of the gasifier, and replaced with fresh bed material (normally inert sand) [63]. This mechanism is feedstock-dependent, as fuels with a higher ash content require a more frequent exchange of bed inventory. In modern applications, fluidized bed plants are better suited to treating RDF than raw MSW. This requires pre-treatment of the waste feedstock to remove recyclable materials, as well as dense, coarse objects, and to reduce particle size. Fluidized beds offer flexibility in terms of feedstock calorific value, moisture, particle size and density, and sulphur content. Nonetheless, limitations may arise if the feed contains a significant portion of large, dense particles or low-melting-point ash. This flexibility centres on the ability to mix and hold the fuel within the fluid bed, providing sufficient residence time for reactions to reach completion. Alkaline

materials (for example, limestone) can also be charged to the bed to help retain acidic impurities or to aid tar cracking and reforming reactions [64]. The heat released by burning char and by the partial combustion of the syngas enhances and allows the endothermic reactions to take place. This provides the basis for controlling the temperature of the bed during steady-state operation. In this respect, the equivalence ratio (ER), which is the amount of oxygen fed relative to that required for stoichiometric complete combustion, is the parameter that determines the difference between combustion, pyrolysis, and gasification [41].

Figure 2.2 shows a typical topology of a fluidized bed gasifier, with the main reacting zones determined by the mixing and segregation behaviour of reacting particles in the case of on-bed feeding. The devolatilization takes place in the upper region of the bed, due to the tendency of light fuel particles to segregate and upon reaching the surface of the bed [58–60]. The remaining solid char particles tend to mix with the bed inventory and descend in the bed. At the bottom of the bed, the inlet gasification agent comes in contact with the hot char particles and oxygen is consumed. In the upper zone mainly char gasification takes place, and to a more limited extent tar and other gas reactions, such as reforming and oxidation.

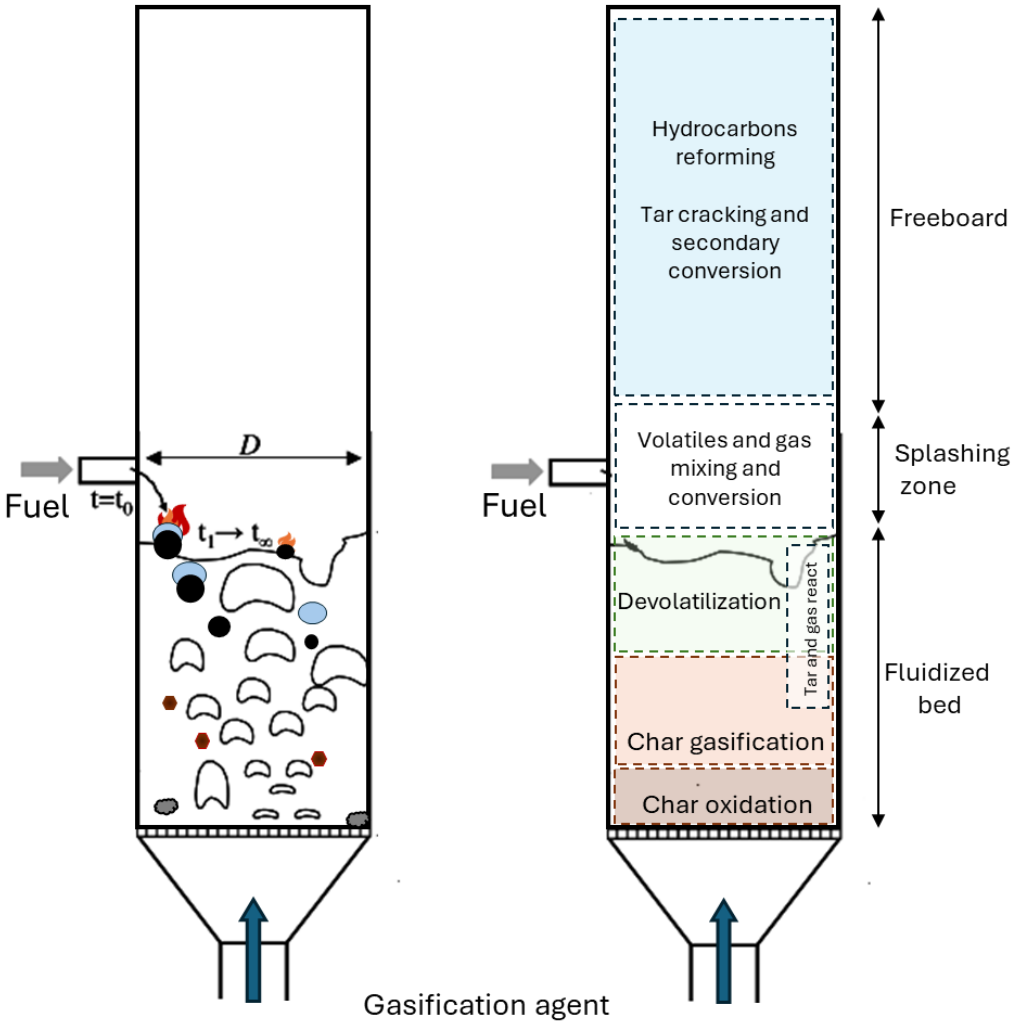

Figure 2.2 – Schematic representation of the topology of bubbling fluidized bed gasifier and the main reacting zones, in the case of buoyant fuel particles that segregate towards the surface of the bed.

The extent of reactivity depends on the bed temperature and degree of mixing. Carbon loss can occur in this region due to the entrainment of fine char particles, produced by comminution and attrition with bed particles [61,62].

The design and placement of the feeding system are key aspects of gasification reactor engineering, typically categorized as either in-bed or on-bed configurations. In-bed systems enhance mixing between the fuel and bed material, which can lead to higher conversion efficiencies [63]. In contrast, on-bed systems are more commonly implemented in large-scale reactors, such as those used in fluidized bed combustion, due to their relative simplicity, operational reliability, and lower cost.

However, when feedstock is introduced onto the surface of the fluidized bed, fuel particles may accumulate due to segregation effects, resulting in lower gas quality and increased tar formation [63]. Bruni et al. [64] conducted experimental studies on particle segregation in fluidized beds and found that segregation occurs more rapidly than the fuel devolatilization process. Consequently, most volatiles are released at the surface, even when fuel is introduced at the bottom of the bed.

These considerations have important implications for the design and operation of feeding systems, especially when handling fuels with high volatile content. While bottom feeding offers advantages in syngas quality and reactor efficiency, it also introduces design complexity and operational challenges, such as particle backflow, feeder blockages, and gas leakage [65]. Conversely, on-bed feeding offers simpler and more manageable operation, making it a practical choice. The experimental setup used in this study adopts an on-bed feeding system (refer to Sections 3.9.1 and 3.9.2.1).

The region above the fluidized bed, i.e. the splashing zone, is characterized by intense mixing induced by bubbles bursting, with homogeneous and heterogeneous reactions taking place. In the freeboard, the uppermost section of the gasifier, endothermic reactions and secondary tar conversion predominate. Oxidation reactions occur only in the case of secondary O_2 injection, as this zone typically lacks oxidizing agents.

Figure 2.3 summarizes the processes and phenomena occurring in a fluidized bed gasifier, leading to the production of syngas from solid fuels.

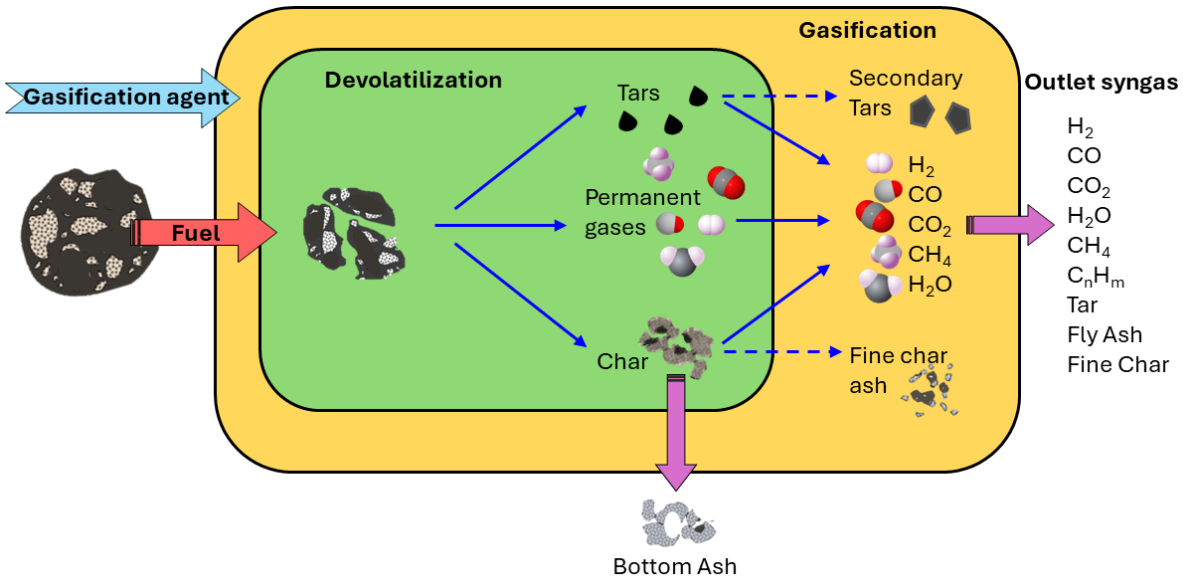

Figure 2.3 – Overview of the processes taking place in the gasifier: devolatilization of the solid fuel, reforming and gasification reaction, char conversion.

2.2.1 Solids devolatilization in fluidized beds.

Fluidized bed reactors applied to thermochemical processes have been investigated since the times when coal dominated heat and power generation, spanning over three decades of research to adapt the technologies to more sustainable feedstocks. Figure 2.4 illustrates the primary stages of feedstock thermal decomposition. Unlike coal, modern feedstocks such as biomass, plastics, and their mixtures (found in RDF, SRF, and similar materials) are characterized by high volatility, undergoing complex thermal transformations including drying, melting, and thermal cracking.

At high temperatures, typically between 200°C and 400°C, the solid structure of the feedstock undergoes rapid decomposition into smaller molecular components. This temperature-driven process, known as devolatilization, generates substantial quantities of vapours and gases, collectively named volatile matter or volatiles. The volatile content in waste feedstocks shows remarkable variation, ranging from 10 wt.% [75] to 99 wt.% [74], depending on feedstock composition.

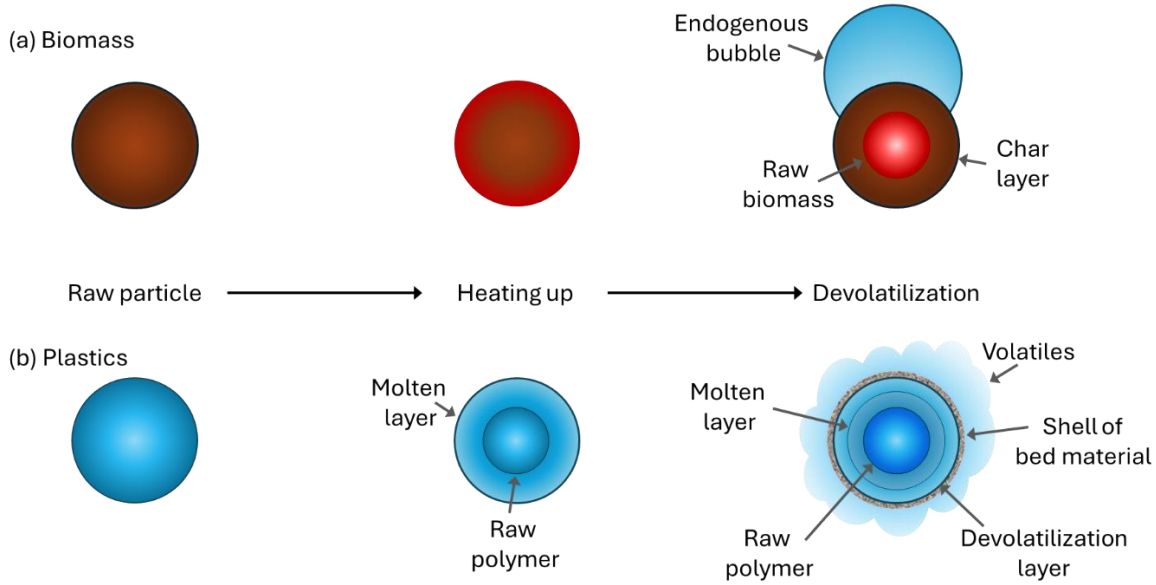

Figure 2.4 – Schematic representation of the main steps of thermal decomposition of feedstock particles, (a) biomass particle and (b) plastics.

The release of volatiles during devolatilization is markedly different across different solid fuels. Biomass produces higher volatile yields than coal due to its composition - lower carbon content but higher oxygen and hydrogen levels. These volatiles include water vapour, CO_2, CO, H_2, CH_4, and tars, primarily originating from the thermal decomposition of cellulose, hemicellulose, and lignin at relatively low temperatures.

Waste-derived solids show variable devolatilization patterns due to their heterogeneous nature. MSW, which contains diverse materials from organics to metals, produces complex gas mixtures during devolatilization, leading to inconsistent gasification behaviour.

Plastics demonstrate distinct devolatilization characteristics, generating primarily hydrocarbons with minimal char formation [66]. Their synthetic, homogeneous nature results in more predictable volatile production at higher temperatures compared to biomass and MSW.

2.2.2 Chemistry of Gasification

Gasification is the process that converts carbonaceous material from a solid to a combustible or synthesis gas (i.e., H_2, CO, CO_2, and CH_4). In general, gasification is defined as the reaction of carbon with air, oxygen, steam, carbon dioxide, or a mixture of these gases at 700°C or higher to produce a

gaseous product that can be used to provide electric power and heat or as a raw material for the synthesis of chemicals, liquid fuels, or other gaseous fuels [43].

The physical and chemical processes which take place between the gasification agents and the fresh solid feed in the conversion route to synthesis gas are complex, influenced by varying feed, process design, and operating conditions; nonetheless, the gasification chemistry may be considered as two distinct conversion mechanisms. When feedstock particles are rapidly heated at high temperatures (above 500 °C) in the reactor, more than 80% of their (dry) mass is rapidly converted into permanent gases and organic vapours, leaving only a variable amount of char and a few mineral ashes in the solid phase. With high volatility (more than 60%) and low ignition temperature (250 – 350° C), the devolatilization occurs immediately after the injection of the fuel into the reactor [9]. This first step is usually referred to as pyrolysis, wherein water vapour, organic liquids, and non-condensable gases, such as CO, H_2, and CO_2, are separated from the solid carbon (i.e. char) and ash content of the fuel. The vapour product comprises mostly polyaromatic hydrocarbons (PAHs) and tar (i.e. dark, oily, viscous material, consisting mainly of heavy organic and mixed oxygenates).

Subsequently, the volatiles and char undergo a second gasification step, and they modify their composition due to the occurrence of several reactions, reported in Table 2.3.

Most of these reactions are endothermic and require a consistent amount of energy to proceed. Most of the oxygen injected into a gasifier, either as pure oxygen or air, is consumed in combustion reactions ($r_{2\text{-}4}$ in Table 2.3) to provide the heat necessary to dry the solid fuel, break up chemical bonds and raise the reactor temperature to promote endothermic gasification reactions.

Table 2.3 – Typical gasification reactions [22,24,25].

r_j	Reaction name	Reaction	Enthalpy of reaction $\left[\frac{\text{kJ}}{\text{mol}}\right]$
1.	Devolatilization	$Fuel \rightarrow \text{Char} + \text{Volatiles} + \text{Tars}$	+200 -400
2	Combustion	$C + O_2 \rightarrow CO_2$	-394
3	Combustion	$H_2 + {}^1/_2\, O_2 \rightarrow H_2O$	-742
4.	Partial combustion	$C + {}^1/_2\, O_2 \rightarrow \text{CO}$	-111
5	Water gas shift	$CO + H_2O \rightleftarrows CO_2 + H_2$	-41
6.	Methane reforming	$CH_4 + H_2O \rightleftarrows CO + 3H_2$	206
7.	Bouduard reaction	$C + CO_2 \rightleftarrows 2CO$	160
8	Water gas reaction	$C + H_2O \rightleftarrows H_2 + CO$	118

The principal gasification reactions are fuel devolatilization, methane reforming, Bouduard, and water-gas reactions (r_1 and $r_{6\text{-}8}$ in Table 2.3). These are all endothermic and therefore favoured at high

temperatures and low pressures. In particular, the Bouduard and water gas, although favourable, are characterized by a very slow reaction kinetics in the absence of a catalyst. The water-gas shift reaction r_5 can potentially play a crucial role in the performance of the gasification process, being important for enhanced production of H_2. Optimum yield is obtained at low temperatures (up to 300 °C) in the presence of a catalyst and pressure does not affect increasing hydrogen yield. The overall conversion process may be considered a simplified two-step process. The distinction between primary and secondary conversion is based on the different times of conversion of the various processes. Experimental studies have shown that as a result of the rapid heating of the fuel, 90% of devolatilization takes place in a matter of milliseconds, whereas the remainder of gasification processes (mainly heterogeneous reactions) take one or two orders of magnitude longer time [24]. In this sense, char gasification is the most critical of all reactions. Though char from biomass usually constitutes a minor fraction of the fuel, its conversion kinetics has a major effect on the performance of a gasifier, for it is the slowest of conversion processes. When pyrolysis takes place in the presence of steam and oxygen, the O_2 is involved preferably in the combustion of the light volatiles, leaving steam and char [61].

2.2.2.1 Chemistry of tar conversion

Tar is a complex mixture of several different chemical substances. The definition of tars has evolved through the years, upon reaching a consensus with the European Committee for Standardization (CEN) establishing a standardized definition: tars refer to all organic compounds in gasification product gas with molecular masses exceeding that of benzene [67].

During the devolatilization, tar is typically produced as one of the primary components, and it is then involved in through multiple reaction pathways undergoing substantial transformation. Figure 2.5 shows the temperature progression driving tar species evolution produced from waste materials, transitioning from initial products to phenolic structures and ultimately to aromatic hydrocarbons. Tar yield initially increases with temperature, reaching a characteristic peak within the 500-600°C range, after which secondary decomposition reactions in the freeboard lead to decreasing yields. This peak temperature, which varies according to feedstock composition, typically corresponds to the devolatilization stage in thermochemical processes. In operations below 800°C, the predominant tar constituents exceeding 5% commonly include toluene, naphthalene, and phenol.

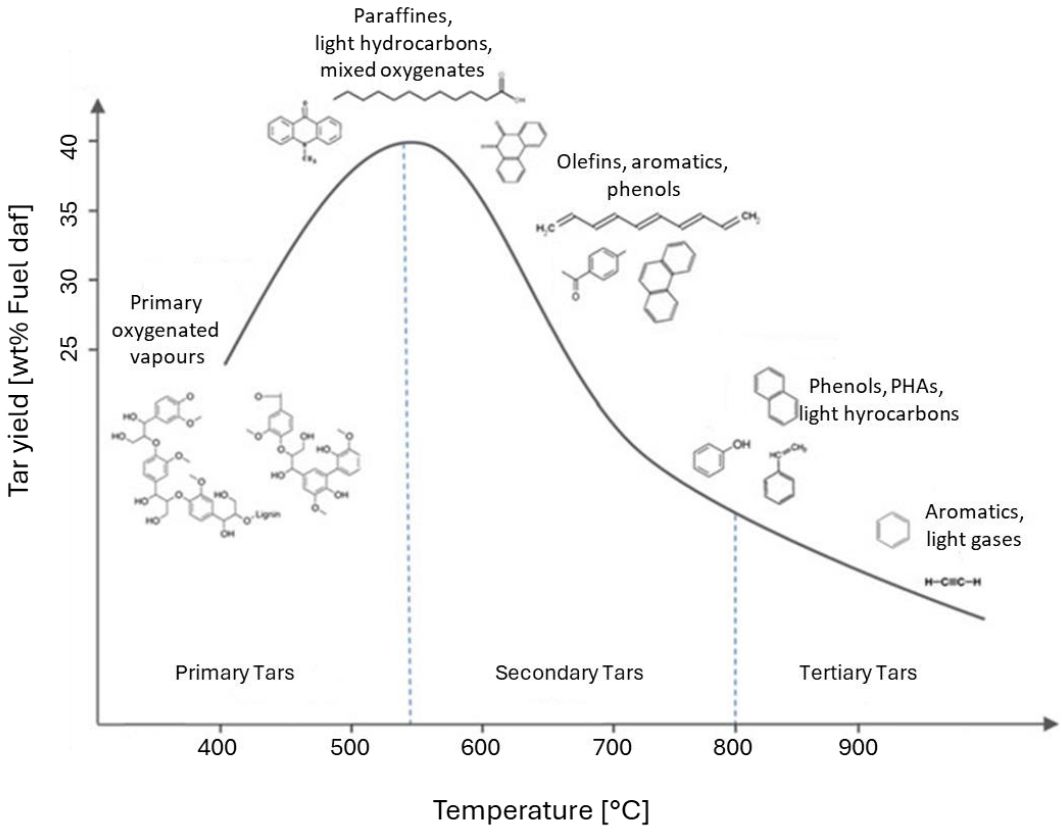

Figure 2.5 – Tar yield in a generic gasification process as a function of the operating temperature. Adapted from [68]

A common classification of tars relies on tars formation in the gasifier [69]:

- Primary tar, characterized by cellulose-, hemicellulose-, plastic- and lignin-derived products.
- Secondary tars, characterized by phenolics and olefins, are products of the conversion of primary tars.
- Tertiary tars, including alkyl and methyl derivates of aromatics and sulphur-containing species
- Condensed tertiary tars, composed of polyaromatic hydrocarbons and polyhydroxyalkanoates (PHAs).

The amount and composition of tar produced are strongly dependent on the feedstock used, reactor design and operating conditions, making tars one of the major challenges in the modelling and design of gasifiers.

2.2.2.2 Note on reactions involving tars

After primary decomposition, a variety of homogeneous and heterogeneous reactions can take place. This is particularly true for tar compounds, which undergo multiple transformations following their initial formation. These transformations can arise from interactions with both gas solid phases. An overview of the main reactions involving tar species are reported in Table 2.4. The reactions include

oxidation (r_9), steam and dry reforming reactions (r_{10} and r_{11}) that convert tars into lighter gases, and thermal cracking (r_{13}) that breaks complex molecules into simpler compounds. Additional reactions encompass dealkylation removing alkyl groups from aromatic structures, deoxygenation eliminating oxygen-containing functional groups, aromatization forming stable ring structures, and polymerization reactions leading to soot formation.

Primary and secondary tar conversion processes take place both within and outside the fuel particles. Solid materials in the bed, such as dolomite and olivine, can catalyse tar conversion reactions. Char and ash particles can exhibit a catalytic effect as well. However, the typically short residence times of volatiles in the bed often limits the extent of catalytic conversion.

The complexity of secondary tar reactions creates significant challenges for prediction and modelling. These reactions produce diverse heavy compounds with non-uniform distribution patterns, reflecting the intricate network of possible reaction pathways.

Table 2.4 – Main reactions involving tar species (assumed as $C_xH_yO_z$) in gasification processes.

r_j	Reaction name	Reaction	Enthalpy of reaction $\left[\frac{\text{kJ}}{\text{mol}}\right]$
9.	Partial oxidation	$C_xH_yO_z + \frac{1}{2}(x-z)O_2 \rightarrow xCO + \frac{y}{2}H_2$	Highly endothermic +(200 to 400)
10.	Dry reforming	$C_xH_yO_z + (x-z)CO_2 \rightarrow (2x-z)CO + \frac{y}{2}H_2$	
11.	Steam reforming	$C_xH_yO_z + (x-z)H_2O \rightarrow \left(\frac{y}{2} + x - z\right)H_2 + xCO$	
12.	Hydrogenation	$C_xH_yO_z + \left(z + 2x - \frac{y}{2}\right)H_2 \rightarrow CH_4 + H_2O$	
13.	Thermal cracking	$C_xH_yO_z \rightarrow \frac{y}{4}CH_4 + zCO + \left(x - z - \frac{y}{4}\right)C$	

2.2.3 Gasification agents

Gasification processes employ various gasifying agents, including air, pure oxygen, steam, carbon dioxide, nitrogen, or their combinations [70–72]. The choice of gasifying agent significantly influences the product gas composition and its calorific value. Air gasification, while offering operational simplicity and independence from complex industrial infrastructure [73], produces syngas with relatively low heating value (4-7 MJ/Nm^3) due to nitrogen dilution [74].

Oxygen and steam gasification generate medium-heating-value gas (10-18 MJ/Nm^3), offering improved gas quality compared to air gasification [43,61]. However, pure oxygen gasification faces economic constraints due to high production costs, limiting its commercial viability. Steam gasification emerges as a more economical alternative while offering enhanced hydrogen yields [75]. This increased hydrogen production stems from steam participation in reforming and water-gas shift reactions [40], making it particularly attractive for hydrogen-focused applications.

The effectiveness of conventional gasification processes depends significantly on feedstock moisture content, with optimal operation typically requiring moisture levels below 10-15% [76]. Process efficiency decreases markedly as moisture content rises [77]. For biomass feedstocks with extremely high moisture content (90-95%), supercritical water gasification has emerged as a promising alternative for hydrogen production, effectively utilizing the feedstock's water content in the conversion process [75]. The technical and safety challenges related to such operating conditions hinder the large-scale development of the technology.

Studies from fixed bed gasification highlight how steam gasification generates syngas with maximized hydrogen content, alongside substantial CO and CO_2 concentrations (Figure 2.6) [21]. In contrast, air gasification yields higher CO concentrations but reduced H_2 and CO_2 levels compared to steam-based processes.

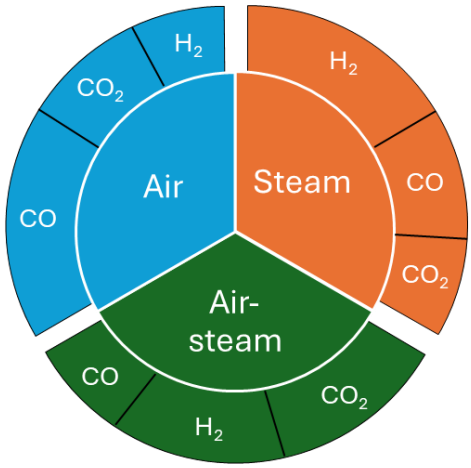

Figure 2.6 – Effect of gasification agent on the syngas composition [21].

Gil et al. [75] collected experimental results of lab-scale fluidized bed gasifiers and compared different gasifying agents (air, pure steam, and steam-O_2 mixtures), inferring the superior performance of steam gasification in hydrogen production. However, the results show large variability and uncertainty, especially when considering the scale-up to larger facilities. These findings highlight how gasifying agent selection can be optimized based on specific process objectives, whether prioritizing operational simplicity, hydrogen yield, or overall gas quality.

However, the choice of gasifying agent influences not only product distribution but also tar formation in char and syngas quality. This should be assessed together with other crucial operating parameters, such as the Equivalence ratio (ER). A description of relevant operating and performance parameters can be found in Section 3.10.

2.3 Overview on Fluidized Beds Hydrodynamics

Fluidization occurs when solid particles achieve fluid-like behaviour through suspension in a gas or liquid medium. [78]. This phenomenon takes place when the upward gas flow through a particle bed generates sufficient drag force to counterbalance the gravitational force acting on the particles. At this point, the bed reaches minimum fluidization, characterized by a specific upward gas velocity known as the minimum fluidization velocity (u_{mf}). Beyond u_{mf}, depending on particle characteristics, gas bubbles may form and rise through the bed, promoting the mixing of the dense phase. This bubbling behaviour resembles a boiling liquid, leading to what is called the bubbling fluidization regime. An overview of fluidization regimes is reported in Figure 2.7.

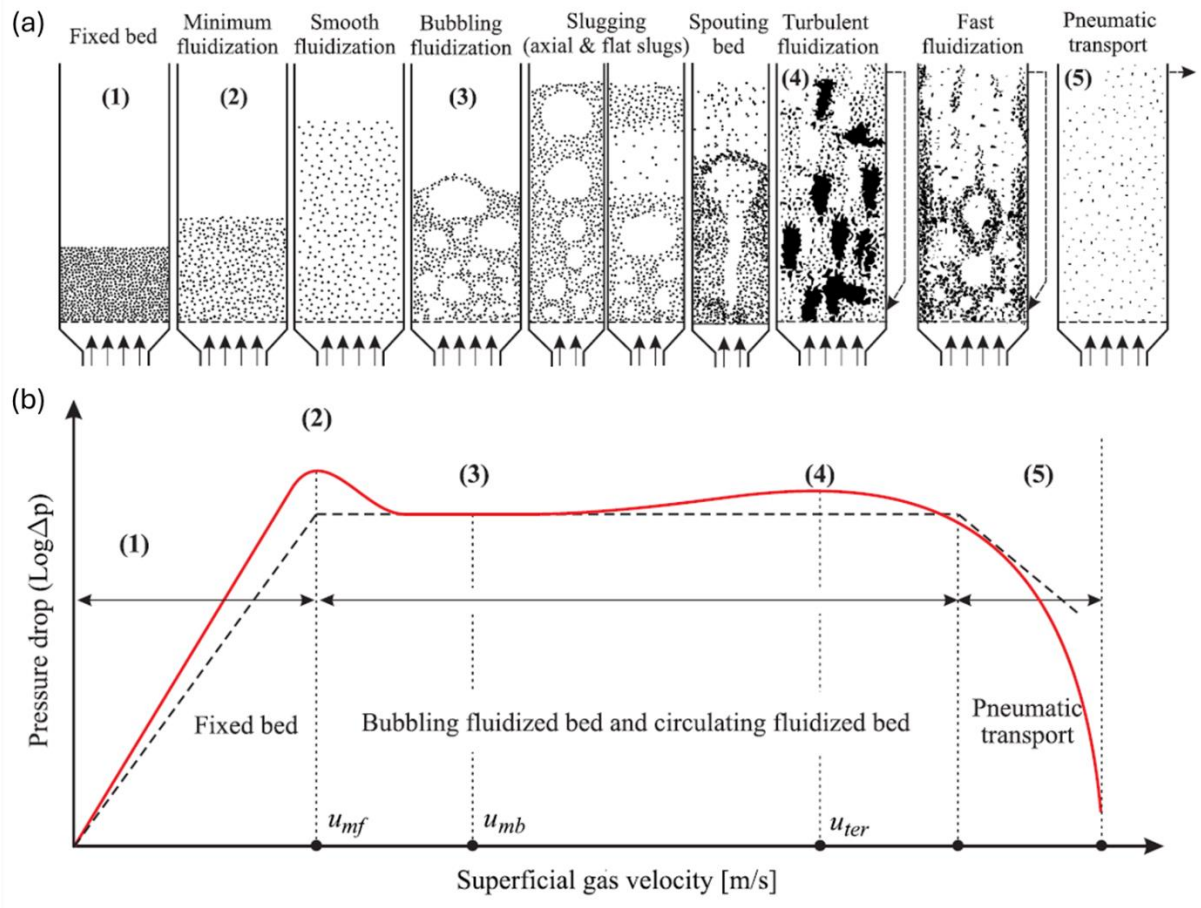

Figure 2.7 – Qualitative representation of (a) fluidization regimes and (b) pressure drop versus superficial fluidization velocity. Adapted from [79]. u_{mf}: minimum fluidization velocity, u_{mb}: minimum bubbling velocity, u_{ter}: terminal fall velocity.

The bubbles in the bed undergo coalescence while moving upward and laterally, creating vigorous particle mixing. This intense agitation makes fluidized beds particularly effective for processes requiring high rates of heat and mass transfer, such as combustion and gasification. In these applications, the bed particles are first heated above the fuel ignition temperature. Once fuel enters the system, it interacts with these hot fluidized particles, initiating combustion or gasification

reactions. During continuous operation, the bed temperature reaches equilibrium through a balance between heat generation from char combustion within the bed and heat removal through both the exit of volatile gases and endothermic gas-phase reactions.

The understanding of the hydrodynamics of a fluidized bed is of prime interest, as it helps characterize not only the fluid dynamic properties of the bed inventory but also the behaviour feedstocks behave in these systems. The intimate interaction between bed and fuel particles is ultimately responsible for the stability and efficiency of the gasifier.

2.3.1 Solids mixing and segregation in fluidized beds

Research has focused on understanding axial mixing and segregation patterns when biomass is introduced into fluidized beds [80]. Studies of cotton stalk-quartz sand mixtures in a three-dimensional bubbling bed, with biomass mass fractions between 1% and 3%, revealed distinct segregation behaviour. [81]. At minimum fluidization conditions, biomass particles accumulate at the bed surface due to buoyancy effects. This stratification becomes more pronounced as fluidization velocity increases, driven by the upward movement of bubbles.

The mixing and segregation patterns for cylinders (length of 4.5 cm, diameter of 1.1 cm) with different values of density ρ_{cyl} are shown in Figure 2.8.

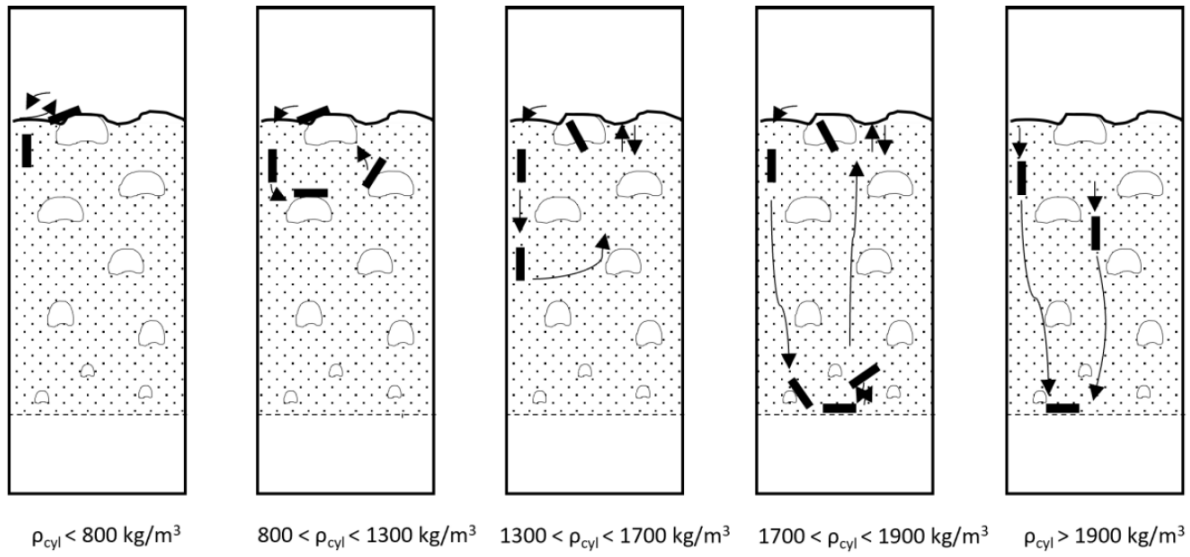

Figure 2.8 – Movement of a cylindrical isolated body of different densities in a fluidized bed. Bulk density of the bed $\rho_b = 1490\ kg\ m^{-3}$. Adapted from [78].

The segregation mechanisms during feedstock devolatilization differ significantly from those observed in non-reactive systems. The formation of volatile bubbles surrounding devolatilizing coal particles was first documented through experimental observations [82]. This led to the development of a theoretical framework suggesting these volatile bubbles function as lifting mechanisms, lifting

feedstock particles toward the bed surface [83]. Further experimental work demonstrated that particles under reactive conditions exhibit substantially higher rise velocities compared to inert conditions [84]. Iannello et al. [59,60,85,86] extensively studied the segregation behaviour of different reacting particles in fluidized beds in a wide range of operating conditions (e.g., temperature, fluidization velocity, fluidizing gas). This enhanced vertical movement can create a stratified conversion pattern where volatile matter predominantly bypasses the bed material and releases directly into the freeboard region [58,87]. Such behaviour presents a significant operational challenge in bubbling fluidized bed systems processing feedstocks with high volatile content.

Fluidized bed gasifiers are usually operated at bubbling or turbulent conditions, promoting further the segregation of lighter reacting particles. Therefore, a certain degree of feedstock segregation to the surface cannot be avoided. This makes information regarding solids mixing behaviour instrumental for the design of fluidized beds gasifier, and the region across the surface of the bed, also called splashing zone, a very sensitive section of the reactor. The effective exploitation of the features and strengths of fluidized bed thermochemical converters depends on volatile matter release patterns and gas phase mixing and segregation [58].

2.3.2 Gas mixing induced in the Splashing Zone

Gas mixing in the splashing zone of gas-fluidized bed reactors plays an important role in fluidized bed processes where fast homogeneous gas phase reactions take place. This has been thoroughly investigated in the literature, particularly in the case of fluidized bed combustion of high-volatile solid fuels. [58,88]. Nonetheless, the same considerations can be extended to gasification processes where, despite the use of sub-stoichiometric quantities of oxygen, the large contribution to overall heat balance is due to the homogeneous combustion of volatile matter.

As a result of the extensive particle segregation and gas bypass with respect to the bed, the homogeneous reactions are often deferred until the splashing region or upper freeboard, increasing the risk of hotspots and uneven reactions. Gas mixing in the splash zone of the fluidized bed becomes the rate-controlling process in most of the practical applications of thermochemical conversion of highly volatile solid fuels when fast gas-phase chemical reactions take place under non-premixed conditions [60,89].

The dynamics of bubble eruption and the flow structures developing in the splash zone determine the gas mixing in the region above the bed, transitioning to a plug-flow behaviour for the rest of the freeboard. Two models have been proposed in the literature to describe the flow structures generated by bubbles bursting at the bed surface. The “Pulsed Jet” theory assumes that the erupting gas bubbles behave like intermittent jets, and the decay of gas velocity along the jet centreline described as free

shear layers [90]. The "Ghost Bubbles" theory assumes that the structure and the internal flow pattern of bubbles in the bed are retained in the freeboard upon bursting, with the ghost bubbles undergoing volume growth by entrainment of the nearby gas. If internal circulation is laminar, the ghost bubble behaves like a vortex ring, otherwise a puff is established. In either case, the bubble progressively slows down after bursting as it entrains the slower surrounding fluid [91].

Later experimental studies investigating the hydrodynamics of isolated bubble bursts show departures from both models. Solimene et al [92] performed a comprehensive characterization of hydrodynamics and gas mixing in the splash zone of a fluidized bed, with a combination of non-intrusive optical diagnostic techniques, namely planar laser light scattering (PLLS) and planar laser induced fluorescence (PLIF).

An example of the sequence of frames showing the flow structures and gas-mixing induced by the bubble bursting in the splashing zone is reported in Figure 2.9.

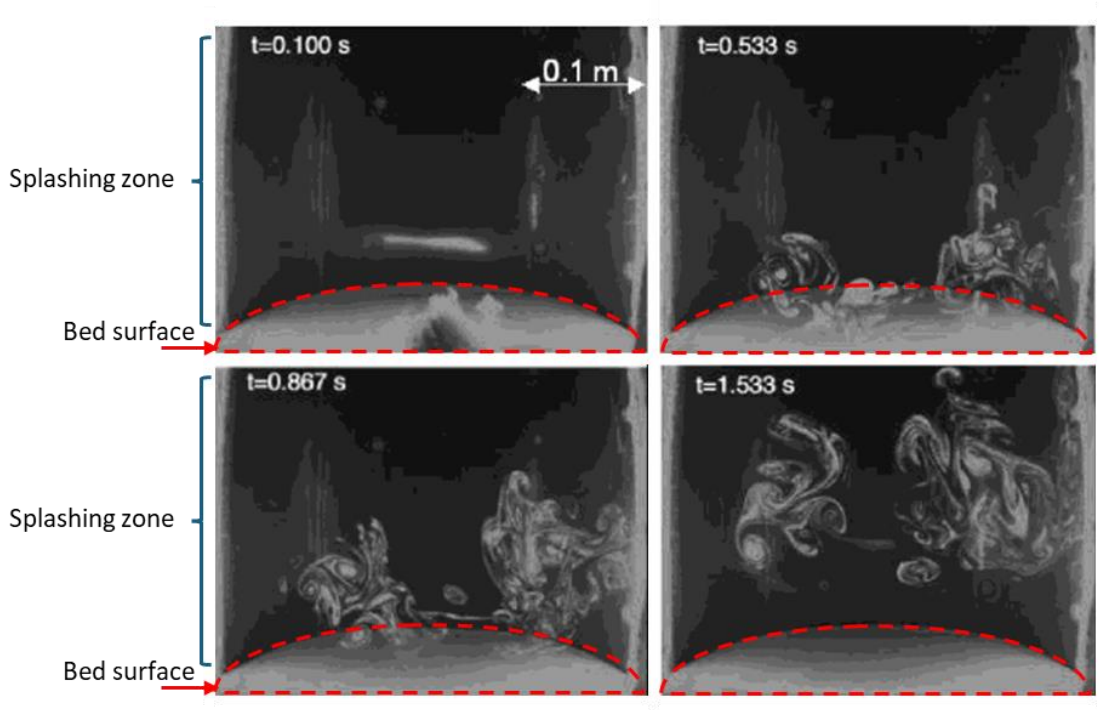

Figure 2.9 – Sequence of frames recorded after injection of two closely time-delayed bubbles into the fluidized bed. Adapted from [92].

They found that the basic flow structure associated with bubble eruption consists of a toroidal downward-rotating vortex ring, induced by ejection and fallback of bed solids. Toroidal vortex rings rise along the splash zone at a relatively steady velocity and the toroidal pocket increases almost linearly with time at a fairly constant rate [88].

The flow structures generated by bubble bursting do not conform to the nearly-spherical structure of the ghost bubbles with internal toroidal circulation. Nonetheless, the ghost bubble theory, unlike

the pulsed jet model, captures the important feature of the enlargement of the flow structures due to gas entrainment from the mainstream which is observed in the experiments [93].

2.4 Modelling Approaches for Fluidized Bed Gasification

The conversion of waste to hydrogen through gasification encompasses multiple research areas, including process technologies, operating parameters, reactor configurations, separation and purification systems, and feedstock characteristics. Additionally, the optimization of gasifier design and operation requires a comprehensive analysis of system behaviour across various operating conditions. While large-scale experimental studies present significant challenges related to safety, practicality and costs, mathematical models can effectively represent the physical and chemical phenomena within gasifiers, enabling system optimization with reduced time and financial investment [94]. Nonetheless, the inherent complexity of gasification processes makes mathematical modelling for performance prediction a challenging endeavour.

Model validation requires thorough comparison against real data from systems of relevant scale, to verify accuracy beyond simple comparisons with syngas composition or other modelling approaches [43,66]. Although the overall system efficiency and practical viability of hydrogen production depend significantly on downstream processes, current modelling efforts in literature concentrate primarily on the gasification unit operation, this stage being the main bottleneck of the successful deployment of such process [76].

Comprehensive modelling of fuel conversion in fluidized beds is based on a detailed description of gas-solid interactions within the reactor. This includes applying the conservation balances of mass, species, heat, and momentum for all species and phases involved, along with appropriate source and sink terms, boundary conditions, and phase-specific constitutive relationships.

The literature presents several modelling approaches, which can be categorised into three main groups based on fluid-dynamics simplification methods according to the classification proposed by Gómez-Barea and Leckner [61]. Table 2.5 provides an overview of the features of the three groups of models, together with the main advantages and disadvantages. The three categories of models are sorted as follows:

1. Computational Fluid-Dynamics Models (CFDM): These models solve all conservation equations while incorporating specific assumptions about phase interactions. The development of advanced Computational Fluid-Dynamics (CFD) approaches has grown exponentially in the last decade, supported by the fast technological advancement of computers and novel software.

2. Fluidization Models (FM): This approach describes the bed as a combination of multiple phases or regions with predetermined topology. This enables solving mass and heat balance equations, with advanced approaches considering also the transport between zones. Instead of solving momentum equations directly, these models utilize semi-empirical correlations to characterize bubble and particle dynamics, providing suitable framework for chemical reactor modelling.
3. Black-Box Models (BBM): These models implement overall system balances, incorporating either equilibrium assumptions or empirical relationships. The most novel and promising approach is the application of Machine Learning techniques to predict the performance of the gasifier, with a notable example represented by physics-informed neural networks.

Table 2.5 – Main modelling approaches for fluidized bed gasifiers. Adapted from [61].

Type	Concept	Potential results	Advantages	Disadvantages
CFD	- Mass and energy balances - Momentum equations solved - Constitutive and closure laws adopted	- Detailed prediction of bed fluid dynamic - 2D and 3D modelling - Uncertain accuracy of prediction of process performance	- Useful for exploring reactor design and fluid dynamic	- Time consuming solution - Uncertainty with respect to design parameters and closure relations
FM	- Usually 1D modelling, following the two-phase theory: emulsion and bubble phase - Momentum balance not required - Semi-empirical correlation used for gas and solids flow patterns	- Temperature and concentration profiles - Useful insights in fluidized bed design, although less detailed than CFDM.	- Compromise between precision and numerical complexities - Fast and easy to operate, useful for engineering and design application.	- Flow structures is assumed, accuracy limited by semi-empirical correlations - Limited by the range of validity of the correlations implemented
BBM	- Overall mass and energy balance - Only global models - Often thermodynamic equilibrium assumed for reaction	- Amount of produced gas and heating value - Syngas composition with lower accuracy for heavier species	- Very easy to use and limited number of inputs required (Equilibrium-based models) - Accuracy and reliability (Neural networks)	- Lacking proper description of the fluid dynamic and reactor behaviour - Extensive experimental data required for model training and testing (Neural networks)

FM currently represents the most developed approach for fluidized bed gasifiers (FBGs), building upon five decades of theoretical advancement and experimental validation. While CFDM shows promise, significant development remains necessary to overcome the limitations related to computational complexity. BBM offers practical utility in specific applications but demonstrates limited predictive capability compared to FM and CFDM. The substantial solving times requirements of CFD simulations, particularly when incorporating chemical reactions, maintain FM as the predominant modelling approach. For these reasons, the focus of this review will be mainly on the development of FMs.

2.4.1 Computational fluid-dynamic models

The two-fluid model has been widely applied to fluidized-bed systems in different engineering sectors. However, there are still relatively less models of this type compared to the many models of other classes [61]. Alobaid et al. [79] report that most of the studies developing CFD models are found in the field of thermochemical processes (pyrolysis/gasification, and combustion) and CO_2 capture. However, the largest part of modelling efforts in CFD has been focused in the field of non-reactive simulations, with over 800 studies reported in the literature [79]. Most of them investigate gas-solid interaction (drag modelling) or hydrodynamics or deal with mathematical aspects of the two-fluid model.

The fundamental distinction between (CFDM and alternative modelling approaches lies in their detailed treatment of fluid mechanics, though source terms remain similar across all models. CFDM solves momentum equations for both gas and solid phases. The gas phase analysis employs a continuum approach within a Eulerian framework, comparable to single-phase flow modelling but incorporating additional terms to account for solid-phase interactions. The selection of an appropriate turbulence model for the gas phase represents a critical modelling decision.

The solid phase characterization in CFDM follows two distinct methodologies. The first treats the solid phase as a continuum using a Eulerian framework [95]. The second tracks individual particles through their equations of motion. These approaches are designated as Eulerian-Eulerian Models (EEM) and Eulerian-Lagrangian Models (ELM), respectively.

Conversion of various biofuels in bubbling FBG (BFBG) has been simulated by CFD tools: beech and pine wood [96], sewage sludge [97], eucalyptus and miscanthus [98,99] and coffee husks [100]. In all cases, despite the reasonably good agreement with experimental data, the validation has been carried out in lab-scale fluidized bed setup. Notable examples of successful model development have been produced by Couto et al. [101–106]. The authors first presented experimental and numerical results for the gasification of coffee husk biomass, with the two-dimensional CFD model developed in ANSYS-

FLUENT showing good agreement with measured outlet gas compositions with an approximately 20 % error [104,106]. However, the CFD model did not show good predictive capabilities and sensitivity towards heavy hydrocarbons, lacking tar production as well as detailed devolatilization reactions [105]. To model municipal solid waste (MSW) gasification, Couto et al. [101–103] applied the same previous CFD model with an improved pyrolysis model, taking into account secondary tar production [107]. Good agreement was achieved for most process conditions. However, some gas components, especially hydrocarbons (CH_4 and C_2H_4), deviate up to 40 %.

Overall, CFDMs presented in the literature do not demonstrate better process performance prediction capabilities compared to FMs. Although CFDM achieves high accuracy in representing the reactor fluid dynamics, the associated intensive computational requirements and extended processing times do not justify the selection of this kind of model over FMs.

2.4.2 Black box models

This set of models is called BMM because the process inside the reactors is not resolved in detail. BMMs instead address reactor processes through overall mass, species, and heat balances across the entire gasification unit, supplemented by assumptions about material distribution within the gasifier. The complexity and underlying assumptions of BBM vary significantly based on their intended purpose, ranging from basic performance prediction through mass and heat balances to detailed gas and solid composition analysis. BBM encompasses several modelling approaches, two of the most relevant ones are analyzed more in depth below. The classification of these models often presents challenges, as many implementations combine multiple approaches to achieve their objectives.

2.4.2.1 BMM – Equilibrium

Equilibrium Models (EM) operate on the principle that outlet streams achieve equilibrium conditions, where the system reaches its most stable composition through the minimization of Gibbs free energy. The equilibrium modelling approach can follow either stoichiometric or non-stoichiometric formulations. Stoichiometric approaches require the specification of complete reaction mechanisms, including all relevant chemical reactions and species. In contrast, non-stoichiometric formulations do not require defined reaction mechanisms but need preliminary specification of potential outlet gas species. EM requires only the elemental composition of fuel as input data, which is obtained through ultimate analysis [38,108].

Non-stoichiometric formulations have demonstrated utility in biomass gasification system simulation, accounting for various gaseous components and solid species, including carbon and inorganic matter from biomass ash [108]. Most biomass gasification EM focus on predicting outlet stream composition for primary gaseous components: CO, CO_2, H_2, H_2O, CH_4, N_2, and solid carbon in

graphite form, along with process temperature and heating value [109]. The model can either calculate bed temperature through heat loss estimation or use an imposed temperature value. Several examples of successful equilibrium modelling are available in the literature [108,110–114]. However, the relevance of these is either surpassed by FM and CFDM approaches or subdued to the assessment of larger plants.

Equilibrium simulations of fluidized bed gasification indicate negligible oxygen content, minimal solid carbon above approximately 800°C, and absence of tar regardless of the representative compound selected [103,382]. While experimental measurements confirm the absence of oxygen in fluidized bed biomass gasification, observed tar and char concentrations deviate significantly from equilibrium predictions. Comparative analysis of equilibrium and kinetic predictions [206] reveals that steam reforming of methane and water gas shift operates far from equilibrium under typical gasification conditions, indicating substantial kinetic limitations.

2.4.2.2 BBM – Neural networks

Artificial neural networks represent a mathematical modelling approach that utilizes regression to establish correlations between process input and output streams. This method requires extensive experimental data for implementation. While neural networks have gained prominence across various fields, their application to renewable energy system modelling and prediction has emerged more recently [115]. This approach requires a less detailed understanding of system phenomena compared to equilibrium and kinetic modelling methods. Neural network modelling has demonstrated improved accuracy in predicting gasification product gas composition [116]. However, the development of these models requires comprehensive experimental datasets, which are often scarce in biomass gasification literature. This data limitation explains the relatively small number of published neural network models in this field. Guo et al. [117] demonstrated the practical implementation and effectiveness of artificial neural networks in biomass gasification process simulation. A recent and notable example of the potential of this type of modelling approach has been proposed by van Wyk [118]. The author developed a physics-informed machine learning model for predicting the outputs of gasification. A dataset was compiled from experimental data of a lab-scale reactor, encompassing a wide range of feedstock characteristics (biomass to plastics) and process conditions, which served as input for the model. The results showed very good predictive accuracy (RMSE of 2.7 and R^2 0.95), with an optimum physics contribution of 30% (70% data contribution) to improve carbon closure [118]. Although still at an early stage of development, limited by the extensive data requirement at the relevant scale, this represents a promising first step towards improving data-driven ML models for application to thermochemical systems.

2.4.3 Fluidization models

FM represent the predominant approach in comprehensive fluidized bed gasifier modelling [61]. FM achieves an effective balance between BBM and CFDM by simplifying complex gas-solid dynamics while retaining the overall fluid-dynamic, capturing the multiphase pattern in the bed. This approach divides the bed into two phases and makes use of semi-empirical correlations to represent the predetermined characteristics of each phase. One-dimensional models are the most common among FMs. A schematic representation of bubbling fluidized bed and the two-phase theory is shown in Figure 2.10.

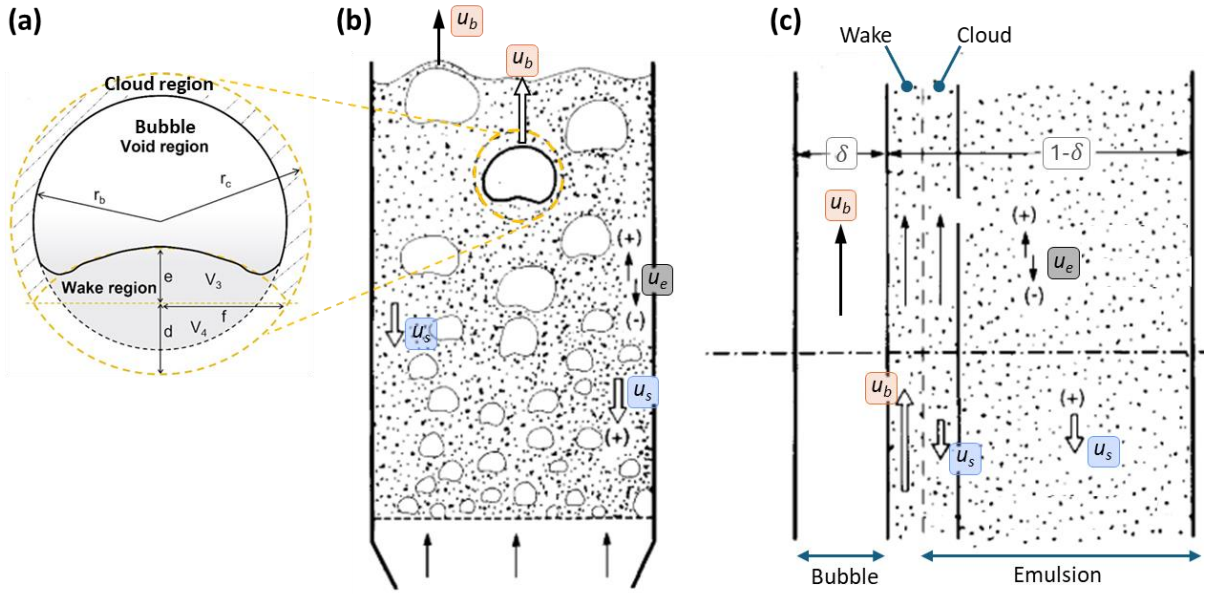

Figure 2.10 – Schematic representation of (a) regions of the bubble, (b) bubbling fluidized bed, and (c) two phase theory. u_b is the bubble rise velocity, u_e the velocity of the emulsion phase, u_s the solids downward velocity, δ the fraction of the bed occupied by bubbles. Adapted from [78,119].

Initial modelling attempts treated fluidized bed reactors as systems with uniformly mixed gas and solids, disregarding the multiphase nature of the bed. These simplified approaches proved inadequate for accurate predictions and reactor design optimization [61]. Recognition of these limitations led to the development of multiphase descriptions, which better captured the effective contact time between phases in fluidized beds. The following models adopted the elegant two-phase theory of fluidization [120] for a more realistic description of the bed. Two-phase reactor models are characterized by emulsion and bubble phases. The original FM assumes the emulsion phase as containing all solid particles and a fraction of the gas in perfect mixing conditions, while the bubble phase consists of gas in plug-flow. Rather than solving momentum balances explicitly, these models utilize Davidson's approach [121] to calculate the bubble rise velocity, along with other semi-empirical correlations and additional assumptions to determine key parameters. This entails determining gas

flow distribution between phases, bubble fraction in the bed, emulsion phase voidage and velocity (several of these correlations have been used to develop this work and presented in Table 3.7).

Over recent decades, researchers have introduced various modifications and simplifications to FM for application across different reaction systems. The evolution of FM for simulating fluidized bed processes has led to numerous adaptations tailored to specific reaction conditions and operational requirements. Information regarding reactors and processes modelled in literature is reported in Table 2.6. A comprehensive description of the FM available in the literature and developed for gasification in fluidized beds is provided in Table 2.7.

Table 2.6 – Summary of reactor type and operations modelled in the FMs available in literature. BFB: bubbling fluidized bed. FB: fluidized bed. CFB: circulating fluidized beds. DCFB: dual circulating fluidized bed, EF: entrained flow.

Authors	**Reactor type**	**Fuel type**	**Gasification agent**
Nikoo [122]	BFB – lab scale D_{bed} 4 cm, H 140 cm	Pine sawdust	Air and steam
Radmanesh et al. [123]	BFB – Lab scale D_{bed} 7.8 cm, H 165 cm	Beech wood	Air
Sadaka et al. [124–127]	BFB	Wheat straw	Air and steam
Fiaschi and Michelini et al. [128]	FB – Lab scale, with dual distributor plate D_{bed} 15 cm, H 50 cm	Wood chips, Almond shell, Gass straw, Corn stalk	Air enriched
Bilodeau et al. [129]	FB – small pilot scale D_{bed} 30 cm, H 290 cm	Wood and a mixture of wood and plastic	Air
Jiang and Morey [130]	FB – Large lab scale D_{bed} 16 cm, H 136 cm	Corncob	Air
van den Aarsen [131]	BFB Dbed 30 cm	Beech wood	Air
Raman et al. [132]	BFB – large lab scale D_{bed} 23 cm, H 173 cm	Feedlot manure	Air
Corella and Sanz [133,134]	CFB – from pilot to commercial scale: $D_{bed,c}$ 330 cm, H_c 1480 cm	Pine wood chips	Air
Petersen and Werther [71,135]	CFB – pilot scale D_{bed} 10 cm,H 1500 cm	Pelletised dried sewage sludge	Air
Panopoulus et al [136]	FB	Olive kernel residue	Air, air and steam, steam only
Nguyen et al. [137]	DCFB	Biomass	Steam and air
Adeyemi et al. [138]	EF – lab scale D_{bed} 6.6 cm, H 154 cm	Kentucky coal and wood waste	Air
Kaushal et al. [139]	BFB – small pilot scale D_{bed} 15 cm, H 215 cm	Various biomasses	Air, oxygen, steam or a mix
Eikeland et al. [140]	BFB	Wood chips	Steam
Agu et al. [141]	BFB- lab scale D_{bed} 28 cm, H 127 cm	Sawdust	Air, and steam
Sebastiani et al. [65]	BFB- pilot scale D_{bed} 25 cm, H 410 cm	RDF	Steam-oxygen
Pitkäoja and Ritvanen [142]	CFB- pilot scale D_{bed} 15 cm, H 900 cm	Biomass	Steam-oxygen and air

Table 2.7 – Collection of FMs of gasification from literature. LM: Learning model, DM: design model, SS: Steady state, US: unsteady state TM: Transient model, 2PT:2-phase theory, PC: Particle conversion.

Authors	**Type of reactor model**	**Fluidized bed model**	**Freeboard model**	**Energy balance**	**Devolatilization model**	**Char conversion and elutriation**	**Gas-phase reaction kinetics**	**Tar model**	**Validation**
Nikoo [122]	LM, SS 1D	Based on modified 2PT	Yes – assumed perfect mixing Char conversion reactions only	No – Temperature imposed	Instantaneous and equilibrium	Reactivity from coal No fragmentation	Equilibrium assumed for reactions	No	Outlet gas composition and temperature from literature Reasonable/poor predictions agreement. No Tar content
Radmanesh et al. [123]	LM, SS 1D	Based on modified 2PT [78]	No	No	Yes – from literature and own tests on particle level	CCBMM for char mixing No PC, no fragmentation	Some – oxidation of H_2, CO, CH_4 and tar	Yes – secondary tar cracking from literature	Outlet and profiles of gas composition and temperature from own experiments Reasonable predictions agreement. No Tar content
Sadaka et al. [124–127]	LM, SS 1D	3 zones modelled: jet, bubbling and slugging	No	Yes	Simplified – based on C, H and O balances of fuel composition	No	Equilibrium assumed for reactions	Empirical cracking model from literature	Outlet gas composition and temperature from literature Good predictions agreement. No Tar content
Fiaschi and Michelini et al. [128]	LM, SS 1D	Based on 2PT with reactions in emulsion phase	No	Simplified: overall bed only	Instantaneous	Yes – PCM from literature, elutriation considered	Not reported	No	Outlet gas composition from 3 literature sources. No Tar content
Bilodeau et al. [129]	LM, SS 1D	Based on semi-empirical literature model [143]	Yes – homogeneous plug flow	Yes – overall for compartments	Instantaneous and equilibriums	Kinetic model but not elutriation	Instantaneous volatiles oxidation	No	Outlet gas composition and temperature from own experiments

Table 2.7 – Continued.

Authors	Type of reactor model	Fluidized bed model	Freeboard model	Energy balance	Devolatilization model	Char conversion and elutriation	Gas-phase reaction kinetics	Tar model	Validation
Jiang and Morey [130]	LM, SS 1D	Based on literature model on extended 2PT [131]	Yes – with concentration of solids	Simplified – bed temperature fixed to determine freeboard temperature	Product distribution from own experiments	Shrinking core approach for char particles From literature [131]	Assumed equilibrium of water gas shift (WGS) to determine gas species concentrations	One lumped compound. From literature [131]	Outlet gas composition and freeboard temperature from own experiments Good agreement at high temperature, poor at low. No tar content
van den Aarsen [131]	LM, SS 1D	Extended 2PT with parameters validated by own experiments	No	No - T imposed and adjusted by air flowrate	Assumed confined area of the reactor where devolatilization takes place, depending on particle size. Product distribution determined by own experiments	Yes – Shrinking core model with kinetics and physical parameters with own experiments No elutriation	Simplified: assumed oxidation in the bottom bed and WGS equilibrium.	One lump compound determined experimentally	Outlet gas composition and tar content from own experiments. Good agreement of predictions.
Raman et al. [132]	LM, TM 2D	Based on modified 2PT, properties varying with reactor height	No	No	Assumed volatiles yields distribution and relative yield from thermogravimetric analysis (TGA)	Assumed reactivity of coal, no elutriation	Only WGS kinetics considered	No	Outlet gas composition from own experiments. Reasonable agreement
Corella and Sanz [133,134]	LM, SS 1D	Constant solids porosity assumed for the bed	Qualitative description of comminution but no modelling Constant solids concentration in freeboard in two zones	Yes – over 4 zones defined. Overall heat balance in each zone	Instantaneous, with product distribution form literature. Tar and char content as a function of temperature	No	Most of the representative reactions of the process (in Table 2.3) with some ad-hoc corrections	Two lumps reacting with O_2, steam and thermal cracking	Not validated

Table 2.7 – Continued.

Authors	Type of reactor model	Fluidized bed model	Freeboard model	Energy balance	Devolatilization model	Char conversion and elutriation	Gas-phase reaction kinetics	Tar model	Validation
Petersen and Werther [71,135]	DM, SS 1D/3D	Modified 2PT with parameters from own tests	Core-annulus with solids distribution, key parameters from own tests	No – Temperature imposed	Instantaneous. Product distribution from own measurements	No	Most of the reactions (in Table 2.3) from several sources	Benzene taken as tar representing species	Outlet gas composition from own experiments. Reasonable agreement No Tar content
Panopoulus et al [136]	LM, SS	Configuration with multiple reactors network	No	No	Instantaneous, determined from feedstock composition	No	Equilibrium approach	One lumped species	Not validated
Nguyen et al. [137]	DM, SS	Three-stage steady-state model depending on reactions	No	No - Temperature studied as a parameter	Simplified: from mass balance of feed composition and literature data	Assumed reactivity of char being all carbon. No elutriation	Only WGS, methane reforming reactions considered	No	Outlet gas composition from literature data. Reasonable agreement. No tar content
Adeyemi et al. [138]	LM, SS	Configuration with multiple reactors network	No	No	Assumed instantaneous, product distribution from literature	Kinetic approach for char gasification reactions. No elutriation	Stoichiometric approach for oxidation reactions	Benzene used as tar species	Outlet gas composition from own experiments. Poor agreement. No tar content
Kaushal et al. [139]	DM, SS 1D	Based on 2PT with literature correlations	Yes – homogeneous plug flow	Simplified – global energy balances	Yes – semi-kinetic approach with assumed pattern release	Yes – Shrinking core model No elutriation	Most of the reactions (in Table 2.3) from literature	One lumped primary tar, and a secondary inert tar	Outlet gas composition and temperature from literature Good agreement
Eikeland et al. [140]	DM, SS	Configuration with multiple reactors network, perfectly mixed reactor	No	No – Temperature imposed	Simplified – kinetics from literature and balance from feedstock composition	Assumed reactivity of char being all carbon. No elutriation	Most of the reactions (in Table 2.3) from literature	No	No – comparison with results from Computational Particle Fluid Dynamic (CPFD)

Table 2.7 – Continued.

Authors	Type of reactor model	Fluidized bed model	Freeboard model	Energy balance	Devolatilization model	Char conversion and elutriation	Gas-phase reaction kinetics	Tar model	Validation
Agu et al. [141]	DM, 1D US	Solids and gas momentum equations solved: Eulerian for gas flow and dispersed flow behaviour for particles. Empirical correlations for 2PT used	Yes	Yes – studied both isothermal and non-isothermal cases	Kinetic approach and product distribution derived from literature.	Assumed reactivity of char being all carbon. Limited elutriation	Water gas shift and methane reforming	One lumped tar species	Outlet gas composition from literature Good agreement. No tar content
Sebastiani et al. [65]	DM, SS 1D	Based on 2PT with literature correlations	Yes – homogeneous plug flow	Simplified – bed temperature fixed, freeboard profile solved	From own experiments in TGA	Simplified: assumed reactivity of char, fragmentation and elutriation from literature [144–146]	Most of the reactions (in Table 2.3) from several sources	Benzene, naphthalene and one lumped species, with relevant reaction kinetics	Outlet gas composition and freeboard temperature profile from own experiments. Good agreement Limited in tar content
Pitkäoja and Ritvanen [142]	DM, TM, 1.5D	Modified 2PT, including the core-annulus approach	Yes	Yes	Yes – form literature [147]	Assumed reactivity of char being all carbon.	Extensive reaction kinetic considered, including calcium looping	One lump and naphthalene	Outlet gas composition and freeboard temperature from literature. Very good agreement. Limited in tar content

2.4.3.1 Preliminary modelling study

A preliminary kinetic model was developed following the typical literature approach for FM, i.e. following the 2PT, to better identify any discrepancy and inconsistency between typical FM-based results and real-plant operations [65]. The model simulates the operation of a pilot-scale fluidized bed gasifier operating with steam-oxygen situated in Swindon (UK), described in Section 3.9.1. The feedstock used for reference testing was a standard UK RDF, which was also tested to determine the RDF primary decomposition product and kinetic. This was done through ad-hoc thermogravimetric analyses to verify the hypothesis of instantaneous devolatilization, and to determine the product distribution of devolatilization, identifying a limited number of key components (H_2, CO, CO_2, CH_4, H_2O, C_6H_6, $C_{10}H_8$) used as a starting for the following reaction pathway. The model divided the whole reactor into two regions: a lower section represented by the bubbling fluidized bed, and the homogeneous gas-phase freeboard above. To describe the fluid dynamics of the fluidized bed, the model followed the simple2PT, as described in Section 2.4.3, which assumes the emulsion phase to operate at isothermal conditions. Furthermore, the model assumed sharp separation between the bubbling bed and the freeboard, with the gas phases being perfectly mixed at the boundary of the two regions (i.e. when entering the freeboard). A more extensive description of the model and the work can be found elsewhere [65]. Figure 2.11 shows a fairly good agreement between the predicted gas composition and the experimental value.

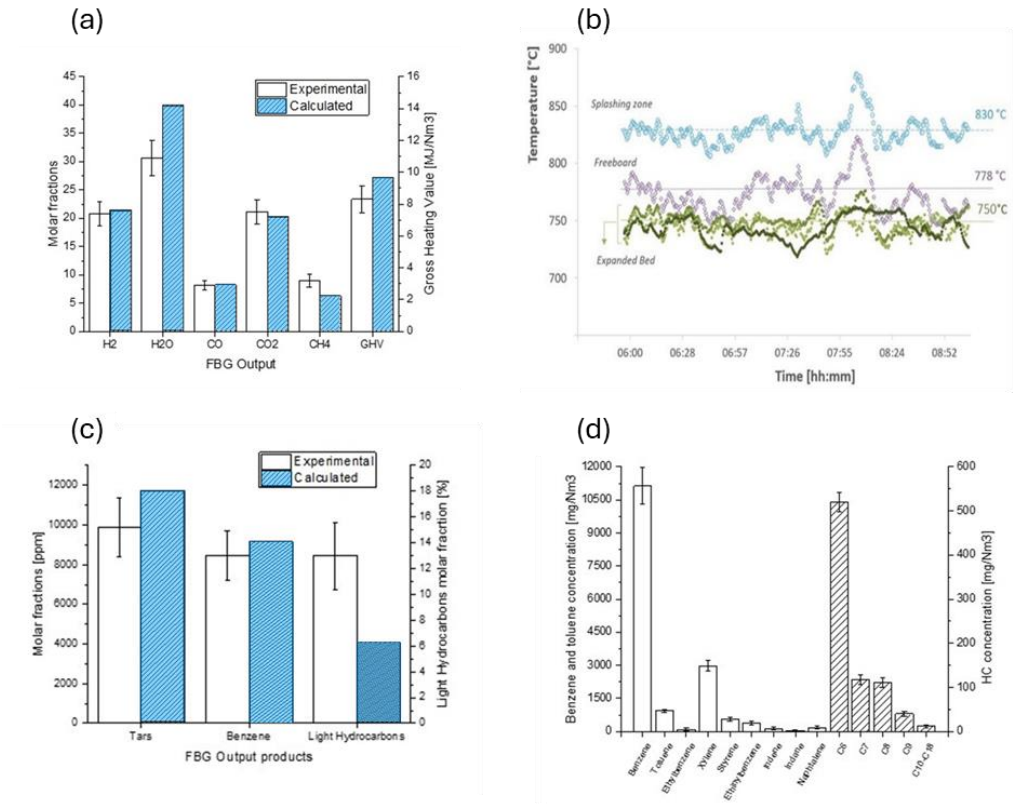

Figure 2.11 – Preliminary model results for (a) outlet syngas composition and (b) temperature profile, (c) hydrocarbon species and (d) experimental tars distribution.

Overall, the model proved to be reliable in the estimation of the output of the gasifier, with the most relevant deviation being related to steam and methane molar fractions (10% and 3% respectively). Despite the reasonable prediction of the total amount of hydrocarbons (Figure 2.11 (c)), the model overestimates the content of light hydrocarbons, with CH_4 representing all the non-condensable hydrocarbons measured experimentally. Furthermore, the model fails to provide a breakdown of heavy hydrocarbon species (Figure 2.11 (d)), with the composition of tars playing a crucial role in the overall performance of the process and operations of the plant.

The assumption of mono-dimensional axial variation provided ease of computation, and less time of simulation compared to available kinetic models. Nonetheless, it also highlighted limitations related to the input information needed, such as bed temperature and feedstock properties, as well as other improvements, including the number of chemical species produced by devolatilization and fuel particle mixing behaviour. In particular, some of the limitations can be identified as follows:

- Feedstock devolatilization and product composition. TGA tests provide an unrealistic devolatilization behaviour of particles, justifying the assumption of instantaneous conversion. This has the potential of hindering the reactor hydrodynamic, with the whole volatiles being released at one point. Additionally, the chemical species considered as representative of the product of devolatilization were limited in light and heavy hydrocarbons.
- Reaction kinetics. The reactions considered and implemented, although involving all the species, failed to represent the intricate network of reactions involving hydrocarbon species.
- Isothermal conditions of the emulsion phase. Despite being a common assumption, the operating temperature is not always available beforehand, limiting the predictive capabilities of the model.
- Gas mixing. The model did not properly take into account the splashing zone, but assumed the ideal behaviour of the two regions (bottom bed and top freeboard), with perfect gas. This impacts not only the concentration profiles through the freeboard, but also promotes the reaction otherwise limited by the non-perfect mixing. Salatino et al. [58] highlighted the extent to which gas mixing in the splashing zone may affect the apparent kinetics of different reactions, finding that at all relevant mixing scales the Damköhler number is larger than unity, suggesting that the mixing becomes the rate-limiting step.

2.4.3.2 Analysis of FM literature

Analysis of fluidization models reported in Table 2.7 reveals several common characteristics, as outlined below:

1. Most implementations utilize one-dimensional, steady-state approaches based on two-phase fluidization theory. Models differ primarily in their methods for calculating bubble parameters, including diameter, velocity, and bed fraction. Standard assumptions include the complete mixing of solids in the bottom bed region and plug flow behaviour for gas in both bubble and emulsion phases. At elevated fluidization velocities, some models adapt to treat the emulsion phase as perfectly mixed instead of plug flow.
2. The freeboard is not modelled in many BFBG models. When included, it has been assumed homogeneous and perfectly mixed, without any elutriation of solids.
3. In modelling biomass conversion, instantaneous devolatilization represents the most common simplifying assumption. Under this approach, devolatilization gases provide initial conditions for subsequent bed conversion processes. The specification of volatile species composition following devolatilization often lacks clear documentation across the literature. Some models adapt correlations from different biomass types or coal studies to describe this composition.
4. Particle size reduction by fragmentation and attrition of fuel and char is typically disregarded.
5. Modelling of tar species and conversion typically follows simplified approaches, either omitting the process entirely or representing tar species through lumped components that undergo a limited set of reactions. Kinetic parameters for these reactions are sourced from literature, though significant variations exist between different sources.
6. Model validation typically relies on temperature measurements and gas composition analysis of outlet streams. The axial concentration profiles of chemical species within the gasifier remain unvalidated in most studies. Furthermore, most validations are carried out using lab-scale experiments, which may not accurately represent the fluid-dynamic behaviour observed in full-scale gasification systems.
7. Models generally demonstrate reasonable accuracy in predicting major gaseous species concentrations at reactor outlets, though validation often relies on a limited number of experimental data. Notable discrepancies appear primarily in CO and H_2 concentration predictions. The common practice of grouping light hydrocarbons and tar compounds into CH_4 or lumps can account for observed variations in methane concentration predictions. Tar modelling remains largely unaddressed in most studies, and when included, predictions frequently show significant deviations from experimental measurements.

8. The majority of modelling studies incorporate sensitivity analysis to examine variable effects. This analytical approach enhances understanding of gasification processes and aids in interpreting experimental observations under specific operating conditions. However, most models are ‘‘learning models’’ that only allow for prediction of process performance but do not aid the design of the reactor. This makes the model less sensitive to design variations and investigation of operational challenges. ‘‘Development-design-models’’ are more rarely dealt with, although are the most suited for searching for the best operating conditions [61].

2.5 Refined research questions and objectives of the thesis

The initial two chapters have established the research motivation and presented a comprehensive literature review, providing essential background for modelling investigations to follow. These are aimed at investigating the performance of large-scale fluidized bed gasifiers operating with different waste feedstocks, as well as gaining a deeper understanding of the role of gasification agents and other operating parameters. This is done to support the design optimization of gasification reactors, as well as bolster the overall process of H_2 production from waste. Thus, the main research questions addressed in this Thesis can be summarized as follows:

1. Determining the feasibility of building a simple but accurate gasification model for better control and performance predictions. This is deemed essential for process development considering the difficult and expensive large-scale gasifier operations, which makes it unfeasible to test different conditions. The lack of extensive experience and comprehensive literature data regarding the gasification of waste-derived feedstock was also a driving factor for this quest. The best candidate appears to be a 1D FM, but some features should be improved. Extensive validation employing relevant-scale data is deemed essential for the comprehensive utilization of the model.

2. The primary emphasis in waste gasification is to maximize the yield of the product gas which in turn ensures high hydrogen yield. The performance of waste gasification processes is influenced by several operation parameters, however, the relative importance and effect of these is still uncertain. Model investigation can support the identification of the best range of operations.

3. The successful development of hydrogen production from waste faces several operational challenges, with the most crucial being tar formation. Controlling tar levels is vital for the steady operations of the plant, however, current models prove to be inadequate at addressing this aspect, including at best a limited number of chemical species to represent

the behaviour of a complex and heterogeneous family of compounds. In addition, typical fluidized bed reactors are characterized by a long freeboard region, where homogeneous reactions and secondary tar reactions can become predominant, having enough residence to proceed. This can change significantly the composition of tars from the primary species released with devolatilization, however, most of the models in literature either neglect the importance of the freeboard, or fall short in accounting for relevant phenomena.

4. Devolatilization represents a highly complex phenomenon that determines the overall decomposition of solid feedstock during gasification. The duration required for complete devolatilization and yield of products depends on both operating conditions and the physicochemical properties of the feedstock material. Accurate characterization of the devolatilization process, with respect to the mixing and segregation behaviour of reacting particles proves essential for predicting the performance of the. However, most modelling and simulation studies tend to oversimplify this critical step assuming instantaneous conversion or a non-realistic release of volatiles.
5. Particularly with regards to waste conversion into hydrogen via gasification, the overall plant efficiency is still uncertain, considering the number of process units still required to deliver the high-purity H_2. The complexity of the process opens unexplored integration opportunities, together with the evaluation and design of critical units of the plant. A holistic and consistent approach to the full plant would be required to address this research question

In light of this assessment, the research objectives of this Thesis have been refined and are outlined below:

1. To develop an accurate and easy-to-operate model to predict the operation of waste gasification in large-scale fluidized beds, extensively validated with real plant data. The model is to be developed with a flexible and modular approach, making it easy to be adapted depending on reactor design requirements.
2. To identify the most suited operating conditions for different configurations, including different types of feedstocks and gasification agents. Particular emphasis is given to the two extremes represented by the most conventional, air, and the most promising, steam-O_2.
3. To accurately predict tar formation and behaviour by including a broad spectrum of heavy hydrocarbon species. The model has to be particularly accurate and detailed concerning the freeboard and the complex pathway of reaction kinetics that can occur.

4. To develop an empirical semi-kinetic devolatilization pattern release to overcome the common assumption of instantaneous reaction. This approach has to account for the complex interplay of mixing and segregation behaviour with volatlies release that characterize reacting particles in fluidized beds.
5. To develop a full-plant process simulation, informed by the detailed kinetic model, to investigate the technical feasibility and environmental benefits of a Waste-to-H_2 plant.

Having set these objectives, the primary focus of this research endeavours was to attain a deeper understanding of the intricate mechanisms governing fluidized bed gasifiers, and untangle the intricate relationships among the process operating variables. Part of this work has been conducted in collaboration with the Department of Environmental, Biological, Pharmaceutical Sciences and Technologies, University of Campania “Luigi Vanvitelli” (Prof U. Arena research group) and the engineering design team of Advanced Biofuel Solutions Ltd (Swindon, UK).

Chapter 3. Methodology

From the available literature, a kinetics-based, mono-dimensional approach appears to offer the best compromise between accuracy and computational complexity, while a modular structure bolsters the flexibility required for a model to be comprehensive. Nonetheless, real plant data are necessary to validate such models, especially for novel applications using waste-derived feedstock and steam-oxygen operation.

This chapter describes the development of the one-dimensional kinetic model for different feedstocks gasification in bubbling fluidized bed reactors. Other than information from literature on similar approaches, the model development builds on findings from a preliminary modelling study and the needs of plant operators regarding the main operational issues.

The information reported in this chapter follows the modular structure of the model itself, organized into sub-models and subroutines. The core of the chapter is characterized by descriptions of the novel modelling approach for feedstock devolatilization, the fluid-dynamic and relevant semi-empirical correlations implemented for the fluidized bed, splashing zone and freeboard, moving then to the reactions implemented and the reaction kinetics sub-routine.

The model incorporates the reaction network of different gasification agents within the fluid dynamics of a bubbling fluidized bed to predict feedstock and tars conversion, gas composition, and overall gasification performance A dedicated model for the freeboard that allows for a detailed description of secondary tar reactions. The chapter concludes with a description of the large-scale facilities chosen for validation and the investigative approach.

Parts of this chapter have been published in:

Sebastiani, A., Parrillo, F., Ardolino, F., Arena, U., Iannello, S., Materazzi, M. (2025). Modelling of Oxygen-Steam Gasification of Waste Feedstock in Industrial Fluidized Bed Reactors. *Chemical Engineering Journal*, *506*, 159763. https://doi.org/10.1016/J.CEJ.2025.159763

3.1 Advanced model structure

The model described in this study for the gasification process is based on chemical reaction kinetics, coupled with the typical features of a BFB. The whole gasification model is divided into three parts, representing the main sections that can be identified in the gasifier: the bottom zone, which includes all the phenomena occurring in the BFB, the top of the reactor, which represents the freeboard section, and the intermediate region represented by the splashing zone. The freeboard is modelled as a homogeneous plug flow reactor (PFR). The hydrodynamic of the fluidized bed was modelled following the two-phase theory [78]. The standard approach has been adapted to the gas of thermochemical conversion of solid fuels, introducing a third gas phase representing the endogenous bubbles released by the feedstock. The bed model is further divided into two sub-models to decouple the primary feedstock decomposition and secondary conversion in the BFB. Primary decomposition includes devolatilization of the fuel particle in the absence of oxygen, while the subsequent conversion consists mostly of extra particle reactions like oxidation, cracking and reforming of the gas species [61,148]. The two phenomena are considered to occur in series and have been investigated separately. Lastly, the modified ghost-bubble theory is followed to describe the mixing induced by the bubbles bursting at the surface of the bed in the splashing zone. In order to have a realistic approach toward the overall gasification process, the model has been divided into sub-routines, which include hydrodynamics characterization, reaction kinetics and stream properties. A schematic overview of the general structure of the model, together with the relevant sub-models and subroutines, is reported in Figure 3.1, while a graphic representation of the model and the discretized FBG is shown in Figure 3.2. To simplify the computational load of a kinetic model and handling of the phenomena involved in the process, it is assumed that there are no variations of temperature and concentrations in the radial direction; therefore, the model is one-dimensional and predicts changes only in the axial direction. The height of the bed has been divided into a series of compartments of finite volume where the set of differential equations of mass and energy balances are solved. The discretisation of the solutions could affect the accuracy of the model; therefore, the grid size has been chosen as an optimized compromise between precision and computational time. Differently from CFD simulations which are computationally resource-intensive and time-consuming, making it challenging to control the production process in real-time, executing 1D models allows for quick process evaluation and decision-making by operators. Mass and energy balances are solved in each compartment, whereas the output solution is used as input for the subsequent one.

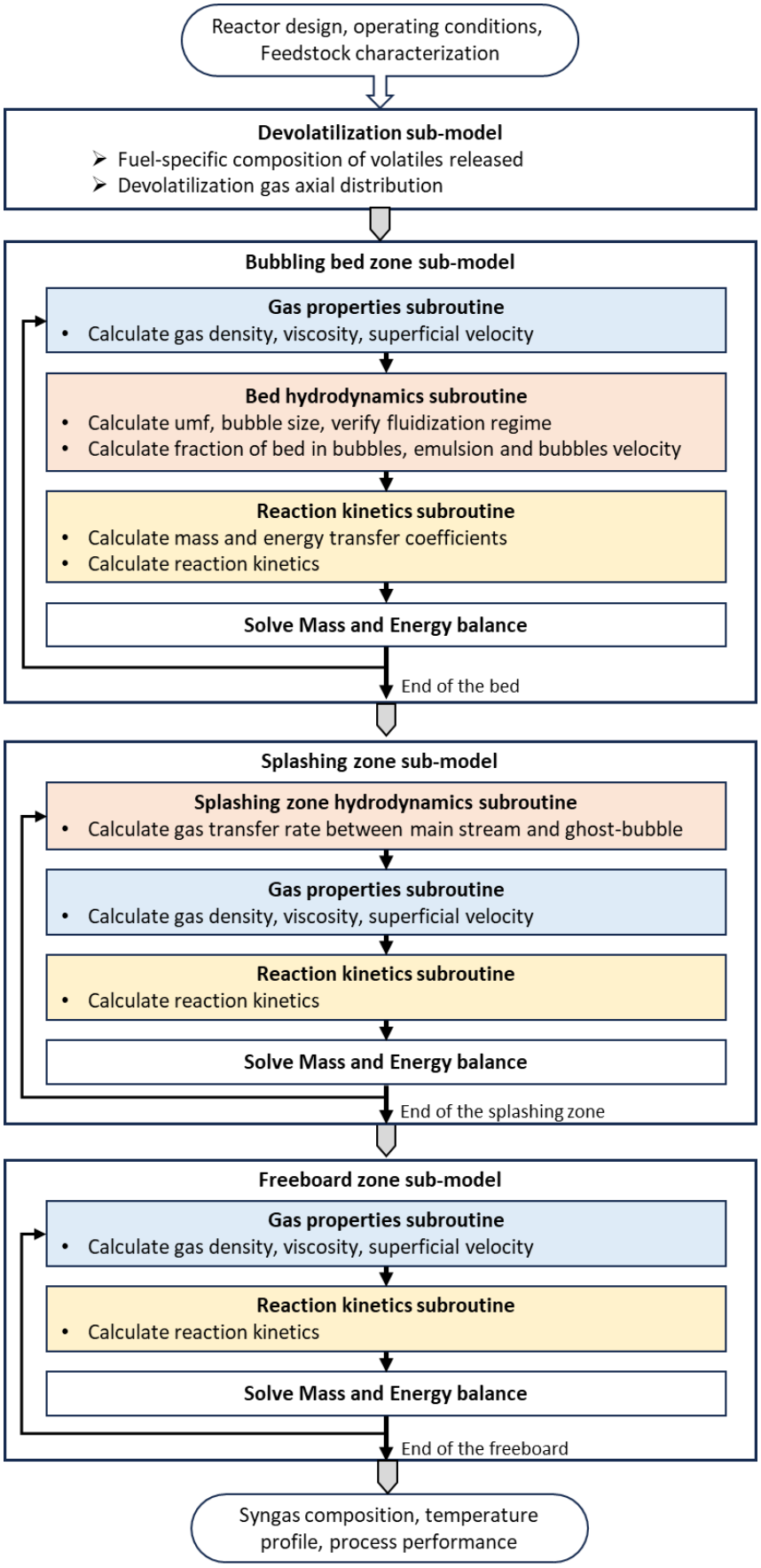

Figure 3.1 – Structure of the model

The overall model relies on the two-phase theory to describe the behaviour of the bubbling bed. The fluidizing agent splits between the emulsion and bubble phases, while the fuel solid particles are added to the emulsion phase, where they undergo primary devolatilization. The volatile matter is released in the form of endogenous bubbles, forming an additional gas phase in the bed involved in the mass balances in each compartment. Char is assumed to remain and react in the emulsion phase, while gas species are transferred between the two gas phases and the emulsion phase depending on the difference in concentration. At the end of the bed, all the gas passes to the splashing zone, which is modelled to account for the turbulence gas flow and mixing induced by the bubbles bursting at the surface of the bed freeboard. Along both the freeboard and splashing zone, only homogenous reactions are assumed to take place.

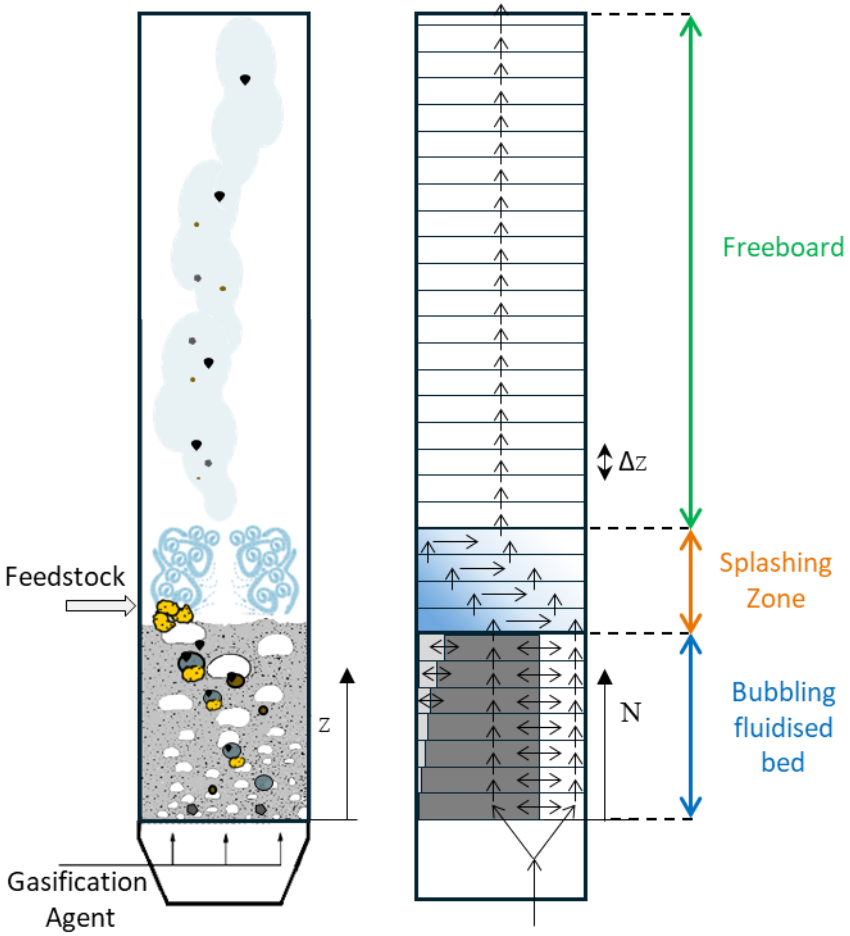

Figure 3.2 – Compartment structure of the reactor modelled.

3.2 Feedstock characterization and devolatilization sub-model

Devolatilization is a critical stage in the gasification of various feedstocks, including biomass, waste-derived solids, and plastics. During this phase, the feedstock undergoes thermal decomposition, where volatile compounds are released as the material is heated. This process results in the formation of a solid residue known as char, alongside a mixture of gases and tar. The efficiency and composition of the devolatilization products are highly fuel-specific, influenced by the intrinsic properties of the feedstock such as its chemical composition, moisture content, and structural characteristics. Therefore, devolatilization is an extremely complex feedstock-specific phenomenon, highly dependent on the temperature and heating rate of the particle, making the modelling of this step challenging, especially in the coupling with the fluid dynamic of the reactor.

The nature of the release of volatiles during this stage plays a crucial role not only in determining the overall efficiency and output of the gasification process but also in operating the reactor. The operational challenges can be related to:

- Temperature control: Rapid or uneven devolatilization can lead to temperature gradients, necessitating efficient heat management systems to maintain uniform reactor temperatures.
- Gas Composition: The composition of the syngas produced is influenced by the volatiles released during devolatilization. Feedstocks with high volatile content (e.g., biomass and plastics) produce more combustible gases, impacting the design and operation of downstream gas cleaning and utilization systems.
- Tar and Particulate Management: High tar production, especially from biomass, can lead to operational challenges such as fouling and clogging. Effective tar mitigation strategies, including the use of catalysts and secondary reactors, are essential.
- Segregation of fuel particles. Uneven axial and radial distribution of fuel particles is commonly experienced in industrial-scale thermochemical converters and may, in turn, give rise to uneven profiles of gas and heat release and reduced tar conversion. This is determined by the self-segregation behaviour of highly volatile feedstock at the bed surface, resulting in poor mixing within the fluidized bed and “stratified” conversion patterns.

For a model to represent accurately the process, the chemical reactions and processes should be predicted quantitatively. However, due to the complexity of the conversion and the highly case-specific phenomena involved, suitable simplifications have to be developed [149]. The first assumption is that the quantity of moisture in the feedstock is quickly released as vapour, adding to the inlet steam content. A feedstock-specific approach is followed to determine the overall product distribution of the primary decomposition (i.e., char, moisture, gases, and tars). The tar fraction is further divided into toluene, phenol and naphthalene (representative of multi-aromatic species) and

a primary lumped tar component. All the species are then subject to thermal cracking and reforming reactions to yield more gas or secondary tars [150]. The initial gas fraction is composed of hydrogen, carbon monoxide, carbon dioxide, methane, and benzene according to Equation (1). The solid residue is composed of carbon and ashes, the latter considered inert. The char is assumed as carbon only, and calculated on an ash-free basis.

$$F \rightarrow \alpha H_2 + \beta H_2O + \gamma CH_4 + \zeta C_2H_4 + \omega C_3H_6 + \vartheta C_6H_6 + \varphi C_7H_8 + \iota\, C_6H_6OH + \eta C_{10}H_8 + \xi tar + \kappa char \qquad (1)$$

Despite devolatilization being typically faster compared to gasification reactions, leading to this often being assumed instantaneous, this represents one of the most critical aspects of a kinetic model. The main limitation of assuming instantaneous devolatilization is the implication of all the volatile matter being mixed with the up-flowing gasifying agent at one point. This results in a detrimental impact on the overall process, affecting the hydrodynamic behaviour of the fluidized bed and the overall final product composition. Gas mixing and evolution are sensitive parameters for the operation of the fluidized bed and the reliability of the model, since these affect primarily the residence time within the reactor. The challenge related to implementing an appropriate model for gas release from devolatilization is crucial for a 1D model and is closely related to the type of feedstock used for the process and the volatile content. Therefore, in this study, the steam and gas released during drying and devolatilization are not added instantaneously to the gas stream. A simplified semi-kinetic approach is used to model the devolatilization process. A feedstock-specific predefined release pattern along the height of the gasifier is developed depending on the characteristics and behaviour of the fuel particles in the fluidized bed, supported by experimental evidence on particle segregation and volatiles release.

3.2.1 Axial segregation of reacting particles in a fluidized bed

The main governing mechanism that determines the mixing or segregation of particles is driven by differences in size and density: finer/lighter solids tend to rise fast and get layered on top of the bed, while coarser/heavier solids tend to accumulate at the bottom of the bed. In addition, another fuel-segregation mechanism typical of thermochemical processes like gasification is determined by the interaction between gas-emitting fuel particles and the fluidized bed.

As proposed by Solimene et al [58], quantitative criteria for uniform volatile matter release may be established by assessment of the relative importance of competing processes by means of dimensionless numbers. It is possible to define the characteristic time scales of axial segregation time and total devolatilization time. The comparison of the characteristic times is accomplished by defining the axial Damköhler number according to Equation (2):

$$Da_{AS} = \frac{t_{AS}}{tD} \quad (2)$$

Criteria for uniform distribution of volatile matter in the bed required that $Da_{AS} \gg 1$. The overall devolatilization time of different reacting particles (namely wood, plastic material and waste-derived solids) has been determined experimentally at different conditions, both for particle size and fluidization regime. The complete devolatilization time for in-bed particle feeding ranges between 50 - 140 seconds for polypropylene and 60 – 110 seconds for biomass [59]. The time required for complete devolatilization in the case of on-bed feeding falls within the same range, although in the higher end, highlighting how the particle segregation on the surface of the bed hinders the overall conversion and performance of the process.

The axial segregation time was determined experimentally using the X-Ray radiography system, allowing to obtaining a time-resolution tracking of fuel particles within the fluidized bed. Additional information regarding the experimental apparatus is reported in Appendix A. Experiments were carried out using spherical beechwood or polypropylene particles with different diameters (8, 10 and 12 mm), under inert conditions, using nitrogen as a fluidization agent. All the samples were half-drilled in order to insert a small tracer particle of lead, ranging from 1.5 to 2 mm in diameter, to make the particle visible upon X-ray exposure during the experiments. The fluidized bed reactor was operated at different temperatures, ranging between 500°C and 700°C, and different fluidization regimes, from minimum fluidization to vigorous bubbling. Figure 3.3 shows the procedure followed for single particle tracking to determine the segregation profile.

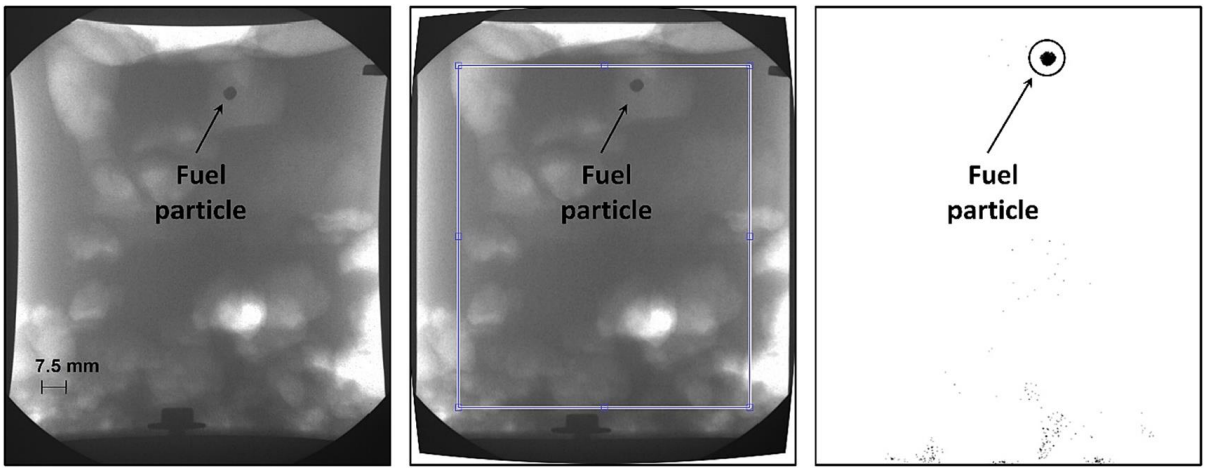

Figure 3.3 – Main steps of the X-ray image analysis. From left to right: raw image, correction of pincushion distortion and selection of the region of interest, particle tracking and final post-processed image. From [60].

Segregation studies show how the density of the particle and fluidization regime are the parameters that mostly influence the mixing behaviour of feedstock particles. As expected, lighter particles tend to segregate at the surface of the bed, while more vigorous fluidization regimes

promote in-bed mixing. Nonetheless, two different behaviours for biomass and plastics were highlighted. Despite both being expected to behave like buoyant bodies, having lower density compared to the average bed density, this is not the case for plastic particles, which tend to sink within the bed instead. Figure 3.4 shows the experimental particle segregation profiles of single particles of biomass (a-b) and plastics (c-d) for on-bed. The profiles are reported with dimensionless axial position, with 0 and 1 corresponding to the bottom and surface of the bed respectively, and a time scale between 0 corresponding to the feeding time and complete devolatilization. In the case of plastic feedstock, the particles showed a larger degree of mixing within the bed compared to biomass particles, or the expected behaviour of a buoyant bed. This is attributed to the formation of an unfluidized sand region on the upper surface of the polymer particle, resulting in a local increase of the average density, which can exceed that of the emulsion phase. Others [59,85] ascribe this characteristic to the slow rate of devolatilization that does not form endogenous bubbles responsible for the lift force that contributes to the rise of the particles to the surface.

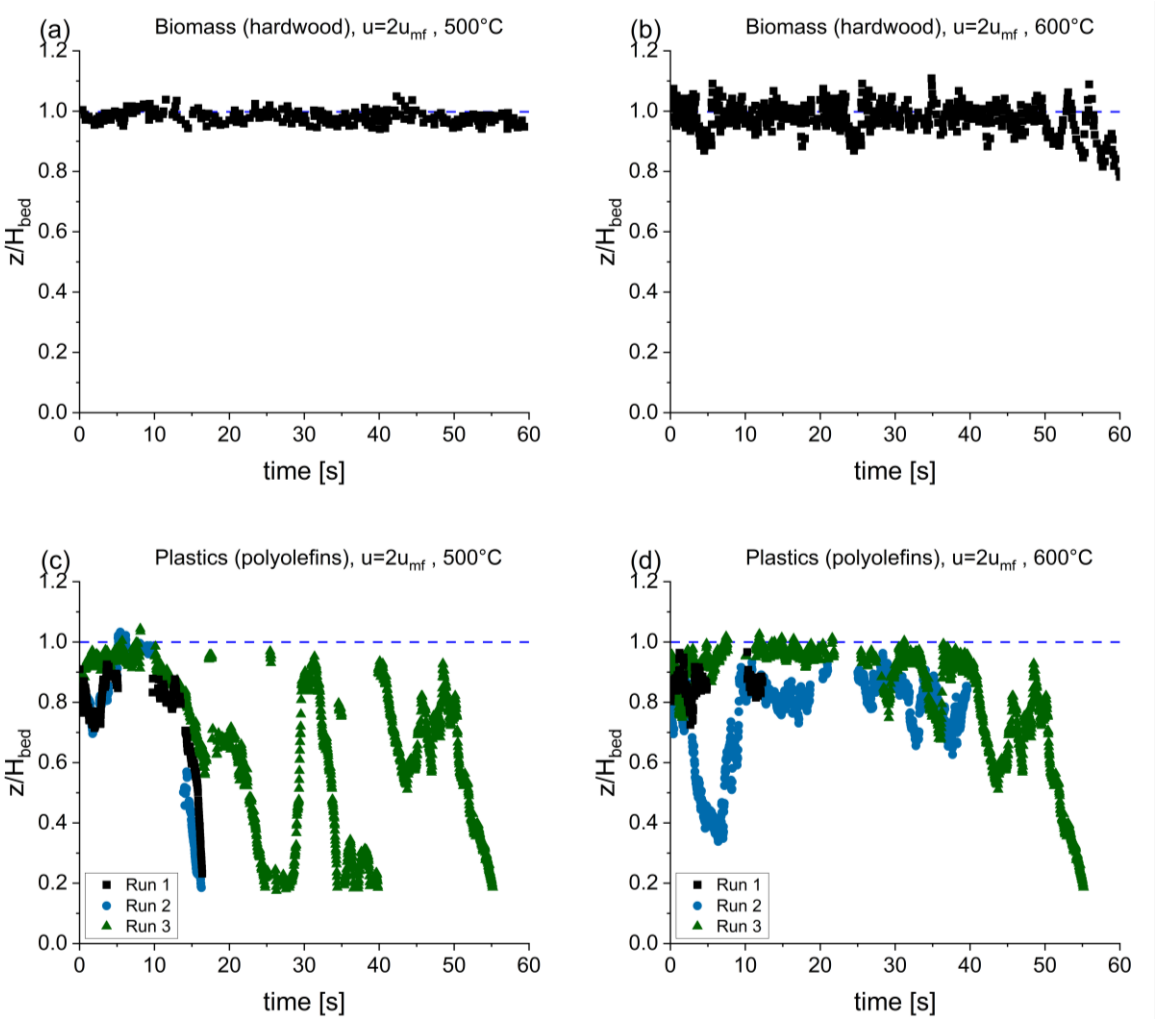

Figure 3.4 – Axial segregation profiles at fluidization index 2 and different temperatures for (a-b) biomass, adapted from Iannello et al. (2023), and (c-d) plastics, adapted from [85].

A further noticeable difference is that once reaches the surface of the bed, biomass particles are ejected into the splashing zone due to the eruption of exogenous bubbles, generating a more vigorous motion with the particle falling back within the bed. This is not observed in the case of plastic particles, which are always found below the surface of the bed. Furthermore, in the case of on-bed feeding, plastic particles tend to sink deeper into the bed.

Segregation studies allow to identify and predict the position of the fuel particles within the bed and the average time spent in each position. The fraction of time spent by the fuel particle in each section of the fluidized bed is then related to the fuel particle conversion and release of volatile matter.

Figure 3.5 shows the frequency, defined as the number of times the particle transits in a specific location of the bed over the entire devolatilization time, obtained from the segregation profiles in [25,26]. This is directly related to the time spent by the reacting particle at a certain axial position in the bed, which is proportional to the amount of devolatilization products released at that location [26]. The predefined pattern release of volatiles is different between biomass and plastic to account for the differences in the mixing behaviour of the two materials. This more realistic approach would incorporate devolatilization kinetics into the model, with appropriate reaction rates that capture the finite time required for volatiles to release, thus improving the accuracy of predictions regarding gas, tars, and char formation.

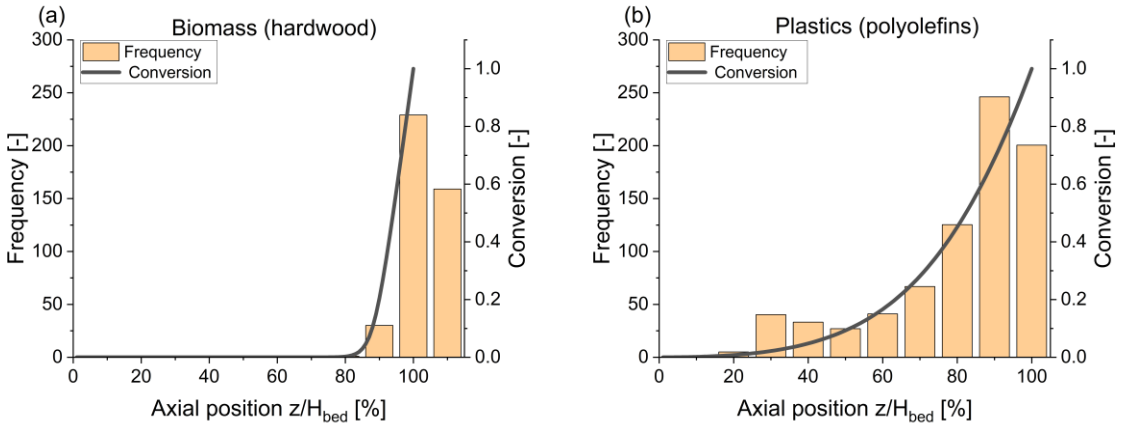

Figure 3.5 – Fuel particles frequency distribution within the fluidized bed and related conversion profile. (a) biomass particles; (b) plastics.

One limitation of this approach is the marginal difference between the material available and used to derive the segregation profile and hence the predefined pattern release of volatiles, and the specific material used in the experimental tests (Sections 3.9.1 and 3.9.2.1). Nonetheless, the profiles obtained are distinctive of the overall behaviour of biomass and plastic-derived feedstock, and representative of the materials investigated in Chapters 4 and 5.

Once the fuel conversion rate has been determined, the composition of the volatiles released needs to be considered. Devolatilization is a highly fuel-specific process where the nature of the volatile species released is directly influenced by the intrinsic properties of the feedstock, such as its chemical composition, moisture content, and structural characteristics. Given the variability and differences among the feedstocks considered, relying on primary direct data to determine the product distribution during devolatilization is preferred [147,151]. This direct approach is deemed more accurate at simulating the process, proven that these are fuel and process specific, i.e. obtained for a specific type of fuel (e.g. beechwood, eucalyptus chips, polypropylene) and in similar conditions of the process (e.g. in a bubbling fluidized bed, similar range of particle size). In contrast, secondary methods or proxies, which often involve generalized assumptions, can lead to significant inaccuracies and suboptimal reactor performance. Therefore, the use of suitable literature data involving detailed empirical studies and direct measurements of devolatilization products is prioritized when available. This is especially the case for biomass and plastics, which usually have very specific composition and have been characterized in several studies in literature. However, due to the intrinsic heterogeneous and complex nature of MSW-derived materials, and the lack of suitable literature data, a more generalized approach is adopted. In the mixed waste case, it is assumed that the behaviour and product distribution follow that of the main constituents, i.e. biomass and plastics. Therefore, a weighted average of biomass and plastic is used, balancing the lower accuracy with the flexibility of application to different feedstocks.

3.2.2 Biomass devolatilization model: Eucalyptus woodchips

Different biomass types can be used for pyrolysis and gasification processes, depending on availability, costs and process specification, affecting the overall devolatilization stage. With the aim of balancing model accuracy and flexibility, literature data for the devolatilization product distribution have been adopted in the case of a specific type of biomass being used within the process and relevant suitable data are available. This is the case of eucalyptus chips, which have been widely used for thermochemical processing [152]. Eucalyptus grandis wood is globally used as hardwood feedstock for the paper and pulp industry, producing large quantities of waste. The characterization of the biomass of Eucalyptus in terms of properties, proximate and ultimate analysis is reported in Table 3.1.

Table 3.1 – Eucalyptus chips characterisation. Adapted from [153].

Proximate analysis (wt% as received)	South African eucalyptus chips
Fixed Carbon	13.3
Volatile matter	78.5
Moisture	7.9
Ash	0.3
Ultimate analysis (wt% dry)	
C	49.8
H	6
N	0.1
O	43.7
S	<0.1
Biomass properties	
Density (kg/m^3)	240
Particle size (mm)	1.5-5.5
Heating value (MJ/kg)	19.4

Heidari et al [153] studied the fast pyrolysis of eucalyptus wood sourced from South Africa in a continuous-feed fluidized bed reactor, investigating the effect of different operating conditions on the product distribution of both light gases and condensable vapours. This study was selected due to the similarity of reactor configuration (i.e. bubbling fluidized bed), operating conditions and feedstock used when compared with the relevant experimental results obtained from the operation of the large-scale gasifier. The product distribution and composition of liquid, char and gas fractions produced from biomass pyrolysis were assessed at different temperatures (450 °C-600°C) and feed particle size (1-3mm) in an inert N_2 atmosphere.

The relevant literature data (obtained at 600°C and 1.5mm particle size) were then adapted in this work and used to calculate the stoichiometric coefficient, given as weight percentage, needed for equation *(1)*. In particular, the provided composition of the light gases was normalized to the gas fraction. The resulting pyrolysis product distribution used in the model is given in Table 3.2.

The bio-oil, representing the condensable fraction of the volatile matter, has been attributed to the heavy hydrocarbons and tar species, with fractions allocated according to the characterization provided in the literature. A further gravimetric lumped “tar” species has been identified based on the overall atomic balance between the feedstock characterization and the products of devolatilization. The gravimetric tar is assumed to have the properties of phenol.

Table 3.2 – Characterisation of product distribution and composition of chemicals released from pyrolysis of Eucalyptus chips.

Pyrolysis product distribution ($\%\ \mathrm{wt_i/wt_{biomass}}$)	
Gas	48.5
$Liquid$	37.2
$Char$	14.3
Gas product distribution ($\%\ \mathrm{wt_i/wt_{gas}}$)	
H_2	8.25
CO	49.32
CO_2	25.84
CH_4	12.74
C_2H_4	2.56
C_3H_6	1.28
Liquid product distribution ($\%\ \mathrm{wt_i/wt_{liquid}}$)	
C_6H_6	0.40
C_6H_6O	34.25
C_7H_8	13.43
$C_{10}H_8$	42.0
$tar\ (CH_xO_y)^*$	9.91
*Calculated from the feedstock proximate and ultimate analysis	

3.2.3 Plastics devolatilization model

Although there are different types of plastics of interest for thermochemical processes, and the composition of plastic waste can be heterogeneous, polyolefin constitutes the largest fraction of plastic waste and holds great potential in the chemical recycling scenario. Therefore, this work was focused on polyolefins as plastic feedstock.

A similar approach of biomass devolatilization has been followed for the case of plastic feedstock, with the product distribution resulting from the devolatilization of plastic material adapted from literature data. Kaminsky [154,155] extensively studied the pyrolysis of different types of plastics in a pilot-scale fluidized bed reactor. The characterization of the types of plastics considered in this work is reported in Table 3.3.

The product composition of PE and PP was assessed with different fluidizing gases, mainly steam, nitrogen or pyrolysis gas itself, and different temperatures. Data referring to operating conditions closer to the ones relevant to this work have been adapted to obtain the stoichiometric coefficient needed for equation 1. In particular, the selection was restricted to fast-pyrolysis data, obtained at high temperature (740°C), and using steam as the fluidizing gas.

Table 3.3 – Characterisation of different plastics. Adapted from [85].

Proximate analysis (wt% as received)	PE	PP
Fixed Carbon	0.12	-
Volatile matter	95.95	99.30
Moisture	0.5	-
Ash	3.4	0.70
Ultimate analysis (wt% dry)		
C	81.5	84.62
H	12.4	15.23
N	0.29	0.14
O	1.6	-
S	-	0.01
Plastics properties		
Density (kg/m^3)	910	697
Particle size (mm)	2-4	2-4
Heating value (MJ/kg)	38.7	44.70

The composition of the light gases was taken as provided for the same chemical species considered and normalized to close the mass balance. The fraction of heavy condensable hydrocarbons has been lumped according to the functional group and molecular weight. This was deemed necessary to match the extensive number of chemical species reported in the literature and the more limited, but representative, ones implemented in the model. The resulting pyrolysis product distribution used in the model is given in Table 3.4.

Table 3.4 – Characterisation of product distribution and composition of chemicals released from pyrolysis of plastics. Adapted from[154].

Pyrolysis product distribution ($\% wt_i/wt_{plastic}$)	BluPolymer-L	BluPolymer-L
H_2	0.5	0.46
H_2O	0.52	0.48
CO	0	0.00
CO_2	0	0.00
CH_4	17.4	15.97
C_2H_4	32.8	30.10
C_3H_6	9.8	8.99
C_6H_6	13.19	12.11
C_7H_8	4.94	4.53
C_6H_6O	0	0.00
$C_{10}H_8$	1.31	1.20
$tar\ (CH_xO_y)^*$	20.02	23.85
$Char^*$	0.12	2.30

**Calculated from the feedstock proximate and ultimate analysis*

3.3 Bubbling fluidized bed sub-model

The gasification process of various solid feedstocks in a bubbling fluidized bed was modelled adapting the two-phase theory to accurately capture the complex fluid dynamics within the reactor. The two-phase theory divides the fluidized bed into two distinct regions: the emulsion phase and the bubble solid-free phase. All gas in excess of that required for minimum fluidizing condition passes through the bed as bubbles [156]. The emulsion phase consists of solid particles that are well-mixed with the gas. In this phase, the gas velocity is approximately equal to the minimum fluidization velocity, ensuring that the solid particles remain suspended. Key characteristics of the emulsion phase in the model include:

- Homogeneous mixing: The solid particles are uniformly distributed within the gas, promoting efficient heat and mass transfer.
- Heat Transfer: The heat required for devolatilization and subsequent gasification reactions is predominantly supplied by the solids making up the bed material, which acts as thermal well due to the high thermal inertia. The overall heat balance is further sustained by the partial oxidation reaction occurring in the gas phase.
- Chemical Reactions: Devolatilization, partial oxidation, and the primary gasification reactions occur mainly in this phase, involving the gas in the emulsion.

The bed material is composed by inert particles, and a constant Sauter mean diameter is used to characterize the bed particles. This common approach allows accurate description of the bed behaviour even when information about the particle size distribution of the bed material is not available. The possible entrainment of bed particles is verified calculating the terminal fall velocity corresponding to the given value of mean diameter. It is assumed that there is no mass loss due to the entrainment of fine sand particles. This assumption allows to consider the bed height as a constant parameter. In reality, the particle size distribution of bed material changes over time, and particles elutriation can occur to a varying extent depending on fines fraction, which for simplicity was not considered in this model. The residual solid fraction from devolatilization (i.e. carbon and ashes in char) is added to the emulsion phase. In particular, while the ashes are considered to be inert, the carbon in char coarse particles is exposed to heterogeneous reactions ($r_{12\text{-}14}$ in Table 3.13). A fraction of char particles can elutriate with the gas flow depending on particle size [62,157].

The bubble phase, or lean phase, is characterized by gas bubbles rising through the bed, which are relatively free of solid particles. These bubbles provide the primary mechanism for gas transport through the bed and mixing enhancement. Key characteristics of the bubble phase include:

- Gas Transport: Bubbles transport reactant gases such as oxygen, steam, or air through the bed, enhancing contact with the solid feedstock. Nonetheless, depending on the

operations of the fluidized bed, gas in the bubble phase tend to bypass the bed, limiting the in-bed conversion efficiency.

- Interphase Exchange: There is a continuous exchange of gas between the bubble and emulsion phases, facilitating the transfer of reactants and products.
- Reaction Environment: Conditions within the bubbles are different from the emulsion phase, providing an additional mean for temperature control.
- Bubbles dynamic: growth due to coalescence.

An additional gas phase, representing the endogenous bubbles formed by the release of volatile matter by the reacting feedstock, is added within the model. This has the aim to better couple the complex hydrodynamic of the fluidized bed and the mixing and segregation behaviour of reacting solids that emit gas. The endogenous bubble gas phase behaves like the bubble phase in terms of interphase mass exchange, although it is closely related to the distribution predetermined by the devolatilization sub-model. A schematic representation of the three-phase fluidized bed model is shown in Figure 3.6.

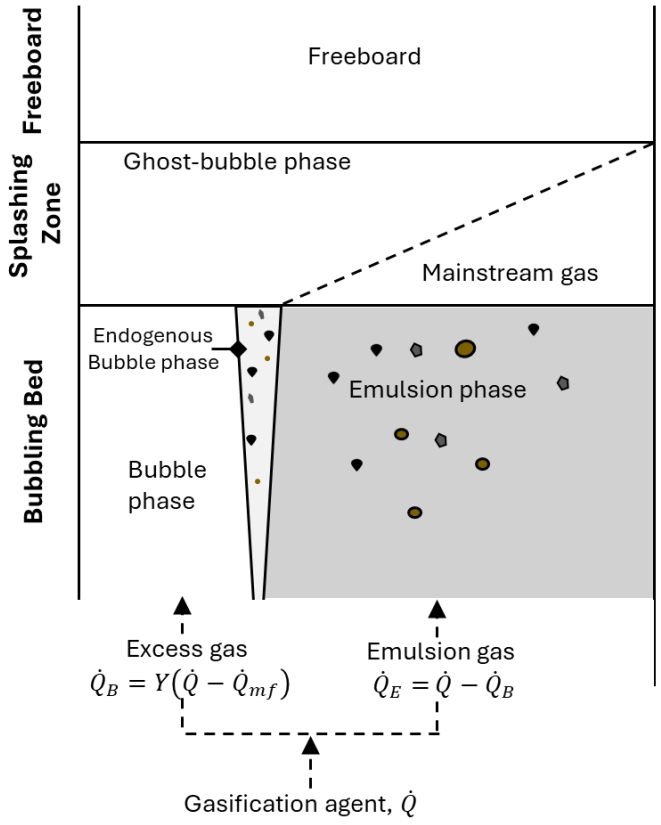

Figure 3.6 – Schematic representation of the three-phase system modelled for the fluidized bed.

The overall gasification process is strongly affected by the reactor temperature profile, which determines the extent of the reaction kinetics therein but also regulates mass transfer between the phases and affects the overall operation of the fluidized bed.

The conservation equations, in the form of mass balances, for gas species account for volatile matter input, reaction products, and interphase mass transfer. The rate of change in molar concentration of the i-th species, in both emulsion, bubble phases, and additional endogenous bubble phase, is expressed by Equations (3)-(5) in Table 3.5. Boundary conditions at the inlet of N_{fb}-th compartment of the bed for the i-species in all phases are reported in Table 3.5 as well.

Table 3.5 – Mass balance equations for the i-th chemical species and j reactions solved for the fluidized bed.

Phase	Mass balance equation	Eq. #
Emulsion phase (e)	$\frac{dc_{ei}}{dz} = \frac{\delta}{1-\delta}\frac{\varepsilon_e}{u_e}\left[K_{b,e}(c_{ei} - c_{bi}) + K_{eb,e}(c_{ei} - c_{ebi})\right] + \frac{\varepsilon_e}{u_e}\sum_j \nu_{i,j}\, r_j$	*(3)*
Bubble phase (b)	$\frac{dc_{bi}}{dz} = \frac{K_{b,e}}{u_b}\,(c_{bi} - c_{ei})$	*(4)*
Endogenous bubbles phase (eb)	$\frac{dc_{ebi}}{dz} = \frac{K_{eb,e}}{u_b}\,(c_{ebi} - c_{ei})$	*(5)*
Inlet boundary condition of compartment N_{fb}		
Emulsion phase (e)	$\dot{n}_{ei}(N_{fb}, in) = \dot{n}_{ei}(N_{fb} - 1, out)$	*(6)*
Bubble phase (b)	$\dot{n}_{bi}(N_{fb}, in) = \dot{n}_{bi}(N_{fb} - 1, out)$	*(7)*
Endogenous bubbles phase (eb)	$\dot{n}_{ebi}(N_{fb}, in) = \dot{n}_{ebi}(N_{fb} - 1, out) + \chi(N_{fb}) \cdot \frac{\nu_{i,Dev}}{MW_i}$	*(8)*

Where the fraction of the bed occupied by bubbles is expressed by δ, while ε is the voidage and u represents the superficial velocity of the relevant phase. In the emulsion phase, the last term takes into account of the reaction kinetics r_j according to the stoichiometric coefficient $\nu_{i,j}$.

The $K_{b,e}$ is the interchange coefficient between bubble and emulsion phase [78], while $K_{eb,e}$ is the interchange coefficient between endogenous bubbles and emulsion phase. The expression to calculate the mass transfer coefficient and the other parameters required for the mass balance equations are reported in Section 3.3.1, which details the bubbling bed hydrodynamic subroutine.

The boundary conditions at the inlet of N_{fb}*-th* compartment are based on continuity of the molar flowrates leaving compartment N_{fb}*-1* for emulsion and bubble phases. An additional term is added for the endogenous bubbles phase to represent the amount of volatiles released by devolatilization of the solid feedstock, with the conversion ($\chi(N_{fb})$) being determined from Figure 3.5 and the product distribution ($\nu_{i,Dev}$) given in Table 3.2 and Table 3.4. The inlet conditions of the first compartment (i.e. N_{fb}*=1*) is determined by the fluidizing agent, which depends on the operating conditions of the gasifier.

One of the main advantages of a fluidized bed is good solid mixing due to the upward gas stream that globally results in temperature homogeneity across the whole bed [158]. This is also promoted by the large contact surface and the high heat exchange rates between gas and solid particles. These reasons often lead to assuming the emulsion phase is modelled as isothermal. This assumption will be verified in the results section.

The temperature profile is affected by chemical reactions and heat losses. Energy balances for emulsion and bubble phases, together with the boundary conditions, are reported in Table 3.6.

Table 3.6 – Energy balance equations for the N_{fb}-th compartment and j reactions solved for the fluidized bed.

Phase	Energy balance equations	Eq.#
Emulsion phase (e)	$\frac{dT_e}{dz} = \frac{1}{\sum_i c_{ei} c_{pi}} \frac{\varepsilon_e}{u_e} \left[\sum_j r_j \Delta H_j^r + \frac{\delta}{1-\delta} \mathcal{H}_{be} (T_e - T_b) + \mathcal{J} A_{bed} C_s (T_e - T_{avg}) \right]$	*(9)*
Bubble phase (b)	$\frac{dT_b}{dz} = \frac{\mathcal{H}_{be}}{u_b} \cdot \frac{1}{\sum_i c_{bi} c_{pi}} (T_e - T_b)$	*(10)*
Endogenous bubbles phase (eb)	$\frac{dT_{eb}}{dz} = 0$	*(11)*
Inlet boundary conditions of compartment N_{fb}		
Emulsion phase (e)	$T_e(N_{fb}, in) = T_e(N_{fb} - 1, out)$	*(12)*
Bubble phase (b)	$T_b(N_{fb}, in) = T_b(N_{fb} - 1, out)$	*(13)*
Endogenous bubbles phase (eb)	$T_{eb}(N_{fb}, in) = T_{eb}(N_{fb} - 1, out)$	*(14)*

Where $\mathcal{H}_{be}$ represents the heat transfer coefficient between emulsion and bubbles, $\mathcal{J}$ is the solids flux to represent the solids circulation rate induced by the mixing in the bed, C_s is the specific heat capacity of the bed material. Expressions for the heat of reaction ΔH_j^r and heat capacities c_{pi} are taken from the literature [159] The heat of reaction $\Delta H_j^r(T)$ can be calculated through equation *(15)* [160].

$$\Delta H_j^r(T) = \Delta H_j^r(T_0) + \int_{T_0}^{T} \Delta c_{p,j} dT \qquad (15)$$

Where, $\Delta H_j^r(T_0)$ is the enthalpy of reaction at reference temperature T_0 and can be calculated from the enthalpy of formation of each species involved in reaction j, according to equation *(16)*.

$$\Delta H_j^r(T_0) = \sum_{i,k} \nu_{i,k} \Delta H_{i,k}^f(T_0) - \sum_{i,n} \nu_{i,n} \Delta H_{i,n}^f(T_0) \qquad (16)$$

Where, ΔH_i^f is the heat of formation of component *i* at reference temperature T_0=25°C, ν is the stoichiometric coefficient for component *i* in reaction *j*, *k* refers to the products and *n* to the reactants.
Bed hydrodynamics sub-model

3.3.1 Bubbling bed hydrodynamic subroutine

The hydrodynamic behaviour of a fluidized bed is strongly influenced by the characteristics of the solid material making up the bed and the fluidization agents. These characteristics (namely particle size and density relative to the fluidization gas) determine their class within the Geldart powder classification system. Each class exhibits unique fluidization properties and behaviours. For instance, Group A powders, with smaller particle sizes and lower densities, demonstrate smooth fluidization and are prone to bubbling only at higher gas velocities. Additionally, bubbles size along the height of the bed reach a maximum, when the equilibrium between the growth due to coalescence and the splitting establish. In contrast, Group B powders, with moderate particle sizes and densities, do not incur in smooth fluidization, and bubble growth is not limited by splitting, typically forming large, stable bubbles. In turn, this leads to vigorous mixing and enhanced gas-solid contact, although there is the risk for the bed to enter slugging regime when the bubble diameter approaches that of the reactor. These hydrodynamic differences significantly impact the gasification process, influencing parameters such as temperature distribution, mass transfer rates, and reaction kinetics within the fluidized bed. Understanding the Geldart classification of the solid feedstocks and tailoring the fluidization conditions accordingly are crucial for optimizing the performance and efficiency of fluidized bed gasifiers. For the model to be versatile and describe the different features of the fluidized bed and fluidization regimes, all relevant correlations have been implemented within the bed hydrodynamic subroutine.

The correlations in Table 3.7 describe the bubble rise velocity and other fundamental parameters to describe the hydrodynamic behaviour of the modelled BFB.

Table 3.7 – Mathematical correlations for the modelling of BFB [80].

Name	Expression	Eq.#
Initial bubble size [cm]	$d_{b0} = \frac{1.30}{g^{0.2}}\left[\frac{u_0 - u_{umf}}{N_{or}}\right]^{0.4}$	*(17)*
Limiting size of bubble [cm]	$d_{bm} = 0.65\left[A_{bed}(u_0 - u_{mf})\right]^{0.4}$	*(18)*
Bubble diameter [cm] [161]	$d_b = \frac{0.54}{g^{0.2}}(u_0 - u_{mf})^{0.4}\left(z + 4\left(\frac{A_{bed}}{N_{or}}\right)^{0.5}\right)^{0.8}$	*(19)*
Minimum fluidizing velocity [cm s^{-1}]	$u_{mf} = \frac{\mu_g}{\rho_g d_p}(27.2^2 + 0.0408Ar)^{0.5} - 27.2)$	*(20)*
Rise velocity of a single bubble [cm s^{-1}]	$u_{br} = 0.711(g\, d_b)^{0.5}$	*(21)*
Rise velocity for bubbles in bubbling beds [cm s^{-1}]	$u_b = u_0 - u_{mf} + u_{br}$	*(22)*
Rise velocity of emulsion gas	$u_e = \frac{u_{mf}}{\varepsilon_{mf}}$	*(23)*
The fraction of bed in bubbles, $\frac{m^3\ bubbles}{m^3\ bed}$	δ	
- Vigorously bubbling beds, $u_0 \gg u_{mf}$	$\delta = \frac{u_0}{u_b}$	*(24)*
- Fast bubbles, $u_b > 5\frac{u_{mf}}{\varepsilon_{mf}}$	$\delta = \frac{u_0 - u_{mf}}{u_b - u_{mf}}$	*(25)*
- Slow bubbles, $u_b < u_e$	$\delta = \frac{u_0 - u_{mf}}{u_b + 2u_{mf}}$	*(26)*
- Intermediate bubbles, $\frac{u_{mf}}{\varepsilon_{mf}} < u_b < 5\frac{u_{mf}}{\varepsilon_{mf}}$	$\delta = \begin{cases} \frac{u_0 - u_{mf}}{u_b + u_{mf}} & when\ u_b \cong \frac{u_{mf}}{\varepsilon_{mf}} \\ \frac{u_0 - u_{mf}}{u_b} & when\ u_b \cong 5\frac{u_{mf}}{\varepsilon_{mf}} \end{cases}$	*(27)*
Mass interchange coefficient bubble-cloud [s^{-1}]	$K_{bc} = 4.5\left(\frac{u_{mf}}{d_b}\right) + 5.85\left(\frac{\mathcal{D}_{ij}^{0.5} g^{0.25}}{d_b^{1.25}}\right)$	*(28)*
Mass interchange coefficient cloud-emulsion [s^{-1}]	$K_{ce} = 6.77\left(\frac{\mathcal{D}_{ij}\varepsilon_{mf} u_{br}}{d_b^3}\right)^{0.5}$	*(29)*
Total mass interchange coefficient bubble-emulsion [s^{-1}]	$\frac{1}{K_{be}} = \frac{1}{K_{bc}} + \frac{1}{K_{ce}}$	*(30)*
Solids circulation rate [kg m^{-2} s^{-1}]	$\mathcal{J} = \rho_p Y(1 - \varepsilon_{mf})(u - u_{mf})(\beta_W + 0.38\beta_d)$	*(31)*
	$\beta_W = 0.26, \beta_d = 0.42$	*(32)*
Gas phase diffusivities [cm^2 s^{-1}] [162]	$\mathcal{D}_{ij} = \frac{\left(10^{-3}T^{1.75}\left(1/MW_i + 1/MW_j\right)^{0.5}\right)}{p\left[\left(\sum_i v_i\right)^{\frac{1}{3}} + \left(\sum_j v_j\right)^{\frac{1}{3}}\right]^2}$	*(33)*
Gas phase density	$\rho_{gas} = \frac{p}{RT} MW_{gas}$	*(34)*
	$MW_{gas} = MW_i \frac{\dot{n}_i}{\sum_i \dot{n}_i}$	*(35)*
Gas viscosity [Pa s] [163]	$\mu_g = \frac{\sum_i(\mu_i x_i MW_i^{0.5})}{\sum_i(x_i MW_i^{0.5})}$	*(36)*
Heat transfer coefficient bubble-cloud [W m$^{-3}{}_b$ K^{-1}]	$H_{bc} = 4.5\left(\frac{u_{mf}\rho_g c_{pg}}{d_b}\right) + \frac{5.85\left(\lambda_g \rho_g c_{pg}\right)^{0.5} g^{0.25}}{d_b^{1.25}}$	*(37)*
Heat transfer coefficient cloud-emulsion [W m$^{-3}{}_b$ K^{-1}] [164]	$H_{ce} = 6.78\left(\frac{\varepsilon_{mf}\lambda_g \rho_g c_{pg} u_b}{MW_g d_b^3}\right)^{0.5}$	*(38)*
Total heat transfer coefficient bubble-emulsion	$\frac{1}{\mathcal{H}_{be}} = \frac{1}{H_{bc}} + \frac{1}{H_{ce}}$	*(39)*

In particular, equations (17) to (19) are used to characterize the bubble growth in the bed due to coalescence, with (17) and (18) representing the minimum and maximum bubble size in the case of Geldart group A powders. Darton et al.[161] determined experimentally a correlation for the bubble

size as a function of the axial position within the bed (Equation (19)) and the catchment area, defined as the ratio between bed cross section and the number of orifices in the distributor plate.

Among the many different correlations available in literature to estimate the minimum fluidization velocity, the one implemented in the model is the most suited when operating at high temperature, like in the case of thermochemical conversion processes [2,61].

3.4 Splashing Zone sub-model

The splashing zone of fluidized bed reactors is a region of crucial interest for the operation of the gasifier, and therefore its modelling as well. The peculiar gas mixing pattern above the bed can determine the performance of the gasifier, as well as pose detrimental challenges related to hotspot formation. Above the surface of the bed, the eruption of the bubbles exiting the bed releases the unreacted gas. This causes vortex-like perturbation resulting in the mixing of all the gas species emerging from the bed: bubbles, the upward main gas stream and the gas released by the reacting particles either on the surface of the bed or in the form of endogenous bubbles.

The splashing zone has been modelled as a two-gas phase plug-flow system: one representing the mainstream gas flow exiting the emulsion phase, and the second represented by the gas released by the bubbles bursting, with a phenomenological approach similar to the ghost-bubble theory. Whilst the complex flow structure resulting from the mixing induced by the bubbles bursting at the surface of the bed was not represented in the model, the result of the complex hydrodynamic with the two phases mixing was accounted for within the balance equations, in terms of growth rate $\dot{V}$ of the ghost bubbles entraining gas from the mainstream. The gas entrained from the mainstream phase is mainly composed by syngas, while the gasification agent bypassing the bed in the form of bubbles constitutes a large part of the ghost-bubble phase. The model considers the continuity of mass and temperature at the interface between fluidized bed and splashing zone (sz), and it is expressed in Table 3.8.

Table 3.8 – Continuity conditions at the interface between fluidized bed and splashing zone.

Phase	Balance	Equation	Eq. #
Ghost-bubble phase (gb)	Mass	$\dot{n}_{gbi}(N_{sz}=1,in)=\dot{n}_{bi}(N_{fb}=end,out)+\dot{n}_{ebi}(N_{fb}=end,out)$	*(40)*
Main stream gas phase (m)	Mass	$\dot{n}_{mi}(N_{sz}=1,in)=\dot{n}_{ei}(N_{fb}=end,out)$	*(41)*
Ghost-bubble phase (gb)	Energy	$T_{gb}(N_{sz}=1,in)=T_{b}(N_{fb}=end,out)$	*(42)*
Main stream gas phase (m)	Energy	$T_{m}(N_{sz}=1,in)=T_{m}(N_{fb}=end,out)$	*(43)*

A schematic representation of the splashing zone and the mixing of the two gas phases is shown in Figure 3.7. Since the mixing of the two phases entails the transport of reactants from the mainstream gas phase, the model assumes that homogeneous gas-phase reactions occur only within the ghost-bubble phase.

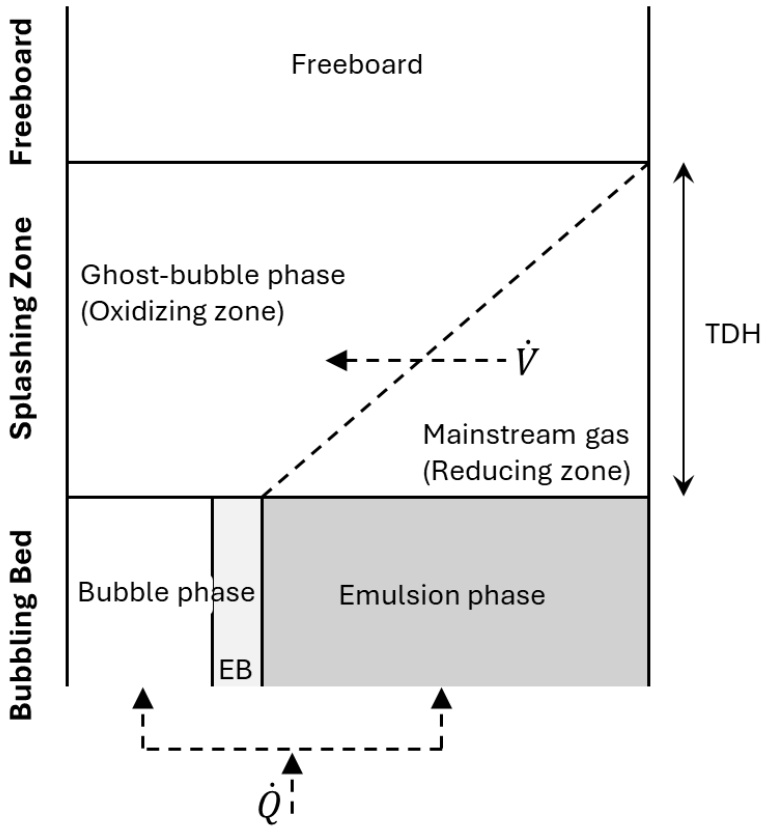

Figure 3.7 – Schematic representation of the splashing zone and the mixing of the two gas phases. $\dot{V}$ represents the entrainment rate from the reducing zone to the oxidizing region associated with the growth of the ghost-bubbles.

The mass and energy balance equations solved for both phases are reported in Table 3.9, together with the boundary conditions at the inlet of N_{sz}-th compartment of the splashing zone.

Table 3.9 – Mass and energy balance equations for the N_{sz}-th compartment and j reactions solved for the splashing zone.

Phase	Balance	Equation	Eq.#
Ghost-bubble phase (gb)	Mass	$\frac{d\dot{n}_{gbi}}{dz} = A_{bed} \cdot \sum_j \nu_{i,j}\, r_j$	*(44)*
Main stream gas phase (m)	Mass	$\frac{d\dot{n}_{mi}}{dz} = 0$	*(45)*
Ghost-bubble phase (gb)	Energy	$\frac{dT_{gb}}{dz} = \frac{A_{bed}}{\sum_i n_{gbi} c_{pi}} \frac{1}{u_f} \left(\sum_j r_j \Delta H_j^r - \frac{(T_f - T_a)}{R_{tot}} \right)$	*(46)*
Main stream gas phase (m)	Energy	$\frac{dT_m}{dz} = 0$	*(47)*
Inlet boundary condition of compartment N_{sz}			
Ghost-bubble phase (gb)	Mass	$\dot{n}_{gbi}(N_{sz}, in) = \dot{n}_{ebi}(N_{sz} - 1, out) + \dot{V} \frac{n_{gbi}}{\sum_i n_{gbi}}$	*(48)*
Main stream gas phase (m)	Mass	$\dot{n}_{mi}(N_{sz}, in) = \dot{n}_{mi}(N_{sz} - 1, out)$	*(49)*
Ghost-bubble phase (gb)	Energy	$T_{gb}(N_{sz}, in) = T_{gb}(N_{sz} - 1, out) + \frac{\dot{V}}{\sum_i \dot{n}_{gbi}} T_m(N_{sz} - 1, out)$	*(50)*
Main stream gas phase (m)	Energy	$T_m(N_{sz}, in) = T_m(N_{sz} - 1, out)$	*(51)*

Where R_{tot} is the total thermal resistance to the heat losses to the surrounding and $\dot{V}$ is the term accounting for the gas entrained in the ghost-bubble phase.

The hydrodynamics of the splash zone of fluidized bed reactors has been the subject of considerable research effort. However, the attention has been mainly focused on solids flow patterns related to the bubble bursting, as a key to characterize solids entrainment and elutriation. The solids present in this region consist mainly of ejected bed or unreacted particles, and elutriated fines. The solids concentration decays rapidly along the splashing zone and they are inert towards the chemical reactions[58,61]. Therefore, the presence of solids has been neglected in the present work. Nonetheless, the height of the splashing region is usually calculated as the maximum height reached by bed solids in their ejection/fall-back and referred to as total transport disengagement height (TDH) [87]. Horio et al. [90] defined TDH as the height at which mass transfer of solids from the particle ascending zone to the particle descending zone near the wall becomes negligible. Based on this assumption, they suggested that TDH corresponds to a position where the fluctuating gas velocity decays by 95% and obtained an expression for the TDH given by Equation (52).

$$TDH = 14 \sqrt{\frac{D_b}{g}} \qquad (52)$$

In this work, the splashing zone height is given by the TDH, with a compartmentalized structure as presented in Section 3.1.

The two gas phases are completely mixed at the end of the splashing sone, with the axial location determined by the TDH, and assuming the growth rate of the ghost-bubble being constant and linear, as determined experimentally by Solimene et al [88,89,92], the two phases are mixed at a predetermined constant rate. The mixing rate $\dot{V}$ is determined as the ratio between the total mainstream gas and the number of layers the splashing zone is divided into.

3.5 Freeboard Zone sub-model

Gas in the freeboard is modelled as a non-adiabatic plug flow. The freeboard height is given by the total reactor height minus the expanded bed and splashing zone heights. The model considers continuity of mass and temperature at the interface between splashing zone and freeboard (f), where the two gas phases in the splashing zone are completely mixed. Table 3.8 reports the boundary equations between freeboard and splashing zone.

Table 3.10 – Continuity conditions at the interface between fluidized bed and splashing zone.

Phase	Balance	Equation	Eq. #
Splasing zone main stream gas phase (m)	Mass	$\dot{n}_{mi}(N_{sz} = end, out) = 0$	*(53)*
Freeboard (f)	Mass	$\dot{n}_{fi}(N_f = 1, in) = \dot{n}_{gbi}(N_{sz} = end, out)$	*(54)*
Freeboard (f)	Energy	$T_f(N_f = 1, in) = T_{gb}(N_{sz} = end, out)$	*(55)*

Mass and energy equations, and boundary conditions at the inlet of N_f-th compartment of the freeboard are reported in Table 3.11.

Table 3.11 – Mass and energy balance equations for the N_f-th compartment and j reactions solved for the freeboard.

Balance in the freeboard (f)	Equation	Eq.#
Mass balance	$\frac{d\dot{n}_{fi}}{dz} = A_{bed}\ \sum_j \nu_{i,j}\, r_j$	*(56)*
Energy balance	$\frac{dT_f}{dz} = \frac{A_{bed}}{\sum_i \dot{n}_{fi} c_{pi}}\left(\sum_j\ r_j \Delta H_j^r - \frac{(T_f - T_a)}{R_{tot}}\right)$	*(57)*
Inlet boundary condition of compartment N_f		
Mass	$\dot{n}_{fi}(N_f, in) = \dot{n}_{fi}(N_f - 1, out)$	*(58)*
Energy	$T_f(N_f, in) = T_f(N_f - 1, out)$	*(59)*

The freeboard mass balance accounts for the homogeneous gas phase reactions involving the chemical species. A more detailed and complex pathway of reaction kinetic has been adopted for the freeboard, with further detail reported in the following Section 3.5.1. The energy balance considers both the heat released/absorbed by the reactions and the heat lost to the surrounding environment.

3.5.1 Detailed reaction pathway freeboard sub-model

Tars are considered to be the major challenge in the application of biomass and waste gasification, especially for fixed and fluidized beds in which operating temperatures are below 900 °C.

In the case of waste or biomass feedstock, the problem is even more serious, due to the higher volatility of wastes and the high propensity to fragmentation [165]. Although not classified as tars, other volatile organic hydrocarbons can be detrimental to syngas utilization in fuel synthesis. Unsaturated hydrocarbons such as benzene, ethylene, and acetylene, for example, pose serious challenges to hydrogenation or water gas shift catalysts leading to deactivation by carbon deposition or coke formation, especially when the synthesis catalyst is applied in adiabatic fixed bed reactors [166]. In most practical cases, tar contents in the producer gas are in the order of 10 g/Nm^3 [167–169], with a composition that can vary depending on the feedstock used, operating conditions, and geometry of the reactor. Tar and heavy hydrocarbon species are initially produced during the pyrolysis of solid carbonaceous fuels, and this primary tar formation is not avoidable due to the nature of the devolatilization process itself. However, after their evolution from the solid phase, the primary tar species are subject to secondary homogeneous reactions that alter the distribution of hydrocarbons and the overall composition of the produced gas. Due to the reduced residence time of volatiles within the bed gas mixing, these secondary reactions take place mainly within the freeboard.

As discussed in Section 2.4.3.1, one of the limitations of the preliminary modelling work, as well as of other models reported in the literature is the accuracy in modelling the tar species [61,76]. Therefore, to improve the capability of the model to predict both the amount of tars and the composition, an alternative freeboard sub-model has been implemented to increase the number of chemical species and reactions, accounting for a detailed reaction pathway. For the best results to be obtained, this alternative modelling approach has been developed using Chemkin. Chemkin is a powerful software and part of ANSYS Fluent. It has been created for modelling and simulating complex chemical kinetics, widely used in combustion, atmospheric chemistry, and other reaction systems and process engineering. Chemkin is particularly renowned for its ability to handle detailed kinetic mechanisms involving thousands of species and reactions, including detailed kinetic modelling, and high-performance simulations with extensive chemical databases. Although Chemkin outcompetes

other software for handling advanced reaction pathways, it is limited with respect to reactor design and configuration, hence the choice of using of this software has been limited to the freeboard.

The model developed by Ranzi et al. [170–173] has been adapted in this work, and it consists of 402 chemical species, including permanent gases (i.e. H_2, CO, CO_2, N_2), steam, a wide range of hydrocarbons, as well as radical species. The reaction mechanism entails overall 14903 reactions, with decomposition reactions, partial and total combustion, water gas shift, reforming and hydrogenation reactions, radical and all other relevant reactions [170–173]. A one-dimensional open plug flow reactor model has been used, with inlet conditions given by the output of the splashing zone, and geometrical parameter same as the freeboard section. Figure 3.8 shows the simplified reaction pathway of destruction of naphthalene, the heaviest hydrocarbon species within the fluidized bed model, and production of H_2 (a) and CO_2 (b). The reaction connections are coloured logarithmically according to heat rate of production, with positive heat being red, and negative heat being blue.

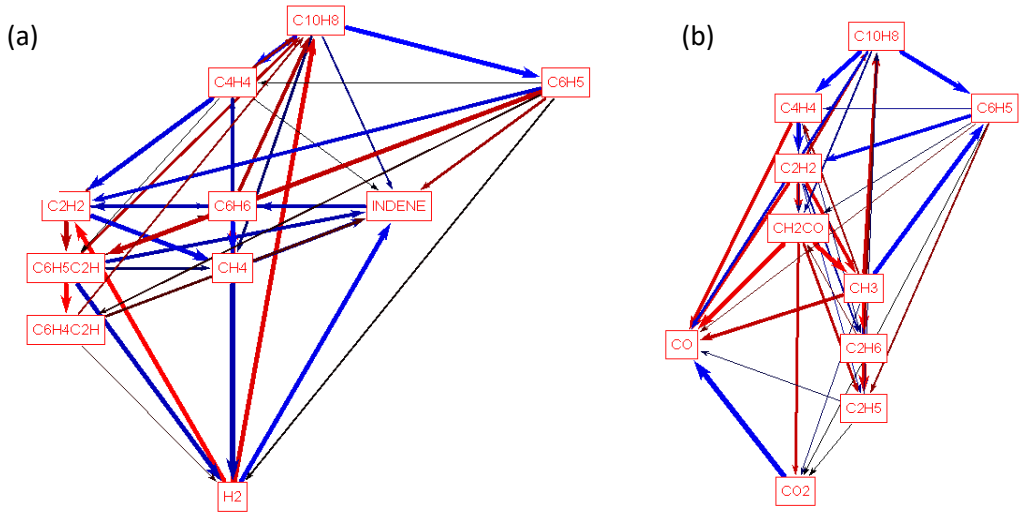

Figure 3.8 – Simplified reaction pathways for H_2 (a) and CO_2 (b).

3.6 Reaction Kinetics sub-routine

The homogeneous reactions are listed in Table 3.12 along with their kinetic equations. These take place simultaneously but at different rates, according to the conditions that occur in each compartment. The dependence from the temperature of each kinetic is expressed by the Arrhenius-type equation (60):

$$k_j = A_j \exp\left(-\frac{E a_j}{RT}\right) \qquad (60)$$

No heterogeneous reactions take place in the freeboard, assuming that fine char particles are rapidly carried over with the gas. The fraction of fine char is produced inside the bed due to the comminution of coarse particles [145,146].

Table 3.12 – Homogeneous reactions that occur in the bed gasifier. Reaction rates are expressed in mol/m³s, concentrations in mol/m³, Activation energy in J/mol.

r_j	Reactions	Reaction rates (mol/m³s)	Ref.
1	$CO + H_2O \rightleftarrows CO_2 + H_2$	$r_1 = k_1\left(c_{CO}\, c_{H_2O} - \frac{c_{CO_2}\, c_{H_2}}{K_{eq,1}}\right)$ $A_1 = 2.778$ $Ea_1 = 12560$ $K_{eq,1} = 0.022\exp\left(-\frac{34730}{RT}\right)$	[174]
2	$CH_4 + H_2O \rightleftarrows CO + 3H_2$	$r_2 = k_2\left(c_{H_2O}\, c_{CH_4} - \frac{c_{CO}\, c_{H_2}^3}{K_{eq,2}}\right)$ $A_2 = 4.916 \cdot 10^{-10} T^2 \cdot \frac{c_C}{M_C \rho_C d_p}$ $Ea_2 = 36150$ $K_{eq,2} = 3.106 \cdot 10^{14}\exp\left(-\frac{208800}{RT}\right)$	[174,175]
3	$H_2 + \frac{1}{2}O_2 \rightarrow H_2O$	$r_3 = k_3\, c_{O_2}\, c_{H_2}$ $A_3 = 1.08 \cdot 10^{10}$ $Ea_3 = 125525$	[174]
4	$CO + \frac{1}{2}O_2 \rightarrow CO_2$	$r_4 = k_4\, c_{CO}\, c_{H_2O}^{0.5}\, c_{O_2}^{0.25}$ $A_4 = 1.78 \cdot 10^{10}$ $Ea_4 = 180032$	[174]
5	$CH_4 + \frac{1}{2}O_2 \rightarrow CO + H_2$	$r_5 = k_5 c_{CH_4}^{0.7} C_{O_2}^{0.8}$ $A_5 = 1.58 \cdot 10^{10}$ $Ea_5 = 202641$	[174]
6	$CH_4 + 2O_2 \rightarrow CO_2 + H_2O$	$r_6 = k_6\, c_{CH_4}^{0.3}\, c_{O_2}^{1.3}$ $A_6 = 2.06 \cdot 10^{6}$ $Ea_6 = 202500$	[176]
7	$C_6H_6 + 3O_2 \rightarrow 6CO + 3H_2$	$r_7 = k_7\, c_{C_6H_6}\, c_{O_2}$ $A_7 = 1.58 \cdot 10^{12}$ $Ea_7 = 202641$	[174]
8	$C_6H_6 + 5H_2O \rightarrow 5CO + 6H_2 + CH_4$	$r_8 = k_8\, c_{C_6H_6}$ $A_7 = 4.4 \cdot 10^{5}$ $Ea_7 = 220000$	[176]
9	$C_{10}H_8 + 4H_2O \rightarrow C_6H_6 + 4CO + 5H_2$	$r_9 = k_9\, c_{C_{10}H_8}\, c_{H_2}^{0.4}$ $A_9 = 9.97 \cdot 10^{10}$ $Ea_9 = 324000$	[176]
10	$CH_xO_y + zO_2 \rightarrow \left(\frac{x}{2} - y - 2z + 2\right)CO + \left(y + 2z - \frac{x}{2} - 1\right)CO_2 + \frac{x}{2}H_2O$	$r_{10} = k_{10} c_{O_2} c_{CH_xO_y}$ $A_{10} = 1.58 \cdot 10^{7}$ $Ea_{10} = 201000$	[149]
11	$CH_xO_y \rightarrow (1-y)CH_4 + \left(\frac{x}{2} + 2y - 2\right)H_2 + yCO$	$r_{11} = k_{11} c_{Tar}$ $A_{11} = 4 \cdot 10^{4}$ $Ea_{11} = 76600$	[177]
12	$C_2H_4 + O_2 \rightarrow 2CO + 2H_2$	$r_{12} = k_{12} c_{C_2H_4}^{0.1} c_{O_2}^{1.65}$ $A_{12} = 2.4 \cdot 10^{12}$ $Ea_{12} = 125590$	[71]
13	$C_2H_4 + 2O_2 \rightarrow 2CO + 2H_2O$	$r_{13} = k_{13} c_{C_2H_4}^{0.1} c_{O_2}^{1.65}$ $A_{13} = 2.4 \cdot 10^{12}$ $Ea_{13} = 125590$	[178]
14	$C_2H_4 + 2H_2O \rightarrow 2CO + 4H_2$	$r_{14} = k_{14} c_{C_2H_4} c_{H_2O}$ $A_{14} = 0.12$ $Ea_{14} = 17111$	[178]

Table 3.12 – Continued.

r_j	Reactions	Reaction rates (mol/m³s)	Ref.
15	$C_3H_6 + 3O_2 \rightarrow 3CO + 3H_2O$	$r_{15} = k_{15} c_{c_3H_6}^{-0.1} c_{O_2}^{1.85}$ $A_{15} = 5 \cdot 10^{11}$ $Ea_{15} = 125590$	[178]
16	$C_3H_6 + 4.5O_2 \rightarrow 3CO_2 + 3H_2O$	$r_{16} = k_{16} c_{c_3H_6}^{0.1} c_{O_2}^{1.65}$ $A_{16} = 1.3 \cdot 10^{12}$ $Ea_{16} = 125590$	[178]
17	$C_3H_6 + 3H_2O \rightarrow 3CO_2 + 6H_2$	$r_{17} = k_{17} c_{c_3H_6} c_{H_2O}$ $A_{17} = 0.12$ $Ea_{17} = 17111$	[178]
18	$C_7H_8 + H_2 \rightarrow C_6H_6 + CH_4$	$r_{18} = k_{18} c_{C_7H_8} c_{H_2}^{0.5}$ $A_{18} = 3.3 \cdot 10^{10}$ $Ea_{18} = 247000$	[179]
19	$C_6H_6O \rightarrow CO + 0.4C_{10}H_8 + 0.15C_6H_6 + 0.1CH_4 + 0.75H_2$	$r_{19} = k_{18} c_{C_6H_6O}$ $A_{19} = 10^7$ $Ea_{19} = 100000$	[178]
20	$C_6H_6O + 3H_2O \rightarrow 4CO + 2CH_4 + 2H_2$	$r_{20} = k_{20} c_{C_6H_6O} c_{H_2O}^3$ $A_{20} = 10^7$ $Ea_{20} = 100000$	[178]

Coarse char particles, which have a terminal fall velocity higher than superficial gas velocity, instead, are consumed in the emulsion phase by heterogeneous reactions listed in Table 3.13.

Table 3.13 – Heterogeneous reactions that occur in the bed gasifier. Reaction rates are expressed in mol/m³s, concentrations in mol/m³, Activation energy in J/mol.

r_j	Reactions	Reaction rates (mol/m³s) [174,176]	Ref.
21	$C + CO_2 \rightleftarrows 2CO$	$r_{21} = k_{21} \frac{c_{CO_2}}{1 + K_{k,CO_2}^{(21)} c_{CO_2} + K_{k,CO}^{(21)} c_{CO}}$ $A_{21} = 4.89 \cdot 10^7 \left(\frac{\rho_{char}}{M_{char}}\right)$ $Ea_{21} = 268000$ $K_{k,CO_2}^{(21)} = 6.60 \cdot 10^{-2}$ $K_{k,CO}^{(21)} = 1.2 \cdot 10^{-1} \exp\left(-\frac{25500}{RT}\right)$	[174]
22	$C + H_2O \rightleftarrows H_2 + CO$	$r_{22} = k_{22} \frac{c_{H_2O}}{1 + K_{k,H_2O}^{(22)} c_{H_2O} + K_{k,H_2}^{(22)} c_{H_2} + K_{k,CO}^{(22)} c_{CO}}$ $A_{22} = 2.39 \cdot 10^2 \left(\frac{\rho_{char}}{M_{char}}\right)$ $Ea_{22} = 129000$ $K_{k,H_2O}^{(22)} = 3.16 \cdot 10^{-2} \exp\left(-\frac{30100}{RT}\right)$ $K_{k,H_2}^{(22)} = 5.36 \cdot 10^{-3} \exp\left(-\frac{59800}{RT}\right)$ $K_{k,CO}^{(22)} = 8.25 \cdot 10^{-5} \exp\left(-\frac{96100}{RT}\right)$	[174]
23	$\alpha C + O_2 \rightleftarrows 2(\alpha - 1)CO + (2 - \alpha)CO_2$	$r_{23} = k_{23} c_{o_2}$ $A_{23} = 5.957 \cdot 10^2 \cdot T_p \left(\frac{6}{d_p}\right)$ $Ea_{23} = 149440$ $\alpha = \frac{1 + 2f_r}{1 + f_r}, f_r = 4.72 \cdot 10^{-3} \exp\left(\frac{37737}{RT_p}\right)$	[174]

Table 3.12 and Table 3.13 provide all the reactions and their respective kinetics as considered in the model. Partial and total combustion reactions were included in the reaction network (r_{3-7}, r_{10}, r_{14}) as the effect of the presence of oxygen in the inlet gas stream. These reactions are responsible for the heat production that supports endothermic reactions, and for the consumption of H_2 and mostly hydrocarbon species with the increase of CO, CO_2, and H_2O content. As a consequence, the variation of those species affects the rate of reaction of both water gas shift reaction r_1 and methane reforming r_2. These reactions appear to play a significant role in the final composition of the syngas. In particular, the water gas shift reaction is found to approach faster the thermodynamic equilibrium, without reaching this state mostly because of the low residence time [174].

Morf et al. [177] studied experimentally the change of mass and composition of tars due to homogeneous secondary reactions in the absence of oxidising agents. The kinetic of tar conversion and formation of aromatic compounds were obtained and reported with the general reaction r_{11}. In this work, this reaction kinetics has been used to take into account the thermal degradation and secondary reactions of tar species that break into lighter gases, (i.e. CO, CH_4, and H_2) and a secondary lumped heavy hydrocarbon compound.

3.7 Gas properties subroutine

A separate subroutine was developed to calculate the properties of the chemical species at different conditions, namely temperature, and determine the overall properties of the gas streams as weighted average depending on the composition. For the gravimetric tar species, it has been assumed the same value of phenol for enthalpy of formation and heat capacity and viscosity. Heats of formation are listed in Table 3.14, while the expression of heat capacity for each compound as a function of the temperature is reported in Table 3.15.

Table 3.14 – Standard enthalpy of formation of the species [160,180].

Component	ΔH_i^f $[kJ\ mol^{-1}]$
C	0
H_2	0
H_2O	-241.81
CO	-110.53
CO_2	-393.51
CH_4	-74.52
C_6H_6	82.88
$C_{10}H_8$	150.58
N_2	0
O_2	0
C_2H_4	52.47
C_3H_6	20.41
C_6H_6O	-96.4
C_7H_8	50.1

Table 3.15 – Heat capacity at constant pressure for each component as a function of the temperature [160,180].

Component	$c_{p,i}$ [kJ mol^{-1}K^{-1}]	Eq.#
C	$c_{p,C} = \left(2.673 + 0.002617T - \frac{116900}{T^2}\right) 4.184 \cdot 10^{-3}$	*(61)*
H_2	$c_{p,H_2} = (6.62 + 0.00081T)\ 4.184 \cdot 10^{-3}$	*(62)*
H_2O	$c_{p,H_2O} = \left(8.22 + 0.00015T + \frac{0.00000134}{T^2}\right) 4.184 \cdot 10^{-3}$	*(63)*
CO	$c_{p,CO} = (6.60 + 0.00120T)\ 4.184 \cdot 10^{-3}$	*(64)*
CO_2	$c_{p,CO_2} = \left(10.34 + 0.00274T - \frac{195500}{T^2}\right) 4.184 \cdot 10^{-3}$	*(65)*
CH_4	$c_{p,CH_4} = (5.34 + 0.0115T)\ 4.184 \cdot 10^{-3}$	*(66)*
C_6H_6*	$c_{p,C_6H_6} = (-5.9488 + 0.99T - 4 \cdot 10^{-5}T^2)\ 4.184 \cdot 10^{-3}$	*(67)*
$C_{10}H_8$*	$c_{p,C_{10}H_8} = (-14.213 + 0.1863T - 10^{-4}T^2 - 3 \cdot 10^{-8}T^3)\ 4.184 \cdot 10^{-3}$	*(68)*
N_2	$C_{p,N_2} = (6.50 + 0.001T)\ 4.184 \cdot 10^{-3}$	*(69)*
O_2	$c_{p,O_2} = \left(8.27 + 0.000258T - \frac{187700}{T^2}\right) 4.184 \cdot 10^{-3}$	*(70)*
C_2H_4	$c_{p,C_2H_4} = -6.39 + 184.40\frac{T}{1000} - 112.97\left(\frac{T}{1000}\right)^2 + 28.50\left(\frac{T}{1000}\right)^3 + 0.32\left(\frac{T}{1000}\right)^{-2}$	*(71)*
C_3H_6	$c_{p,C_3H_6} = 18.812 + 0.1847T - 7 \cdot 10^{-5}T^2 + 9 \cdot 10^{-9}T^3$	*(72)*
C_6H_6O	$c_{p,C_6H_6O} = 0.0434 + 0.2445\left(\frac{1152/T}{\sinh(1152/T)}\right)^2 + 0.1512\left(\frac{507/T}{\cosh(507/T)}\right)^2$	*(73)*
C_7H_8*	$c_{p,C_7H_8} = -28.644 + 0.5384T - 0.0003T^2 + 7 \cdot 10^{-8}T^3$	*(74)*

*Obtained interpolating literature data for heat capacities at different temperatures [181,182].

The equations describing the variation of viscosity with temperature for all chemical species is reported in Table 3.16.

Table 3.16 – Vapor viscosity for each component as a function of the temperature [160,180].

Component	μ_i [$Pa \cdot s$]	Eq.#
H_2	$\mu_{H_2} = \frac{1.797 \cdot 10^{-7} T^{0.685}}{1 - 0.59/T + 104/T^2}$	*(75)*
H_2O	$\mu_{H_2O} = 1.7096 \cdot 10^{-8} T^{1.1146}$	*(76)*
CO	$\mu_{CO} = \frac{1.1127 \cdot 10^{-6} T^{0.5338}}{1 + 94.7/T}$	*(77)*
CO_2	$\mu_{CO_2} = \frac{2.148 \cdot 10^{-6} T^{0.46}}{1 + 290/T}$	*(78)*
CH_4	$\mu_{CH_4} = \frac{5.2546 \cdot 10^{-7} T^{0.59}}{1 + 105.67/T}$	*(79)*
C_6H_6	$\mu_{C_6H_6} = \frac{3.134 \cdot 10^{-8} T^{0.9676}}{1 + 7.9/T}$	*(80)*
$C_{10}H_8$	$\mu_{C_{10}H_8} = \frac{6.4318 \cdot 10^{-7} T^{0.5389}}{1 + 400.16/T}$	*(81)*
N_2	$\mu_{N_2} = \frac{6.5592 \cdot 10^{-7} T^{0.6081}}{1 + 54.714/T}$	*(82)*
O_2	$\mu_{O_2} = \frac{1.101 \cdot 10^{-6} T^{0.5634}}{1 + 96.3/T}$	*(83)*
C_2H_4	$\mu_{C_2H_4} = \frac{2.0789 \cdot 10^{-6} T^{0.4163}}{1 + 352.7/T}$	*(84)*
C_3H_6	$\mu_{C_3H_6} = \frac{7.3919 \cdot 10^{-7} T^{0.5423}}{1 + 263.73/T}$	*(85)*
C_6H_6O	$\mu_{C_6H_6O} = \frac{1.0094 \cdot 10^{-7} T^{0.799}}{1 + 103.1/T}$	*(86)*
C_7H_8	$\mu_{C_7H_8} = \frac{8.7268 \cdot 10^{-7} T^{0.49397}}{1 + 323.79/T}$	*(87)*

3.8 Numerical solution procedure

The 1D gasification model consists of a system of ordinary differential equations (ODEs), in particular:

- 47 mass and energy blances for the fluidized bed for each compartment
  - 45 mass balances for each bed compartment (15 for the bubble phase, 15 for the emulsion phase, 15 for the endogenous bubble phase)
  - 2 energy balances, one for the emulsion phase and one for the bubble phase
- 16 mass and energy balances for the splashing zone for each compartment
  - 15 mass balances for the ghost-bubble phase
  - 1 energy balance for the ghost-bubble phase
- Up to 400 mass and energy balance equations for the freeboard, depending on the reaction mechanism pathway

Initial conditions of the model depend on the operation of the gasifier, and discussed in Capters 4 and 5. Each feedstock used is characterized according to type of material used in the experimental tests, and reported in Sections 3.9.1 and 3.9.2.1.

For each compartment, the calculated concentrations and temperature are used as boundary conditions for the following compartment (i.e. Dirichlet conditions), as detailed in Sections 3.3, 3.4 and 3.5.

These equations have been solved through the Matlab® subroutine ode15s for the bed and splashing zone, and CHEMKIN-Pro for the freeboard. The simulatneous solutions provide the concentration of the different species in each phase along the reactor, and the temperature profile in the gasifier.

For every compartment, the fluidization condition is analyzed to ensure that the system is within the bubbling fluidization regime and no slugging takes place. Elutriation of sand and char particles is evaluated. The algorithm of the computational procedure is shown in Figure 3.9.

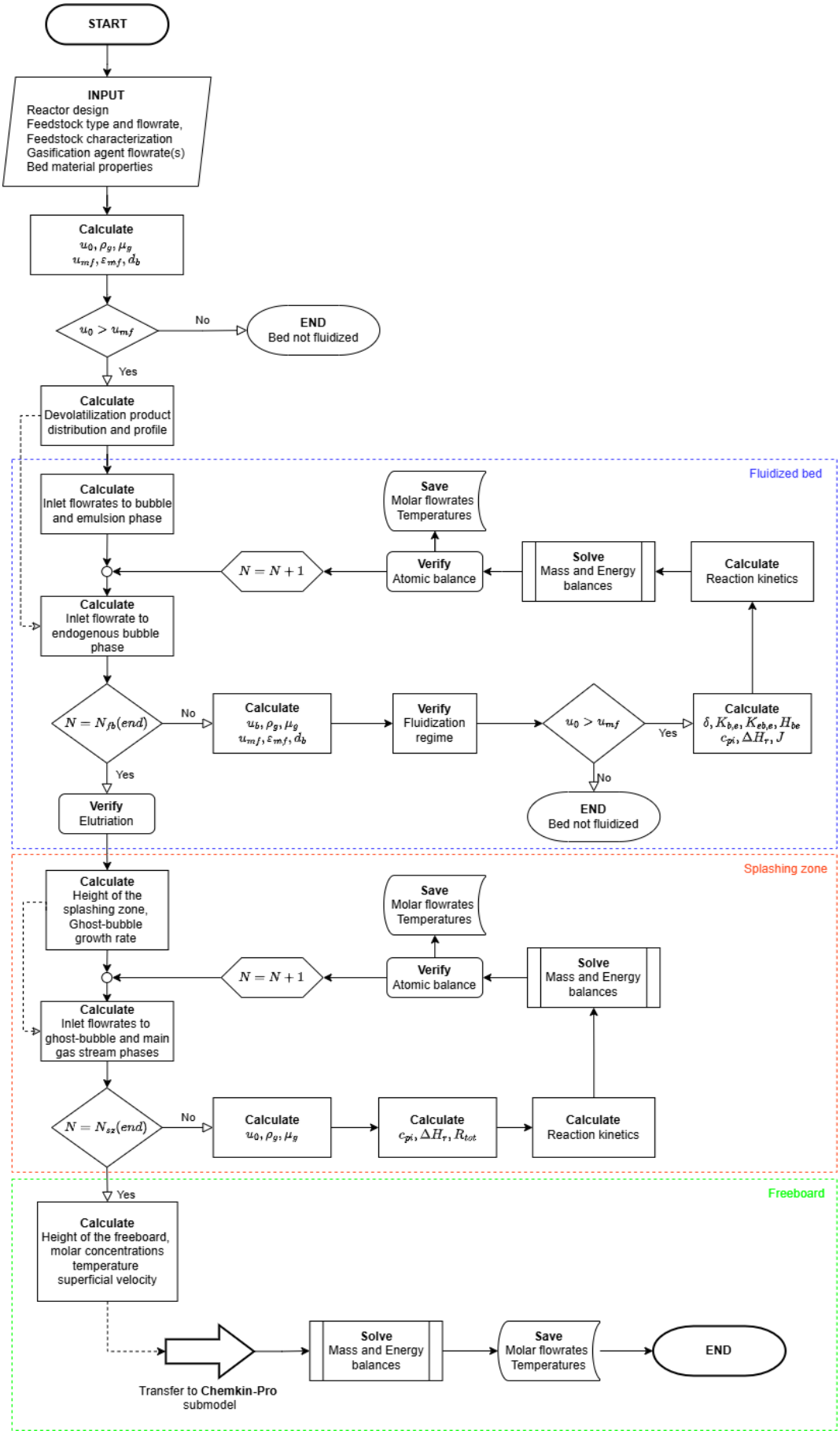

Figure 3.9 – Algorithm of the model.

3.9 Experimental apparatus and validation

3.9.1 Pilot plant: the APP gasplasma reactor

The FBG that was used to generate experimental results for model validation is part of the waste gasification pilot plant based in Swindon (UK). The Swindon plant has been extensively used for R&D purposes and an accurate description of plant components and operation is available elsewhere [183,184]. The experimental setup is shown in Figure 3.10.

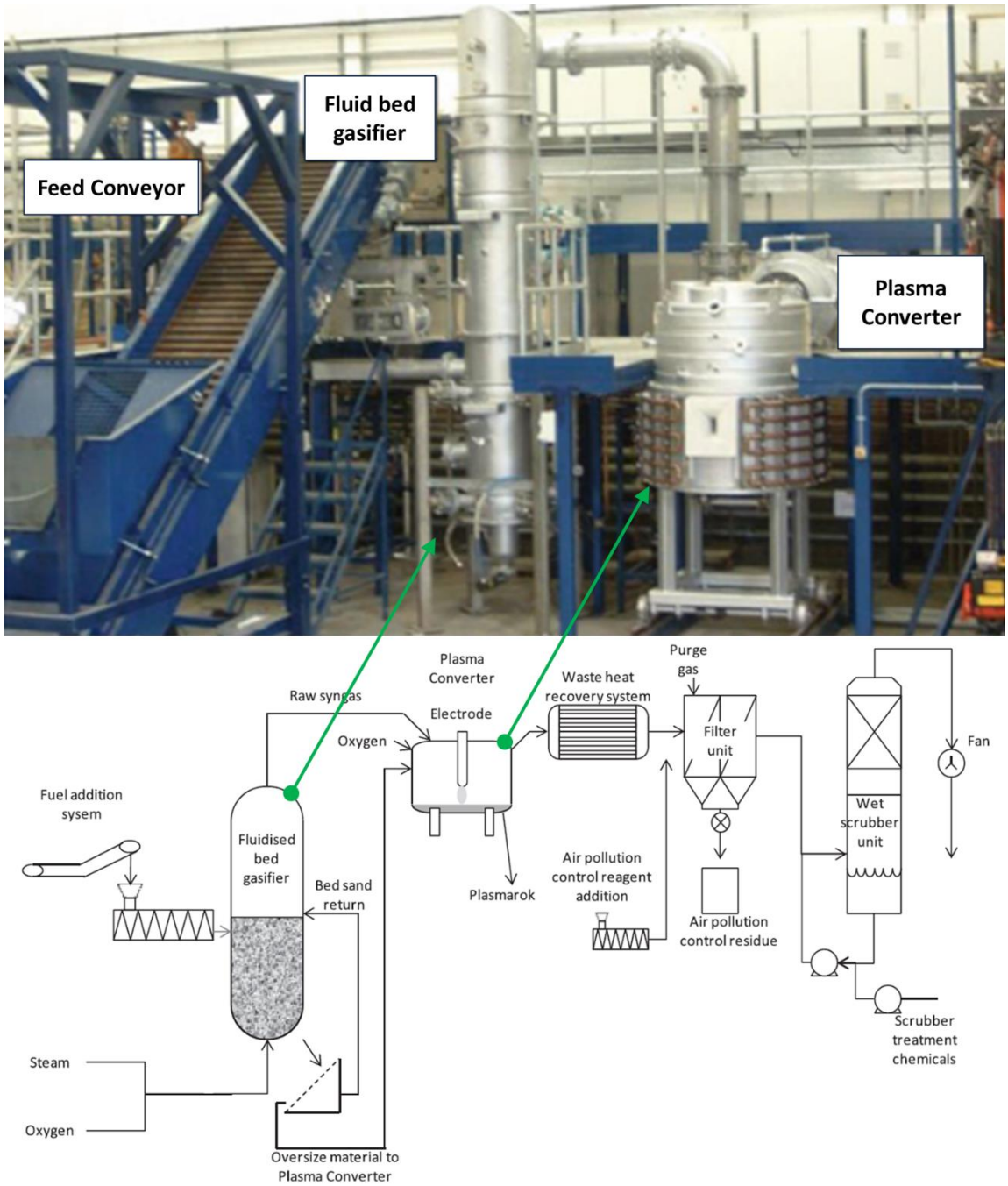

Figure 3.10 – Schematic flow sheet of the pilot scale gasifier, with a picture of the plasma-assisted large bubbling fluidized bed apparatus, part of the Gasplasma plant owned by Advanced Plasma Power, in Swindon, UK. Adapted from [185].

The feedstock (waste material) is initially stored in a buffer hopper mounted on load cells and fitted with level indication and alarm. The waste is extracted from the hopper at a controlled rate using a variable feed screw. A rotary valve after the variable feed screw provides an airlock before the RDF is fed to the gasifier by a constant-speed screw. Gasification takes place in a bubbling fluidized bed gasifier at about 750 °C using steam and oxygen as fluidizing gases. During start-up, the system is warmed up to about 600 °C using hot air supplied by a natural gas burner.

The trials began with 75 kg of virgin bed material in the BFB. During the trial, this material was discharged frequently to maintain a bed differential pressure of 50-70 mbar and prevent the build-up of oversize. Bed material, along with any solid residue from gasification of the RDF (e.g., inert glass, metal fractions, etc.) are extracted automatically from the bottom of the bed, cooled, and finally screened using a vibrating screen to separate the sand from the solid residues. Sand is then recycled back into the process. The extracted bed material is metered using a slide gate valve. The slide valve opens for a fixed period of a few seconds, discharging approximately 0.03 m^3 per pulse, the pulsing being used to meter the flow of bed material. The on-line extraction screening and the recycling of bed material was not a feature of the model, as their effect on syngas quality is expected to be minimal.

The actual operating conditions of the gasifier depend on fuel characteristics and desired reaction profiles. Bed temperature is controlled to not exceed 850 °C by adjusting the steam/oxygen ratio and fuel feed. This is to avoid the risk of incipient ash melting and the possible formation of agglomerates, which represent a major issue in RDF gasification. Maintaining a nearly constant bed temperature also helps to minimise reactor upset conditions due to fuel variations (moisture, ash, heating value, etc) providing near steady-state conditions for the performance of the gasifier. The plant is specifically instrumented with direct and continuous measurements of flows, gas composition, temperatures and pressures. The on-line syngas composition was monitored using a Gasmet Fourier Transform Infrared (FTIR) Spectroscopy gas analyser. Additional CO:CO_2 monitoring is undertaken utilising a XEntra 4210 analyser. The calorific value and the Wobbe index of the gas are monitored using a CWD 2005 Calorimeter.

The feedstock used for testing in the APP facility – and in the relevant model runs – was a standard UK municipal solid waste derived RDF [65].

Table 3.17 shows the average chemical and mechanical properties, and heating value of the waste feedstock samples.

Table 3.17 – Characterization of the waste feedstock used in the experimental tests carried out in the APP facility [42,65].

Ultimate analysis, %wt	RDF	Eucalyptus
C	41.76	40.74
H	5.05	4.61
N	3.02	0.22
O	23.39	34.40
S	0.13	0.01
Cl	0.25	0.01
Moisture	14.60	19.68
Ash	11.80	0.33
Proximate analysis, %wt		
Fixed Carbon	8.90	11.48
Volatile matter	64.70	64.24
Moisture	14.60	19.68
Ash	11.80	0.33
GHV [MJ/kg_{fuel}]	20.51	19.08
Average particle size [mm]	5	4
Bulk density [kg/m^3]	200	250

The main design and operation characteristics of the pilot FBG are summarised in Table 3.18.

Table 3.18 – Design and characteristics of the pilot BFB [65].

Parameter	Values
Bed diameter [m]	0.25
Bed expanded height [m]	1.10
Freeboard height [m]	3.00
Bed temperature [°C]	700-800
Fuel feeding rate [$kg\ h^{-1}$]	40-60
Oxygen to fuel ratio [wt/wt]	0.28-0.33
Steam to oxygen ratio [mol/mol]	2.5-3
Bed inert material density [$kg\ dm^{-3}$]	2.7
Bed inert material mean diameter [µm]	615

3.9.2 Pilot plant: the Faber reactor

The pilot scale bubbling fluidized bed gasifier employed in this study has a maximum thermal input of 400 kW, with a plastic waste capacity of up to 50 kg/h, and a reactor total height (5.73 m) and internal diameter (0.489 m) that are large enough to exclude any scale-related implications [186]. This allows transferring obtained results to larger (even commercial) scale reactors, and it contributes to bridging the gaps between research and industrial deployment. Additional information regarding the main geometric parameters and features of the pilot scale BFBG are reported in Table 3.19.

Table 3.19 – The main geometric parameters and features of the pilot scale FABER gasifier [187].

Parameter	Values
Geometrical parameters	internal diameter: 0.489 m; total height: 5.73 m
Plastic waste capacity	up to 50 kg/h
Thermal output	up to 400 kW
Typical bed amount	234 kg
Feeding system	over-bed (air/water) cooled screw feeders, able to feed two fuels in co-gasification mode
Fluidizing/Gasifying agents	Air, pure oxygen, steam, alone and as their possible mixtures
Fluidizing velocity range	0.4-1.0 m/s
Syngas cleaning	cyclone, wet scrubber
Safety equipment	water seal, safety valves, rupture disks, alarms, nitrogen line for making inert the reactor environment, flare at the syngas exit

The gasifier zones are schematically shown in Figure 3.11: the plenum, the bed zone (up to 1.0 m), the splashing zone (up to about 1.5 m), and the low (up to 2.45 m), medium (up to 3.45 m), and high freeboard (up to 5.7 m). K-type thermocouples and pressure transmitters (Kobold) monitor the temperature and pressure of each zone, which are continuously recorded and processed by a data acquisition and control system. The raw syngas is cleaned by a cyclone and a wet scrubber to make it suitable for different final applications. More details about the pilot scale gasifier can be found in [188,189].

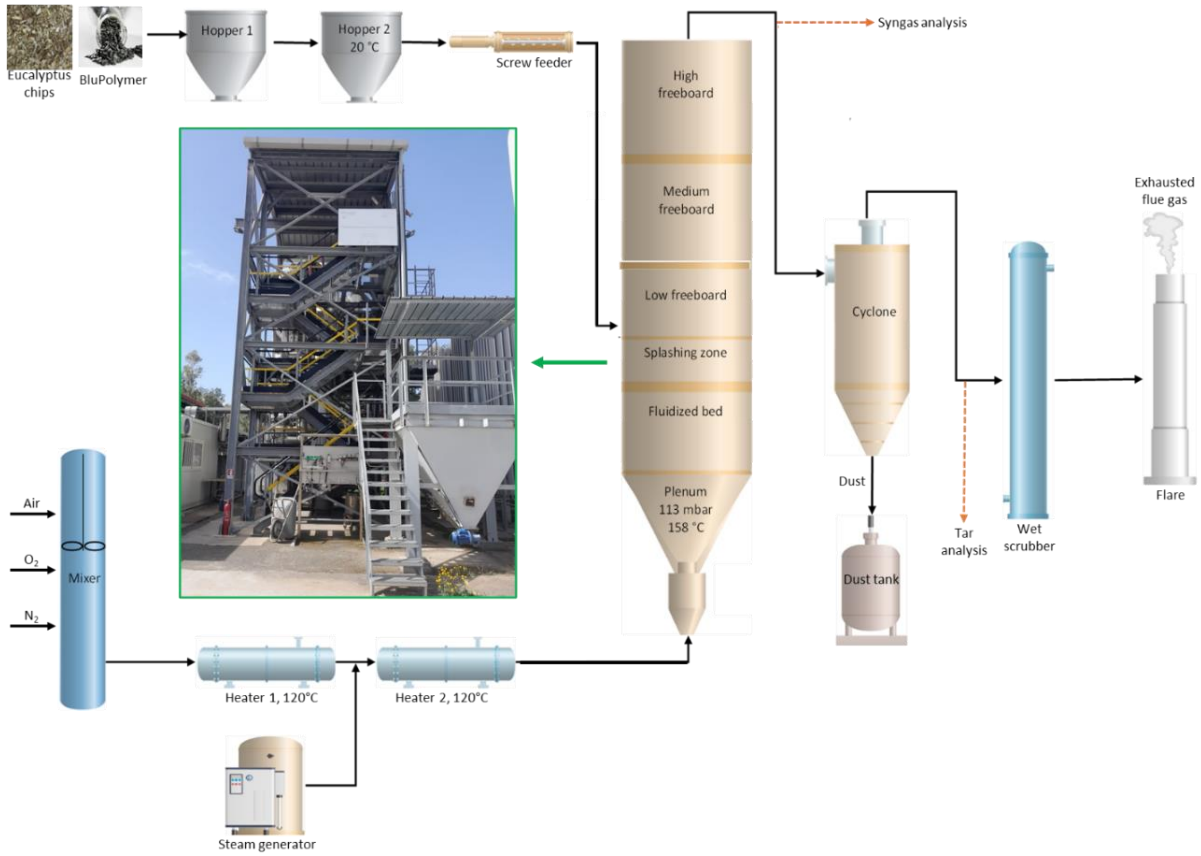

Figure 3.11 – Schematic flow sheet of the pilot scale gasification plant, with a picture of the large bubbling fluidized bed apparatus, named FABER, at the Research Centre of Sotacarbo, Sardinia (Dashed lines refer to sampling points) [190].

3.9.2.1 The experimental procedure and material tested.

The gasifier requires about 3 hours to be heated up to about 700 °C by means of pre-heated blast gases and three electric heaters located along the reactor. At this temperature, the fluidizing gas and the plastic waste flow rates are set to obtain the desired values of the process parameters. The mass flow rate of fluidizing gas (a mixture of air, oxygen, and steam) is measured by means of a Bronkhorst, MF-C40 mass flow meter. Under the selected operating conditions, and without any thermal assistance of external heaters, the reactor gradually reaches thermal and chemical steady states, which are generally maintained for about 2 hours. During this time, gas and solids sampling procedures are activated and measurements of pressure, temperature, blast flow rates, and syngas composition (at four points: two levels along the reactor, at the reactor exit, and downstream of the wet scrubber) are taken. The reliability of syngas composition measurements is guaranteed by a double system of on-line monitoring downstream of the cleaning section: a series of Siemens analyzers to detect CO, CO_2, O_2 and CH_4 (Ultramat 23) and H_2 (Calomat 6); and an Agilent 3000 gas-chromatograph (GC) equipped with 4 different columns (MolSieve, PoraPlot, OV, Alumina) for the detection of a wide spectrum of syngas compounds. Gas is also sampled at two points within the reactor (2450 mm and 3450 mm from the bottom) and at the reactor exit using Tedlar bags and sent to off-line measurements, which are performed using the same GC mentioned above.

Experimental tests were designed by selecting a plastics waste and a biomass with a uniform and constant composition [189]. The plastic waste is a polyolefin blend of two different types, named Blupolymer-L (referred to as Blu-L in this work) and Blu-C respectively, provided by Corepla (Italian Consortium for Plastic Packaging), and prepared by the I.Blu company [191] from non-recyclable residues of separated collection of plastic packaging. Table 3.20 reports their ultimate and proximate analyses (obtained via a LECO Truspec CHN/S), along with low heating value. The biomass particles are obtained by shredding Eucalyptus camaldulensis wood. Properties of biomass feedstock (Eucalyptus) are also provided for comparison, and for analysis of co-gasification simulations.

Table 3.20 – Characterization of the waste feedstock used in the experimental tests carried out in the FABER facility [190].

Ultimate analysis, %wt	Blu-L	Blu-C	Eucalyptus
C	81.5	76.0	43.1
H	12.4	8.16	4.3
N	0.29	0.37	0.4
O	1.6	6.8	36
Moisture	0.52	0.86	14.0
Ash	3.4	7.6	2.2
Proximate analysis, %wt			
Fixed Carbon	0.12	2.3	19.2
Volatile matter	95.9	89.2	64.6
Moisture	0.52	0.86	14.0
Ash	3.4	7.6	2.2
LHV [MJ/kg_{fuel}]	40.5	31.1	13.68
Average particle size [mm]	3	3	5
Density [kg/m^3]	900	900	250

3.10 Operating and performance parameters for process evaluation

3450 mm from the bottom) and at the reactor exit using Tedlar bags and sent to off-line measurements, which are performed

A number of parameters can be defined and identified to characterize the operations of a gasifier. Depending on the nature of the parameters, these can be divided into operating and performance parameters.

Operating parameters define the input conditions and settings that control how a system runs, providing information regarding the reactor operating conditions. The most common parameters for gasification purposes, and the ones considered in this work, are:

- *Equivalence ratio* (ER) is defined as the molar ratio between the O_2 feed to the gasifier and the stoichiometric O_2 required for complete combustion of the fuel. This parameter is

crucial for all advanced thermochemical technologies, whereby the different processes operate within a specific range of ERs. The ER can be calculated with Equation (88).

$$ER = \frac{\dot{n}_{O_2}^{in}}{\dot{n}_{O_2}^{stoic}} = \frac{\dot{n}_{O_2}^{in}}{F\left(\frac{C^{wt}}{AW_C} + \frac{1}{4}\frac{H^{wt}}{AW_H} + \frac{N^{wt}}{AW_N} + \frac{S^{wt}}{AW_S} - \frac{1}{2}\frac{O^{wt}}{AW_O}\right)} \quad (88)$$

Where $\dot{n}_{O_2}^{in}\ [kmol\ h^{-1}]$ is the inlet O_2 molar flowrate, $F\ [kg\ h^{-1}]$ is the fuel feeding rate, i^{wt} is the fuel weight composition of component i and values are given in Table 3.1 and Table 3.3, while $AW_i\ [kg\ kmol^{-1}]$ is the atomic molar mass of component i.

- *Steam-to-Carbon* molar ratio (StC) is calculated as the relative amount of inlet steam to the amount of carbon fed to the gasifier with the fuel. This parameter is relevant for processes using steam as gasification agent, and indirectly determines the thermal and chemical stability of the process via the feeding steam. The StC can be calculated through Equation (89)

$$StC = \frac{\dot{n}_{H_2O}^{in}}{\dot{n}_{C}^{in,feed}} = \frac{\dot{n}_{H_2O}^{in}}{F\frac{C^{wt}}{AW_C}} \quad (89)$$

Where $\dot{n}_{H_2O}^{in}\ [kmol\ h^{-1}]$ is the inlet steam molar flowrate.

- *Oxygen molar fraction* (x_{O2}). This parameter is mainly relevant for gasification processes using air or air-enriched streams as gasification agent. The x_{O2}, also referred to as enrichment ratio, is defined as the oxygen molar fraction in the gasification medium. The x_{O2} is calculated with Equation (90).

$$x_{O_2} = \frac{\dot{n}_{O_2}^{in}}{\dot{n}_{O_2}^{in} + \dot{n}_{N_2}^{in}} \quad (90)$$

Where $\dot{n}_{N_2}^{in}\ [kmol\ h^{-1}]$ is the inlet N_2 molar flowrate.

- The *Feedstock composition* has a strong influence on the operations of the reactor, especially when dealing with highly heterogeneous feedstocks like waste-derived material. The study of feedstock composition is often addressed considering the categories of materials that constitute waste and the relative blends. Waste is composed of a biogenic fraction (i.e. paper, cardboard, wood, etc.), fossil-derived materials in the form of non-recyclable plastics, and inert fractions. In this work, the effect of feedstock

composition is studied via the blending ratio between plastics and biomass to address both the case of co-gasification of biomass and plastic, or the gasification of RDF

- *Gasifier temperature*. The operating temperature is a crucial parameter for all advanced thermochemical technologies. This information is often given as a range or average value for the whole reactor. However, operating complex multiphase reactors like fluidized beds require extensive information regarding the temperature distribution in the reactor, both local and axial profile.

Performance parameters, instead, are related to the output of the process and measure how well the system is performing under those operating conditions. The performance parameters used in this work to evaluate the efficiency of the process are:

- *Cold gas efficiency* (CGE) is a standard efficiency criterion in gasification processes, and it is the ratio on an energy basis between the outlet syngas and inlet fuel to the gasifier. The CGE can be calculated with Equation (91)

$$CGE\ [\%] = \frac{\dot{V}_{Syngas}^{out} \cdot LHV_{Syngas}}{F \cdot GHV_{Fuel}} \cdot 100 \qquad (91)$$

Where $\dot{V}_{Syngas}^{out}\ [Nm^3\ h^{-1}]$ is the outlet syngas flowrate measured or calculated at normal conditions (20°C and 1atm), $LHV_{Syngas}\ [MJ\ (Nm^3)^{-1}]$ is the syngas heating value, while $F\ [kg\ h^{-1}]$ is the feedstock feeding rate and $GHV_{Fuel}\ [MJ\ kg^{-1}]$ is the fuel gross heating value.

- *Net energy efficiency* represents a generic formulation of the CGE that accounts for other energy requirements of the plant. It Is determined with Equation (92)

$$\eta\ [\%] = \frac{\frac{\dot{V}_P^{out}}{3600} \cdot LHV_P}{\frac{F}{3600} \cdot GHV_{Fuel} + \sum W + \sum Q} \cdot 100 \qquad (92)$$

Where the quantity at the numerator refers to the main product of the plant, while $\sum W$ and $\sum Q$ are added at the denominator to account for the additional power and heat required in the plant.

- C*arbon conversion efficiency* (CCE) represents the percentage (%) of total carbon in the gasifier with the feedstock converted to product gas species contain carbon (i.e. CO, CO_2, CH_4 and light hydrocarbons). In this work, the CCE has been calculated using Equation (93).

$$CCE\ [\%] = \frac{\dot{n}_{Syngas}^{out} \cdot \left(x_{CO} + x_{CO_2} + \sum_n n \cdot x_{C_nH_m}\right)}{F\,\frac{C^{wt}}{AW_C}} \cdot 100 \qquad (93)$$

Where $\dot{n}_{Syngas}^{out}\ [kmol\ h^{-1}]$ is the outlet syngas molar flowrate, x_i represent the molar fraction of the gas species i. The light hydrocarbons were considered for $n \leq 5$, which corresponds to species that would be in vapour phase at 20°C and 1atm. The quantities at the denominator have been already defined for Equation *(88)*.

- *Hydrogen specific yield* (g_{H2}/kg_{Fuel}) quantifies the yield of production of H_2 form the feedstock, and it is calculated as the weighted ratio between the H_2 in the outlet syngas and the feedstock flow rate, according to Equation (94).

$$g_{H_2}/kg_{Fuel} = \frac{x_{H_2} \cdot \dot{n}_{Syngas}^{out}}{MW_{H_2} \cdot F} \qquad (94)$$

Where $MW_{H_2}\ [kg\ kmol^{-1}]$ represents the H_2 molecular weight.

  - *Hydrogen-to-Carbon monoxide ratio* (H_2/CO) is the molar ratio between the H_2 and CO content in the outlet syngas, and it is mainly relevant for processes where the produced syngas undergoes further catalytic conversion into synthetic fuels. This parameter can be obtained as a combination of other parameters considered in this work, therefore it has not been analyzed in detail.

- *Dry syngas outlet flowrate* is the total syngas obtained from the gasification process at normal conditions (20°C and 1atm). It is referred to as $\dot{V}_{Syngas}^{out}\ [Nm^3\ h^{-1}]$ in Equation (91). In this work, this parameter is also investigated as ratio against the feedstock feeding rate *F* according to Equation (95).

$$Dry\ syngas - to - Fuel\ ratio = \frac{\dot{V}_{Syngas}^{out}}{F} \qquad (95)$$

- *Syngas purity* refers specifically to tar content in the produced syngas, and it is measured as g_{tar}/Nm^3_{Syngas}. In this work, Equation (96) has been used to quantify the syngas purity.

$$Tar\ content = \frac{\dot{n}_{Syngas}^{out} \cdot \left(\sum_n \frac{x_{C_n}}{MW_{C_n}}\right)}{\dot{V}_{Syngas}^{out}} \qquad (96)$$

Where x_{c_n} represent the molar fraction of the heavy hydrocarbon species having $n > 5$ and molecular weight higher than benzene.

3.11 Investigative Approach

Table 3.21 shows a summary of the investigative approach adopted in this work. Further information about the operating conditions and findings are discussed in the relevant Chapters.

Table 3.21 – General investigative approach adopted in each Chapters of the Thesis, with respective main objective.

<table>
<tr><td rowspan="2">Performance parameters measured against</td><td colspan="5">Operating parameters investigated</td></tr>
<tr><td>ER</td><td colspan="3">Feed composition</td><td>StC</td><td>x_{O2}</td></tr>
<tr><td>Syngas composition</td><td rowspan="7">Chapter 4</td><td rowspan="7">Chapter 4</td><td rowspan="7">Chapter 5</td><td></td><td rowspan="7">Chapter 5</td><td rowspan="7">Chapter 5</td></tr>
<tr><td>Temperature profile</td><td></td></tr>
<tr><td>Tar content</td><td></td></tr>
<tr><td>CCE</td><td></td></tr>
<tr><td>CGE</td><td rowspan="3">Chapter 6</td></tr>
<tr><td>g_{H2}/kg_{Fuel}</td></tr>
<tr><td>Syngas to fuel ratio</td></tr>
<tr><td>Net efficiency</td><td></td><td></td><td></td><td></td><td></td></tr>
<tr><td>Chapter number</td><td colspan="6">Main Objective</td></tr>
<tr><td>4</td><td colspan="6">Air gasification of biomass, plastic waste and blends</td></tr>
<tr><td>5</td><td colspan="6">Steam-oxygen gasification of different waste feedstock</td></tr>
<tr><td>6</td><td colspan="6">Waste-to-H2 overall plant assessment</td></tr>
</table>

Chapter 4. Air gasification of biomass, plastic waste and blends

This chapter presents the results of the model predictions for the operations of the FABER pilot scale fluidized bed gasifier using air as a gasification agent. The results of an extensive validation for gasification of biomass, plastic waste and blends at different proportions are first presented. The model well predicts the composition of the outlet syngas and performance metrics for all feedstocks studied and at different operating conditions.

The chapter then continues showing the main features and capabilities of the model, providing the concentration profiles of all chemical species and phases. Particular emphasis is given to the profile of heavy hydrocarbons and tar composition in the freeboard. Finally, the model is used to investigate the effect of the main operating parameters on the overall performance of the air-gasifier and tar distribution.

4.1 Introduction

Air-blown gasification dominates large-scale waste treatment facilities, offering advantages in terms of operational simplicity and cost-effectiveness compared to other gasification methods. While process aspects of biomass conversion units have been extensively studied in the literature [24,192], including the technical feasibility [18,61,193–195] and environmental sustainability [38,39,196] of alternative operation modes, limited experience exists regarding plastic waste and biomass-plastic blends as feedstock. Moreover, existing research on fluidized bed gasification primarily focuses on syngas composition at the reactor exit or post-cleanup, analysing it as a function of main operating and design parameters [189].

Despite the technical advantages, operating air gasification systems in bubbling fluidized beds presents several challenges. These include predicting the effect of operating conditions on syngas composition and tar formation, optimizing the air-to-fuel ratio to balance the quality of the syngas with process efficiency, and managing feedstock variability. This chapter aims to validate the capability of the model to predict pilot-scale gasifier operations under varying equivalence ratios and feedstock compositions, while providing deeper insights into the complex phenomena occurring within the gasifier, particularly regarding secondary tar formation, freeboard reactions and temperature profiles.

4.2 Air-gasification of biomass, plastic waste and their blends: tests summary and experimental results

Several autothermal air gasification tests, most of which are available in the literature, have been carried out by treating eucalyptus chips, BluPolymer-L or various mixtures of the two feedstocks and fixed air flowrate. In particular, the biomass flow rate was reduced (from 94.0 kg_{fuel}/h to 57.8 kg_{fuel}/h) to obtain values of ER progressively increasing from 0.21 to 0.35, which is in the range of variation of main interest for BFBGs. This was done with the purpose of keeping the fluidization regime constant while assessing the reactor behaviour when operated at different values of ER. Table 4.1 reports the operating conditions of all the performed autothermal gasification tests, carried out with plastic waste (BluPolymer-L), biomass (Eucalyptus chips) and their blends.

Table 4.1 – Operating conditions and main results of the pilot scale tests with different waste feedstock. BluPolymer-L is referred to as BP-L and Eucalyptus as E.

Test #	Gasification agent		Fuel		ER
	Air [NL/h]	Air [kmol/h]	Fuel type	Feed rate [kg/h]	
1	66711	2.98	BP-L	29.2	0.22
2	109653	4.89	BP-L	42	0.25
3	77560	3.46	E	80.0	0.25
4	87559	3.91	E	84.40	0.27
5	89455	3.99	E	81.80	0.28
6	77914	3.48	E	69.90	0.29
7	87575	3.91	E	75.00	0.30
8	76555	3.42	E	64.50	0.31
9	86297	3.85	E	65.50	0.34
10	77586	3.46	E	57.80	0.35
11	76001	3.39	E	94.00	0.21
12	88309	3.94	E	95.50	0.24
13	116076	5.18	BP-L 80% E 20%	60.00	0.21
14	114838	5.12	BP-L 70% E 30%	53.00	0.25
15	111661	4.98	BP-L 60% E 40%	72.00	0.20
16	108920	4.86	BP-L 60% E 40%	67.00	0.21
17	110322	4.92	BP-L 60% E 40%	63.00	0.22
18	114794	5.12	BP-L 60% E 40%	60.00	0.25
19	114451	5.11	BP-L 60% E 40%	51.00	0.28
20	111820	4.99	BP-L 30% E 70%	85.00	0.24
21	109967	4.91	BP-L 40% E 60%	89.00	0.19
22	115379	5.15	BP-L 40% E 60%	71.00	0.28
23	119501	5.33	BP-L 40% E 60%	71.00	0.26
24	115689	5.16	BP-L 40% E 60%	65.00	0.27

The relative results for main process performance parameters are reported in Table 4.2.

Table 4.2 – Main process performance results of the pilot scale test with different waste feedstock.

Test #	Reactor Temperature		Syngas			Process			
	Bed [°C]	Freeboard Outlet [°C]	Outlet flowrate, [Nm^3/h]	LHV, [MJ/Nm^3]	Tar content [g/Nm^3]	CCE [%]	CGE [%]	g_{H2}/kg_{Fuel}	g_{CO}/kg_{Fuel}
1	852	691	88	9.2	3.5	78	71	12.0	110.9
2	890	758	145	7.5	9.0	78	64	20.0	138.0
3	764	725	142	5.6	4.0	71	60	19.8	235.8
4	764	712	143	5.9	4.7	74	53	16.5	267.9
5	764	714	143	5.8	n.a.	87	n.a.	21.9	335.4
6	764	747	143	5.7	5.1	84	56	17.2	276.6
7	764	776	144	5.5	4.4	85	57	19.2	323.2
8	764	650	135	5.3	2.0	86	73	22.9	342.4
9	764	677	136	5.3	3.2	82	57	17.6	314.3
10	764	720	130	5.2	1.9	91	74	19.5	381.7
11	764	804	138	5.0	n.a.	97	71	20.8	369.9
12	764	693	124	4.7	1.2	91	71	19.3	376.9
13	865	745	159	10.1	8.0	92	80	13.48	135.73
14	868	749	149	7.8	7.2	82	67	13.55	161.55
15	849	749	164	10.3	n.a.	87	78	12.40	142.27
16	864	720	160	9.6	n.a.	86	74	12.57	143.19
17	888	750	159	8.4	3.2	85	70	15.31	186.01
18	872	755	155	8.2	6.6	88	73	13.60	154.90
19	920	737	148	7.4	4.9	86	71	14.50	134.13
20	823	764	182	8.0	n.a.	92	81	20.63	264.81
21	797	737	182	9.6	3.1	88	76	16.42	199.26
22	861	734	168	8.1	4.1	91	76	16.89	215.78
23	889	732	166	7.1	3.3	87	71	18.15	251.18
24	908	748	165	7.2	n.a.	94	75	17.67	253.69

4.3 Air gasification of plastic waste

4.3.1 Outlet gas composition

The comparison between predicted and experimental syngas composition for air gasification of BluPolymer-L (Figure 4.1) shows generally good agreement across all gas species. The model accurately predicts the dominant presence of N_2 in the syngas, with values around 70% that closely matched experimental measurements (approximately 65%). For the other species, the model adequately captures the trends, with slight variations in accuracy across different components. CO_2 predictions (approximately 10%) aligned well with experimental values, while a modest underestimation can be found for H_2 and CO, with model predictions slightly below the experimental measurements (around 2-3% for both species). CH_4 predictions (approximately 5%) are reasonably consistent with experimental data, though showing minor overestimation. The predictions for heavier hydrocarbons (C_nH_m) and the LHV are very close, with the difference falling within the experimental error. These results suggest that the developed model provides a reliable framework for predicting syngas composition from plastic waste gasification, though with some limitations in accurately capturing the formation of hydrogen and carbon monoxide. The error bars in experimental results reflect the uncertainties in the measurement devices, as well as fluctuations in the recorded signal and repeated tests.

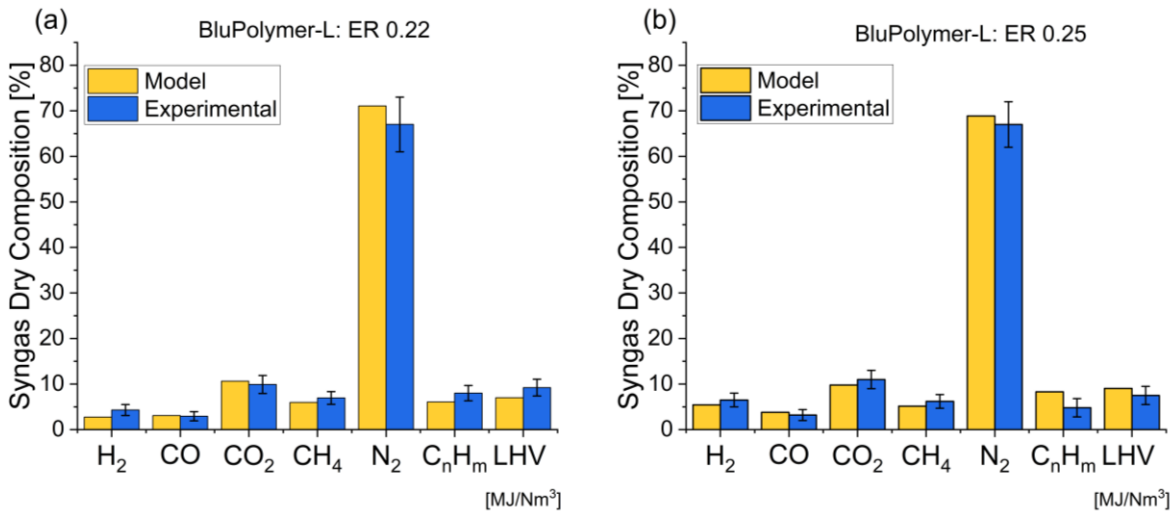

Figure 4.1 – Comparison between model predictions and measured data of syngas composition and heating value for air gasification of plastic waste (BluPolymer-L) at different ERs.

4.3.2 Temperature profile

Figure 4.2 reports the predicted temperature profile along the reactor with the available experimental data for air gasification of plastic waste. There is a good match between the predicted profile and the experimental values throughout the length of the reactor. The model accurately

captures the trends observed in the measured data, showing the increase in temperature from the colder bottom of the reactor, where the fluidization gas enters at around 200°C, and the higher region of the bed, which operates at around 850°C. Nonetheless, a marginal discrepancy can be found towards the outlet of the gasifier (T3), with the predicted temperature falling in the lower end of the experimental range. The model effectively predicts the balance between exothermic and endothermic reactions, but also the heat loss with the surroundings and the crucial role of nitrogen as a temperature moderator. This predictive capability is crucial, as higher temperatures are typically associated with enhanced cracking and devolatilization of the plastic feedstock, leading to improved gasification performance, and potentially hindering the model reliability in case of significant mismatch.

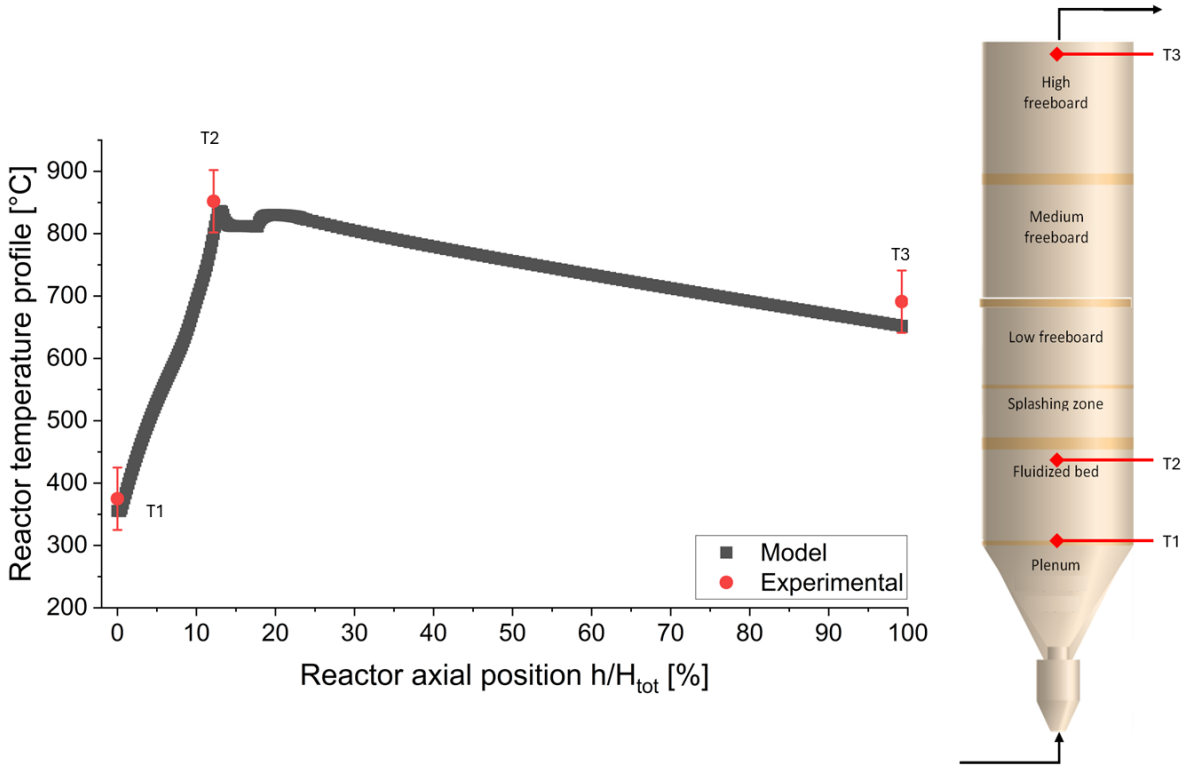

Figure 4.2 – Comparison between predicted axial profile and measured values of gasifier temperature for air gasification of plastic waste. 29.2 kg/h of BluPolymer-L, at ER 0.22.

4.3.3 Process performance

The results in Figure 4.3 demonstrate a strong agreement between the model predictions and the experimental data for various performance parameters of air gasification of plastic waste across different values of equivalence ratio (ER) values. The process of plastics gasification shows overall good conversion efficiencies (in Figure 4.3(a)), with both CCE and CGE in the range of 60% to 80%. The

model predicts very close results for both efficiency parameters, with the overall error within 7%, reflecting the discrepancies in syngas composition as seen in Figure 4.1. The model gives a moderate increase in CGE as the ER is raised. This can be attributed to the ability of the model at accounting for the higher production of light gases, which are likely generated through the enhanced cracking of heavier hydrocarbon compounds at the higher operating temperatures.

The model also demonstrates an excellent match for the outlet syngas volumetric flowrate, as presented in Figure 4.3(b). Both experimental and predicted values show an increase in outlet flowrate when the ER is increased. This is the combined result of the higher amount of air needed to achieve larger ERs, with a larger fraction of inert N_2 in the outlet syngas, but also an overall higher amount of light gases being produced, as also confirmed by the increase in CCE.

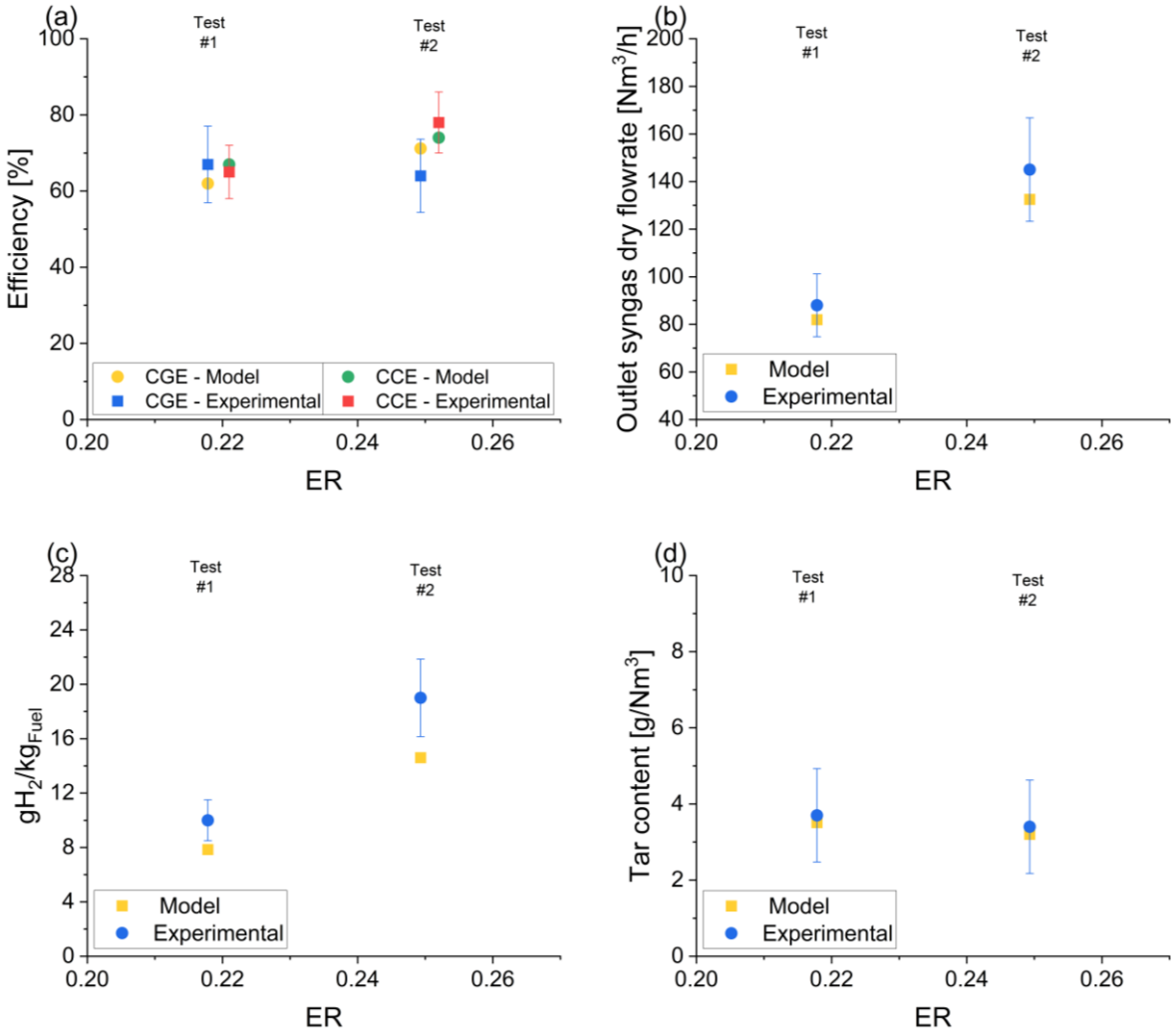

Figure 4.3 – Comparison between model results and experimental data of performance parameters of plastics gasification at different values of ER. (a) CGE and CCE, (b) outlet syngas dry flowrate, (c) specific yield of hydrogen and (d) tar content in the produced syngas.

Both model and experimental values show an increase in H_2 production at higher ERs (Figure 4.3(c)), although this result is also affected by the different operating conditions used with regard to the amount of fuel used. The model shows a very moderate decrease in tar content in the outlet syngas, as can be seen in Figure 4.3(d), potentially caused by the higher temperatures promoting the cracking of heavy compounds.

The overall strong correlation between the model predictions and the experimental observations across the key performance parameters provides confidence in the ability of the model ability to reliably simulate the air gasification. This predictive capability can be leveraged to optimize the design and operation of such waste-to-energy systems, ultimately improving their efficiency and environmental performance.

4.4 Air gasification of biomass

4.4.1 Outlet gas composition

The model has been tested to simulate the air-gasification of eucalyptus chips in a wide range of operating conditions, determined by the ER as shown in Figure 4.4.

The model confirms the robust predictive capabilities across multiple equivalent ratios (ER 0.21-0.34). A consistent trend is observed across all operating conditions, with nitrogen being the predominant species in the syngas composition (45-55%), which is characteristic of air-blown gasification systems. The high N_2 content, while unavoidable when using air as the gasification agent, acts as a temperature moderator within the reactor, but also a diluent that reduces the syngas heating value. Minor discrepancies between predicted and experimental N_2 concentrations are primarily attributed to experimental uncertainties in mass balance and flow rate measurements. The model accurately predicts the concentrations of major combustible components (H_2, CO, CH_4) and CO_2, with variations typically falling within the experimental error bars. H_2 content ranges from 15-20%, CO from 15-25%, and CH_4 from 8-12%, with the model successfully capturing the slight variations in these species across different ERs. The predictions for higher hydrocarbons (C_nH_m) and the resulting lower heating value (LHV) also show excellent agreement with experimental data.

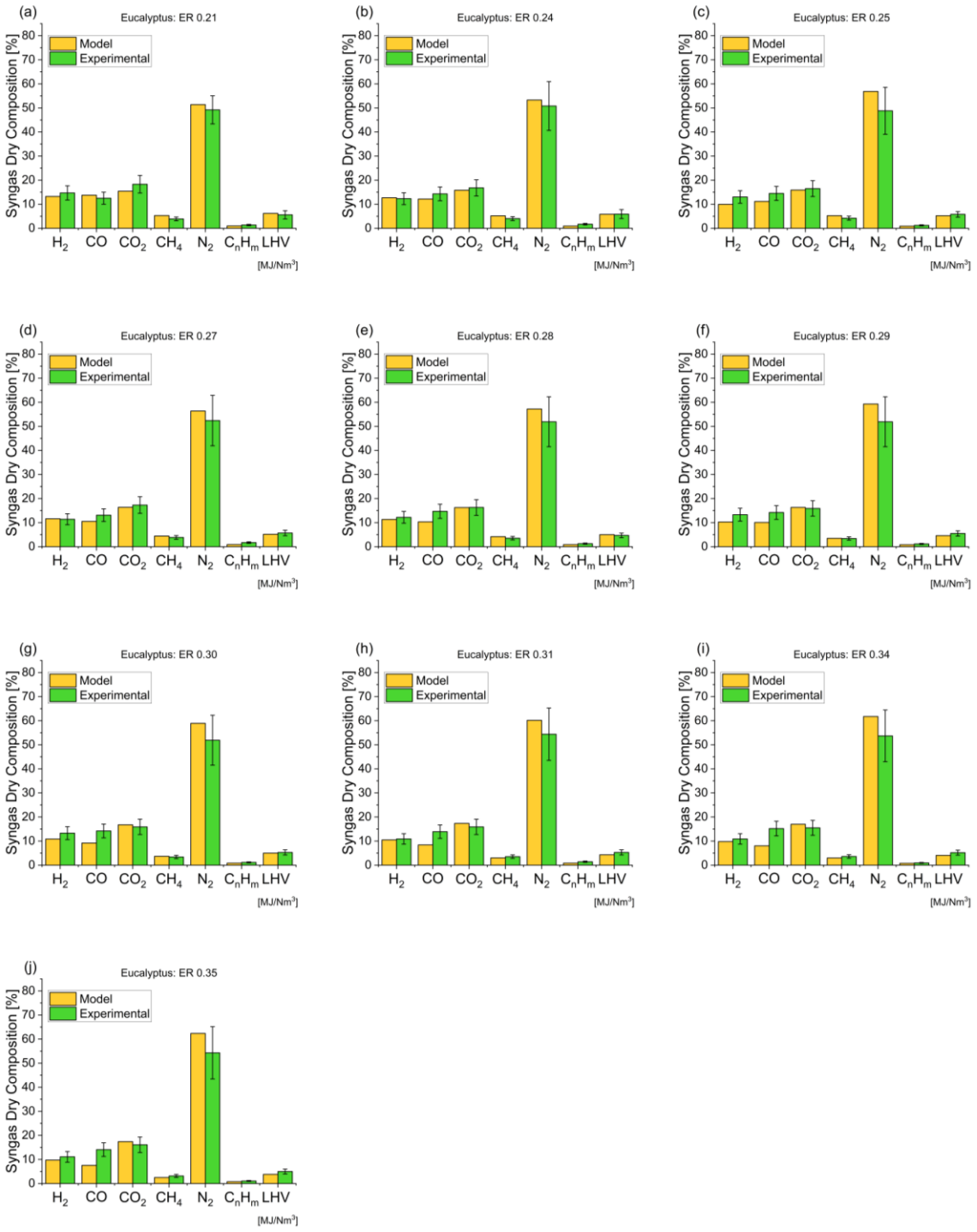

Figure 4.4 – Comparison between model predictions and measured data of syngas composition and heating value for air gasification of biomass (Eucalyptus) at different ERs.

These comprehensive validation results across multiple operating conditions demonstrate the reliability of the model and robustness in predicting syngas composition from woody feedstock gasification.

4.4.2 Temperature profile

A similar temperature profile similar to the case of plastic-air gasification (Figure 4.3) is predicted for the case of biomass gasification (Figure 4.5), with a sharp increase in temperature in the bed, peaking between the surface of the bed and splashing zone, to then decrease along the freeboard due to endothermic reactions and heat losses. However, there are some differences strictly related to feedstock-specific considerations, as analysed more in detail in Section 4.6.2. The peak in temperature (T2) at the surface of the bed is caused by the high heat released by the combustion reactions involving the species released during devolatilization. As discussed in Section 3.2, due to the biomass tendency to segregate at the surface of the bed, a large amount of volatiles is released high in the bed and in the splashing zone, affecting the thermal equilibrium of the reactor and the risk of hotspot formation.

There is overall a good match between the predicted profile and the experimental values throughout the length of the reactor. The higher region of the bed operates at around 800°C, while the syngas exits at around 700°C. Nonetheless, a marginal discrepancy can be found towards the outlet of the gasifier (T3), with the predicted temperature falling in the lower end of the experimental range.

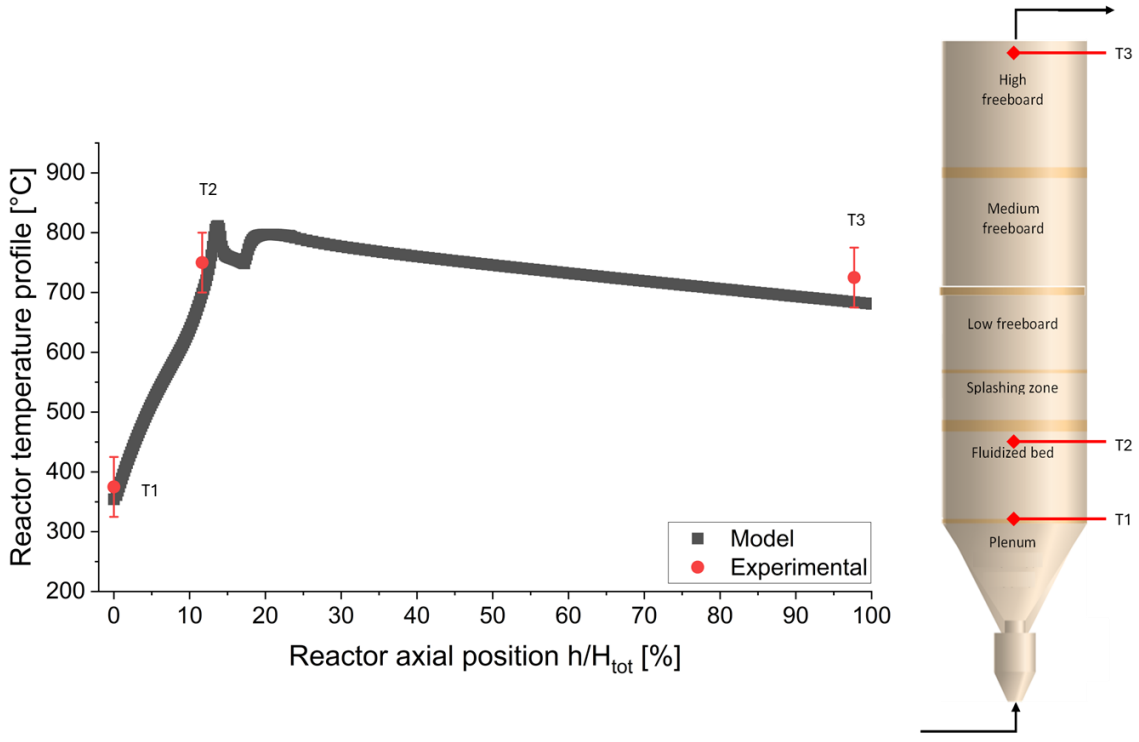

Figure 4.5 – Comparison between predicted axial profile and measured values of gasifier temperature for air gasification of biomass feedstock. 80 kg/h of Eucalyptus, at ER 0.25.

4.4.3 Process performance

The predictive capabilities of the model have been further verified against the main indicators of performance parameters as reported in Figure 4.6, which shows the comparison between the

experimental data and model results as a function of ER. Overall, the model shows good agreement with the experimental data, capturing the trends and orders of magnitude as observed across the key performance indicators.

The model shows a lower variation of CCE when increasing the ER, while the experimental values approach a steady value of around 80% (Figure 4.6(a)). This is reflective of a limitation of the model at best representing the range of heavy hydrocarbon species released during the devolatilization. Despite the excellent level of accuracy in describing the reaction pathway in the freeboard, the overall accuracy is limited by the tar-representing molecules used in the model for the fluidized bed. A further limitation then arises from the product distribution of devolatilization itself, which is obtained with similar feedstock and operating conditions, but subject to experimental error and variations. The underprediction in CCE is mirrored by the overprediction of tar content in Figure 4.6(d). Nonetheless, the conservative predictions of the model are still within the relevant order of magnitude and well capture the experimental trend of variation with the ER.

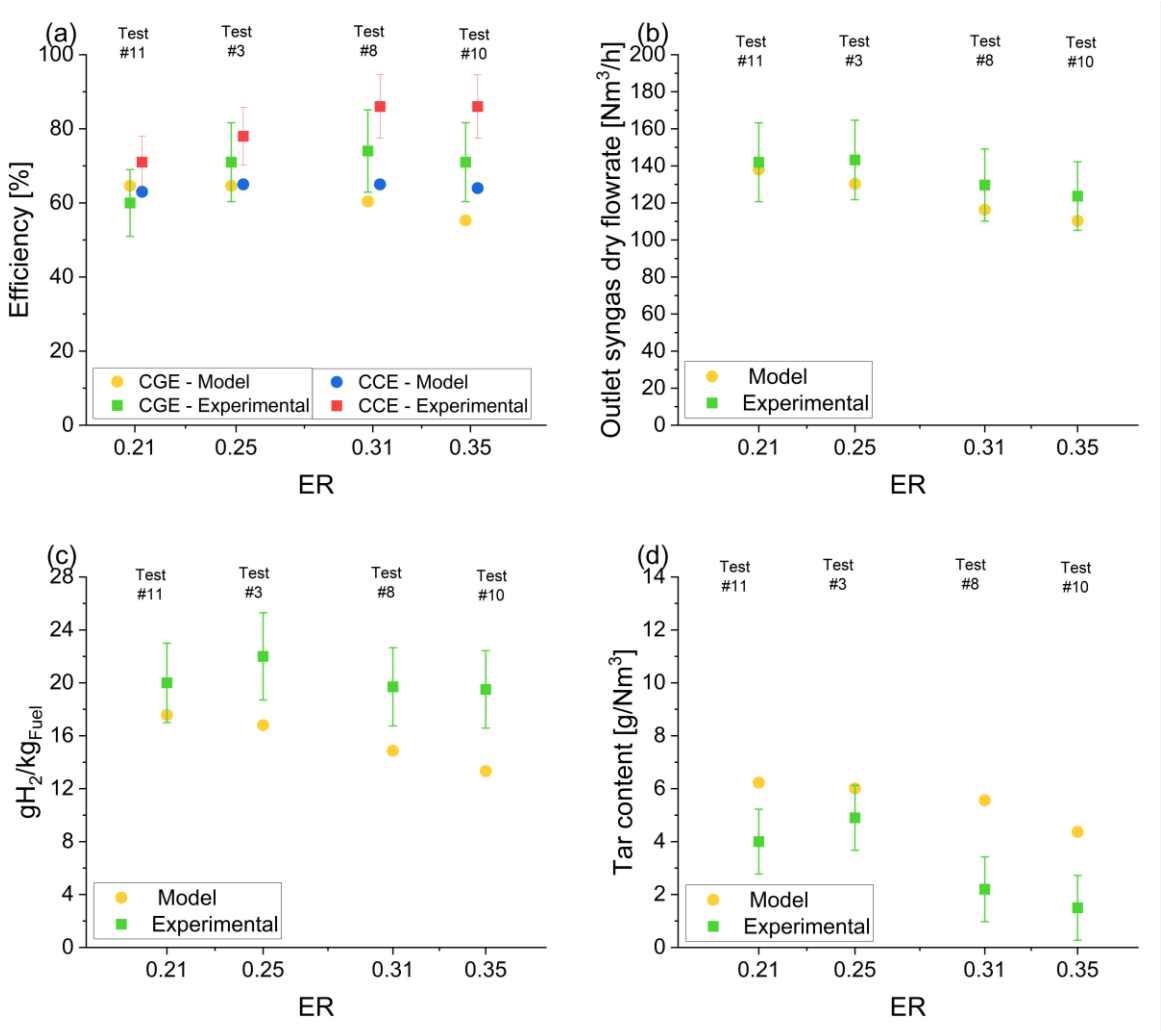

Figure 4.6 – Comparison between model results and experimental data of performance parameters of biomass gasification at different ERs. a) CGE and CCE, (b) outlet syngas dry flowrate, (c) specific yield of hydrogen and (d) tar content in the produced syngas.

These discrepancies can also be attributed to inherent experimental uncertainties as well as challenges in accurately analysing tar content, which is linked to the syngas composition. The lower predicted tar content in the model may indicate a higher conversion of heavier hydrocarbons into lighter species, contributing to the slightly lower syngas flowrate prediction.

4.5 Air gasification of plastic waste and biomass blends

4.5.1 Outlet gas composition

The predictive capabilities of the model have been further evaluated in the case of co-gasification of biomass (eucalyptus chips) and plastic waste (BluPolymer-L) blends across various ER (0.19-0.28). A systematic investigation of different compositions, from plastic only to biomass, demonstrated the versatility of the model in handling heterogeneous feedstock compositions, as reported in Figure 4.7, subject to the availability of relevant experimental data.

The predicted syngas compositions show good agreement with experimental data across all tested conditions, with notable accuracy levels given the inherent complexity of co-gasification processes. As with single-feedstock cases, nitrogen remains the dominant species (50-65%) due to air-blown operation, with the model adequately predicting its concentration. Despite this aspect appears trivial and not the main objective, it is worth considering how the N_2-dilution effect impacts the overall performance of the process and the relevant indicators, as analysed in Section 4.5.3.

Besides N_2, the relative proportions of light gases show subtle variations with changing feedstock ratios. Higher plastic content in the feed mixture affects the syngas composition with increasing amounts of light hydrocarbons. The model captures this trend reasonably well, although with slightly higher deviations compared to single-feedstock scenarios. The average error is well within 5% for the main species and below 10% for N_2. These marginally increased discrepancies can be attributed to potential synergistic interactions between the biomass and plastic components during co-gasification, which are not fully captured by the current model formulation. Nevertheless, the overall error remains within acceptable bounds, and the model successfully predicted the overall impact of varying both the ER and feedstock composition on the resulting syngas properties. This comprehensive validation across different operating parameters and varied feedstock compositions suggests that, despite the increased complexity compared to single-feedstock operations, the fundamental assumptions and mathematical formulation are robust enough to handle the increased complexity of multi-component feedstock systems.

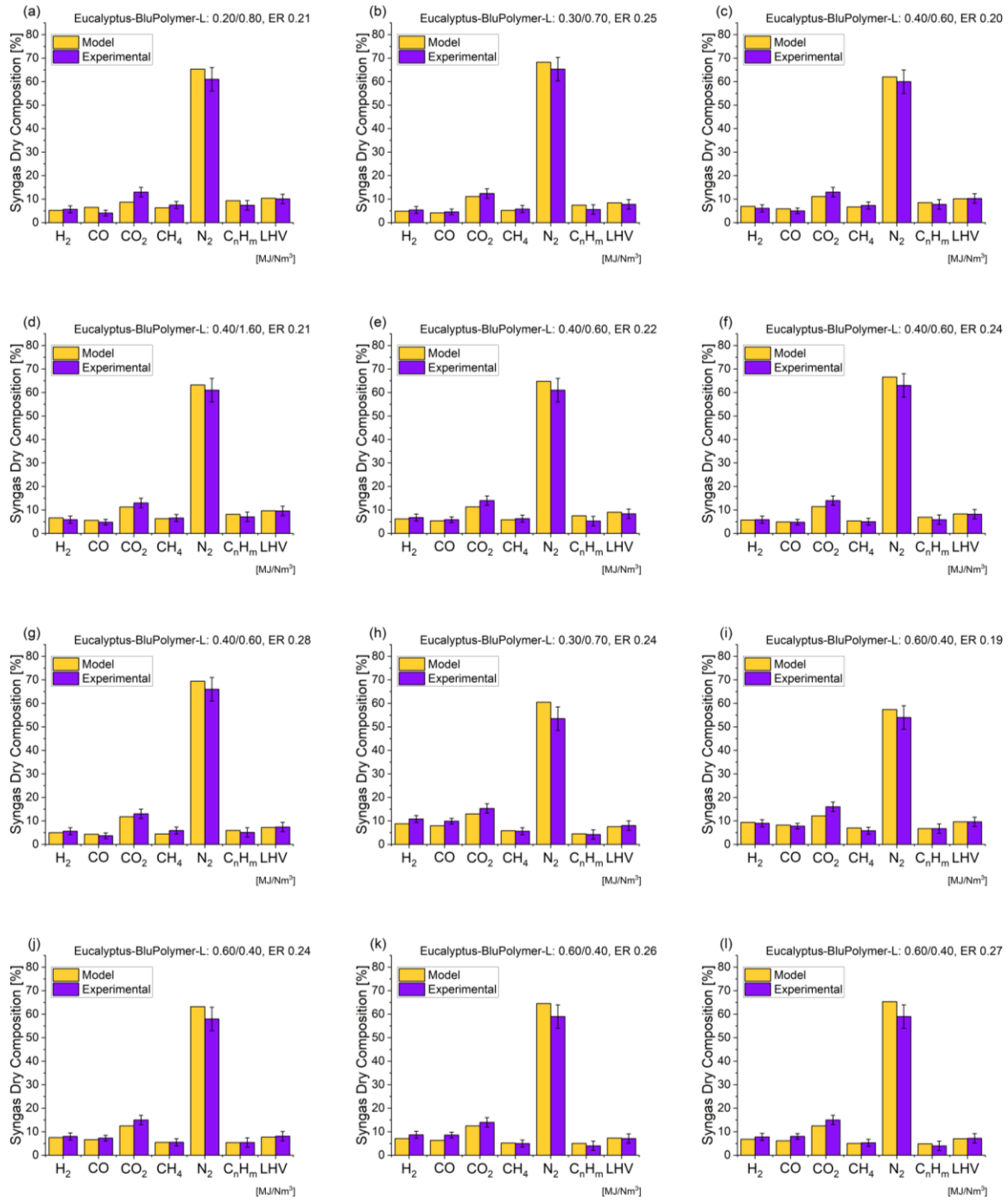

Figure 4.7 – Comparison between model predictions and measured data of syngas composition and heating value for air gasification of mixed feedstocks at different operating conditions of ERs and blending ratio

4.5.2 Temperature profile

Figure 4.8 reports an example of the temperature profile along the reactor for two different feedstock blends at ER 0.25. The predicted profiles show a good match with the experimental values throughout the length of the reactor. The model predictions are in line with experimental values for the bed temperature, with average bed temperatures below 850°C for both feedstock blends, with a

margin of 10°C difference predicted by the model, with higher temperature for the plastic-richer case. A similar order of magnitude of difference can be found at the outlet of the freeboard, with 710°C in the case of biomass-rich feedstock (Figure 4.8(a)) and 720°C for the specular plastic-rich case lower. The experimental values are around 732°C and 737°C respectively.

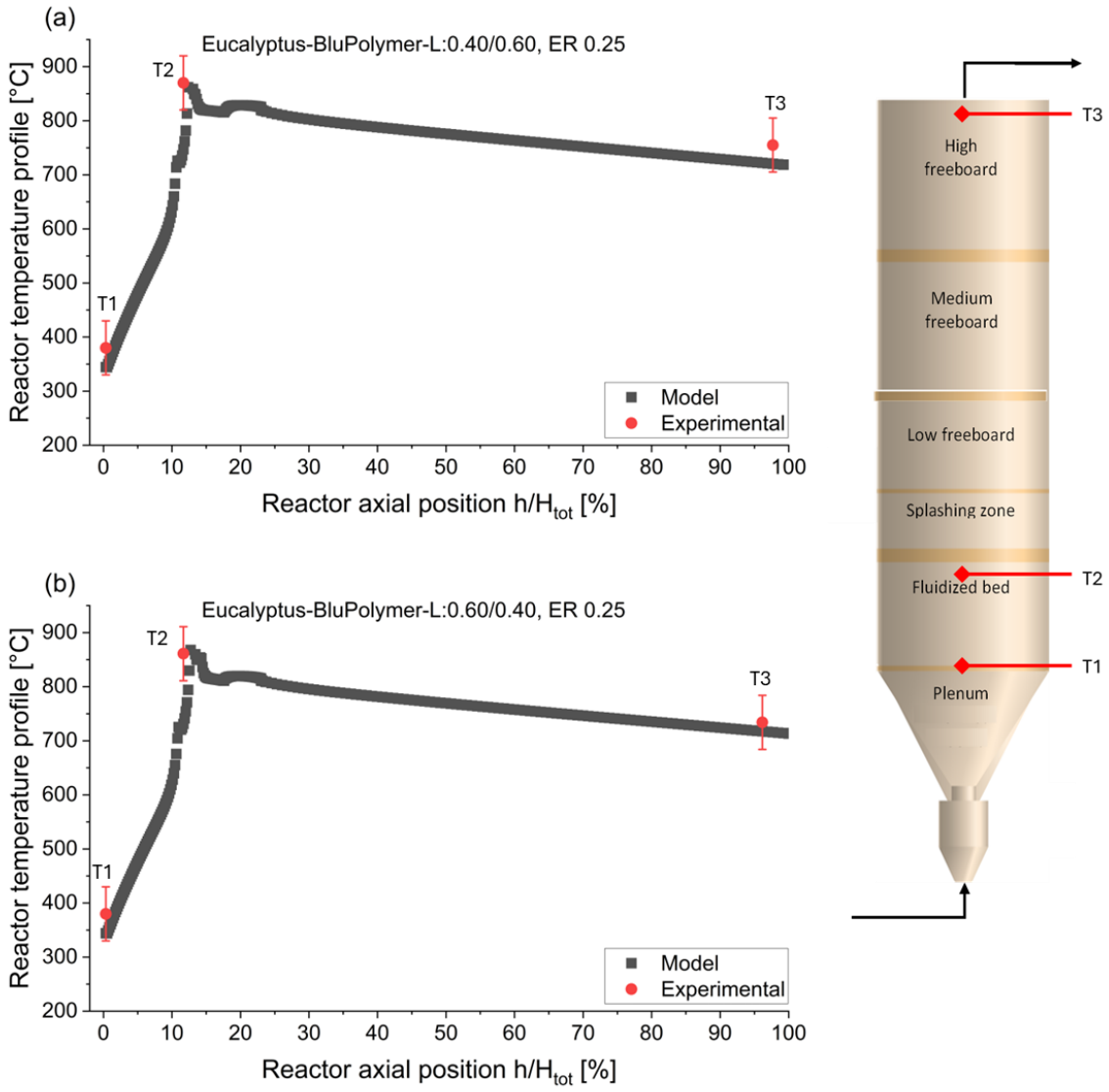

Figure 4.8 – Sample comparison between predicted axial profile and measured values of gasifier temperature for air gasification of mixed feedstocks at different blends. (a) 60 kg/h of 60% BluPolymer-L and 40% Eucalyptus, at. ER 0.25, and (b) 71 kg/h of 40% BluPolymer-L and 60% Eucalyptus, at. ER 0.25.

4.5.3 Process performance

The graphs presented in Figure 4.9 provide an insightful comparison between the experimental data and model results for various performance parameters of a gasification process that utilizes a blend of plastic waste and biomass as the feedstock at an equivalence ratio (ER) of 0.25. Overall, the gasification of mixed blends of biomass and plastics shows very good efficiency, consistent with the pure feedstock cases, with good conversion efficiencies with both CCE and CGE in the range of 60% to

80%. This result further supports the promising development of gasification as not only an alternative waste management solution, but also a key enabler for the recovery of natural resources and the generation of valuable commodities from the produced syngas.

The model predictions are in agreement with the experimental data, accurately capturing the experimental trends across the key performance indicators. Similarly to the case of pure biomass gasification (analysed in Section 4.4), the model has lower accuracy for the case of biomass-rich feedstock at predicting the CCE, while the CGE falls within the experimental variability (Figure 4.9(a)).

The model also provides an excellent match for the outlet syngas flowrate, as shown in Figure 4.9(b). While the values do not exhibit a clear trend due to the different conditions at which the reactor was operated, the model is still able to capture the observed behaviour. This could be attributed to the fact that, despite keeping the same ER, the amount of fuel feedstock was changed to operate the gasifier in safe conditions, which may have introduced some uncertainty.

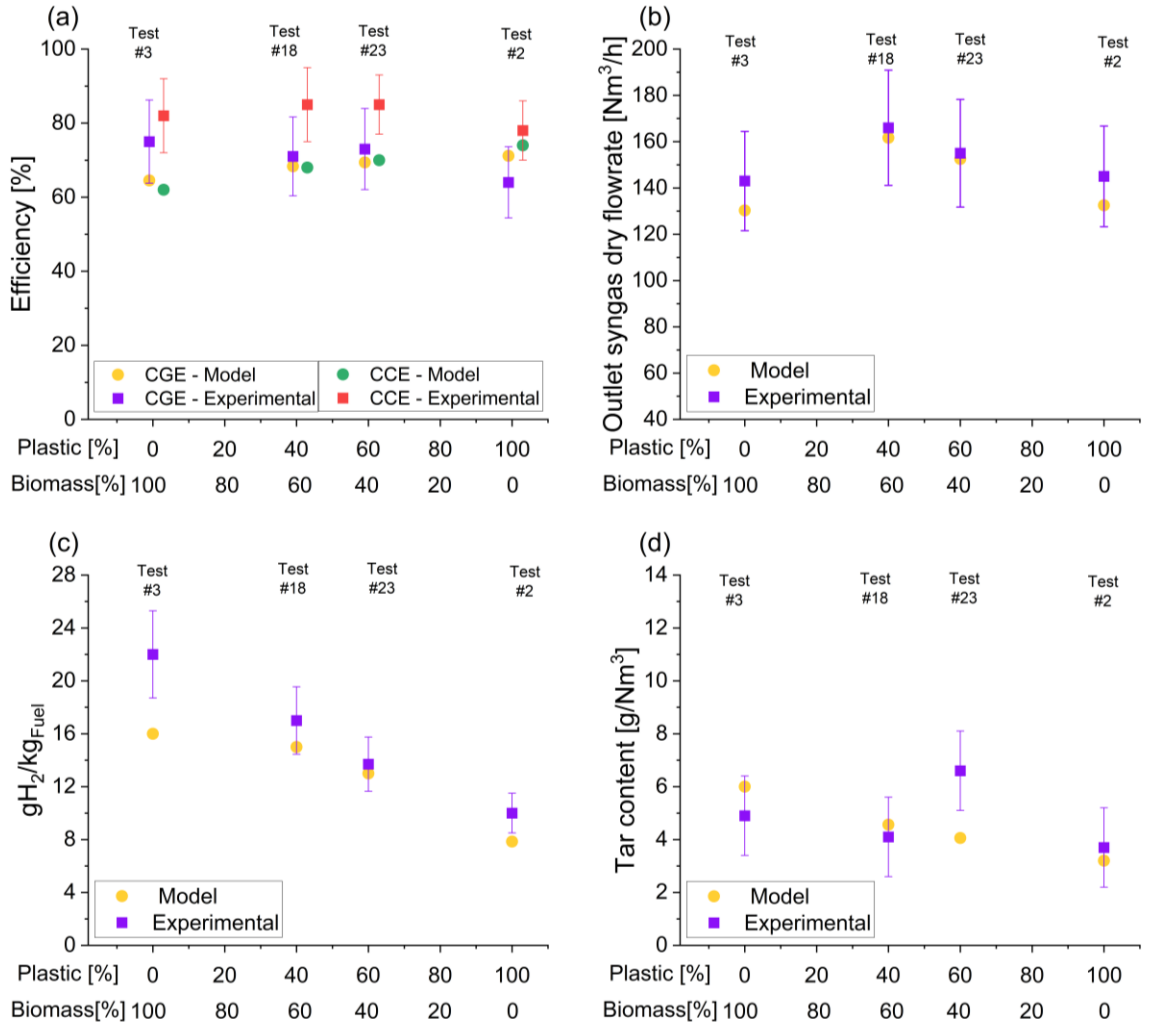

Figure 4.9 – Comparison between model results and experimental data of performance parameters of mixed feedstock gasification at different blending ratios and ER 0.25. (a) CGE and CCE, (b) outlet syngas dry flowrate, (c) specific yield of hydrogen and (d) tar content in the produced syngas.

Nonetheless, the model demonstrates a good match with the H_2 production and tar content trends, as presented in Figure 4.9(c) and (d). Interestingly, the model predicts lower tar content for higher plastic waste content in the feedstock. This could be attributed to the differences in the polymeric structure of the feedstock, where the easier cracking of polyolefins in the plastic waste may lead to lower tar formation compared to the more complex organic structures found in biomass. These initial observations on the effect of feedstock composition and blending ratio spurred further systematic investigation on syngas composition, process performance and the nature of tar compounds, as can be found in Section 4.7.2.

4.6 Process modelling analysis

One of the strengths of the model is the ability to provide precise information along the axial profile of the gasifier, both with respect to chemical species and temperature. This section analyses how the modelling approach affects the axial profiles, reflecting the operations of the bubbling fluidized bed with biomass at ER 0.25.

4.6.1 Axial profiles of syngas composition

The graphs presented in Figure 4.10 to Figure 4.12 provide insights into the complex multi-phase phenomena occurring within the fluidized bed section of the gasification system. Figure 4.10 shows the flowrates of the species inside the bubbling fluidized bed, split according to the three phases modelled to represent the bed. Three distinct phases are shown: the solid-free bubble phase, the solid-rich emulsion phase, and the endogenous bubble phase. The mass transfer between these phases is determined by the differences in concentrations of the chemical species. This is further enhanced by the close contact between phases, a typical feature of fluidized beds, and determined by the size of the bubbles.

At the inlet of the fluidized bed (for $h/H_{tot} = 0$), the injection of air results in a high concentration of N_2 and O_2 in both the bubble and emulsion phase, with the split depending on the fluidization regime. All gas species in the endogenous bubble phase are instead zero in the low bed region, reflecting the profile of volatiles release as described in Section 3.2. The gas species in the endogenous bubble phase gradually increase moving upwards in the bed, peaking at the feeding point towards the surface of the bed. The chemical species produced by devolatilization are gradually transferred to the bubble and emulsion phase, where they are mixed and react with O_2 in combustion reactions. This is shown by the reduction of O_2 in the emulsion phase (Figure 4.10(b)) with the corresponding increase in CO and CO_2 levels. This trend indicates the progression of combustion and pyrolysis reactions taking place within the bed. Concurrently, the continuous consumption of O_2 in the emulsion phase further

promotes the transfer of additional O_2 from the surrounding bubbles (Figure 4.10(a)). This complex dynamic of interphase mass transfer is crucial for the operations of the fluidized bed to ensure efficient utilization of the reactants and optimizing the overall gasification performance.

Figure 4.11 shows the molar flowrates of chemical species in the splashing zone, where two distinct gas phases interact above the bed surface. As described in Section 3.4, when bubbles erupt upon reaching the bed surface, they gradually entrain and incorporate the gas stream emerging from the emulsion phase. This entrainment process is reflected in Figure 4.11(b), which shows a progressive decrease in the main gas stream flowrates until complete mixing is achieved at the splashing zone's upper boundary. The gas stream, as it becomes incorporated into the ghost-bubble phase, continues to participate in ongoing chemical reactions.

The approach followed to model the gas behaviour in the splashing zone exemplifies the complex interplay between hydrodynamics and chemical kinetics in fluidized bed gasification. The continuous exchange of chemical species between phases occurs simultaneously with chemical reactions, creating a dynamic environment where mass transfer and reaction rates are intimately coupled. Understanding these complex multi-phase interactions is essential for accurate process modelling and optimization, as well as for the design and operation of the gasification system, ultimately improving its efficiency and overall performance.

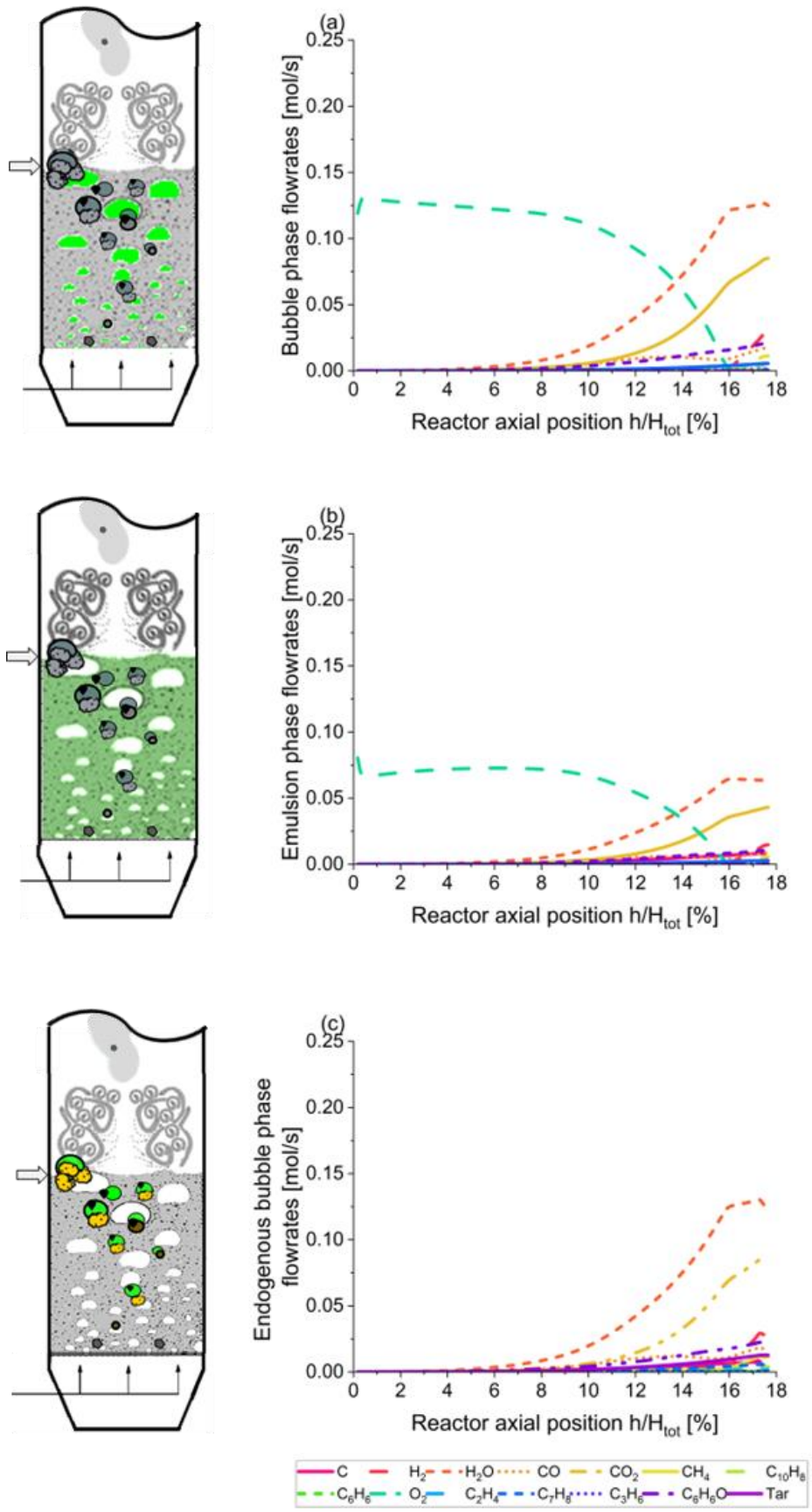

Figure 4.10 – Chemical species flowrate in the different phases of the fluidized bed for biomass gasification at ER 0.25. (a) bubble phase, (b) emulsion phase and (c) endogenous bubble phase. The relevant phase is highlighted in green in the schematics on the left-hand side of each graph.

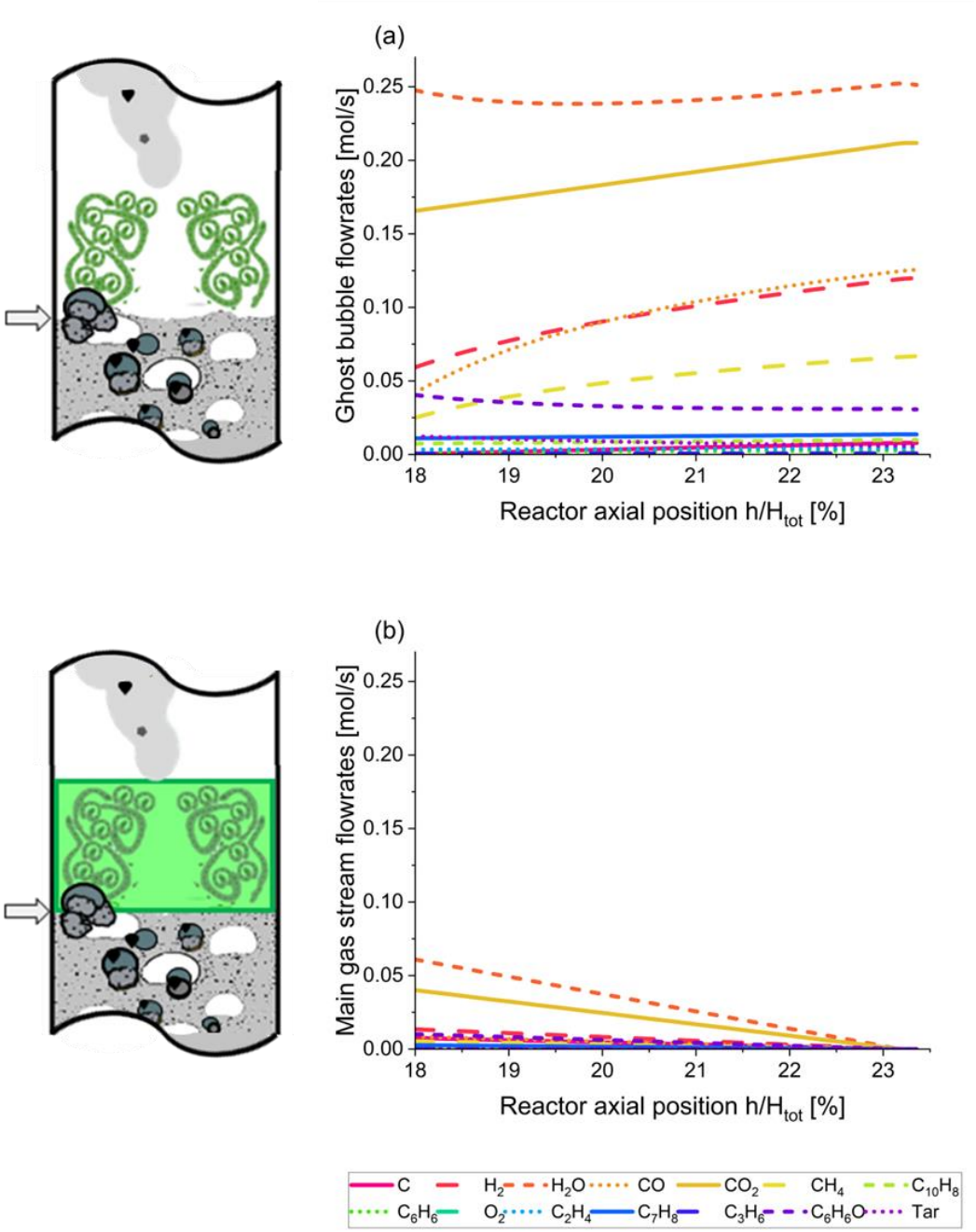

Figure 4.11 – Chemical species flowrate in the different phases of the splashing zone for biomass gasification at ER 0.25 (a) ghost-bubble phase and (b) main gas stream. The relevant phase is highlighted in green in the schematics on the left-hand side of each graph.

A detailed profile of light species and hydrocarbon content at different gasifier levels is shown in Figure 4.12.

Heavy hydrocarbons (represented by the C7+ class) are at their peak in the splashing zone, affected by the direct release of devolatilization products, characterized by 45% wt. of the feedstock transformed into heavy hydrocarbons and tar species. Despite the high temperatures generated on

the bed surface, the conditions are not sufficient to ensure the complete cracking/reforming of the heavier molecules. As the gas moves along the freeboard, heavy hydrocarbons are progressively converted to lighter species, including benzene and phenol, and mostly light alkenes (ethylene and propylene) and single-ring cyclic compounds (e.g. Cyclobutadiene and cyclopentadiene). Despite the high temperatures and reactive atmosphere, the concentration of benzene remains stable along the freeboard, due to the high stability associated with the chemical structure of benzene and aromatic compounds, with the concentration increasing as the result of cracking of the heavier species.

These results show the critical importance of the freeboard in ensuring adequate residence time for reforming and slower depolymerisation reactions to take place, although the residual tar content (4-6 g/Nm^3) demands additional tar conversion and/or removal actions for the use of syngas in chemical recycling applications.

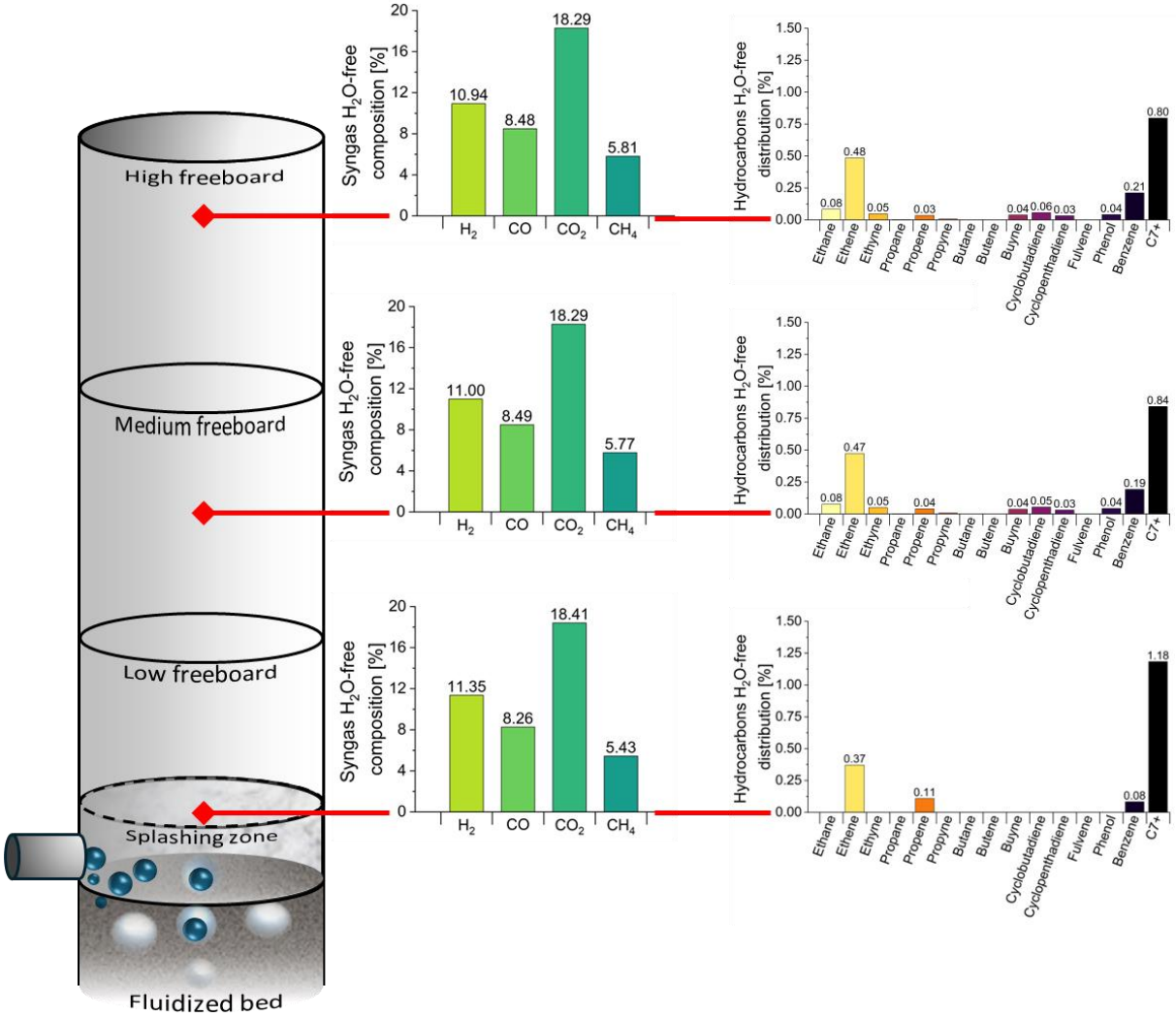

Figure 4.12 – Light gas and hydrocarbons profile in the freeboard of the gasifier. 80 kg/h of Eucalyptus, at ER 0.25.

4.6.1.1 Tar distribution

A more detailed distribution of C7+ species is reported in Figure 4.13, often reported in the literature as a percentage of the condensable liquid phase [197,198]. The results refer to the biomass air gasification at ER 0.25. The distribution appears to be influenced by toluene and naphthalene being the tar-representing species used in the model. This broader distribution in the model results suggests that the kinetic mechanisms for tar evolution and breakdown may need refinement, particularly for primary tar species, despite the most common approach in the literature of adopting one compound to represent the tars, either toluene, phenol or naphthalene, while in this work all three of them have been included.

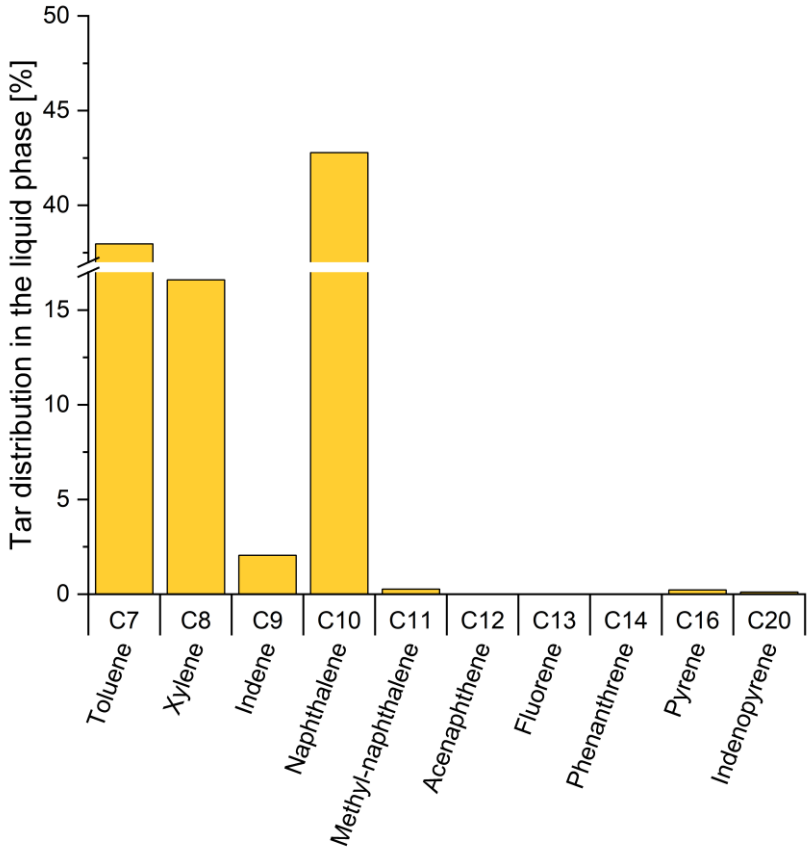

Figure 4.13 – Tar distribution as a percentage of the condensable liquid phase.

Figure 4.14(a-e) shows the comparison of absolute rates of production of the different tar-representing species and heavy hydrocarbons as calculated by the freeboard model developed on Chemkin-pro. The column presents the values of the global rate of reaction, proportional to the length of the bars. The negative values indicate reactions that lead to the depletion of the considered species, while the positive ones are those in which the species is produced. The figure confirms the intricate pathway of reactions involving tar species, although these are mainly associated with cracking to produce lighter species. Figure 4.14(f), instead, shows the rate of production analysis of steam. As

expected, since the gasifier is operated with air, the rates of reaction are limited and involve the moisture and secondary steam produced by the other reactions.

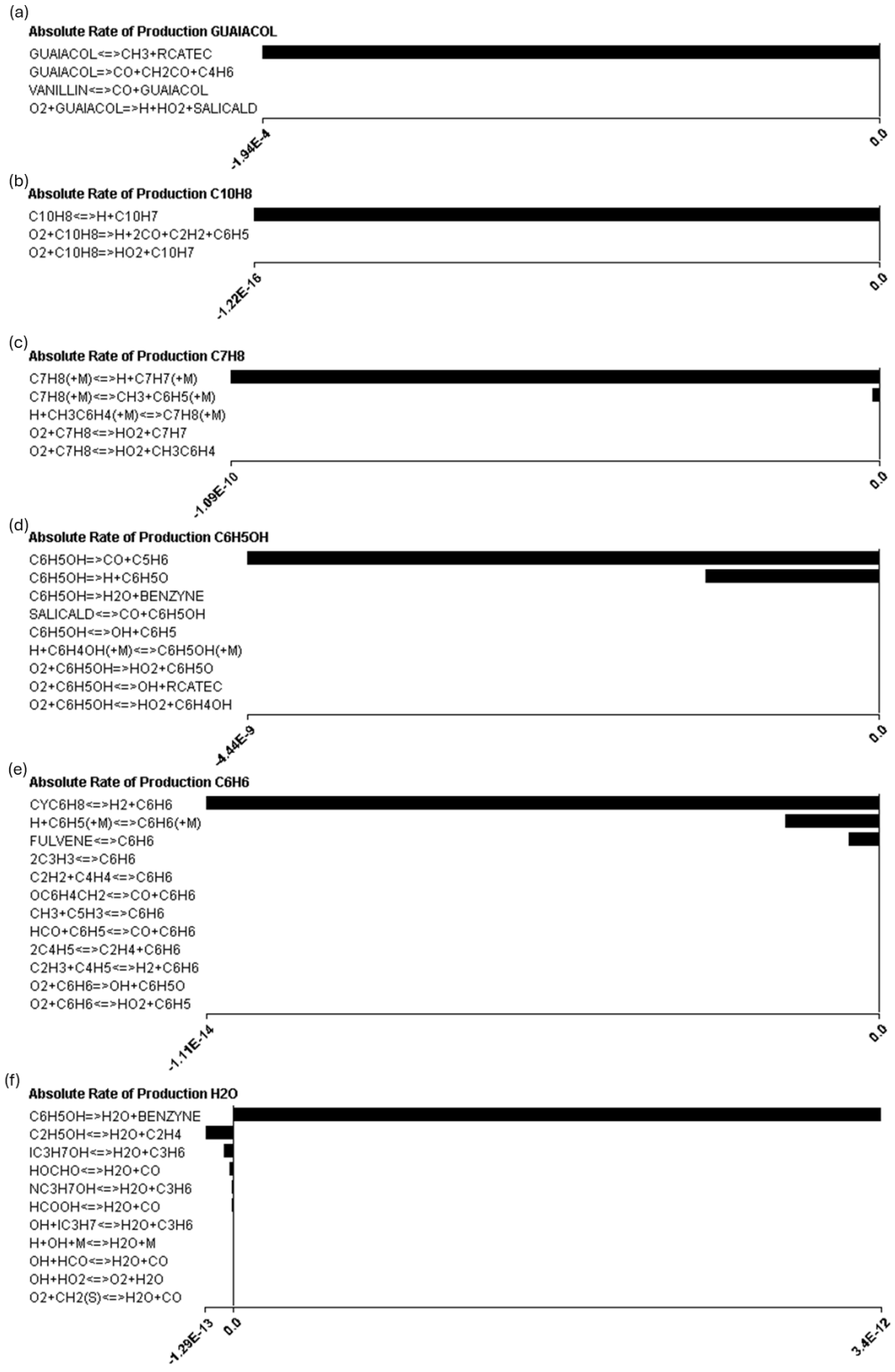

Figure 4.14 - Rate of production analysis (kmol m^{-3} s^{-1}) of different tar species (a-e) and steam (f).

4.6.2 Axial temperature profiles

The model demonstrated good predictions of the axial temperature profiles within the gasifier, with a trend in line with experimental values, despite the limited availability of experimental data. As shown in Figure 4.15, all feedstock configurations exhibit a characteristic sharp temperature increase in the upper regions of the fluidized bed, a phenomenon caused by the combined effects of feedstock segregation patterns and the localized release of volatile matter. Furthermore, the extent of the sharp peak is higher in the case of pure biomass gasification, as a result of the higher degree of segregation of the feedstock particles towards the surface of the bed and the overall pattern of volatiles release.

At the same equivalence ratio (ER) of 0.22 for all three cases, the temperature profile in the bed for the Eucalyptus-BluPolymer-L blend (50:50) falls between those of pure biomass and pure plastics gasification. However, a different trend is predicted in the freeboard, where the blend shows overall lower temperatures. This appears to be the result of combining the temperature profiles of plastic and biomass, although not as a straightforward linear combination. These variations in the thermal profiles underscore the complex interplay between feedstock composition, residence time, and heat transfer mechanisms during co-gasification processes, highlighting the capability of the model to capture such non-linear thermal behaviours.

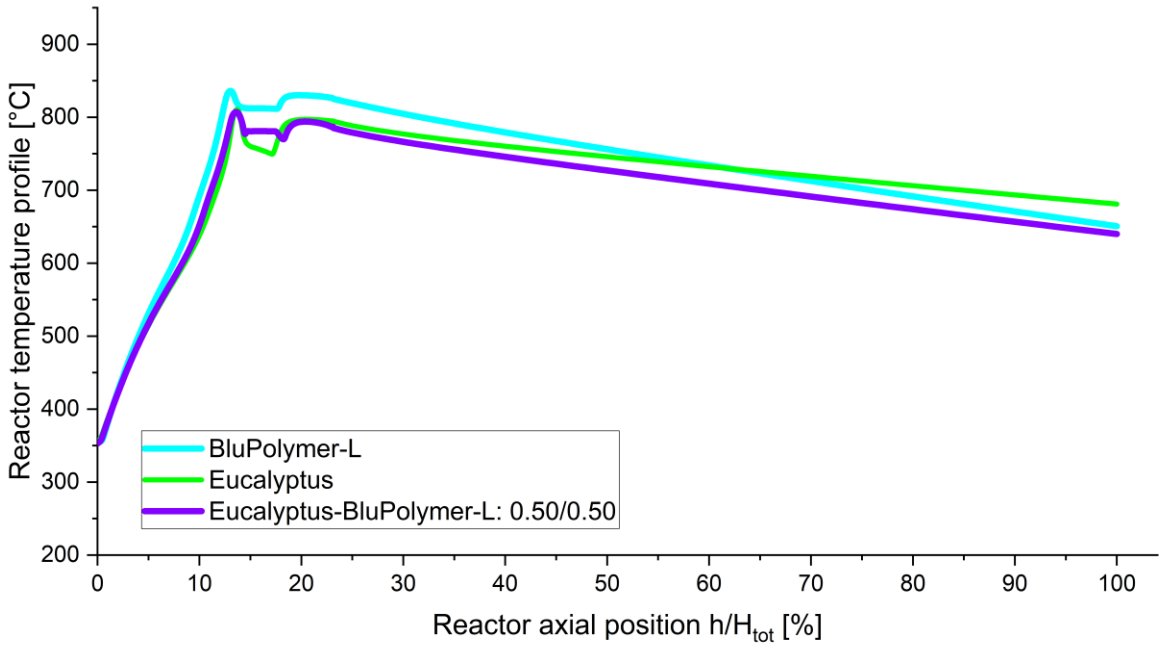

Figure 4.15 – Model predictions of axial temperature profiles for (a) biomass, (b) plastics and (c) 50% plastics and 50% biomass, at ER 0.22 and a total waste energy throughput of around 300 kW.

4.7 Analysis of the effect of operating parameters on process performance

The validated model has been utilized to investigate how key design parameters affect the air-gasification process, with a particular focus on the amount of oxygen and the impact on temperature profiles, distribution of hydrocarbons and composition of tars. This systematic analysis of the effect of ER provides insights into the complex relationships between operating conditions and gasifier performance, enabling the prediction of optimal parameters based on specific end-use requirements for the syngas, whether for power generation, chemical synthesis, or other industrial applications.

Following the ER, the effect of feedstock composition has been examined, in the form of the blending ratio between plastic waste and biomass. This analysis is particularly relevant as the interaction between these dissimilar materials during co-gasification can significantly influence the process dynamics. The plastic fraction in the feedstock bled has been varied while maintaining other operating conditions constant, i.e. ER at 0.25 and waste throughput, the model enabled the identification of synergistic and antagonistic effects on temperature profiles, gas composition, and overall performance indicators. This approach provides valuable insights for optimizing feedstock formulations in practical applications, especially considering the growing interest in waste-to-energy solutions that can handle multiple feedstock types.

4.7.1 Effect of ER

In air-based gasification systems, the ER serves as the primary control parameter that governs the process performance. As demonstrated in Figure 4.16, variations in ER significantly impact both the temperature profile and the resulting gas composition. When operating at higher ER values, the enhanced oxygen availability promotes exothermic oxidation reactions, especially towards the surface of the bed where the bulk biomass decomposition occurs. Increasing the ER leads to an expected reduction in the concentrations of valuable combustible components such as H_2, and CH_4 in the output stream, with a concurrent moderate increase in CO_2. The intensification of combustion reactions induced by the higher ER results in elevated bed temperatures (Figure 4.16(b)), as expected by the autothermal operation of the gasifier. The model predictions show that temperature increases from 750°C to 850°C in the bed and from 770°C to 890°C in the splashing zone, approaching critical values that would trigger the shutdown of the reactor. With increasing ER values, the syngas heating value showed a marked decrease (Figure 4.16(c)). This trend stems from the enhanced oxygen availability promoting complete oxidation reactions over partial oxidation, at the expense of combustible species like CO and H_2. This is further exacerbated by the resulting high temperatures promoting further reactions. This trade-off between conversion and gas quality represents a key consideration in optimizing the gasification process. Nonetheless, the syngas heating value maintains a favourable

threshold around 4 MJ/Nm^3 up to ER 0.34. Based on these findings, optimal gasification performance for Eucalyptus chips can be achieved within an ER range of 0.25-0.30, where the efficiencies are balanced (Figure 4.16(d)).

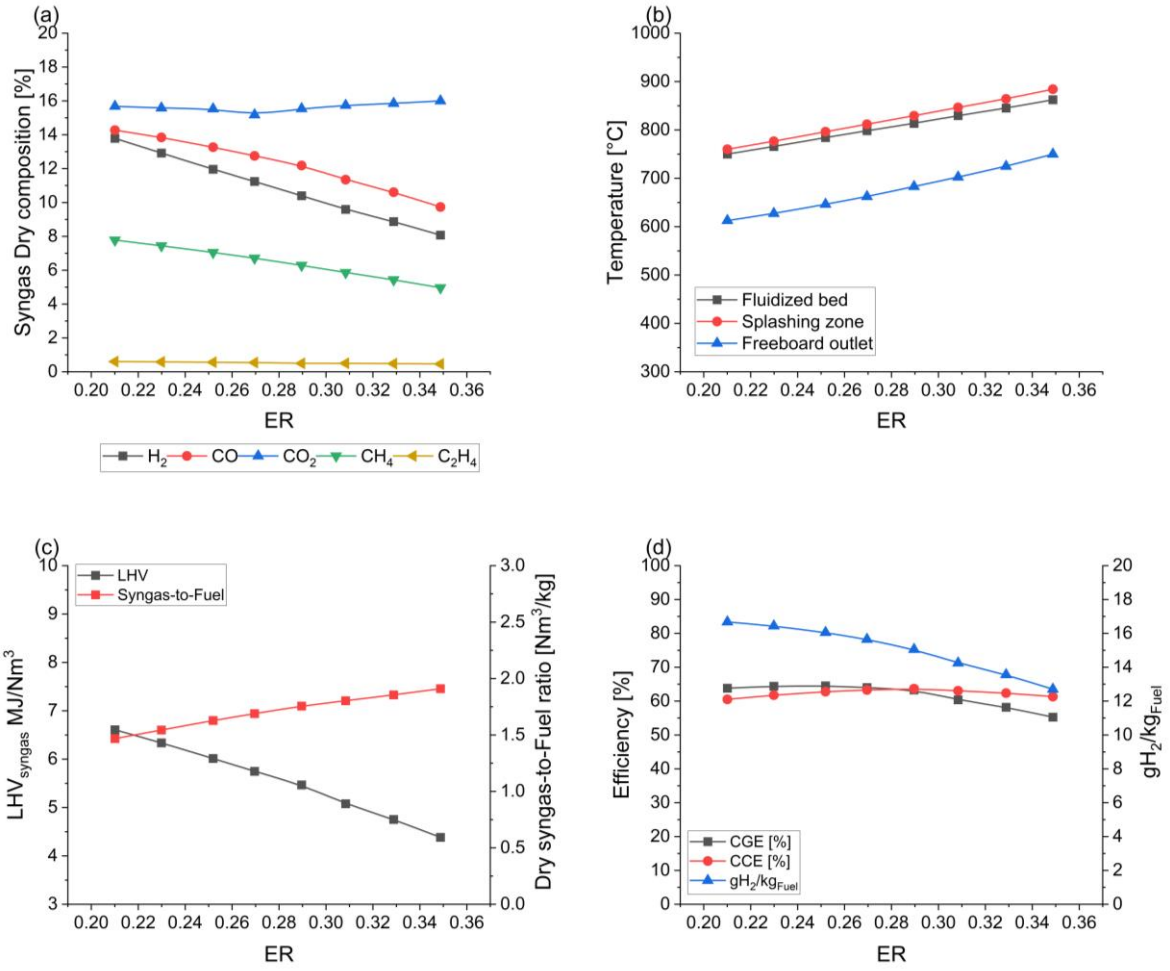

Figure 4.16 – Model predictions of different performance indicators for biomass gasification as a function of the ER for (a) Syngas composition at the reactor exit, (b) reactor temperature in the bed and splashing zone and exit, (c) syngas heating value and syngas volumetric flow ratio, (d) CGE, CCE and specific yield of hydrogen.

Figure 4.17(a) shows how the increase in ER affects also the distribution of hydrocarbons (in Figure 4.17(a)) and tar species (Figure 4.17(b)). Higher ER results in the reduction of hydrocarbon content, especially C7+ and tars. This is attributed to the combined effect of the increase in combustion reactions and enhanced cracking of heavy hydrocarbons promoted by the higher temperatures. This is supported by the profiles of variation of the gas species shown in Figure 4.16(a), where a smaller slope of reduction is predicted for light hydrocarbons (CH_4 and C_2H_4) than the other species. This suggests that the light hydrocarbons produced by tar cracking partly counterbalance the expected reduction caused by combustion and dilution effects (associated with the higher amount of CO_2). A further interesting trend is revealed for the tars distribution in Figure 4.17(b), whereby the reduction

of total tar content appears to be mostly at the expense of the lighter fractions (C7 and C8), while the amount of heavier compounds remains significant.

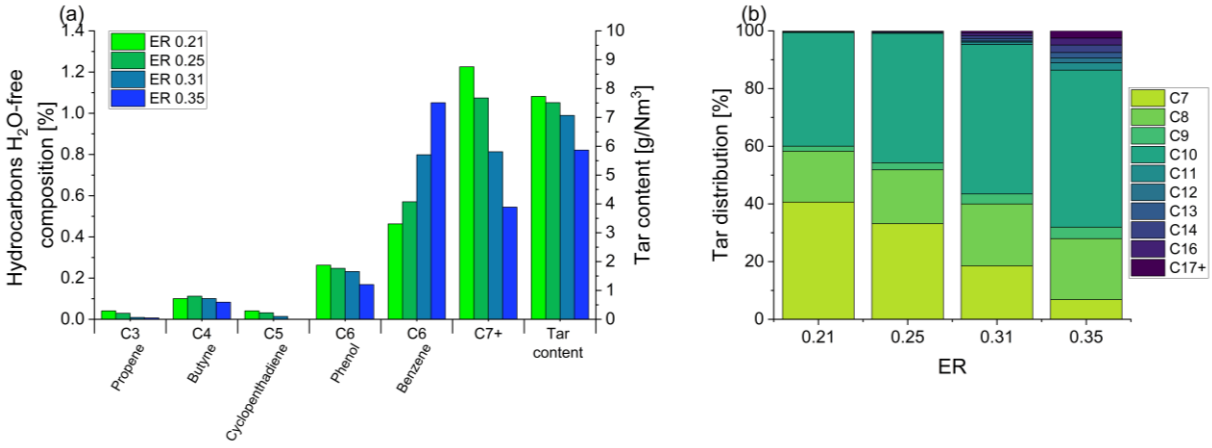

Figure 4.17 – Analysis of heavier hydrocarbons content as a function of the ER. (a) Hydrocarbons C3+ H_2O-free composition and tar content, and (b) specific tar distribution in the C7+ class.

4.7.2 Effect of feedstock composition

The effect of different compositions and biomass/plastics blends has been investigated, analysing the model projections for syngas composition, process performance and tar distribution at ER 0.25. The result of this analysis is reported in Figure 4.18 and Figure 4.19.

Examining the syngas composition in Figure 4.18(a), the data reveal a notable reduction in the hydrogen content as the plastic fraction in the feedstock increases, counterbalanced by a significant increase in the light hydrocarbon (HC). This seems to reflect the differences in chemical structures of the two feedstocks, whereby polyolefins are characterized by simpler hydrocarbon monomers (e.g. ethylene), which tend to be released as constituent monomers from the polymeric. The large differences observed in the hydrocarbon composition are a direct consequence of this feedstock characteristic.

These differences in composition are also reflected in the increase in heating value (Figure 4.18(c)) of the syngas produced with plastic-rich blends, due to the higher quantity of light hydrocarbons and lower inerts (e.g. CO_2). The specific volumetric flowrate of the syngas is observed to increase with higher plastic content in the feedstock Figure 4.18(b). This is likely due to the higher volatile matter content (>96%) in plastics compared to the more complex structure of biomass, which results in a higher proportion of volatiles being released during the gasification process. Consequently, for the same amount of feed, the syngas volumetric flowrate is higher when processing a feedstock with a greater plastic fraction.

Despite the concurrent increase in LHV and outlet flowrate, the CGE shows a rather stable trend, with a moderate increase from 65% to 71%. This is due to the significant differences in heating value between plastic and biomass. While the BluPolymer-L has a very high heating value (around 38 MJ/kg), to the point of posing serious safety technical operating issues, biomass, on the other hand, has a much lower LHV due to its higher proportion of inert compounds.

Finally, the differences in temperature profiles can be attributed to the combined effects of lower syngas flowrates for plastic-rich feedstocks, which may result in shorter residence times, as well as the potential for higher endothermic conversion of tars due to the increased light HC content.

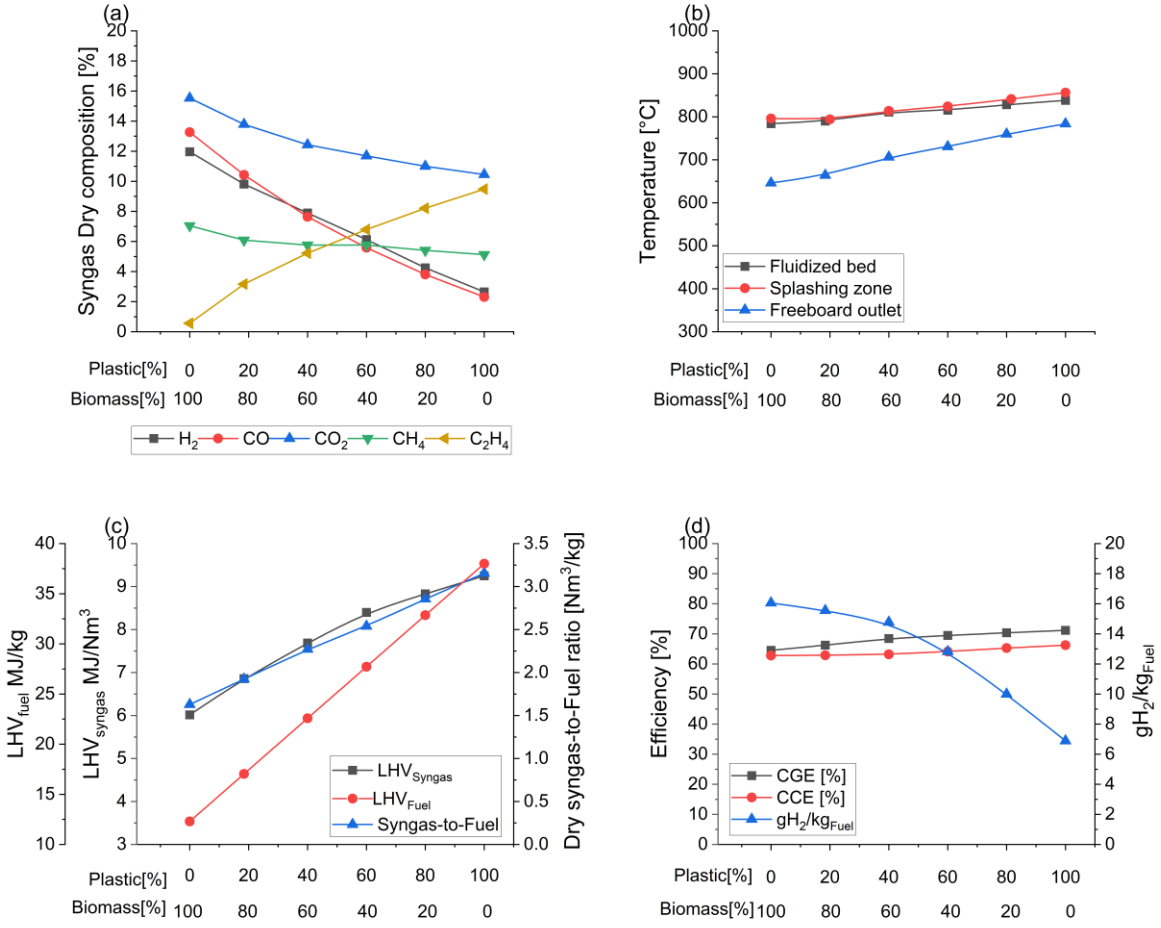

Figure 4.18 – Model predictions of different performance indicators for mixed feedstocks gasification as a function of the blending ratio, with ER 0.25. (a) Syngas composition at the reactor exit, (b) reactor temperature in the bed and splashing zone and exit, (c) syngas heating value and syngas volumetric flow ratio, (d) CGE, CCE and specific yield of hydrogen.

Figure 4.19 presents a detailed analysis of heavy hydrocarbon content as a function of feedstock composition, a crucial factor for successfully integrating the gasifier in waste-to-H_2 processes. The model predictions show higher amounts of light and medium-weight hydrocarbons at higher plastic content in the feedstock, which aligns with the observed trend for ethylene content in the syngas.

The model predicts an opposite trend for tar species (hydrocarbons heavier than benzene), showing decreased total tar content with increasing plastic fraction. While this might initially suggest

that operating with higher plastic fractions could be advantageous for reactor thermal stability, a deeper analysis reveals a more complex scenario.

Nevertheless, as shown in Figure 4.19(b), despite lower total tar content, feedstocks with higher plastic fractions generate tars with a larger proportion of heavier components. This shift in tar composition could potentially create operational challenges, even with reduced total tar quantities.

This nuanced understanding of the hydrocarbon distribution, as captured by the model predictions, highlights the importance of considering both the quantitative and qualitative aspects of the tar formation during the design and optimization of such waste-to-H_2 gasification systems.

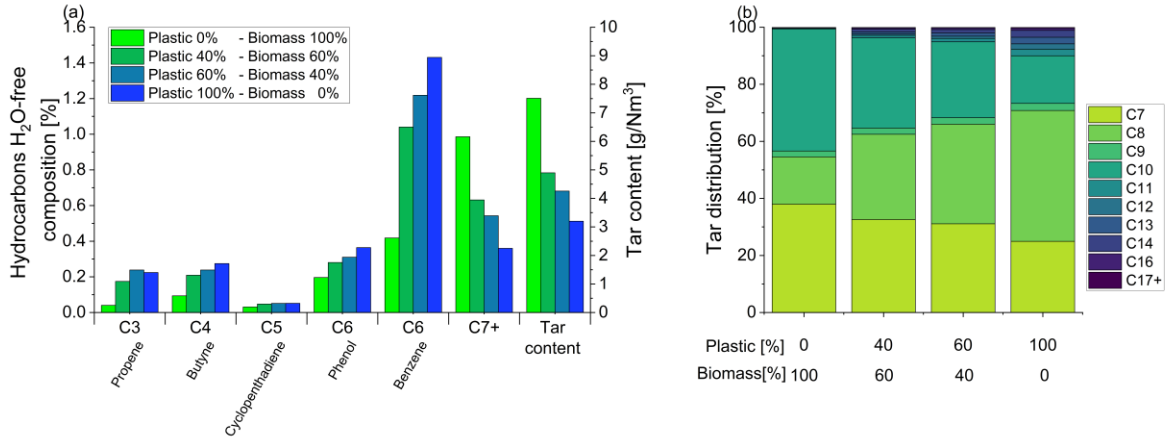

Figure 4.19 – Analysis of heavier hydrocarbons content as a function of the blending ratio, with ER0.25. (a) Hydrocarbons C3+ H_2O-free composition and tar content, and (b) specific tar distribution in the C7+ class.

4.8 Concluding remarks

The developed one-dimensional, steady-state, two-phase model for bubbling fluidized bed gasification has been extensively validated with real plant data from a large-scale air-blow fluidized bed gasifier using different feedstocks and operating conditions. By incorporating the critical parameters of a bubbling fluidized bed and the relevant chemical reaction pathways, the model effectively reproduces the gasification of plastic waste, biomass and mix of the two feedstocks in a FBR. In particular, the accurate representation of the secondary tar reforming reactions occurring in the freeboard by means of an expanded set of chemical species and reactions, allowed for a more in-depth investigation of tars formation and secondary reactions, which is one of the challenges in thermochemical conversion processes, and the main bottleneck for the large-scale deployment of gasification technologies of low-value feedstock.

The validated model was used to predict and assess the fundamentals of gasification in a bubbling fluidized bed, as well as investigate the operations of the gasifier at different conditions and can be summarized as follows:

- **Axial profiles.** The model provides comprehensive and accurate information regarding the concentration and temperature axial profiles. The three-phase approach followed to model the fluidized bed highlights the crucial balance of complex phenomena of mass transfer between the phases. Furthermore, the predefined pattern release of volatiles effectively captures the feedstock segregation behaviour without disrupting the fluidization regime. This is reflected also in the temperature profile, which shows a sharp increase through the bed despite the common assumption of constant isothermal operations. In addition, the model balances the endothermic reactions and heat losses accurately predicting the temperature profile in the freeboard and the outlet syngas.

- **Effect of ER**. The model effectively predicts the influence of ER on the gasification process, providing valuable insights for process optimization and design. While higher ER values lead to reduced tar content, the remaining tar levels are still significant enough to warrant investigation of alternative or additional mitigation strategies. Moreover, high ER values result in temperatures approaching 900°C, which raises safety concerns and should be avoided. The optimal gasification performance is achieved within an ER range of 0.24-0.28, where a satisfactory balance of CGE and CCE is reached.

- **Effect of feedstock composition.** The co-gasification of plastic and biomass blends presents promising opportunities for resource recovery and waste-to-X processes. The model effectively captures how different feedstock compositions influence gasifier performance, providing crucial insights into necessary process adjustments and trade-offs. Plastic-rich feedstocks yield syngas with lower H_2 and CO content compared to conventional gasification processes but produce higher amounts of light olefins and greater heating values. Conversely, biomass-rich feedstocks generate syngas with higher H_2 and CO fractions, though the increased tar content necessitates additional removal strategies. This understanding of composition-dependent behaviour is essential for optimizing process conditions based on available feedstock and desired product specifications.

Chapter 5. Steam Oxygen gasification of biomass and plastics in large-scale fluidized bed reactors

This chapter presents the results of the model predictions for large scale fluidized bed gasifiers using steam-oxygen/air as gasification agent, and converting various types of feedstocks. The model is firstly extensively validated with experimental results, showing excellent predictive capabilities with regards the composition of the outlet syngas, temperature profile and relevant process performance parameters. The model allows for detailed investigation of all feedstocks considered in this work, both biomass and plastic-derived fuels and their blends. Great emphasis is given to the role of steam as gasification agent, with the main interest in the feasibility and implications of replacing N_2 with steam. Therefore, the model has been used to investigate the range of operability of fluidized bed reactors to identify the most suitable conditions, depending on the design specifications and the preferred application, providing interesting insights on trade-offs regarding the use of steam in this kind of processes.

Parts of this chapter have been published in:

Parrillo, F., Ardolino, F., Calì, G., Pettinau, A., Materazzi, M., Sebastiani*, A., & Arena, U. (2024). Plastic waste gasification using oxygen-enriched air and steam: Experimental and model results from a large pilot-scale reactor. *Waste Management*, *183*, 53–62. https://doi.org/10.1016/J.WASMAN.2024.04.045.

*Corresponding author

Sebastiani, A., Parrillo, F., Ardolino, F., Arena, U., Iannello, S., Materazzi, M. (2025). Modelling of Oxygen-Steam Gasification of Waste Feedstock in Industrial Fluidized Bed Reactors. *Chemical Engineering Journal*, *506*, 159763. https://doi.org/10.1016/J.CEJ.2025.159763

5.1 Introduction

Autothermal gasification can be carried out with air, air and steam, or mixtures of air, steam, and pure oxygen. Most large-scale plants operate with air as the gasification agent due to its simplicity and established operational knowledge. However, for the new-generation gasification systems to generate hydrogen and fuels, the operation in the absence of nitrogen is important to reduce the cost of downstream separation [52,199]. This requires the process to employ steam and oxygen as main fluidizing gases as opposed to air, and the operational experience of industrial waste-fuelled fluidized bed reactors on steam and oxygen is still immature. Therefore, the transition to steam-oxygen operations is done gradually by enriching the gasification agent with oxygen and steam. This staged shift helps manage the operational challenges related to steam and improves the understanding of the process.

Under autothermal conditions, the temperature is a state variable of the system, and it is the result of the reacting system to the imposed values of operating parameters [200]. Nonetheless, the temperature values are bounded within an admissible range, mainly related to the reactor material strength (at the higher end) and the optimal progress of gasification reactions (at the lower end). The relevant operating parameters to be considered depend on the gasification agent used in the system. When air is the only gasifying (and fluidizing) agent, the only operating parameter is the equivalence ratio (ER), which is an essential parameter that quantifies the oxygen needed to promote the necessary partial oxidation reactions. The use of oxygen-enriched air, instead, introduces a further parameter of enrichment ratio, represented by the oxygen molar concentration in the air stream. In the case of steam-oxygen, the additional parameter StC (steam-to-carbon molar ratio, defined in Section 3.10), should be taken into account [22,201]. The temperature of the reactor remains a state variable of the system, however, the role of thermal moderator has to be performed by the steam, due to the reduced content or absence of nitrogen. As a consequence, the inlet steam-to-oxygen molar ratio (StO_2) becomes an important parameter. StO_2 is often associated with the moderator role served by the steam over partial combustion reactions, affecting the selection of the StC, possibly resulting in values larger than those of interest for thermodynamic reasons.

5.2 Air enriched-steam gasification of plastic waste

5.2.1 Tests summary

Several autothermal gasification tests have been carried out by treating about 30 kg/h of plastic waste, a mixture of air, oxygen and steam with different proportions as gasification agents. This was done with the purpose of assessing the reactor behaviour when operated with a high heating value

plastic waste and at different values of ER, and experimentally investigating the impact of design parameters, namely ER, x_{O2} and StC, on the performance of the gasifier. Table 5.1 reports the operating conditions of all the performed autothermal gasification tests, carried out with both BluPolymer-L and BluPolymer-C, while the relative results for main process performance parameters are reported in Table 5.2.

Table 5.1 – Operating conditions and main results of the pilot scale tests with different waste feedstock. BluPolymer-C is referred to as BP-C and. BluPolymer-L is referred to as BP-L.

Test #	Gasification agent			Fuel		Operating parameters			
	Air [kmol/h]	Steam [kmol/h]	Oxygen [kmol/h]	Fuel type	Feed rate [kg/h]	ER	StC	x_{O2}	StO_2
1	2.88	1.67	0.00	BP-C	33.3	0.22	0.79	0.21	2.77
2	1.90	1.78	4.34	BP-C	31.0	0.23	0.90	0.28	3.00
3	1.47	1.76	6.90	BP-C	34.7	0.22	0.80	0.35	2.86
4	1.34	1.91	8.93	BP-C	37.0	0.23	0.81	0.39	2.80
5	0.92	2.00	11.64	BP-C	40.1	0.22	0.79	0.49	2.81
6	1.87	2.00	5.02	BP-C	34.4	0.22	0.92	0.29	3.25
7	1.87	2.00	4.93	BP-C	32.0	0.24	0.99	0.29	3.26
8	1.56	1.98	7.57	BP-C	31.0	0.26	1.00	0.35	2.98
9	1.25	1.98	7.65	BP-C	31.0	0.24	1.00	0.38	3.28
10	1.27	1.99	5.23	BP-C	22.0	0.28	1.43	0.33	3.97
11	2.98	0.00	0.00	BP-L	29.2	0.22	0.00	0.21	0.00
12	2.98	1.63	0.00	BP-L	29.0	0.22	0.83	0.21	2.61
13	2.00	1.57	0.22	BP-L	28.0	0.22	0.77	0.29	2.45
14	1.50	1.59	0.31	BP-L	31.7	0.20	0.74	0.34	2.52
15	1.34	1.48	0.41	BP-L	31.7	0.22	0.69	0.39	2.15
16	1.70	1.92	0.31	BP-L	30.0	0.23	0.95	0.33	2.89
17	1.65	1.94	0.32	BP-L	30.0	0.23	0.94	0.34	2.87
18	1.51	2.00	0.36	BP-L	29.5	0.22	1.00	0.36	2.97
19	1.90	1.98	0.22	BP-L	26.0	0.25	1.11	0.29	3.20
20	1.70	1.97	0.30	BP-L	27.0	0.24	1.08	0.33	3.00
21	1.50	1.94	0.32	BP-L	25.0	0.25	1.13	0.35	3.10

Throughout the tests, the reactor temperature appears to reach a thermal steady-state at high temperatures, very close to or above the typical upper limit for safe and optimal operation of the gasifier, for all the tests performed using plastic-derived fuels. This is mainly attributed to the high heating value of plastic, which results in the release of a high amount of heat upon partial combustion.

Interestingly, the values of H_2 specific yield (gH_2/kg_{Fuel}) are similar between the tests performed using air (reported in Table 4.2) and the ones obtained in the case of air-enriched steam gasification in Table 5.2. This result might suggest a limited active role of steam in enhancing the composition of the syngas and overall H_2 yield. However, one relevant consideration involves the experimental limitations in feeding steam into the system, which prevented from being able to test operations in

full steam-O_2 conditions [187]. The reactor has been operated with the highest amount of steam replacing N_2 in test #5, with x_{O2} of 0.49, still close to x_{O2} 0.21 representing air gasification.

Table 5.2 – Main process performance results of the pilot scale test with different waste feedstock.

Test #	Reactor Temperature		Syngas			Process			
	Bed [°C]	Freeboard Outlet [°C]	Outlet flowrate, [Nm³/h]	LHV, [MJ/Nm³]	Tar content [g/Nm³]	CCE [%]	CGE [%]	g_{H2}/kg_{Fuel}	g_{CO}/kg_{Fuel}
1	804	641	86	8.8	3.3	74	73	8.3	125.7
2	824	717	67	9.4	2.4	69	65	9.1	117.2
3	832	714	60	10.8	4.9	64	61	8.6	104.9
4	866	727	63	11.1	3.4	66	61	11.9	103.3
5	870	731	58	13.2	4.4	67	62	11.8	104.6
6	806	698	68	9.7	9.0	67	62	8.0	146.2
7	828	703	68	9.5	6.2	72	66	9.9	125.8
8	862	699	64	10.1	3.0	74	66	12.2	119.4
9	838.	684	54	10.3	4.9	65	58	9.1	124.2
10	837	700	50	9.2	3.5	78	68	10.3	150.2
11	852	691	88	9.2	3.5	78	72	12.0	110.9
12	763	668	87	8.5	3.4	74	66	10.0	221.0
13	843	685	70	9.9	5.6	69	63	11.0	130.0
14	868	703	61	11.1	8.6	63	55	12.0	87.0
15	883	681	59	10.4	6.5	61	50	13.0	93.0
16	857	712	64	9.0	9.6	63	50	13.0	111.0
17	836	702	64	11.4	11.0	72	62	11.0	116.0
18	867	701	63	11.4	8.6	73	63	14.0	101.0
19	821	702	63	8.8	4.5	68	55	9.0	133.0
20	876	687	68	10.3	10.0	79	67	17.0	113.0
21	870	624	58	9.6	7.4	71	56	11.0	112.0

5.2.2 Outlet gas composition

Figure 5.1 and Figure 5.2 present a comprehensive comparison between experimental measurements and model predictions for syngas composition and heating value at various operating conditions. For pure feedstock gasification scenarios (Figure 5.1 and Figure 5.2), the model demonstrates robust predictive, being the error lower than 3% for all species, with larger discrepancies mainly for N_2, and an average error of 1%. The good agreement of the results further demonstrates the successful characterization of the feedstock devolatilization behaviour and product distribution, as well as the reaction pathway considered.

Nevertheless, an appreciable disagreement is found for the hydrocarbon content in the syngas, specifically the species C_nH_m with 2-4 carbon atoms, with the model generally predicting higher quantities. This could be due to the limited availability of specific kinetic studies (and related equations) for C_nH_m in a partially reducing atmosphere and to the assumed distribution of products released from the initial devolatilization stage, which is strongly dependent on the feedstock

composition. This partial limitation of the model affects the accuracy of the predicted heating value of the obtained syngas.

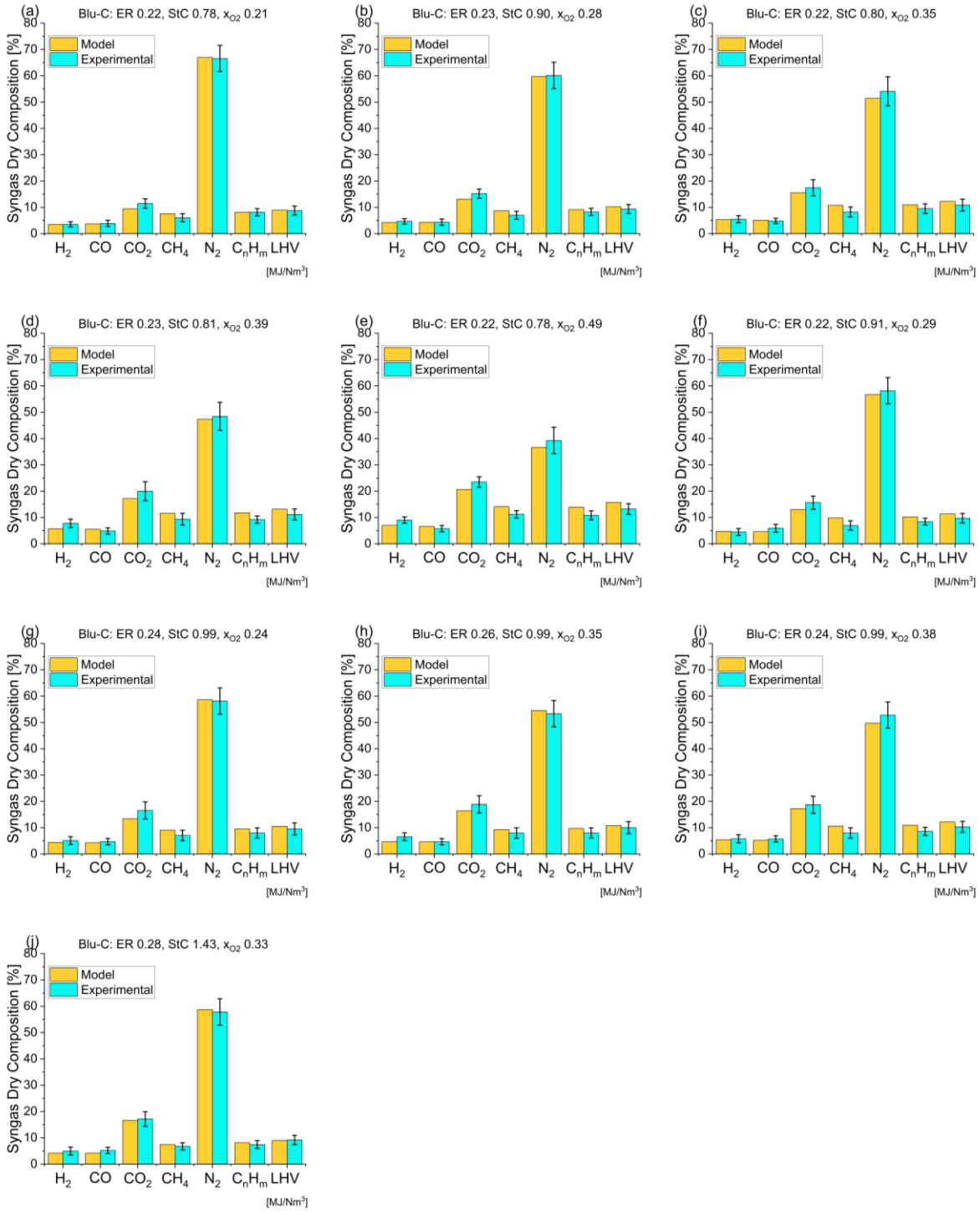

Figure 5.1 – Comparison between model predictions and measured data of syngas composition and heating value for air-enriched steam gasification of plastic waste at different operating conditions. Tests using BluPolymer-C referred to as Blu-C in the figures.

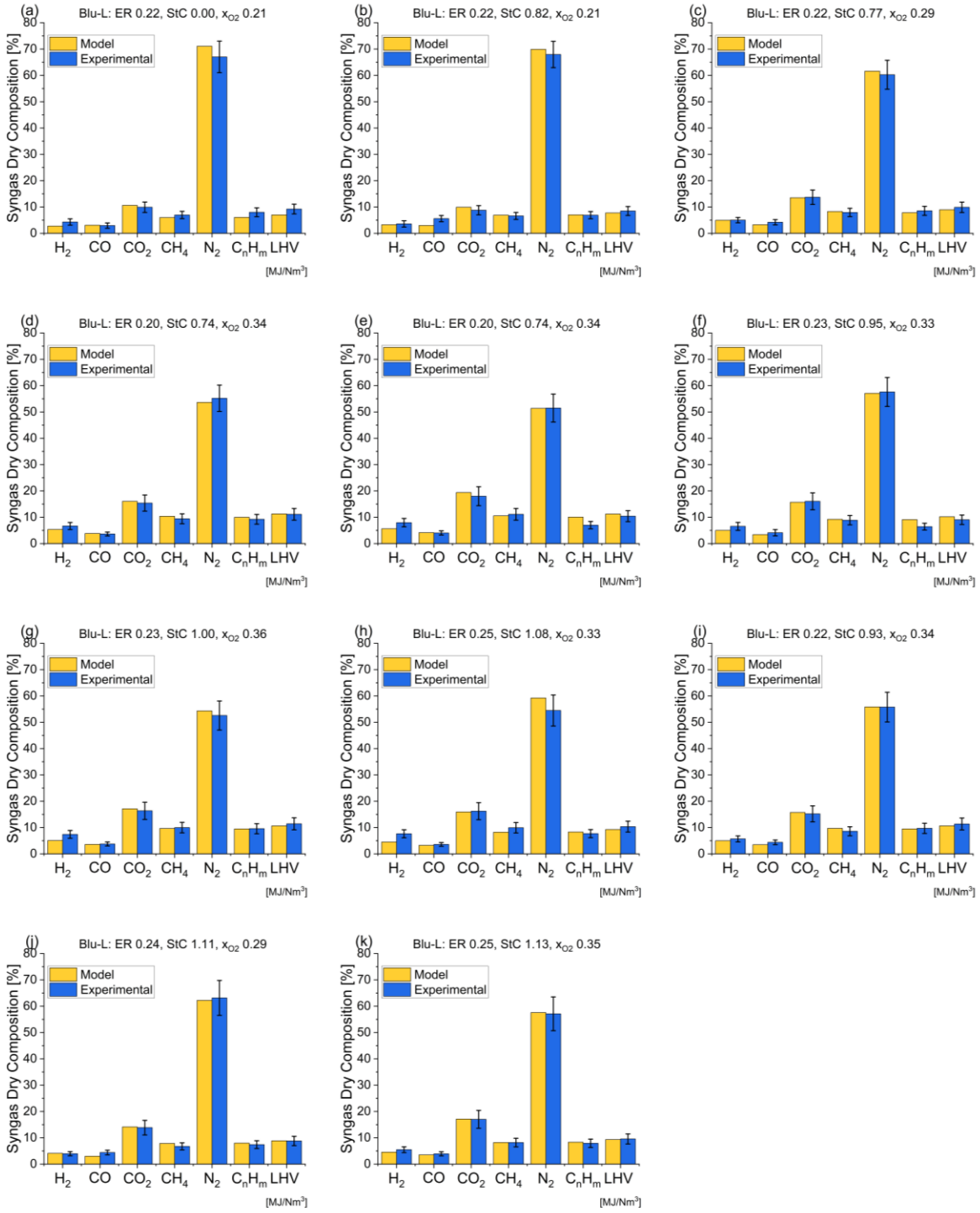

Figure 5.2 – Comparison between model predictions and measured data of syngas composition and heating value for air-enriched steam gasification of plastic waste at different operating conditions. Tests using BluPolymer-L referred to as Blu-L in the figures.

5.2.3 Temperature profile

Figure 5.3 reports the comparison between predicted and measured temperature profiles along the reactor for the different feedstock and two representative operating conditions. The predicted profiles a show remarkably good match with the experimental values throughout the length of the

reactor. Notably, the average value in the bed reaches higher values in the case of operations with plastic fuels, reaching the maximum of 883°C for an oxygen content of 39% at StC=0.75, and slightly lower at StC=1.1, with a limited reduction in the splashing zone. The profiles confirm the crucial role of nitrogen as a temperature moderator. This role must be maintained when, under oxygen-steam operation, nitrogen is not part of the fluidization agent and must be replaced with a suitable amount of steam.

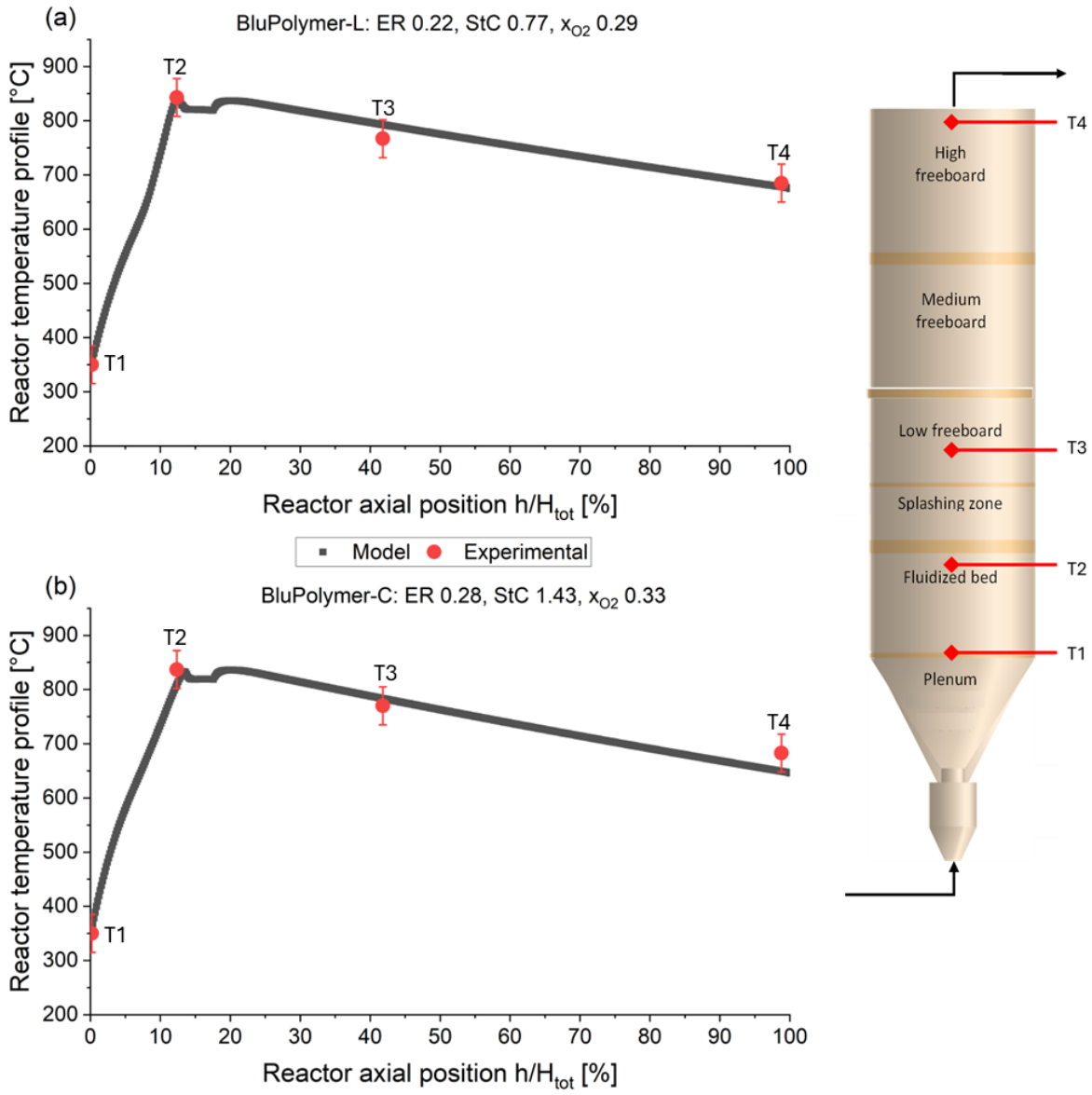

Figure 5.3 – Sample comparison between predicted axial profile and measured values of gasifier temperature for air-enriched steam gasification of plastic waste. (a) 28 kg/h of BluPolymer-L at ER 0.22, StC 0.77 and x_{O2} 0.29, and (b) 22 kg/h of BluPolymer-C at ER 0.28, StC 1.43 and x_{O2} 0.33.

5.2.4 Process performance

The process performance of air-enriched steam gasification has been analysed concerning two relevant operating parameters introduced by the use of air enriched, in the form of oxygen molar fraction (x_{O2}), and steam, in the form of StC.

Figure 5.4 shows good agreement between experimental and model results for different performance parameters of plastics gasification at different oxygen concentrations in the gasification agent, as available from experimental tests. All resulting parameters refer to test at ER 0.22 and StC 0.75 using BluPolymer-L. The process of plastics gasification shows overall good conversion efficiencies (in Figure 5.4(a)), with both CCE and CGE in the range of 60% to 80%. The outlet syngas flowrate reported in Figure 5.4(b) shows a decreasing trend when increasing the oxygen concentration in the gasification agent, which is conversely attributed to the higher amount of steam fed to the gasifier, which is then condensed and separated from the outlet syngas. Lower accordance is found in terms of H_2 specific content (gH_2/kg_{fuel}) and tar content in Figure 5.4c and d. While the model well captures the trend of H_2 specific content variation, a more noticeable difference is found for tar content. In particular, form this preliminary investigation the model suggests that tar content is not affected by the concentration of oxygen (at constant ER), while the experiments show a possible increasing trend. Nonetheless, it is worth factoring in the inherent challenges in sampling and measuring tar content experimentally, leading to uncertainties in the absolute values given from experimental results. In this regard, the good agreement between model results and the tests in terms of order of magnitude of tar content is promising for a reliable systematic investigation of the effect of the oxygen molar fraction in the gasification medium, as can be found in Section 5.6.1.

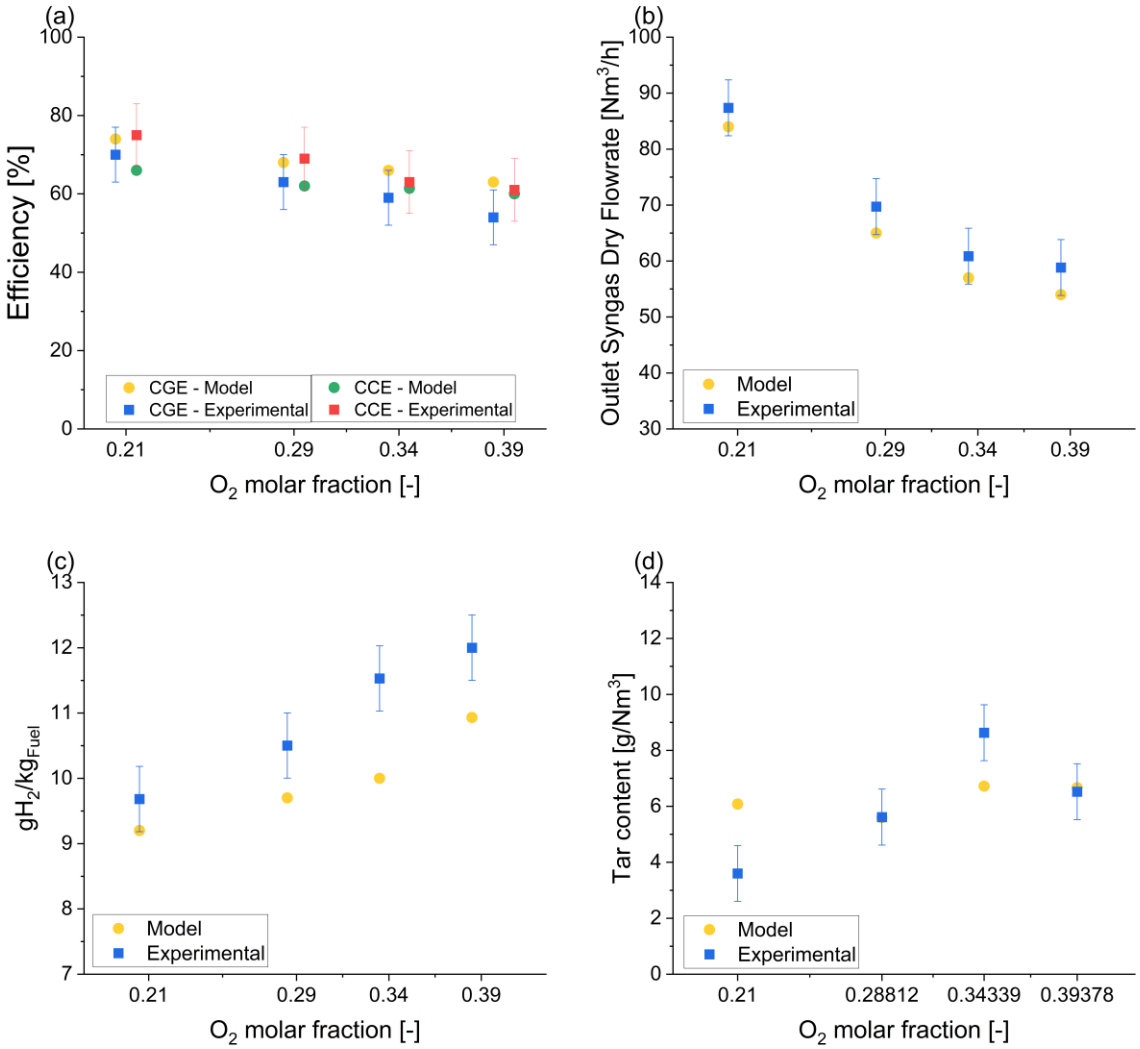

Figure 5.4 – Comparison between model results and experimental data of performance parameters of plastics (BluPolymer-L) gasification at different values of x_{O2}.(a) CGE and CCE, (b) outlet syngas dry flowrate, (c) specific yield of hydrogen and (d) tar content in the produced syngas. ER 0.22, StC 0.75.

In Figure 5.5 instead, the comparison between the model and experimental results for different performance parameters of plastics gasification is reported to investigate the potential effect of the StC ratio. All results parameters refer to results for ER around 0.23 and x_{O2} between 0.21 and 0.28 using BluPolymer-C.

Both experimental results and model predictions demonstrate a consistent slightly decreasing trend in CCE and syngas dry flowrate (Figure 5.5(a) and (b)) as the StC ratio increases from 0.20 to 0.35 mol/mol, with model predictions well within experimental uncertainty. Interestingly, the CGE remains rather steady with increasing steam content which would suggest a rather limited role of steam in promoting reforming reactions, as one would otherwise anticipate[187]. This could result from the concurrent decrease in syngas outlet flowrate and increased heating value (Figure 5.5(c)). This is also indirectly further supported by the increase in H_2 specific content (Figure 5.4c).

A significant finding relates to tar content predicted by the model, which shows minimal variation in concentration (g/Nm³) across different StC ratios, suggesting a minimal effect of steam in affecting the reaction pathway of hydrocarbons, challenging the common assumption and expectation of the role of the steam in tar reduction via reforming reactions. While the tar concentration remains relatively constant, it is still relevant to note that the total of tars produced decreases, counterbalancing the reduction of dry syngas flowrate. These preliminary results have significant implications towards a deeper understanding of the process, highlighting the trade-off between CGE and hydrogen production efficiency, whilst alternative strategies for tar reduction may still be needed depending on the final syngas utilization.

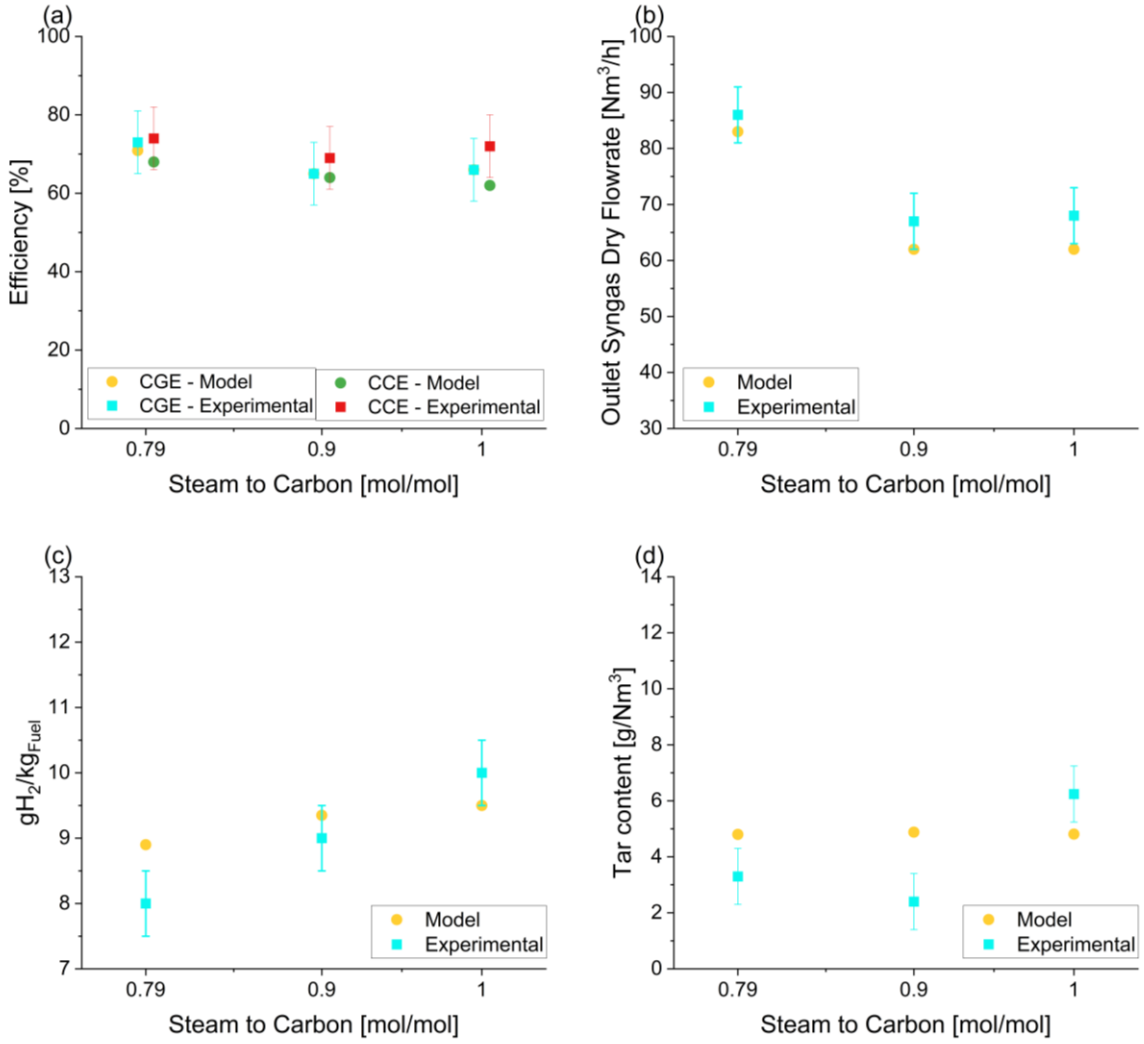

Figure 5.5 – Comparison between model results and experimental data of performance parameters of plastics (BluPolymer-C) gasification at different values of StC.(a) CGE and CCE, (b) outlet syngas dry flowrate, (c) specific yield of hydrogen and (d) tar content in the produced syngas. ER ranging between 0.224. and 0.237 and x_{O2} from 0.21 to 0.28.

5.3 Air enriched-steam gasification of plastic waste and biomass blends

5.3.1 Tests summary

The pilot scale gasifier has been also operated using a blend of biomass and plastic waste as feedstock, with a mixture of air, oxygen and steam with different proportions as the gasification agent. The two fuels are loaded into two different hoppers, where they are weighted, independently of the load cells of the screw feeders to allow a correct evaluation of biomass and plastics flowrates. This was done with the purpose of assessing the reactor behaviour when operated with a heterogeneous feedstock, with a composition representing that of municipal solid waste [42]. Table 5.3 reports the operating conditions of all the performed autothermal co-gasification tests, carried out with different blends of BluPolymer-L and Eucalyptus chips, while the relative results for main process performance parameters are reported in Table 5.4.

Table 5.3 – Operating conditions and main results of the pilot scale tests with blends of biomass and plastics as waste feedstock.

Test #	**Gasification agent**			**Fuel**		**Operating parameters**			
	Air [kmol/h]	Steam [kmol/h]	Oxygen [kmol/h]	Fuel type	Feed rate [kg/h]	**ER**	**StC**	**x_{O2}**	**StO_2**
1	2.22	1.91	0.00	BP-L 40% E 60%	38.3	0.20	1.12	0.21	2.87
2	1.12	1.94	0.22	BP-L 44% E 56%	39.6	0.18	1.07	0.34	2.98
3	1.33	1.87	0.29	BP-L 46% E 54%	33.8	0.26	1.05	0.35	2.53
4	1.60	2.02	0.31	BP-L 44% E 56%	39.3	0.26	1.12	0.34	2.45

Table 5.4 – Main process performance results of the pilot scale test with blends of biomass and plastics as waste feedstock.

Test #	Reactor Temperature		Syngas			Process			
	Bed [°C]	Freeboard Outlet [°C]	Outlet flowrate, [Nm^3/h]	LHV, [MJ/Nm^3]	Tar content [g/Nm^3]	CCE [%]	CGE [%]	g_{H2}/kg_{Fuel}	g_{CO}/kg_{Fuel}
1	763	703	78	8.50	5.64	80	73	14.5	106.3
2	737	644	56	10.13	2.00	70	58	11.6	100.3
3	825	597	68	11.17	0.44	88	78	18.3	160.1
4	866	634	72	7.95	4.29	80	59	16.5	155.1

5.3.2 Outlet gas composition

Figure 5.6 presents the comparison between experimental data and model predictions for syngas composition and heating value at various operating conditions when a blend of plastics and biomass is used as feedstock. The co-gasification of Eucalyptus chips and BluPolymer-L presents additional modelling challenges that contribute to the larger discrepancies between experimental and predicted results compared to the gasification of pure feedstocks, with the error being up to 8%. First, the devolatilization behaviour of biomass represents a significant source of uncertainty due to the complex and uneven structure of the biomass, and variability in proximate and ultimate analysis of feedstock tested, affecting the wide range of products and volatile species that can be formed during thermal decomposition. Furthermore, differences in biomass composition would extend to moisture and ash content, which can significantly impact the gasification process. It is also worth mentioning the lack of capability to represent the potential synergistic effects between biomass and plastic polymers during co-gasification.

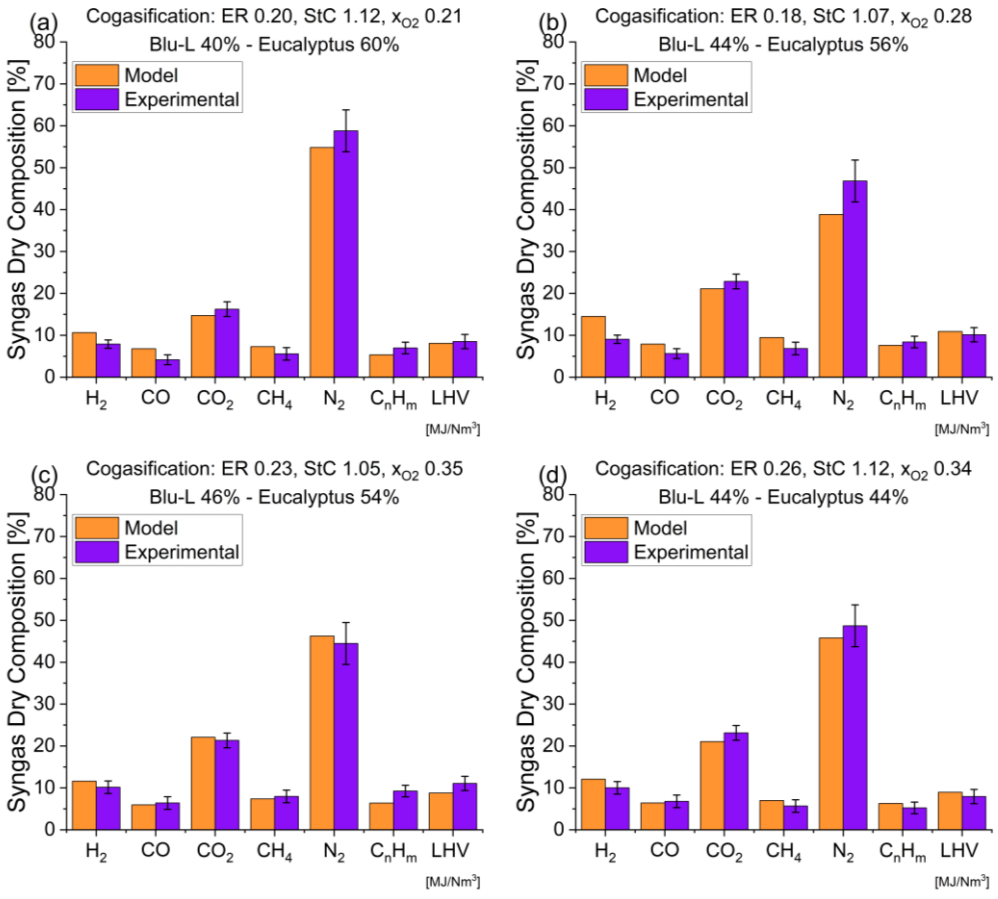

Figure 5.6 – Comparison between model predictions and measured data of syngas composition and heating value for air-enriched steam gasification of mixed feedstocks at different operating conditions and blending ratio.

These synergies might include catalytic effects of biomass ash minerals on plastic and heavy hydrocarbons decomposition, modified reaction pathways resulting from the simultaneous

devolatilization of lignocellulosic and polymer materials, and improved heat transfer due to the different thermal properties of the feedstocks. The combination of these factors results in a more complex gasification environment that deviates from the simple linear combination of the behaviour observed in single-feedstock scenarios. The experimental results do not align well with the findings of Pinto et al. [202], which highlighted that increasing the plastic content results in higher amount of H_2 obtained in the syngas, as a direct result of the higher amount of hydrogen included in the plastic matrix. However, the comparison between the two results is not straightforward due to differences in experimental setup scale and operations. Pinto et al. [202] operated a lab scale circulating fluidized bed using steam only, instead of a steam-O_2 mixture used in this work.

5.3.3 Temperature profile

Figure 5.7 reports a sample temperature profile along the reactor as obtained with the model. The predicted profiles align well with the experimental data along the entire reactor length. The model accurately captures the bed temperature trends, showing average values that are lower than those observed in the pure plastics gasification case (as shown in Figure 5.3). Nonetheless, a marginally larger discrepancy can be found along the freeboard with higher predicted temperatures, which could also be responsible for the differences in syngas composition.

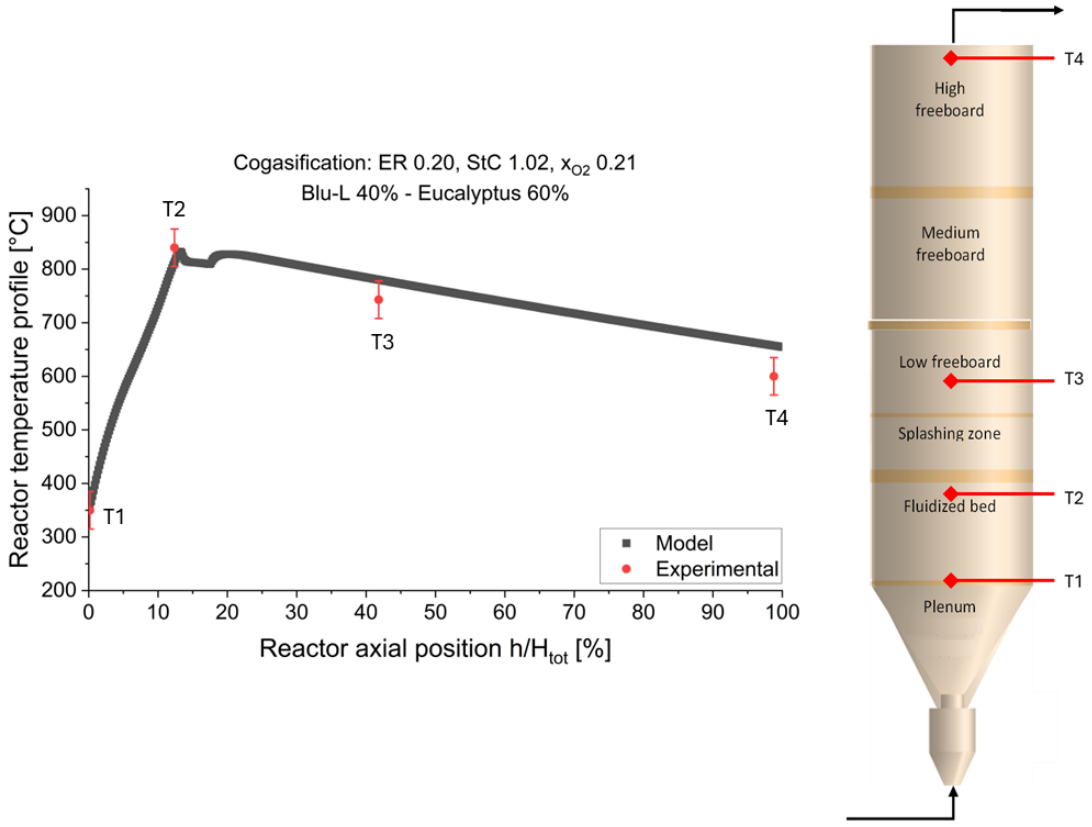

Figure 5.7 – Sample comparison between predicted axial profile and measured values of gasifier temperature for air-enriched steam gasification of mixed feedstocks at different blends. 38.3 kg/h of 40% BluPolymer-L and 60% Eucalyptus, at. ER 0.20, StC 1.12 and x_{O2} 0.21.

5.3.4 Process performance

Figure 5.8 shows a good agreement between experimental and model results for different performance parameters for mixed feedstocks gasification against blending ratios (40-46%) available from experimental tests. These results are reflective of the analysis for syngas outlet composition as discussed in Section 5.3.2. Efficiency and H_2 mass flows are directly related to syngas outlet composition. The model slightly overestimates the hydrogen mass flow rates for a single point, as shown in Figure 5.8(c). This may be explained by the experimental challenges surrounding feeding biomass and polymer blends i.e. consistency of feeding rates and/or ratio of components.

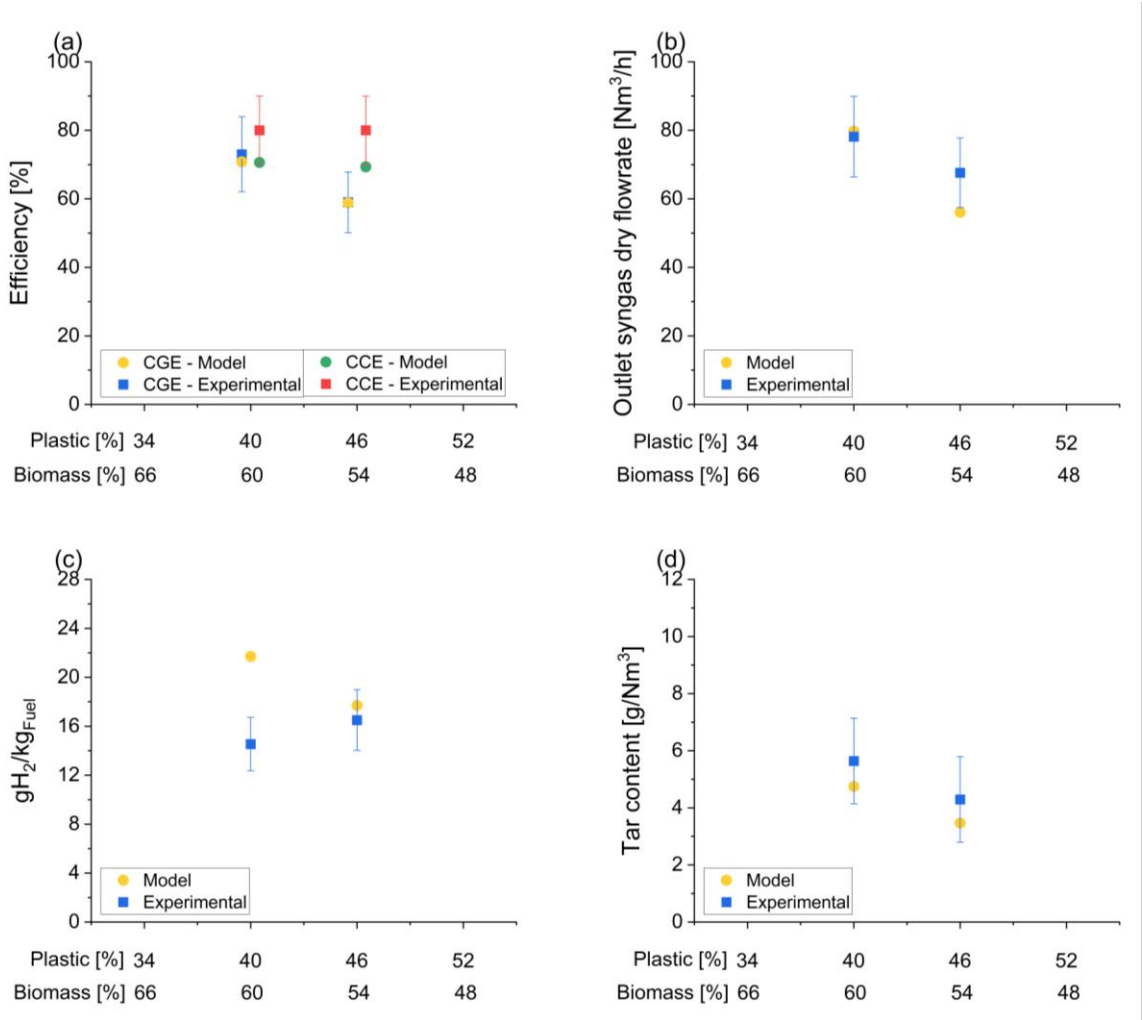

Figure 5.8 – Comparison between model results and experimental data of performance parameters of mixed feedstocks gasification at different blending ratios and operating conditions. (a) CGE and CCE, (b) outlet syngas dry flowrate, (c) specific yield of hydrogen and (d) tar content in the produced syngas.

Nonetheless, the model predictions are in close alignment with experimental data for all other relevant parameters. This preliminary exploration of the effect of feedstock composition with respect to blending ratio seems to suggest a contrasting trend in process performance. For example, higher plastic content leads to a desirable reduction in tar content at the expense of a concurrent reduction

in efficiency. However, this could arise from differences in operating conditions (ER 0.20 vs 0.26). These initial observations on blending ratio spurred further systematic investigation of the effect of syngas composition on process performance in Section 5.7.

5.4 Steam oxygen gasification of biomass and refuse derived fuel

5.4.1 Tests summary

The BFB gasifier that was used to generate the model results, and associated experimental data, is part of the waste gasification pilot plant based in Swindon (UK). The Swindon pilot plant has been extensively used for research and development purposes [183,184] to investigate the gasification of different biomass fuels.

The reactor is a bubbling fluidized bed gasifier that operates at about 750 °C using steam and oxygen as fluidizing gases. Differently from the Faber plant where reactor temperature reached the steady state as a response to the operating conditions, the APP facility is operated to maintain the average bed temperature around the design set point at about 750°C by adjusting the inlet steam and oxygen.

Bed temperature is typically controlled by adjusting the steam/oxygen ratio and fuel feed. Maintaining a nearly constant bed temperature minimises reactor upset conditions due to fuel variations (moisture, ash, heating value, etc) providing near steady-state conditions for the performance of the gasifier. The main design and operation characteristics of the pilot BFB reactor are summarised in Table 5.5.

Table 5.5 – Design and characteristics of the pilot BFB.

Test #	**Gasification agent**			**Fuel**		**Operating parameters**			
	Air [kmol/h]	Steam [kmol/h]	Oxygen [kmol/h]	Fuel type	Feed rate [kg/h]	**ER**	**StC**	**x_{O2}**	**StO_2**
1	0.00	1.76	0.85	E	85	0.28	0.57	1.00	2.10
2	0.00	0.93	0.42	RDF	45	0.24	0.55	1.00	2.20

Table 5.6 – Main process performance results of the pilot scale test with biomass and RDF as feedstock.

Test #	Reactor Temperature		Syngas			Process			
	Bed [°C]	Freeboard Outlet [°C]	Outlet flowrate, [Nm^3/h]	LHV, [MJ/Nm^3]	Tar content [g/Nm^3]	CCE [%]	CGE [%]	g_{H2}/kg_{Fuel}	g_{CO}/kg_{Fuel}
1	750	630	80.4	10.1	n.a.	79	70	32.7	196.1
2	750	670	n.a.	8.0	3.00	n.a.	n.a.	n.a.	n.a.

5.4.2 Outlet gas composition

The model was first run at inlet conditions close to experimental ones, with a margin of error consistent with real plant operation. Figure 5.9 shows the gas composition of the main products and the lower heating value compared to those calculated by the model for both feedstocks tested experimentally, i.e. Eucalyptus chips and RDF. Hydrogen molar fraction is around 20%, which compares well to results reported in different studies [203], while the carbon monoxide fraction is roughly half. As expected, molar fractions of carbon dioxide and steam are quite high, more than 20% and 30% respectively, which is related to the use of steam-oxygen as gasification agents.

The gas composition is generally well-predicted and close to the experimental values, showing a deviation of about 5% between the calculated and experimental data for most species. The model shows better prediction capabilities when Eucalyptus is used as fuel in the process, with discrepancies in line with the ones discussed for Faber predictions, despite the differences in design and operations. Larger discrepancies are found for predictions of RDF gasification, which can be attributed to the extensive heterogeneous composition of the fuel, resulting in more significant uncertainty in the devolatilization product distribution. More relevant discrepancies are related to steam and light hydrocarbon molar fractions (up to 7% and 3% respectively). The difference is mostly due to the high variability of the steam fed into the reactor, and the limited number of species in the model to represent the hydrocarbon distribution. The lower heating value (LHV) is calculated with relation to gases only while the measured one might include some residual vapours (steam mostly) in small percentages. This would explain the slightly higher heating value calculated by the model.

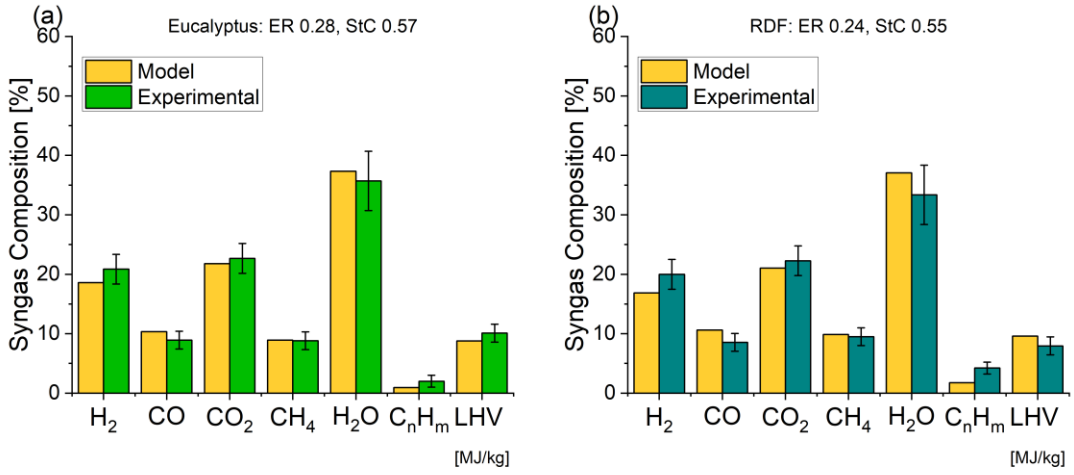

Figure 5.9 – Comparison between model predictions and measured data of syngas composition and heating value for steam-oxygen gasification at different operating conditions. (a) Eucalyptus chips, ER 0.28 StC 0.57 (b) RDF, ER 0.24, StC 0.55.

5.4.3 Temperature profile

Figure 5.10 shows the temperature profile of the FBG during operation at the above conditions. While the temperature at different locations in the bed is maintained fairly constant at around 750°C, the model predicts an increasing profile for continuity with the inlet gas flowrate, which is fed at lower temperatures. The model shows a peak in temperature in the upper bed region. which is attributed to the large amount of volatiles released by the fuel particles fed on the surface of the bed and reacting with the oxygen in the upward fluidization gas. This phenomenon is not present in the relative experimental tests due to the high degree of bed mixing, whereby the hotter layer of bed particles in the upper bed are carried downwards heating the colder bottom region of the bed. Further deviation can be observed in the freeboard temperature profile, which can be attributed to inaccurate heating losses and fluctuations in operating conditions and the high variability of the steam fed into the reactor.

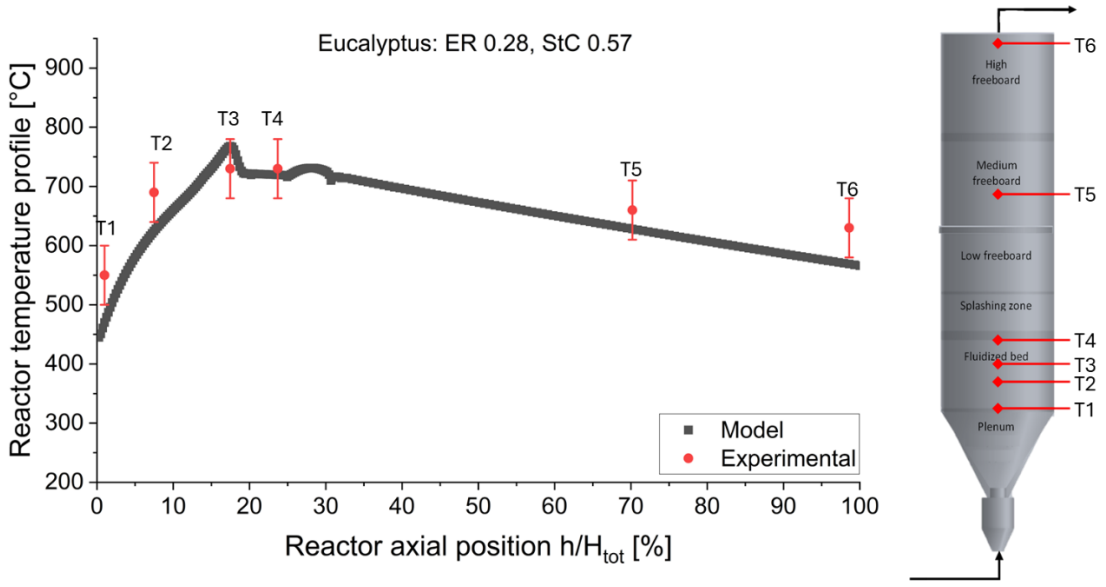

Figure 5.10 – Sample comparison between predicted axial profile and measured values of gasifier temperature for steam-oxygen gasification of biomass. 85 kg/h of Eucalyptus, at. ER 0.28, StC 0.57.

5.4.4 Process performance

Despite a more limited availability of experimental data for the second pilot plant considered, the comparison between model and experimental results for Eucalyptus chips is reported in Figure 5.11 to test the accuracy and reliability of the model predictions for a different gasifier design, but also for full steam oxygen operations. Figure 5.11 shows a remarkable match between predicted and available experimental data, reinforcing the reliability of the model in predicting the full range of operations,

from air to steam-oxygen gasification of both biomass and plastic waste, and therefore making relevant projections to investigate the effect of operating conditions on the process. The error bars in the experimental data are determined by the uncertainty in the primary data used to calculate the variables, affected by the error of the measurement devices, as well as fluctuations in the recorded signal.

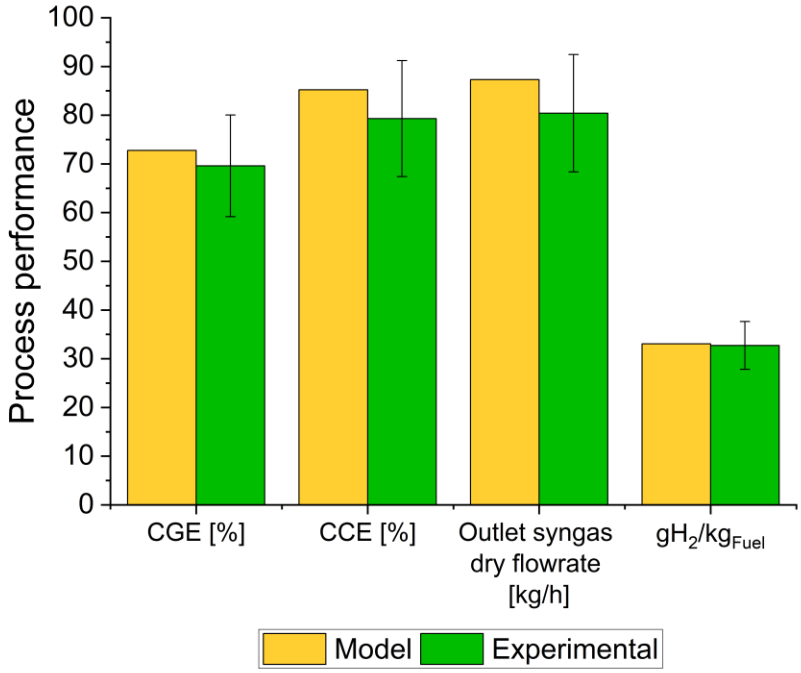

Figure 5.11 – Comparison between model results and experimental data of performance parameters of biomass gasification. (a) CGE and CCE, (b) outlet syngas dry flowrate, (c) specific yield of hydrogen and (d) tar content in the produced syngas.

Based on the experimental data available, the model is reliable also for the evaluation of hydrocarbon species, including benzene and total tars, as shown in Figure 5.12, with close prediction in orders of magnitude. Despite experimental values reporting a higher content of benzene, the model predicts a higher concentration of a range of hydrocarbon species as tars, which include also aromatics that counterbalance the lower benzene predicted. Nonetheless, the model shows a higher total tar content in the outlet syngas.

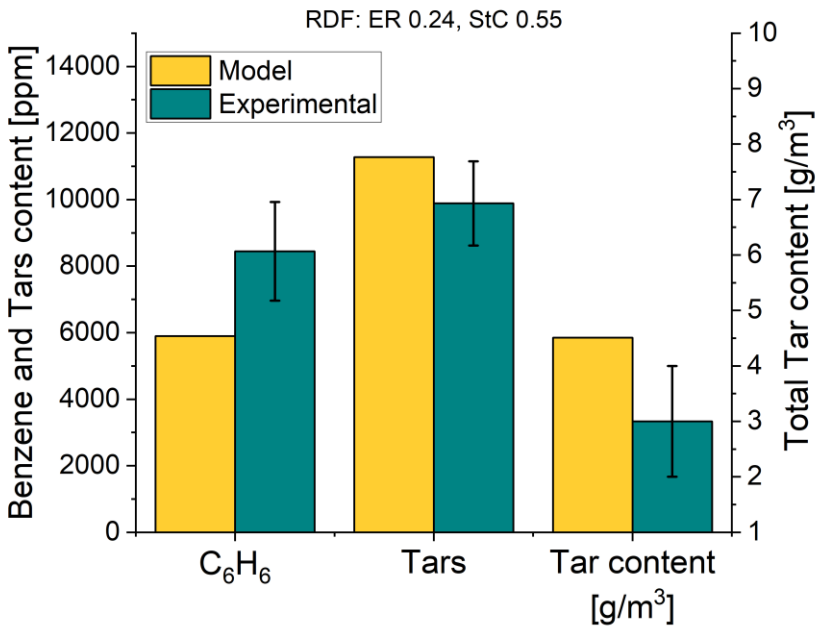

Figure 5.12 – Comparison between model results and experimental data of hydrocarbons content in the syngas produced during RDF steam-oxygen gasification.

It can be observed that tars content in the syngas obtained from RDF gasification is still significantly high, requiring additional reforming for syngas utilization. An example of this is represented by the use of a thermal plasma reactor in the Swindon plant [204]1].

5.5 Process modelling analysis

5.5.1 Axial profiles of syngas composition

Despite the differences in gasification agent, the analysis of the chemical species axial profile in the fluidized bed and splashing zone is the same as the one presented in Section 4.6.1, therefore it is not repeated here. However, different behaviour is expected in the freeboard, where the gasification agent is fully mixed with the gas released from devolatilization, and a more complex pathway is established due to the large quantity of steam replacing N_2.

Tars composition and general hydrocarbons distributions are very often disregarded when modelling FBG. This not only is an important limitation of the modelling approach, but could also lead to inadequate gas cleaning design and to unexpected plant disruption during operation. A detailed profile of hydrocarbons content at different gasifier levels is shown in Figure 5.13.

Tars (C7+) are at their peak in the splashing zone due to their proximity to the feedstock injection point. Here, the influence of devolatilization products is quite marked, and the high temperatures generated on the bed surface are not sufficient to ensure the complete cracking/reforming of the heavier species. As the gas moves along the freeboard, heavy hydrocarbons are progressively converted to lighter species, mostly alkanes and single-aromatic species (e.g. benzene). Ethylene and

propylene contents are also higher in the lower sections of the freeboard, as the effect of direct cracking of the polyethylene and polypropylene fractions in the plastic waste. Similar trends but lower values are observed for increasing oxygen enrichment ratio and steam-to-carbon. Interestingly, the concentration of benzene remains stable along the freeboard, due to the high stability of associated with the chemical structure of benzene and aromatic compounds, making them highly resistant to chemical reactions and challenging to break into lighter components.

These results show the critical importance of the freeboard in ensuring adequate residence time for reforming and slower depolymerisation reactions to take place, although the residual tar content (4-6 g/Nm^3) demands for additional tar conversion and/or removal actions for the use of syngas in chemical recycling applications.

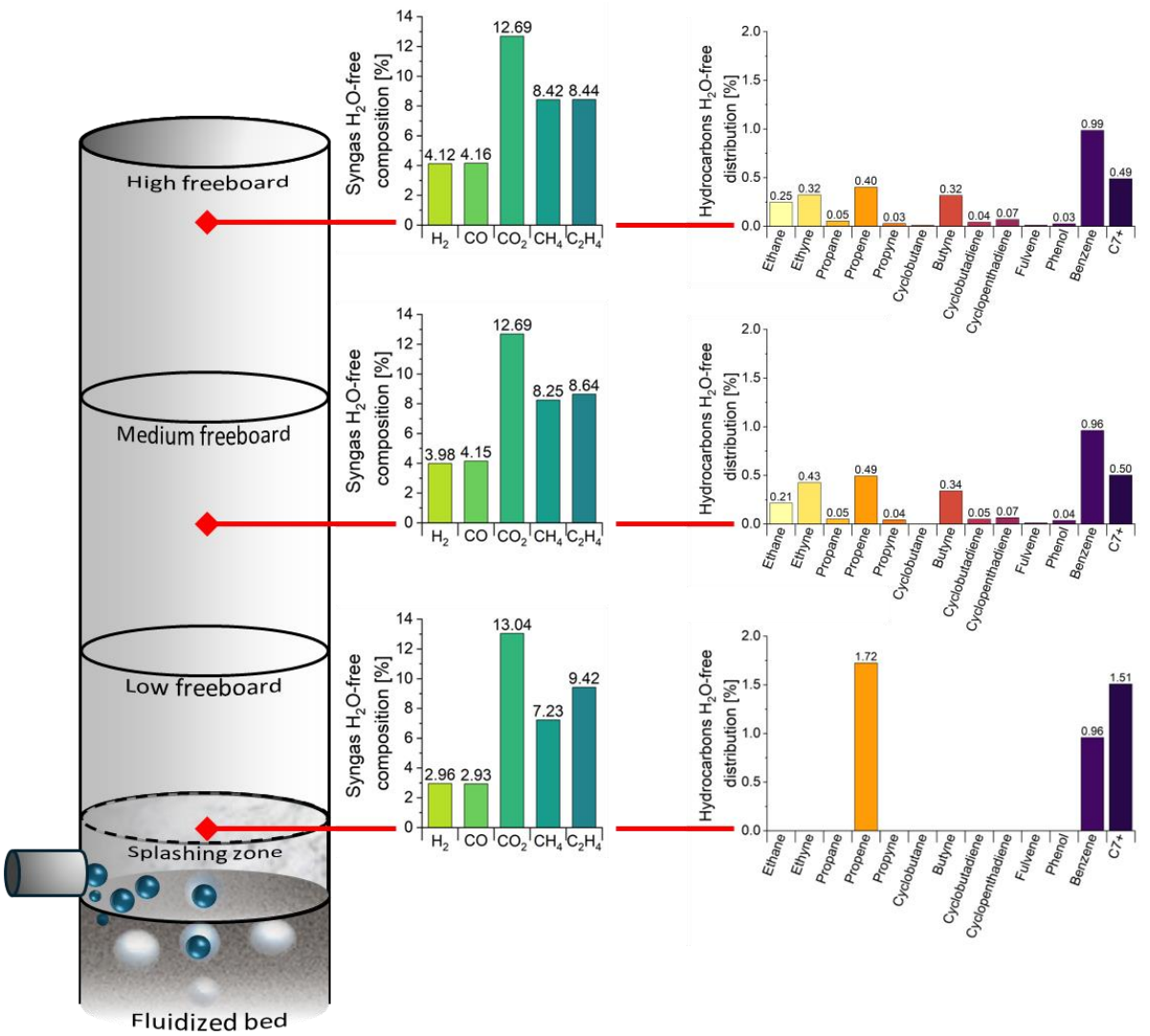

Figure 5.13 – Light gas and hydrocarbons profile in the freeboard of the gasifier. 31 kg/h of BluPolymer-C at ER 0.23, StC 0.90, x_{O2} 0.28.

5.5.1.1 Tar distribution

Figure 5.14 illustrates the tar distribution as a percentage of the liquid phase for BluPolymer-C gasification under specific conditions (ER 0.23, StC 0.90, x_{O2} 0.28). The comparison between experimental data and model predictions shows a generally good agreement, although with some notable differences. Both experimental and model results indicate that C10 compounds dominate the tar composition, accounting for approximately 70-85% of the total tar content. However, the model predicts a slightly more distributed pattern across higher molecular weight compounds (C11-C20+) compared to the experimental data. The discrepancy may be attributed to the challenges in the analysis of tar compounds, as well as the limitation of the model having to represent the tar species via limited defined molecules. This broader distribution in the model results suggests that the kinetic mechanisms for tar evolution and breakdown may need refinement, particularly for primary tar species and secondary tar reactions.

Despite these minor discrepancies, the model successfully captures the overall trend of tar formation, with a clear predominance of lighter tar compounds and a gradual decrease in the proportion of heavier molecular weight species. This validation of tar distribution prediction is crucial for understanding the effectiveness of the gasification process and for designing appropriate downstream tar removal systems.

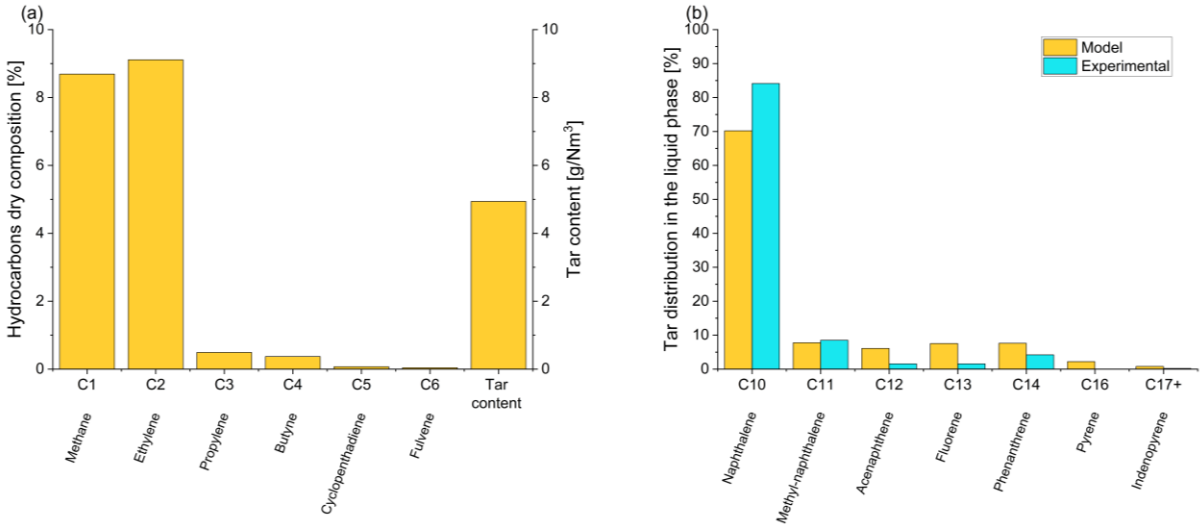

Figure 5.14 – Comparison of tar distribution as a percentage of the condensable liquid phase.

There are multiple reaction pathways for different species in the freeboard. Figure 5.15(a-d) shows the comparison of tar species rate of production analysis along the freeboard as calculated by the Chemkin-pro submodel. The right column presents the values of the global rate of reaction, proportional to the length of the bars for each chemical species. The negative values indicate reactions that lead to the depletion of the considered species, and the positive ones are those in which the species is produced.

The figure confirms the intricate pathway of reactions involving tar species, although the dominant reactions appear to be those associated with cracking to produce lighter species. Figure 5.15(e) represents the rate of production analysis for steam. The results show a limited involvement of steam in reforming reactions of lighter hydrocarbons, where the main limiting factors can be associated with temperature and reaction kinetics. This finding suggests that, while steam can play a major role as an agent controlling the thermal stability of the reactor, it has a rather limited one as chemical agent in the gasification process.

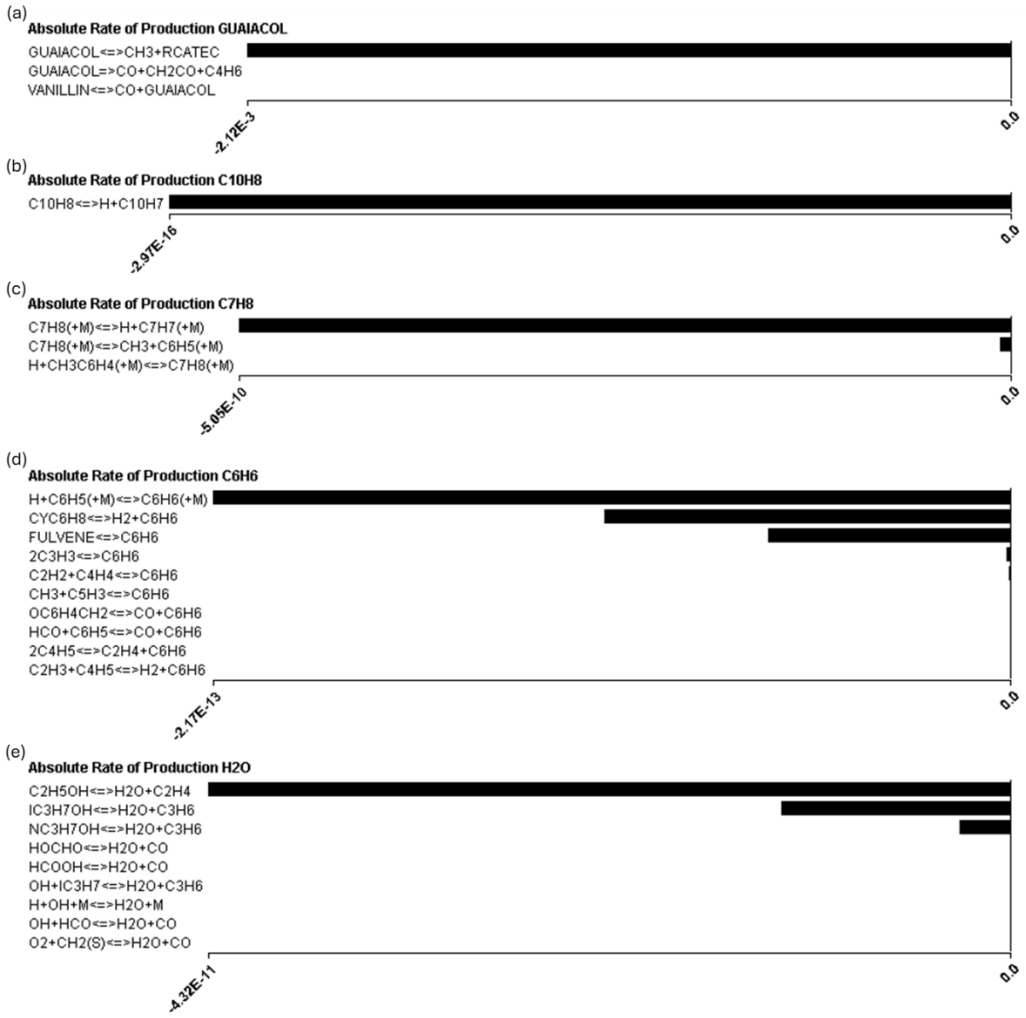

Figure 5.15 – Rate of production analysis (kmol m^{-3} s^{-1}) of different tar species (a-d) and steam (e).

5.6 Analysis of the effect of operating parameters on the process performance

The good matching between results measured during the experimental tests on the large pilot scale gasifier and those obtained by the kinetic model suggests that the model could provide reliable information about the reactor behaviour also when the gasifier is operated at conditions not tested experimentally. The validated model has been used to investigate the impact of design parameters on

the overall performance of the gasifier, in order to better understand the phenomena involved and make predictions on the most suited operating conditions depending on the intended final application of the produced syngas. Among the parameters of interest to be studied, the effect of ER on the performance of the gasifier would be the same as analysed in Section 4.7.1 for all feedstocks, with the main role being that of providing energy to sustain the system. For this reason, ER will not be studied in this case, but the investigation will focus on the other relevant parameters introduced by the use of air enriched and steam as gasification agents, which are the enrichment ratio in the form of x_{O2} and the StC. To ease the assessment, the reactor design has been fixed to be the Faber gasifier and BluPolymer-L the feedstock treated.

5.6.1 Effect of the Oxygen molar fraction: Steam-O_2 vs Air

The model was interrogated to investigate whether the oxygen molar fraction in the enriched air has an impact on the process despite keeping constant ER, and to estimate the extent to which StC (and, in turn, StO_2) must be increased to keep a safe and adequate operating temperature in the reactor (around 850 °C).

Figure 5.16 shows the model results when the oxygen content in the enriched-air stream increases from 0.29 to 1, while the steam injection was increased progressively, from StC 0.79 at x_{O2} 0.29 and StC 1.21 at x_{O2} 0.50, until StC 1.5 under conditions of pure oxygen-steam gasification, i.e. x_{O2} 1. Figure 5.16(a) reports the corresponding dry syngas compositions, as predicted by the model. The results indicate a clear trend with all the chemical species increasing when the oxygen molar fraction is increased.

However, the marked variation cannot be ascribed to the x_{O2} only. Firstly, the increase in x_{O2} in the enriched air is achieved at the expense of N_2 being replaced with steam, therefore the increase in x_{O2} is concurrently associated with a higher amount of steam in the gasification agent, which could participate and promote reforming reactions. Additionally, the results are reported on dry-basis, therefore the above-mentioned higher steam content is condensed and removed from the outlet syngas, increasing the compositions.

Figure 5.16(b) reports the predicted temperature profile when the gasifier is operated at different values of x_{O2}, showing a limited variation that results from the effective replacement of N_2 with steam as a temperature moderation agent.

Similarly, a moderate variation is found for the results of efficiency indicators in Figure 5.16(d) confirming the limited role of x_{O2} in affecting the process. On the other hand, the heating value of the produced syngas increases as a combined result of higher light gas species and lower dry syngas outlet (Figure 5.16(c)).

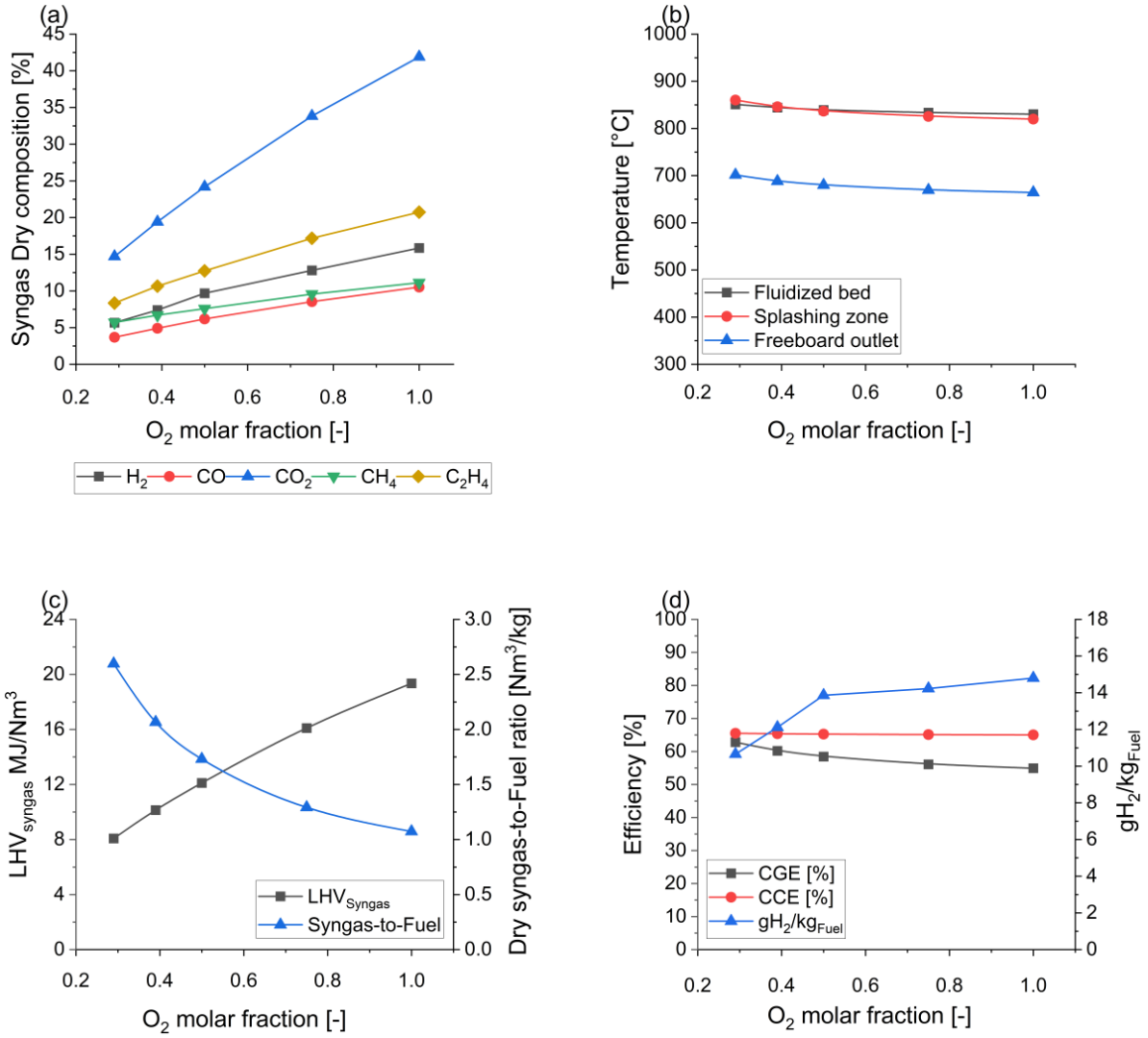

Figure 5.16 – Model predictions of different performance indicators for plastic waste (BluPolymer-L) gasification as a function of x_{O2} and with StC values able to keep the bed reactor temperature at around 850°C with ER 0.25 (a) Syngas composition at the reactor exit, (b) reactor temperature in the bed and splashing zone and exit, (c) syngas heating value and syngas volumetric flow ratio, (d) CGE, CCE and specific yield of hydrogen. Combination of operating conditions are x_{O2}=0.29 StC=0.79 ER=0.25, x_{O2}=0.39 StC=1.05 ER=0.25, x_{O2}=0.50 StC=1.21 ER=0.25, x_{O2}=0.75 StC=1.40 ER=0.25, x_{O2}=1.00 StC=1.50 ER=0.25, using 27 kg/h of BluPolymer-L.

To better identify the role of x_{O2} only, the model projections have been compared on a dry and N_2-free basis in Figure 5.17. A limited increase in CH_4 concentration (from 15% to 11%) and an even more limited decrease in H_2 (from 14.9% to 16.0%) and C_2H_4 (from 22% to 20.7%). These variations appear in agreement with the results provided by [205,206], obtained in a small-scale apparatus. They could be explained by water-gas and steam reforming reactions, whose extensions decrease when StC values are lower than stoichiometric ones.

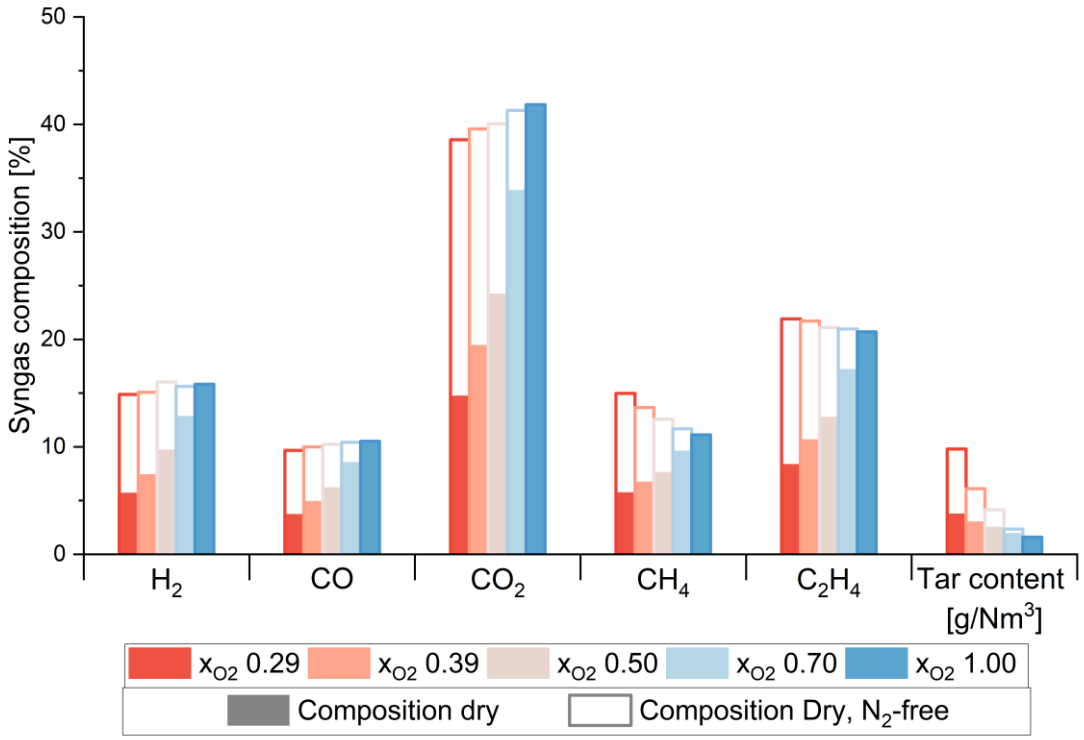

Figure 5.17 – Comparison between syngas composition H_2O-free and H_2O-N_2-free.

Despite the dry and N_2-free syngas composition being marginally affected by x_{O2} and the associated StC, this appears to be an artefact consequence of considering the syngas N_2-free and the concurrent effect of increasing steam content within the system as temperature moderator for higher O_2 concentrations. The full steam-O_2 case, however, should be preferred, as it would overcome the implications of N_2 dilution or the issue of separating the N_2 from products, which in turn incur in significant energy penalties and operating costs, as well as technological challenges. Nonetheless, a slight increase in hydrogen content for higher values of x_{O2} can be seen in the dry-N_2 concentrations, reflecting also the decreased hydrocarbons content, and suggesting that, albeit to a limited extent, the increase in steam would also promote the reforming reactions.

The progressive replacement of N_2 with steam impacts the distribution of light and heavy hydrocarbons, as shown in Figure 5.18. The results suggest an increase in hydrocarbons C3 to C6, with tar content decreasing instead. Interestingly, the tar distribution in Figure 5.18(b) shows a larger content of lighter compounds (C7, C8) within the group of heavy hydrocarbons. This can be attributed to oxygen-rich areas in the bed that could promote the combustion and cracking of the heavier compounds.

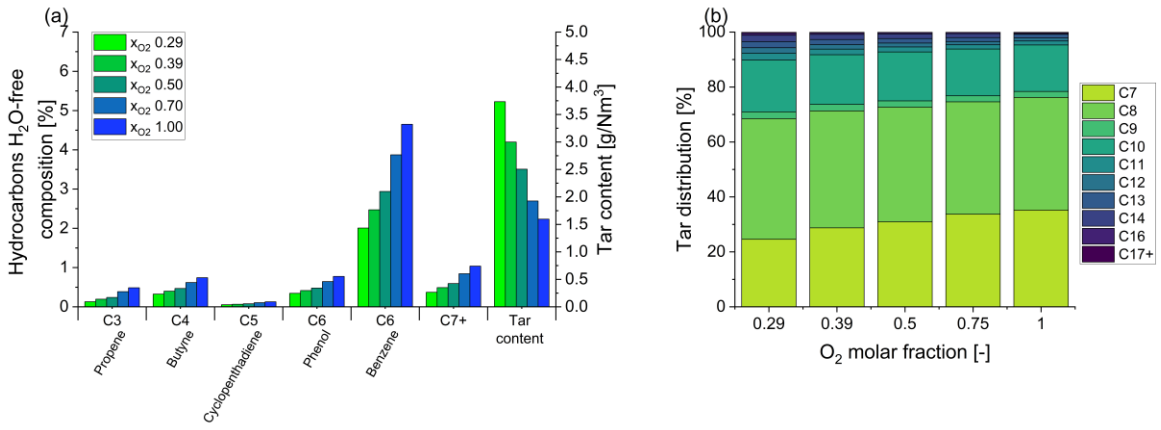

Figure 5.18 – Analysis of heavier hydrocarbons content as a function of the x_{O2}. (a) Hydrocarbons C3+ H_2O-free composition and tar content, and (b) specific tar distribution in the C7+ class.

5.6.2 Effect of the Steam-to-Carbon ratio

The sole effect of steam in the process has been investigated through projections of full-steam-O_2 operations, by varying the Steam-to-Carbon ratio while keeping constant ER at 0.24. This has been done by varying at the same time the amount of fuel, the related oxygen needed to keep the ER constant, and the steam, with the aim of minimizing variations in gas residence time, which would otherwise affect the fluidization regime and the overall model predictions.

Figure 5.19 shows the effect of varying StC on the steam-oxygen gasification of plastic fuels, suggesting dynamics that challenge conventional expectations. Steam plays a crucial role as a temperature moderator, but also as a chemical agent promoting the reforming of char and hydrocarbons, as well as taking part in the water gas shift reaction. The expected effect of increasing the inlet steam would be a reduction of hydrocarbon species and shifting the equilibrium of the water gas shift towards the product, i.e. H_2 and CO_2. Despite this trend holding true on a thermodynamic basis, it is less straightforward for kinetically limited systems, like the one analysed here. Figure 5.19(a) shows the syngas dry composition against the StC; as the StC ratio increases, hydrogen content shows a marginal decrease from 12.3% to 10.6%, while carbon monoxide gradually increases from 9.5% to 12.9%. Carbon dioxide shows a decreasing trend similar to that of the H_2, going from 35% to 32%. The opposite conflicting trend is predicted for methane, showing a marginal decrease from 18% to 14%, and light hydrocarbons, which instead increase with the StC. The higher steam amounts do not significantly promote the reforming of heavier hydrocarbons, suggesting a rather limited influence on the reaction pathway and syngas composition especially at StC larger than 1.5. This behaviour can be attributed to the substantial temperature-moderating effect of steam, evidenced by the marked decrease in both bed temperature (850°C to 750°C) and syngas outlet temperature (700°C to 600°C) with increasing StC ratio in Figure 5.19(b). The lower temperatures appear to overpower the effect of steam in promoting reforming reactions, likely inhibiting the endothermic reforming of heavier

hydrocarbons. This is further supported by the relatively stable efficiencies in Figure 5.19(d). The slight decrease in H_2 and CO_2 suggests a change in the water-gas shift reaction equilibrium affected by the lower temperature. However, the limited change in CH_4 and higher hydrocarbons indicates that steam reforming of these species is not significantly enhanced. It is worth also considering that the reduction in CO_2 content could also be attributed to the relative increase in concentration of the other species, such as the light hydrocarbons. Despite lower temperatures and limited reforming of heavier hydrocarbons, the CGE remains relatively stable at around 60%, with a more substantial increase in syngas LHV from 20 to 25 MJ/Nm³. This can be attributed to the decrease in content of inert species (e.g. CO_2), while the gaseous hydrocarbons increase, contributing to an overall higher heating value.

These results highlight a complex trade-off between syngas composition, process temperature, and overall efficiency. They suggest that kinetic limitations, exacerbated by lower temperatures, may be preventing the system from reaching thermodynamic equilibrium, particularly for steam reforming reactions.

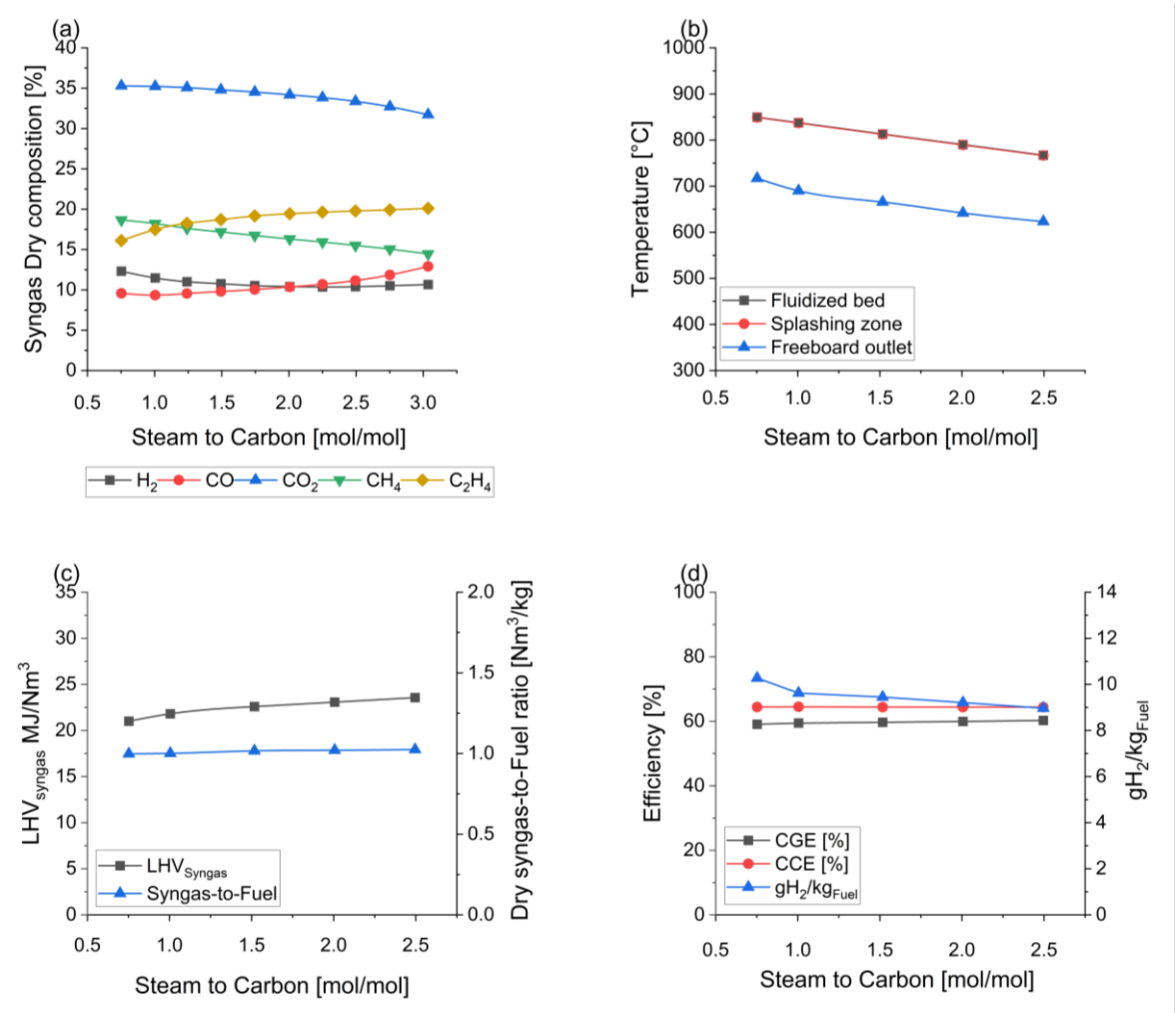

Figure 5.19 – Model predictions of different performance indicators for plastic waste (BluPolymer-L) gasification as a function of the StC, in the case of full steam-oxygen operations at ER 0.24. (a) Syngas composition at the reactor exit, (b) reactor temperature in the bed and splashing zone and exit, (c) syngas heating value and syngas volumetric flow ratio, (d) CGE, CCE and specific yield of hydrogen.

Figure 5.20(a) shows the distribution of hydrocarbons heavier than C2, and a more detailed distribution of tar species is analysed in Figure 5.20(b). The figures show the balance of two contrasting effects induced by the steam. Whilst increasing the steam reduces the operating temperature slowing down reaction kinetics, steam still promotes to a certain extent the reforming reactions of heavier hydrocarbons. The combination of these effects results in a higher content of hydrocarbons with increasing StC, as can be seen for C3 and C6 in Figure 5.20(a), and decreasing tars content, with a wider distribution of heavier species for low StC, as given by the larger fraction of C10+ compounds in Figure 5.20(b).

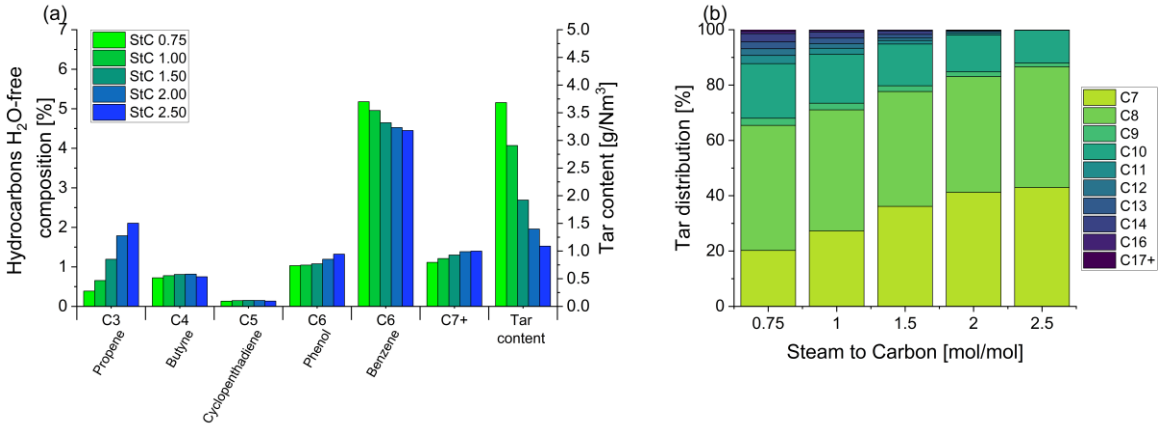

Figure 5.20 – Analysis of heavier hydrocarbons content as a function of the StC, in the case of full steam-oxygen operations at ER 0.24. (a) Hydrocarbons C3+ H_2O-free composition and tar content, and (b) specific tar distribution in the C7+ class.

Overall, StC seems to have a limited effect on syngas composition at values larger than 1.5, possibly due to the limited residence time in the reactor for steam-reforming and water-gas reactions to achieve equilibrium, as already suggested by Basu [22]. However, the role of steam remains crucial to control the temperature profile of the reactor within an acceptable range, highlighting the importance of the steam-to-oxygen molar ratio on the operability of the system. This aspect is particularly important when operating on waste plastic feedstock, due to the extremely high calorific value and the associated risk of hotspots and particles sintering.

The findings underscore the need for careful optimization of the StC ratio to balance syngas quality, process efficiency, and operational constraints. The results point towards the potential benefits of exploring alternative means of maintaining high temperatures at elevated steam ratios to enhance the conversion of heavier hydrocarbons or seeking additional more efficient solutions for tar reforming.

5.7 Effect of feedstock composition

The steam oxygen gasification of plastic and biomass feedstocks presents distinct challenges and opportunities, reflected in the syngas compositions that can be obtained. Figure 5.21 shows the model predictions when operating the gasifier in full steam-oxygen mode, with StC 1.5 and ER 0.24, but using different feedstocks and their blends. In Figure 5.21(a), the biomass-derived syngas exhibited significantly higher hydrogen content (~34%) compared to plastic-derived syngas (~12%), while both feedstocks produced comparable levels of CO and CO_2. Notably, plastic gasification resulted in markedly higher yields of methane (~19% vs ~14%) and other hydrocarbons (~19% vs ~1%) relative to biomass, which can be ascribed to the hydrocarbon-rich nature of plastic devolatilization. The differences in compositions are reflected also in the syngas energy content, with the lower heating value of plastic-derived syngas (~22 MJ/Nm³) being higher than that predicted for biomass-derived syngas (~11 MJ/Nm³).

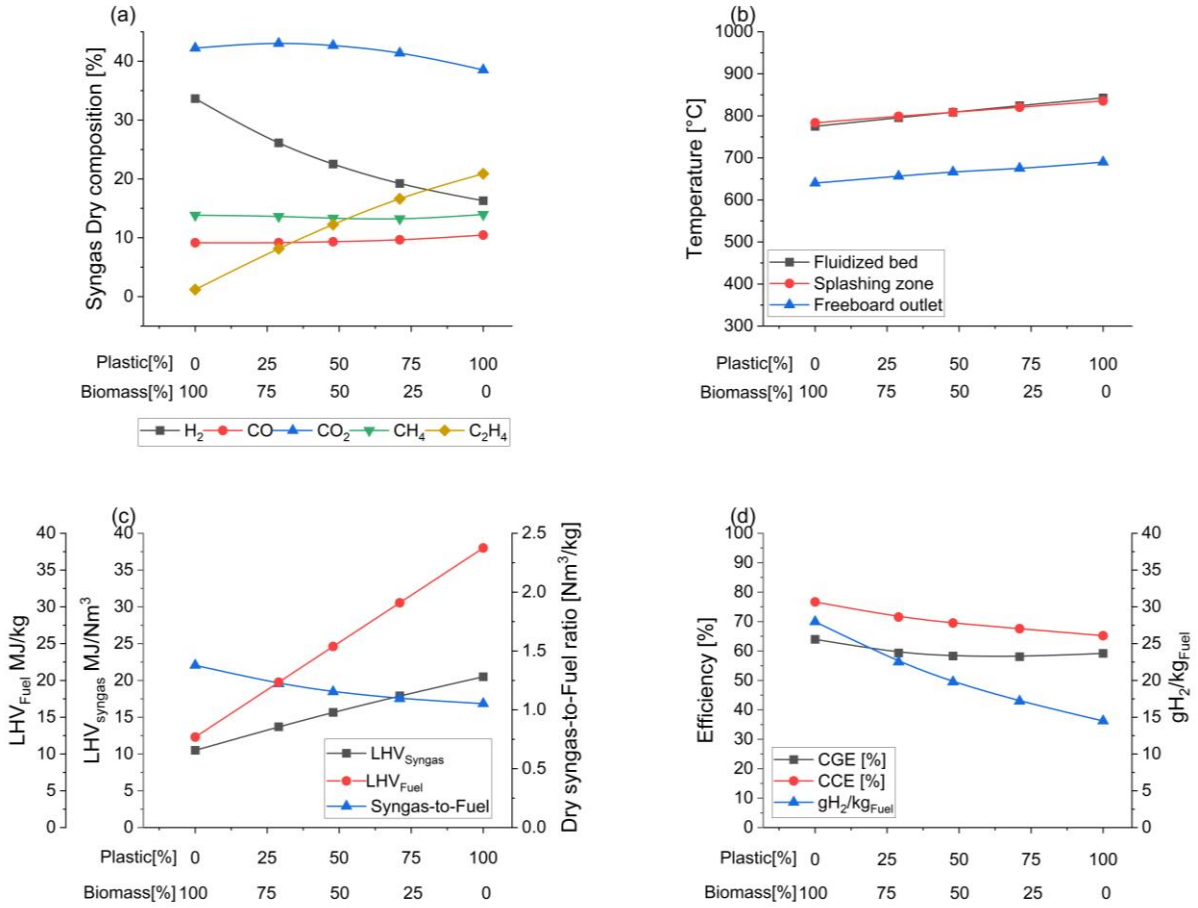

Figure 5.21 – Model predictions of different performance indicators for mixed feedstocks steam-oxygen gasification as a function of the blending ratio, with StC 1.5, ER 0.24. (a) Syngas composition at the reactor exit, (b) reactor temperature in the bed and splashing zone and exit, (c) syngas heating value and syngas volumetric flow ratio, (d) CGE, CCE and specific yield of hydrogen.

These predicted syngas compositions reflect the fundamental differences in feedstock structure: plastic is inherently rich in hydrocarbons, whereas biomass, with its higher oxygen content and complex structure of natural polymers, favours hydrogen and carbon monoxide formation during gasification. Nonetheless, an additional relevant factor impacting the model results is the predicted temperature profile, which is significant between the two feedstocks. As seen experimentally (Section 5.2.3), the high energy content of plastic feedstock poses challenges in the thermal management of the reactor and generally results in higher bed temperatures.

A similar trend can be seen in the distribution of hydrocarbons heavier than C2 as reported in Figure 5.22(a) against different feedstock mixes, from pure biomass to plastics only. Interestingly, the model predicts an overall higher tar content for biomass-rich mixtures, 3.5 g/Nm^3 for biomass against 1.7 g/Nm^3 for pure plastic. When considering the challenges posed by tars during operations of a large-scale gasifier, these results would support the use of plastic-rich blends to minimize the production of tars. Nonetheless, when looking at the specific tar distribution in Figure 5.22(b), this is found to be narrower and skewed towards lighter species (C7 and C8) for biomass-rich blends. Despite the amount of tars being higher, the nature of the chemical species would favour the use of biomass as feedstock instead.

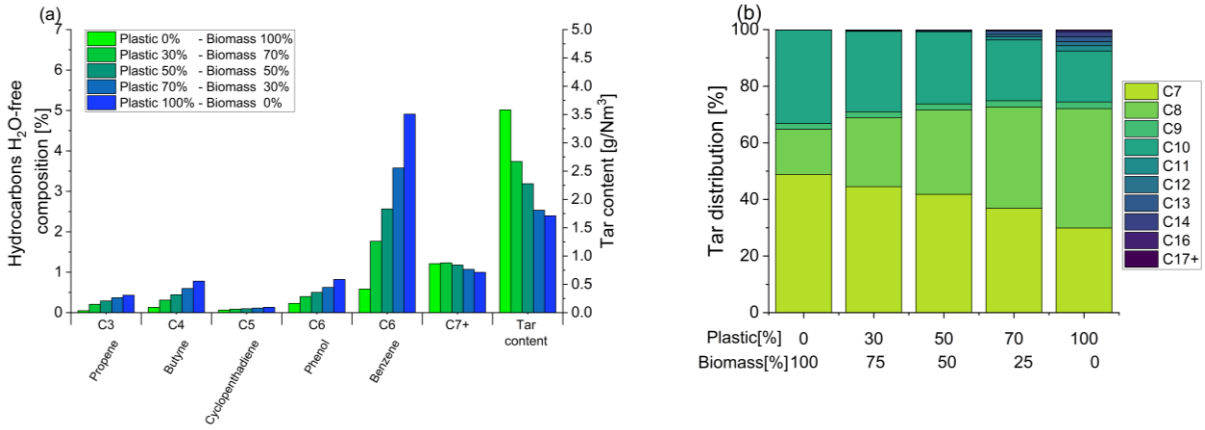

Figure 5.22 – Analysis of heavier hydrocarbons content as a function of the blending ratio, with StC 1.5, ER 0.24. (a) Hydrocarbons C3+ H_2O-free composition and tar content, and (b) specific tar distribution in the C7+ class.

5.8 Concluding remarks

The model effectively reproduces the gasification of plastic waste, biomass and mix of the two feedstocks in a fluidized bed reactor. The results of the model closely align with the available experimental results both in terms of temperature profile and syngas concentration. Where larger discrepancies are found, the model still predicts well the trends and orders of magnitude. In particular, the comprehensive representation of reaction pathways occurring in the freeboard allowed for a more in-depth investigation of tars formation and secondary reactions, which is one of the challenges in

thermochemical conversion processes, and the main bottleneck for the large-scale deployment of gasification technologies of low-value feedstock.

The predictions of the model were used to assess the operations and performance of the gasifier at different conditions to investigate the effect of the main parameters. The results have highlighted clear advantages when operating at full steam-oxygen conditions, but also challenges associated with residual tar content. This offered interesting insights into the potential adoption of the model for reactor design and process optimization. In particular, the results can be summarized as follows:

- **Effect of the oxygen molar fraction**. The model indicates that oxygen concentration in the gasification agent has a limited impact on both process performance and syngas composition on a dry-N_2 free basis. While steam-oxygen gasification offers advantages through nitrogen-free operation, resulting in higher calorific value syngas and simpler downstream separation, the comparable performance with air gasification suggests that the latter might be preferable due to its lower operational costs and energy requirements. This finding has important economic implications for industrial-scale operations.
- **Effect of the steam to carbon ratio**. Steam plays a crucial role in both reaction kinetics and thermal stability of the process. However, at steam-to-carbon ratios above 1.5, the primary influence of the steam shifts to temperature control rather than affecting syngas composition or overall process performance. While steam is commonly believed to promote reforming reactions in thermochemical processes, the model reveals that the system is more sensitive to operating temperature variations. Furthermore, increasing steam content proves ineffective at reducing tar content in the syngas, indicating that additional tar-removal technologies would be necessary depending on downstream applications.
- **Effect of the feedstock composition**. The model predictions reflect the fundamental differences in feedstock characteristics. Plastic-rich feedstocks generate syngas with higher heating value, while biomass-derived syngas exhibits notably higher H_2 content. However, both feedstocks and their blends produce significant amounts of heavy hydrocarbons, necessitating additional tar reduction strategies. Although each feedstock presents distinct challenges, particularly regarding their behaviour in the fluidized bed, both offer opportunities for sustainable resource utilization.

Chapter 6. Analysis of waste gasification for hydrogen production integrated with carbon capture technologies

The recent quest for systems that could potentially provide negative emissions and the requirement of a reliable and constant source of renewable energy has generated new interest towards new classes of low-carbon hydrogen. The transition toward a hydrogen-based economy has gained significant momentum as a promising pathway for decarbonization, yet the technical viability and environmental benefits of hydrogen production have not been fully explored. Bioenergy systems, like waste gasification, associated with Carbon Capture and Storage (BECCS), can make a significant contribution to meeting 2050 climate change targets. Among BECCS, hydrogen from biomass offers the greatest opportunity for carbon-negative emissions.

This chapter presents a comprehensive assessment of a waste gasification plant for waste-to-hydrogen production, integrated with CCS technologies. A large part of the plant inventory data and layout were provided by industrial partner ABSL. A full-plant process simulation has been developed to understand the technical feasibility of the process, with a focus on the environmental implications of H_2 production and CO_2 permanent storage. Different scenarios have been considered to find the process layout associated with the highest energy efficiency and the most successful solution in minimizing the carbon footprint of the overall process.

Part of the work presented in this chapter has been produced as part of the "Hydrogen GGR Demonstration Project", awarded by BEIS for the "Greenhouse Gas Removal Technology Innovation Programme – Phase 1"

Part of this chapter has been published in:

Amaya-Santos, G., Chari, S., Sebastiani, A., Grimaldi, F., Lettieri, P., Materazzi, M. (2021). Biohydrogen: A life cycle assessment and comparison with alternative low-carbon production routes in the UK. Journal of Cleaner Production 319 (2021) 128886. https://doi.org/10.1016/j.jclepro.2021.128886.

6.1 Introduction

In recent years, low-carbon hydrogen has received increasing attention as a high-efficiency energy vector that could be produced from both fossil and non-fossil sources, with low GHG emissions associated with production, and no emissions at the point of use. Around the world, hydrogen is increasingly viewed as a key energy carrier for heating and transportation, especially for sectors such as buses, shipping, and railways where electrification is less feasible. As a result, hydrogen is expected to play a significant part in driving industrial change and features prominently in both the UK's and Europe's long-term industrial strategies. The CCC has recognised the important role that hydrogen plays in decarbonising the UK energy system in its recent Net-Zero report [30].

Sustainable H_2 can be generated by thermochemical treatment (gasification) of biomass or waste feedstocks followed by a sequence of steps for gas conditioning and carbon dioxide removal [207]. An additional purification step is typically needed for transport-grade hydrogen, given the extreme sensitivity of commercial fuel cells to contaminants, such as CO (poison reversible <50 ppm per stack) and sulphur (poison at concentration 0.5 - 1.0 ppm) [208]. The process is most attractive when it uses waste as a feedstock, resulting in lower costs and added environmental benefits, contrary to the current, standard yet polluting waste disposal alternatives (e.g. landfill and incineration). Although hydrogen is a clean fuel at the point of use, its production from waste the operation phase of the plant has both, positive and negative contributions to the environment. Whilst it diverts waste from more polluting practices, such as landfill or incineration, the associated energy consumption of a thermochemical plant carries a significant environmental burden [209].

This final chapter aims at understanding and investigating a possible pathway for sustainable hydrogen production, via waste gasification and integrating the plant with carbon capture and storage technologies. The investigation relies on full plant process assessment using the newly developed model integrated with Aspen Plus simulations to produce mass and energy balances. Understanding the energy efficiency of the process is crucial to investigating the technical feasibility of the proposed process, as well as understanding the environmental benefits. The comprehensive analysis includes first an assessment of the different feedstocks investigated in the previous chapters, namely waste woody-biomass, RDF and plastic waste. The different materials offer unique challenges and opportunities with regards to the overall plant efficiency and H_2 productivity, but even more for environmental benefits associated with the nature and origin of the feedstock. Other important aspects are linked to the end-use of the produced H_2, with different sectors having different purity requirements and limit on other contaminants. Finally, the investigation also considers the role of different carbon capture technologies and the implication of their integration within the waste-to-H_2 plant.

6.2 Technological aspects of a WtH_2 Plant

The overall process examined in this work focuses on the use of waste as sustainable feedstock, mainly due to the typical large availability and low cost of such materials. This study follows and builds upon the extensive investigation of the gasification stage performed with the kinetic model. The different sources considered are waste woody biomass, waste plastics and refuse derived fuel, as analysed in the previous chapters. Although waste poses technical challenges for its use as a chemical feedstock, its suitability has already been proven at pilot and demonstration scale [9,210]. Furthermore, from a climate change perspective, the use of waste as feedstock not only ensures large and economical availability for consistent hydrogen supply, but also avoids the use of current disposal technologies, which are known to contribute enormously to GHG emissions and water and land pollution [211].

A few pilot and demonstration scale examples are present in UK, and this work is specifically based on the plant scheme of one of these [42,51].

Waste cannot be thermochemically treated in the original form upon collection, and different pre-treatments are needed depending on the different sources and types. For example, untreated municipal or commercial waste is first mechanically processed in a material recycling facility (MRF). This is done to homogenise the material and remove part of the moisture, recyclables (e.g., metals and dense plastics) and reject materials (e.g, oversize and inert). Typically, a 100,000 ton MSW feed produces an output of about 60,000 to 80,000 ton of RDF with a moisture content of 10–17 %, 10–20 % ash content and 15–25 MJ/kg calorific value (CV). Generally, the quantity of organic (biomass) content in the feedstock can vary from 40-60% in weight in household waste, while this exceeds 90% in the case of waste woody-biomass. Waste treated to give greater than 90% biogenic content is considered to be on a par with biomass for many of the incentive schemes in UK, although as it is still a waste-derived fuel, it remains subject to all the environmental controls relating to waste. [39].

The mixed plastic waste feedstock, instead, is the stream rejected from an MRF when the majority of metals (ferrous and nonferrous), glass, paper and cardboard, and recyclable plastics are normally recovered. The remaining non-recyclable plastic waste residue from the MRF can be contaminated by some residual organic components, which require additional sorting and cleaning.

After the feedstock-specific pre-treatment, the material is shredded using tearing motion to achieve a rough shred of waste residues, with a homogenous, predetermined particle size between 1-50 mm, depending on the gasification reactor requirements. The final feedstock is in the form of a floc of refuse-derived fuel (RDF), which is then further dried on-site using waste heat from the process. Additional information regarding the feedstocks considered is reported in Section 3.2.

Several sectors can be identified as early adopters of the hydrogen produced, including the use as industrial heat or commodity for the chemical industry (e.g. methanol or ammonia production). Although other sectors present less stringent hydrogen purity requirements and limits on contaminant limits, decarbonizing heavy transport has been regarded as a more urgent priority. Moreover, producing hydrogen at the highest purity standards ensures compatibility with all potential end-users, following a conservative design approach. Therefore, bus fleets have been identified as the earliest adopters of hydrogen for transport. A typical bus will consume around 5 tpa of H_2. A large depot will operate around 100 buses, i.e. 500 tpa or 20 GWh. This equates to around 5% of the yearly production of the Waste-to-H_2 plant scale identified. This suggests that transport applications in the medium term are likely to be serviced by slip streams from larger plants designed to service grid or industrial customer applications.

6.2.1 Plant description

This chapter focuses on the production of H_2 through gasification, with a summary process flow diagram shown in Figure 6.1.

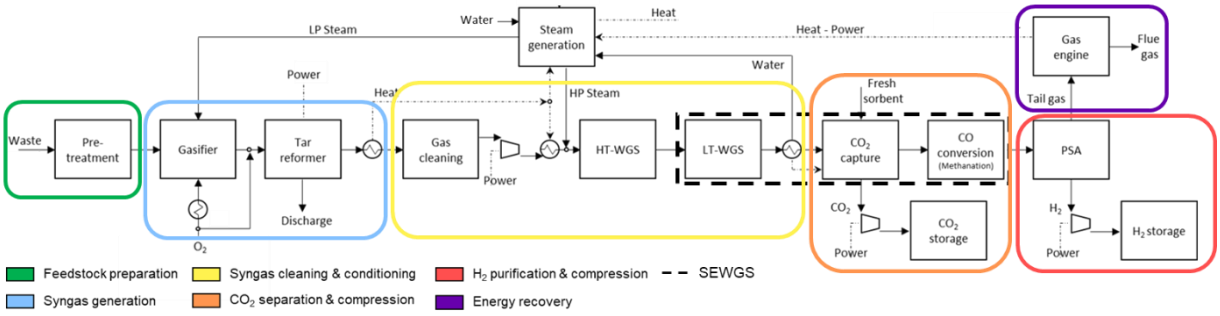

Figure 6.1 – Process flow diagram of the hydrogen production plant from different waste feedstocks integrated with carbon capture and storage.

6.2.1.1 Syngas generation

Following the MRF and pre-treatment, the newly prepared feedstock is fed to the syngas generation block. This includes a two-stage process for gasification and tar reforming; the gasifier is a fluidized bed reactor operated using oxygen and steam as gasification and fluidizing agents. The gasifier is operated with a steam-to-carbon molar ratio of 1.5 and ER of 0.24 for all types of feedstocks. The use of pure oxygen instead of air generates a N_2-free syngas which simplifies the gas cleaning and hydrogen purification downstream. Following the gasifier, a high-temperature tar-reforming stage is always required to decompose the input material into tar-free syngas, and to separate ashes and solid particulate in a vitrified form. The tar reforming unit is usually an energy-intensive stage of the process, powered by oxy-combustion or plasma power, which generates a clean, high temperature syngas (>1200°C) [212]. Materazzi et al [210] have investigated the feasibility and effectiveness of

plasma-assisted gasification for clean syngas production; a preliminary investigation and proof of concept of temperature-induced tar reforming for syngas cleaning has been performed at lab scale and the results are reported in Appendix D.

The hot syngas is then cooled down to approximately 160°C in a waste heat boiler where heat is recovered producing steam at medium pressure (10 bar). This steam is recirculated and used within the process facilities.

6.2.1.2 Syngas cleaning and H_2 production

After heat recovery, the syngas is cleaned from acid gases and other contaminants. A typical cleaning system for small scale (<100,000 tpa) waste-based plants includes dry filters and acid and alkaline wet scrubbers [213]. In the reference case, a dry-cleaning system composed of a ceramic filter is used to remove fine particulate materials from the syngas stream and heavy metal vapours. The syngas acid content is also reduced by means of neutralizing chemical agents (e.g. sodium bicarbonate and activated carbon). The syngas is then sent to a quench-acid scrubber with absorption of ammonia, and an alkaline scrubber to remove the acid compounds and the remaining contaminants. The clean syngas is then passed through a series of guard beds to further reduce the remaining contaminants below 0.1 ppm for use in commercial catalysts and fuel cells [214]. In particular, a zinc oxide bed can be used to further reduce sulphur levels, and additional sacrificial copper-zinc and activated carbon beds to protect the copper catalysts generally used in subsequent water gas shift reactors. The H_2 bulk production stage takes the cool, clean, low-pressure syngas into a series of catalytic water gas shift reactors to increase the fraction of hydrogen, with the remaining fraction being mostly CO_2 and steam, to be separated in the following stage. A final methanation stage is then introduced to further reduce the residual CO to ppm levels, required for the safe operation of proton-exchange membrane (PEM) fuel cells [215].

6.2.1.3 CO_2 separation

After being dewatered, the gas stream is a mixture of H_2 and CO_2, with some other minor components which include N_2, CH_4, and traces of CO and other light hydrocarbons. Whilst post-combustion capture from the flue gas of a biomass power station is not yet a common practice, the technologies used for both power generation and post-combustion capture are mature and each at a state of development where they could be classed as commercially proven.

There are many commercially deployed techniques for separating CO_2 from process streams with the optimal solution depending on factors such as the required specification of the product stream, CO_2 purity, and the temperature and pressure conditions of the inlet and outlet streams [216]. The commercial technologies for pre-combustion CO_2 capture available today differentiate according to the solvent used, and in the reference plant, a monoethanolamine (MEA) carbon capture technology

with 90% carbon capture rate is considered. This technology achieves a high removal efficiency, and the captured CO_2 has a high purity that makes it suitable for other industrial applications or long-term sequestration. Nonetheless, the effect of different carbon capture technologies and the implication of their integration within the H_2 production plant has been investigated in Section 6.6.1.

Once separated, the CO_2 stream is compressed to 60 bar and transported via lorry, sea tankers and finally through pipelines prior to being injected in saline aquifers at 120 bar. Following CO_2 removal, there are residual contaminants in the H_2 stream (mostly CO, CO_2, CH_4 and N_2) that would require a dedicated separation stage to reach the purity required for the transport-grade H_2. The H_2-rich stream is often purified via pressure-swing adsorption (PSA) to obtain a H_2 stream suitable for the final end-use, which is then compressed for storage

6.2.1.4 H_2 purification and electricity production

In the reference process analysed here, the PSA is employed to achieve the minimum requirements of purity and other contaminants for H_2 to be used in low temperature fuel cells. However, achieving the high purity reduces the H_2 recovery and the overall product yield, which results in a significant loss of H_2 into the tail gas. The hydrogen is pressurized at 200 bar and stored, while the remaining tail gas is used for energy recovery for internal use purposes, generating heat and electricity via a Jenbacher gas engine. Besancon et al. [217] studied the link between hydrogen purity requirements for use in fuel cells and the capabilities of production. The authors reviewed different methods for H2 production and purification, and investigated the recovery and purity of a PSA operating at 28 bar and 30°C. They reported that a >99.98% H_2 purity, with CO levels lower than 0.5 ppm can be obtained with H_2 recovery of 83%.

Different H_2 end-users require different purities and requirements, with fuel-cell representing the most stringent application requiring the highest H_2 purity and lowest concentration of contaminants, CO in particular [29]. The effect of different H_2 requirements and the implication on the operations of the PSA has been investigated in Section 6.5.1.

6.3 Integration of the 1D kinetic model for the full plant simulation

Full plant process simulations were developed using Aspen Plus (V12.1). The development of the process simulation was directly informed by the results of the detailed modelling of the fluidized bed gasifier presented in Chapter 4, particularly regarding feedstock-to-syngas conversion and syngas composition. The methodology section outlines the feedstocks used, and the Aspen models used to simulate the production of BioH2 from the feedstock, on a constant energy throughput basis of 65MW. The modelling consists of two sections; the first is the gasification section, with the cleaning of the syngas produced after the gasification, with results taken from the kinetic model. The syngas

composition and feedstock conversion parameters used are reported in Table 6.1. The second section uses the clean syngas to produce H_2 using two stages WGS reactors, followed by carbon capture, and purification of the products with a PSA. Additional information on the parameters regarding each unit developed on Aspen Plus can be found in Table 6.1.

A sophisticated set of models has been developed to predict the performance of different pre-combustion CCS technologies, as well as the balance of plant on a fully integrated biohydrogen system. These models, which have been developed on Aspen Plus simulation software, were validated with a combination of extensive operating experience and data from the Swindon plant (with relation to gasification and gas cleaning sections), and literature data for the CCS systems and hydrogen purification packages. Details of model assumptions and design criteria for the syngas cleaning are provided elsewhere [31,210]. Details related to the syngas–to-hydrogen production model, including the CCS section, are provided in the next section. For this work, the facility is designed and modelled to convert approximately between 60 and 120 tpa of feedstock to approximately 40 MW of high-purity hydrogen. The lower mass flowrate is required in the case of plastic waste due to the significantly higher heating value of the feedstock.

Table 6.1 – Syngas composition and feedstock conversion parameters obtained from the 1D kinetic model and used into the process simulation.

	Waste woody-biomass	RDF	Plastic waste
Syngas/waste wt. ratio	2	2.42	3.31
Steam/waste wt. ratio	0.98	1.23	1.83
Oxygen/waste wt. ratio	0.28	0.42	0.75
Syngas composition (mol/mol)			
H_2O	0.5734	0.6525	0.7386
CO	0.0411	0.0311	0.0258
CO_2	0.1684	0.1450	0.0950
CH_4	0.0601	0.0459	0.0344
H_2	0.1433	0.0880	0.0402
C_2H_4	0.0038	0.0254	0.0483
C_3H_6	0.0002	0.0007	0.0010
C_4H_8	0.0006	0.0010	0.0019
C_5H_{10}	0.0003	0.0003	0.0003
C_6H_6	0.0026	0.0059	0.0121
C_6H_6O	0.0038	0.0002	0.0001
C_7H_8	0.0002	0.0024	0.0014
$C_{10}H_8$	0.0022	0.0016	0.0009

In addition to the equipment required for CO_2 separation (absorption and desorption columns, pumps, heat exchangers, pressure reduction tanks, etc.), heat integration systems and multistage compressors for storage have been included in the models. Flowsheets of the process simulation developed are reported in Appendix C.

6.3.1 Development of the process simulation

Particular attention of this work was paid to thermodynamic models to have an accurate representation of the physic-chemical behaviour of different solvents. This required the selection of different thermodynamic models suited for different sections of the process. Since the overall process involves operations at high pressure, with nonpolar or mildly polar compounds, the Soave-Redlich-Kwong (SRK) cubic equation of state has been chosen as the general thermodynamic model for the simulation. This model is characterized by the Peneloux-Rauzy method for liquid molar volume correction which results in more accurate liquid molar volumes. Furthermore, the model employs the Kabadi-Danner mixing rules when dealing with water-hydrocarbon systems, and NBS steam table are used for calculating properties of water for better accuracy. The NBS steam table provides greater accuracy and SRK is designed to work with it. The enthalpy, entropy, Gibbs energy, and molar volume of water are calculated from the steam tables. The total properties are mole-fraction averages of these values with the properties calculated by the equation of state for other components. Fugacity coefficient is not affected.

When considering the carbon capture technologies, different thermodynamic models were deemed necessary to better simulate the different systems. The electrolyte non-random two-liquid (ElecNRTL) model was used for the aqueous electrolyte system (namely MEA and Benfield). The perturbed-chain statistical associating fluid theory (PC-SAFT) is a method particularly suited for copolymer systems and therefore, chosen for Selexol and Rectisol. The Redlich Kwong equation of state, with the Holderbaum and Gmehling mixing rule is chosen for the CO_2 capture process. The calculation of the activity coefficient model is done by Uniquac for which the interaction parameters are fitted on measured data from the literature. The CO_2 equilibrium was studied and modelled to optimize the methanol loss calculation in the CO_2 stream leaving the desorption column. The simulation of the absorption is performed with a rigorous 2- or 3-phase fractionation for single columns (RadFrac) distillation model. The same model is used to simulate the desorption for the chemical processes (MEA and Benfield), while a depressurization tank is used for physical processes. Finally, the solvent flow rate is selected to perform CO_2 separation with 90% capture rate and minimum steam consumption in the thermal regeneration at the conditions examined. The solvent regeneration column is calculated for each case, as a residual CO_2 concentration is determined in the lean solvent in order to be compatible with the required CO_2 purity (>95%) in the top of the absorption column. Solvent makeup is added to the recycled stream before it enters into the absorber in order to compensate for the solvent loss during the absorption and stripping process. The solvent is added at different pressures and temperatures depending on the specific case. For example, a low operating

temperature of -35°C is chosen for the methanol in order to minimize the solvent losses and to maximize the carbon dioxide solubility.

Additional details of all unit operations and key modelling assumptions for this work are reported in Table 6.2 below.

Table 6.2 – Summary of key assumptions for the process simulations and the different carbon capture units investigated.

Unit block	**Key assumptions:**			**Ref:**
Plasma reactor	Model: Gibbs equilibrium reactor, adiabatic - O_2 inlet added to reach 1100°C - Electricity requirements for power generation informed by plant operators			[9]
Syngas cleaning	Agents: H_2SO_4 and NaOH Model: Stoichiometric reactors with neutralizing agents calculated based on the scrubbers requirements			[218]
Multistage Compressors	Isentropic efficiency: 0.75 Mechanical efficiency: 0.95 Pressure ratio: up to 2.5			[219]
Pumps	Mechanical efficiency: 0.80			[219]
Water Gas Shift	**First Step:** Catalyst: Fe/Cr Inlet temperature: 350 °C Model: Gibbs equilibrium, adiabatic		**Second Step:** Catalyst: Cu-Zn Inlet temperature: 250 °C Model: Gibbs equilibrium, adiabatic	[31]
CCS	**Sorbent**	**Absorption Column:**	**Regeneration column:**	
MEA	Monoethanolamine 30% in water	Pressure: 3 bar Inlet temperature: 55 °C N° stages: 20 Capture rate: 90%	Pressure: 1.5 bar Inlet temperature: 110 °C N° stages: 30 CO_2 purity: 95%	[220,221]
K_2CO_3 (Benfield-like process)	K_2CO_3 30% in water	Pressure: 9 bar Inlet temperature: 70 °C N° stages:15 Capture rate: 90%	Pressure: 1.5 bar Inlet temperature: 115 °C N° stages:30 CO_2 purity: 95%	[220,222]
SELEXOL	Dimethyl ethers of polyethylene glycol (DEPG)	Pressure: 36.5 bar Inlet temperature: 25 °C N° stages:10 Capture rate: 90%	Pressure: 1 bar Inlet temperature: 55 °C N° stages: 1 (depressurization tank) CO_2 purity: 955%	[220,223,224]
RECTISOL	Methanol	Pressure: 36.7 bar Inlet temperature: -35 °C N° stages:10 Capture rate: 90%	Pressure: 1 bar Inlet temperature: 20°C N° stages: 1 (depressurization tank) CO_2 purity: 95%	[220,224,225]
SEWGS	K-promoted hydrotalcite	Pressure: 24 bar (adsorption), 1 bar (desorption) Capture rate: 90%	Productivity: 2.5 molCO_2/kg h Total Steam requirement: 0.28 S/C CO_2 purity: 95%	[226–229]
Methanation	Catalyst: 30% Nickel / Al_2O_3 Inlet temperature: 300 °C Inlet pressure: 27 bar Model: REquil equilibrium, adiabatic operations Reactions: CO and CO_2 hydrogenation to methane			[49]
PSA	Inlet pressure: 40 bar H2 recovery: 83-95%, H2 purity: > 95% Splitting factors: literature data			[230,231]
Gas engine	Efficiency: 40% electricity, 50% thermal energy			[219]

An equilibrium-based approach has been used to simulate additional reactors, using an RGibbs unit for the tar reforming stage, and REquil for the water gas shift reactors. The RGibbs model performs rigorous calculations on reactions and multiphase equilibrium based on the minimization of the Gibbs free energy. The main limitation of this approach is that RGibbs assumes the system reaches the thermodynamic equilibrium, although this can represent an overestimation of the yields of the reactor, it provides reliable information on the potential of the system. Furthermore, the catalytic reactors included in the process are mature and industrial benchmarks, resulting in overall performance close to thermodynamic equilibrium.

Despite this being optimistic, due to the assumption that the system reaches the thermodynamic equilibrium, it appears to be the most suited approach in representing the complex phenomena occurring in the tar reforming unit without over-complicating the process simulation. REquil model instead performs rigorous equilibrium reactor based on a stoichiometric approach, i.e. considering the thermodynamic equilibrium for the given reaction. This unit was specifically chosen to model the H_2 bulk production in the water gas shift reactors, which are reported to have a conversion close to the theoretical equilibrium [232].

A rate-based model is used to simulate that absorption column to have an accurate estimation of solvent required to meet CO_2 purity (>95%). The rate-based calculation allows for a more realistic simulation and sizing of the separation column, based on mass transfer rate calculations on tray and packing and not equilibrium stages. The same rate-based calculation type is used for the simulation of the regeneration column. This is done to provide a conservative, but accurate, estimation of thermal energy required by the reboiler and also for the improved accuracy in sizing of the column. A CO_2 recovery of ~90% is envisaged while modelling all 5 technologies.

6.4 Assessment of H_2 production from different feedstocks

Mass and energy balance analysis serves as the primary tool for assessing plant performance, encompassing feedstock quantities, major process streams (steam and O_2), energy requirements, and final product yields. The analysis evaluates Net Energy Efficiency (NEE), conversion gas efficiency, and biomass-to-hydrogen efficiency as technical parameters for assessing process feasibility and comparing different plant configurations. NEE calculations, particularly crucial for process optimization and scale-up considerations, consider the complete process chain from waste reception to hydrogen and CO_2 generation ready for off-take. This includes all electrical and thermal loads (solvent regeneration and gas compression) and rejected materials, providing a comprehensive view of the process energy requirements and potential optimization points. These parameters are derived from Aspen models, with gasifier outputs informed by detailed 1D kinetic modelling results. The

biomass-to-hydrogen conversion efficiency, a crucial performance indicator, measures the energy content of pure pressurized hydrogen as a percentage of feedstock energy content. This metric parallels the gasification plant's cold gas efficiency (CGE), which relates clean syngas energy to original feedstock energy on a gross heating value basis, enabling direct comparison with other thermochemical conversion processes.

Performance assessment of the H_2-production plant considered three feedstocks: biomass, RDF, and plastic waste, at a fixed scale of 65 MWth waste material input, chosen based on relevant literature applications. Table 6.3 presents the comprehensive mass and energy balance for all three feedstocks. The analysis assumes fuel-cell grade H_2 production (>99.99% purity, CO content below 0.5ppm) and 90% CO_2 capture using MEA as solvent. While maintaining consistent plant scale, efficiency variations arise from specific hydrogen recovery and carbon capture rates, highlighting the impact of feedstock composition on process performance.

Table 6.3 – Summary mass and energy balance for the different feedstocks considered.

		Units	**Biomass**	**RDF**	**Plastic Waste**
Feedstock		ktpa	126.36	97.20	58.68
	[A]	MW_{th}	65.00	65.00	65.00
Steam to gasifier (StC 1.5)		ktpa	123.57	119.19	107.61
O_2 to gasifier (ER0.24)		ktpa	35.03	40.39	44.26
O_2 to tar reformer		ktpa	36.08	34.66	31.19
Clean shifted syngas		ktpa	197.21	183.10	155.85
	[B]	MW_{th}	49.93	48.31	47.85
CO_2 sequestered		ktpa	162.08	150.28	126.21
H_2 produced		ktpa	8.48	8.23	8.13
	[C]	MW_{th}	41.24	39.99	39.51
Net electricity consumption	[D]	MW	8.80	7.39	5.87
Net thermal energy consumption	[E]	MW_{th}	13.17	11.69	9.65
Waste-to-clean syngas conversion efficiency	[B]/[A]	%	76.82	74.33	73.61
Waste to H_2 conversion efficiency	[C]/[A]	%	63.45	61.53	60.79
Net energy efficiency	[C]/ {[A]+[D]+[E]}	%	47.42	47.56	49.07

Analysis of the scenarios reveals significant differences in feedstock quantities processed, reflecting the different heating values, with biomass requiring the highest flowrate due to lower heating value. This implies increased collection and transport costs for biomass, though RDF and plastic waste may incur comparable costs due to complex collection, sorting, and pretreatment

requirements. The feedstock composition significantly influences process parameters and design considerations. For instance, the higher oxygen and moisture content in biomass affects the oxidation reactions in the gasifier, leading to different temperature profiles and syngas compositions compared to plastic waste and RDF. These differences cascade through the entire process, affecting downstream unit operations and overall system integration.

The scenarios also differ in auxiliary feed requirements, despite consistent operating conditions (ER 0.24 and StC1.5) and tar reforming parameters (1100°C). Biomass processing requires less O_2 and steam in gasification due to inherent moisture and oxygen content but demands higher O_2 injection before tar reforming to compensate for lower gasifier outlet temperatures and syngas heating value. This trade-off between gasification and reforming requirements highlights the importance of considering the entire process chain when optimizing operating conditions. Steam requirements significantly impact overall plant efficiency, with heat primarily recovered from the waste-heat boiler post-tar reforming, demonstrating the critical role of heat integration in process optimization.

The waste-to-hydrogen conversion efficiency exceeds 60% across all options investigated, slightly lower than literature values, potentially due to conservative predictions of the 1D model in waste conversion and syngas composition. This high efficiency primarily results from implementing a two-stage water gas shift section, maximizing hydrogen (and CO_2) production while minimizing CO and water content. The WGS section design represents a critical optimization point, balancing conversion efficiency against capital and operating costs. Before entering the WGS stages, clean syngas mixes with steam to promote a shift toward H_2 and CO_2. Steam requirements vary by feedstock composition, maintaining a steam-to-carbon ratio of 1.5 (considering CO and CO_2 forms). This results in different technological implications: approximately 110 ktpa for biomass, 103 for RDF, and 88 for plastics, with each scenario presenting unique challenges for steam system design and heat integration.

Net energy efficiency remains below 50% for all three feedstocks, with plastic waste demonstrating the highest efficiency. A detailed analysis of energy flows reveals multiple contributing factors to efficiency losses. The integration of CO_2 capture introduces significant additional energy demands proportional to capture quantity, requiring both electricity and heat for capture plant operation and dehydration/compression processes. Individual contribution analysis reveals thermal energy as the dominant factor, primarily associated with solvent regeneration requirements. Using MEA as a chemical solvent requires 4-4.2 MJ per kg CO_2 removed. This energy penalty represents a significant optimization opportunity, potentially addressable through advanced heat integration or alternative capture technologies. The relatively low efficiencies also reflect stringent transport application purity requirements, particularly CO content limitations, resulting in approximately 80% H_2 recovery in PSA, with tail gas utilized for energy generation in a gas engine.

Figure 6.2 presents Sankey diagrams illustrating energy flows across the three feedstocks, providing crucial insights into process integration opportunities. While the plastic-to-H_2 scenario produces the least hydrogen (39.5 MWh_{HHV}) compared to biomass and RDF, it requires minimal external energy. This advantage stems from more favourable syngas composition and lower auxiliary stream requirements. Notably, the high-power requirements for tar reforming can be met using energy recovered from PSA tail gas, demonstrating effective energy integration.

The Sankey diagrams also highlight key areas for potential efficiency improvements, particularly in heat recovery and utilization of process streams.

Despite these efficiency limitations, all scenarios demonstrate favourable performance compared to other bioenergy technologies (such as post-combustion CCS) and align with typical biohydrogen plant efficiencies based on biomass feedstock [40,233,234]. The analysis of CO_2 capture performance reveals significant advantages over alternative waste-to-fuel pathways. The CO_2 capture quantity (exceeding 120,000 tons annually) significantly surpasses other Waste-to-Fuel facilities like bioSNG or FT fuels, indicating enhanced environmental benefits where CCS is available. This advantage is particularly pronounced for biomass and waste feedstocks due to the biogenic nature of captured CO_2, contributing with potential negative emissions. The detailed analysis of capture performance also reveals opportunities for optimization through improved solvent selection and process integration.

Two strategies emerge for improving overall plant efficiency: exploring different H_2 end-uses with varying purity requirements to enhance PSA recovery, and investigating alternative carbon capture technologies to identify optimal solutions. The first strategy could significantly impact overall efficiency by allowing higher H_2 recovery rates, though this must be balanced against end-use requirements. The second strategy offers the potential for reducing energy penalties associated with CO_2 capture, particularly through the implementation of alternative solvents or novel capture technologies. Both strategies warrant further investigation in subsequent sections, focusing on RDF feedstock, selected for its balanced technical and environmental considerations, representing a practical compromise between process complexity and environmental benefit.

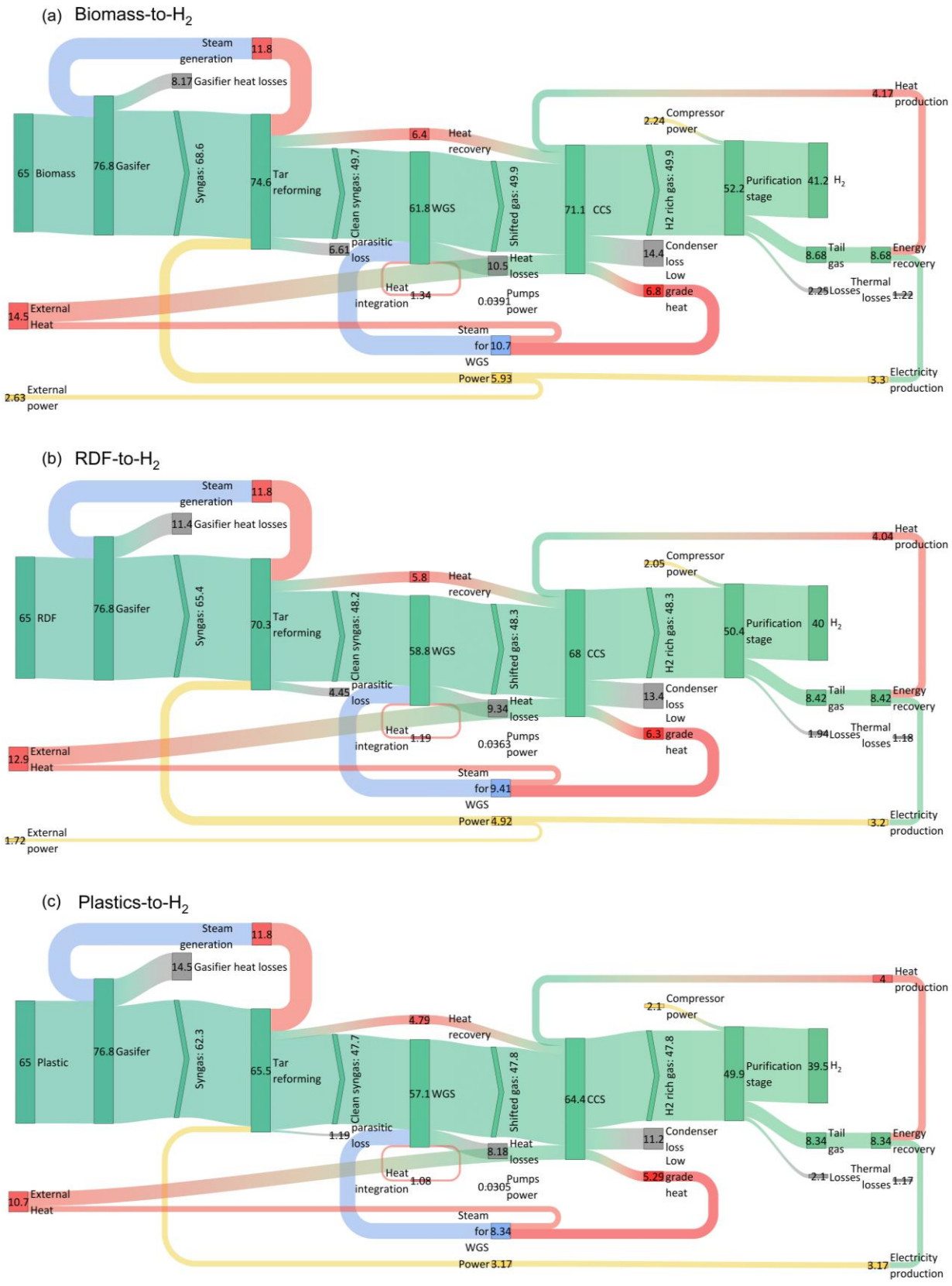

Figure 6.2 – Sankey diagrams representing the energy flows of H_2 production from (a) biomass, (b) RDF and (c) plastic waste. Energy flows reported in MWh_{HHV}.

6.5 Assessment of process performance for different H_2 end-uses: the role of purity

The selection of a process route for hydrogen production with CO_2 capture requires careful consideration of both CO_2 and hydrogen purity requirements, which vary significantly across applications. Figure 6.3 illustrates global H_2 consumption by sector, including projected growth through 2050 aligned with Paris Agreement goals.

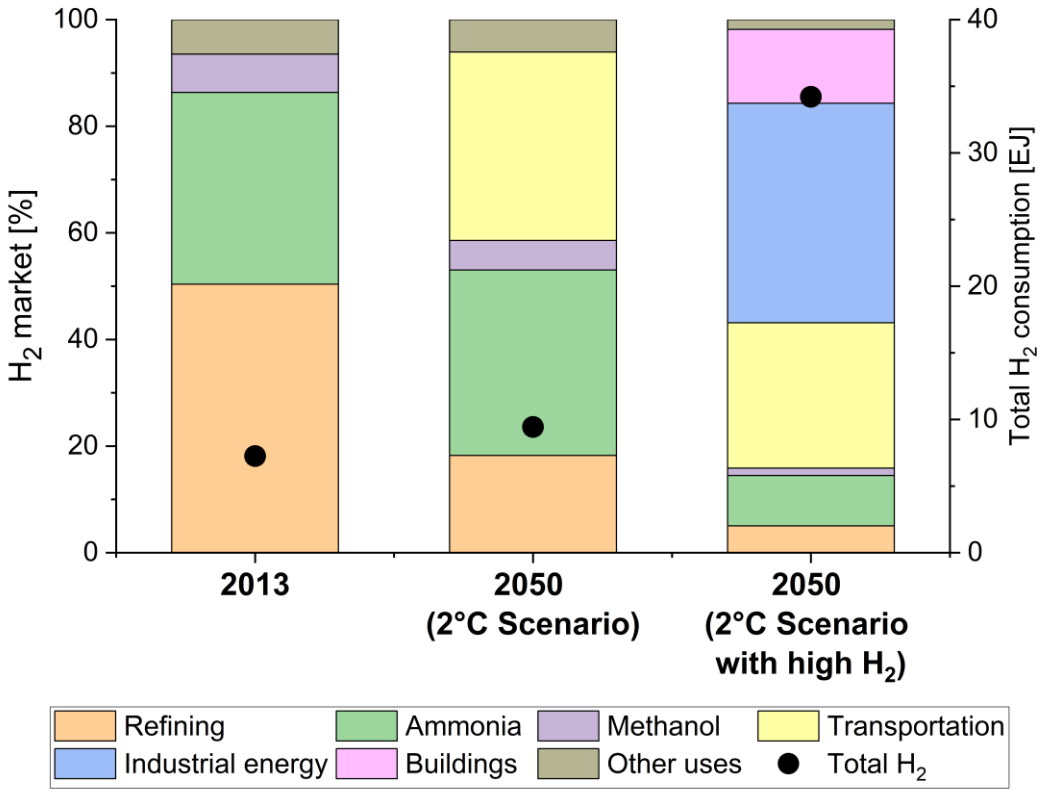

Figure 6.3 – Global hydrogen consumption by sector in EJ in 2013 and anticipated future use in 2050 in the IEA standard 2°C scenario and high-hydrogen 2°C scenario. Adapted from [235].

Hydrogen applications across industries require varying purity levels based on specific process needs. In refining operations, hydrogen at approximately 95% purity supports hydrotreating and hydrocracking processes. These units can utilize hydrogen from external sources or generate it on-site through steam methane reforming or partial oxidation. The processes demand minimal sulphur content to protect catalytic systems [236,237].

Ammonia synthesis requires hydrogen to combine with nitrogen, typically introduced during the reforming stage. This process demands strict control of contaminants including carbon monoxide, carbon dioxide, water, and sulphur species to preserve catalyst functionality [235].

PEM fuel cells represent one of the most demanding applications, requiring exceptional hydrogen purity. These systems are highly sensitive to multiple contaminants: carbon monoxide and sulphur

compounds can degrade catalysts, while ammonia can damage membranes. ISO standards specify strict purity requirements for both mobile and stationary applications.

For gas turbine applications, hydrogen purity requirements focus primarily on combustion characteristics. While inert components have limited impact, the presence of combustible species like methane and carbon monoxide requires careful consideration. Industrial fuel applications follow ISO standards specifying 99.9% minimum hydrogen purity, with specific limits on components such as nitrogen (maximum 400 ppm) to ensure proper turbine operation [238].

Table 6.4 – Hydrogen purity requirements for various end-user sectors. Adapted from [235].

Application	H_2 minimum purity [%]	Impurity limits [ppm]	Ref.
Refining	>95	S: low levels	[239,240]
Ammonia	23-25 (N_2:74-77)	CO_2, CO, H_2O, S: low levels	[235,241,242]
Industrial fuel (heating)	>99.90	O_2:100 ppm, N_2:400 ppm, S:10 ppm H_2O, HC: NC	[238]
PEM fuel cells	>99.97	CO:0.2ppm, S:0.004ppm, CO_2:2ppm, NH_3:0.1 ppm, O_2:5ppm, H_2O:5ppm, HC:2ppm, H_2:300 ppm, N_2+Ar:100 ppm	[238]

S: sulphur compounds, HC: hydrocarbons, NC: Not to be condensed

Transportation applications impose the most stringent purity requirements. When hydrogen requires transport and storage, particularly for liquefaction, additional purification through adsorption becomes necessary to achieve impurity levels below 1 ppm. These enhanced purity requirements distinguish transported hydrogen from cases where production and use occur on-site.

This diverse range of purity requirements adds complexity to process design, particularly as specifications for certain applications continue to evolve. The selection of appropriate purification technologies must therefore balance achieving required purity levels with process efficiency and economic considerations.

6.5.1 Technological considerations arising from H_2 purity requirements per sector

As discussed in section 6.4, one of the major efficiency penalties in the waste-to-H_2 plant is the low PSA recoveries required to achieve high-purity H_2 for fuel cell applications. This analysis considers additional relevant applications, assessing various purification solutions to achieve both required purity levels and maximum overall efficiency. The base case scenario remains transport-grade H_2 production from RDF integrated with MEA-based carbon capture at a 90% capture rate. Additional scenarios were evaluated with an increased capture rate of 95%. Despite higher energy penalties

associated with the increased capture rate, the lower volume flow rate of the gas stream to be purified in the PSA allowed for a reduction in power consumption for gas conditioning, while the reduction of inerts and contaminants in the H_2-rich gas enabled generally higher recovery of H_2 in the PSA. The investigation was expanded to include refining and industrial fuel end-uses (combined as Refining), with H_2 for ammonia production being combined with the industrial fuel scenario due to compatible impurity levels. Figure 6.4 presents a summary of the combinations and different scenarios evaluated.

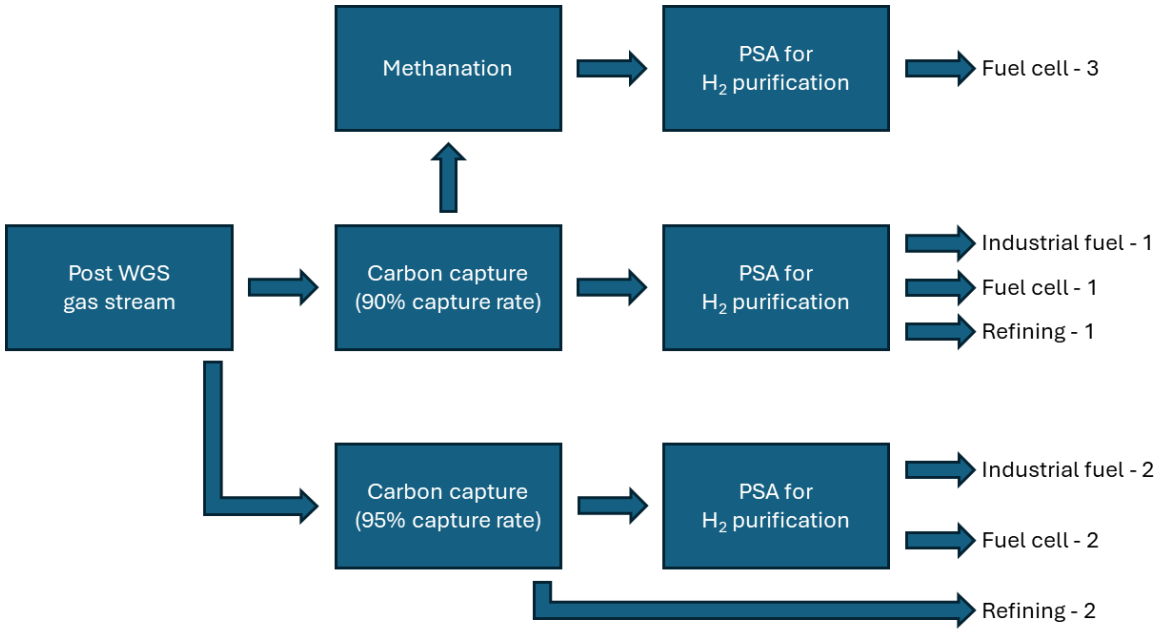

Figure 6.4 – Summary of the H_2 purification solutions considered for each end use.

Due to stringent CO impurity limits, achieving required purity levels results in lower H_2 recovery in the PSA. This led to the development of an additional case, designated as "fuel cell - 3" in Figure 6.4, tailored to the fuel cell impurity limits. This scenario incorporates chemical conversion of CO and CO_2 in a methanation reactor, taking advantage of higher allowable hydrocarbon content and easier separation of CH_4 from H_2 in the PSA. However, this approach has drawbacks, including high energy requirements for the methanation reactor (operating at 27 bar and 300°C) and H_2 consumption during reactions. Table 6.5 presents the comprehensive mass and energy balance results for all scenarios, designed for each of them to meet the standard requirements for the end-use, as outlined in Table 6.4.

The analysis projects that higher capture rate cases are preferable, enabling increased H_2 recovery in PSA and higher overall plant productivity, with Waste-to-H_2 efficiency exceeding 70% for refining, industrial fuel, and ammonia applications. This efficiency increase is offset by additional energy requirements for higher capture rates, resulting in only marginally higher net energy efficiency compared to 90% capture rate cases. Nevertheless, scenarios with 95% capture rate outperform their

90% capture rate counterparts when considering the environmental benefits of increased CO_2 capture and permanent storage.

Table 6.5 – Summary mass and energy balance for all scenarios.

		Units	**Industrial fuel - 1**	**Industrial fuel - 2**	**Refining - 1**	**Refining - 2**	**Fuel cell - 1**	**Fuel cell - 2**	**Fuel cell - 3**
Feedstock (RDF)		ktpa	97.2	97.2	97.2	97.2	97.2	97.2	97.2
	[A]	MW_{th}	65.00	65.00	65.00	65.00	65.00	65.00	65.00
Clean shifted syngas		ktpa	183.10	183.10	183.10	183.10	183.10	183.10	183.10
	[B]	MW_{th}	48.41	48.41	48.41	48.41	48.41	48.41	48.41
CO_2 sequestered		ktpa	150.28	158.63	150.28	158.63	150.28	158.63	158.63
H_2 produced		ktpa	9.13	9.40	9.41	19.91	8.23	9.06	8.83
	[C]	MW_{th}	43.99	45.67	45.67	48.31	39.99	43.99	42.85
Net electricity consumption	[D]	MW	9.13	9.72	9.82	11.20	7.39	9.28	8.96
Net thermal energy consumption	[E]	MW_{th}	13.66	15.21	14.47	16.48	11.69	14.41	13.46
Waste to H_2 conversion efficiency	[C]/[A]	%	67.67	70.26	70.26	74.32	61.53	67.67	65.92
Net energy efficiency	[C]/ {[A]+[D] +[E]}	%	50.10	50.78	51.15	52.12	47.56	49.60	49.01

Among the fuel cell-grade H_2 production routes analysed, scenarios 2 and 3 (increased capture rate and methanation reactor addition) surpass the base case. However, the methanation reactor option proves less favourable, demonstrating lower overall efficiencies and H_2 yield compared to the scenario fuel cell – 2. This reduced performance stems from significant H_2 consumption in CO removal and unavoidable reactions with residual CO_2 [243].

6.6 Assessment of the integration of different carbon capture technologies in the Waste-to-H_2 plant

In the conversion of waste to hydrogen, carbon capture and storage (CCS) technologies serve as indispensable components for reducing environmental impact and enhancing the overall sustainability profile of the process. The separation at industrial scale typically employs absorption technologies, where gases are brought in contact with liquid solvents within scrubber columns to remove specific contaminants. The solvent rich in impurities is then heated and/or undergoes pressure reduction in a dedicated regeneration column, yielding two distinct streams: one containing the

extracted components and another of regenerated solvent that circulates back to the scrubber column.

Various capture technologies have emerged, each offering distinct advantages and operational considerations. These range from conventional chemical absorption methods to physical absorption systems. In chemical absorption, solvents dissolve and react with CO_2, and the process is characterized by fast reaction kinetics that enables reduced plant footprints. Common chemical absorbents include aqueous solutions of amines compounds such as MEA, triethanolamine (TEA), and methyldiethanolamine (MDEA), alongside hot potassium carbonate solutions, as represented by the Benfield process. Physical absorption systems, conversely, operate through CO_2 dissolution and the solvent is regenerated through pressure reduction or increase in temperature. Both approaches result in a reduction of solubility of CO_2 in the solvent, consuming less thermal energy than their chemical counterparts. These systems typically allow for simultaneous CO_2 and H_2S separation in sour-gas sweetening processes. Notable physical solvent technologies include Rectisol®, which employs refrigerated methanol, Selexol™, utilizing dimethyl ethers of polyethylene glycol (DEPG), and Purisol®, based on N-methyl-2-pyrrolidone (NMP).

Chemical solvents are characterized by higher absorption capabilities at rather low CO_2 partial pressures, where the capacity increases with pressure elevation until reaching saturation thresholds. Physical solvents, while having lower absorption rates at low CO_2 partial pressures, have a direct proportional absorption capacity with CO_2 partial pressure in accordance with Henry's law. This characteristic makes chemical solvents particularly suitable for low CO_2 partial pressure applications, despite their substantial thermal energy requirements for regeneration.

In this section, the technical implications of adopting different carbon capture technologies have been investigated. Conventional chemical absorption methods utilizing MEA and potassium carbonate have been compared to the physical absorption processes Selexol™ and Rectisol®. The investigation has expanded to include advanced solid sorbent technologies, and in particular sorption enhanced water gas shift (SEWGS). SEWGS represents an innovative approach that combines the water gas shift reaction with in-situ CO_2 capture in an integrated unit operation. SEWGS systems operate with multiple columns in parallel, following the concept of PSA. Despite not being available at large commercial scale, the SEWGS offers several advantages: it overcomes equilibrium limitations associated with the WGS reaction by means of in situ removal of CO_2, and it can achieve nearly 100% carbon capture rate with minimal increases in energy requirements from typical rates of 90-95%.

6.6.1 Impact of different carbon capture technologies on the performance of the plan

Five different carbon capture technologies were evaluated for integration with a waste gasification plant for H_2 production. The comparison was conducted using the same input conditions across all technologies: clean syngas (approximately 19,000 kg/h at 0.175 barg and 40°C) first processed through two-stage water gas shift reactors for H_2 production. This pre-shift configuration was chosen to ensure a fair comparison between conventional technologies (MEA, K_2CO_3, Selexol, and Rectisol) and SEWGS, which instead combines low-temperature WGS and CO_2 capture. All technologies were designed to achieve 90% capture rates, with CO_2 purity exceeding 95% and fuel-cell grade H_2 production.

The results for the overall mass and energy balance for all the technologies investigated are reported in Table 6.6. The Net Energy Efficiency (NEE) calculations consider the entire process chain, from waste wood reception to final H_2 and CO_2 processing for transportation and storage, including all electrical and thermal loads, solvent regeneration, gas compression, and material rejection. The plant scale remained constant across all cases, maintaining identical capture rates, syngas input, and H_2 production. Consequently, while waste-to-hydrogen conversion efficiency remained constant, net energy efficiency varied based on specific hydrogen recovery and energy requirements of each carbon capture technology.

Table 6.6 – Summary mass and energy balance for the different carbon capture technologies, with capture rate of 90%.

		Units	**MEA**	**K_2CO_3**	**Selexol™**	**Rectisol®**	**SEWGS**
Feedstock (RDF)		ktpa	97.2	97.2	97.2	97.2	97.2
	[A]	MW_{th}	65.00	65.00	65.00	65.00	65.00
Clean shifted syngas		ktpa	183.10	183.10	183.10	183.10	183.10
	[B]	MW_{th}	48.41	48.41	48.41	48.41	48.41
CO_2 sequestered		ktpa	150.28	158.63	150.28	158.63	150.28
H_2 produced		ktpa	8.23	8.23	8.23	8.23	8.23
	[C]	MW_{th}	39.99	39.99	39.99	39.99	39.99
Net electricity consumption	[D]	MW	8.04	8.23	9.64	9.23	8.39
Net thermal energy consumption	[E]	MW_{th}	11.69	12.662	0.77	2.57	-1.23
Waste to H_2 conversion efficiency	[C]/[A]	%	61.53	61.53	61.53	61.53	61.53
Net energy efficiency	[C]/ {[A]+[D]+[E]}	%	47.20	46.59	53.04	52.07	55.42

The analysis revealed that NEE ranges from 46% for K_2CO_3 (Benfield-like technology) to 55% for SEWGS. While all CCS technologies demonstrated high CO_2 selectivity, minimizing product losses, they exhibited different energy penalties. For chemical technologies, including MEA and K_2CO_3, the primary energy penalties were associated with reboiler duties for solvent regeneration, with MEA showing marginally better performance through lower heat requirements. The thermal energy requirements were found to be 4-4.2 MJ per kg CO_2 removed, consistent with literature data [244].

The physical technologies showed lower thermal energy consumption due to pressure-based solvent regeneration, though they required higher electricity consumption due to elevated operating pressures (~47 bar). Selexol outperforms Rectisol due to the different CO_2 solubility characteristics of the two solvents, but also due to the cryogenic operating conditions which Rectisol entails, requiring specialized equipment. The cryogenic operations limited heat integration opportunities for Rectisol within the thermochemical process, which typically operates in a higher range of temperatures.

SEWGS technology achieved the highest efficiency at 55.42% due to reduced steam requirement for combined WGS and CO_2 release, generating excess thermal energy (~1 MWth). It demonstrated the lowest total net electricity consumption among physical technologies, with the capability for higher capture rates with minimal additional energy penalties.

The energy analysis (Figure 6.5 and Figure 6.6) revealed that thermal energy represents the dominant factor, particularly for chemical separation techniques

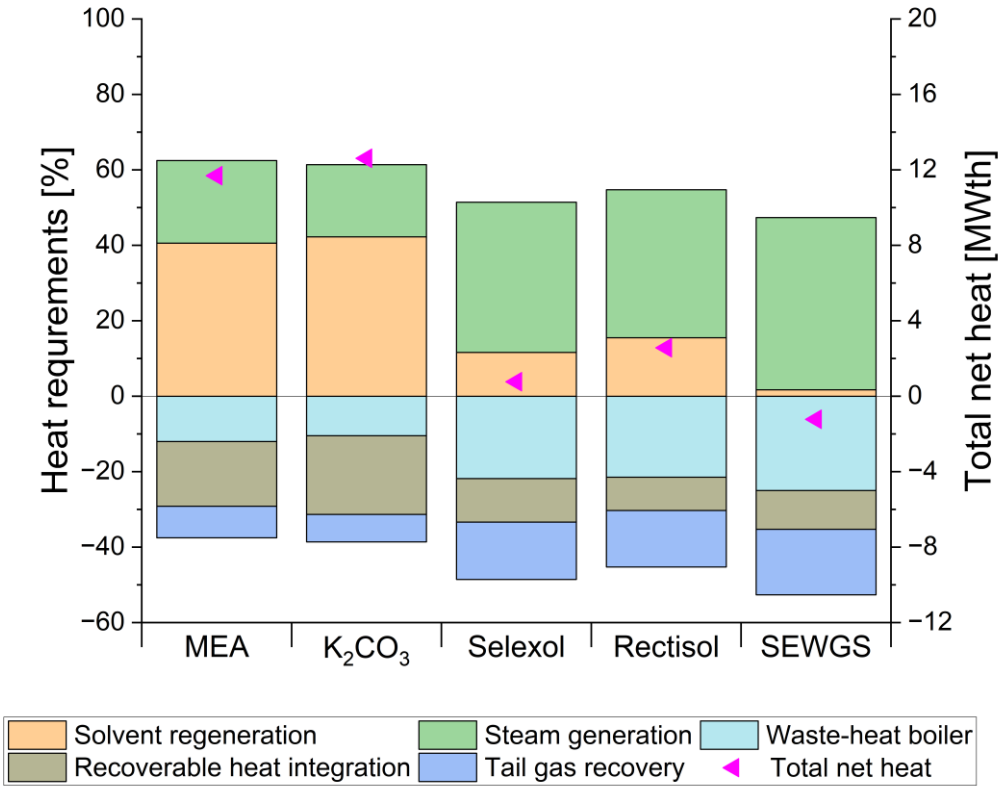

Figure 6.5 – Breakdown of contributions of heat requirements in the Waste-to-H2+CCS plant with the different technologies investigated for CO_2 removal.

. While chemical solvents showed higher heat requirements for regeneration, they offered greater potential for heat integration. Electrical consumption remained relatively consistent across technologies, primarily due to H_2 purification requirements in PSA, which offset the benefits of low-pressure operation in chemical solvents.

Other relevant contributions are associated with the additional compressors required for delivering hydrogen and CO_2 products at pressure in all cases investigated, as well as the electricity to power the tar reforming unit. SEWGS shows the lowest total net electricity consumption when compared to the other physical technologies, however, it entails more complex technological design and operations compared to the other technologies.

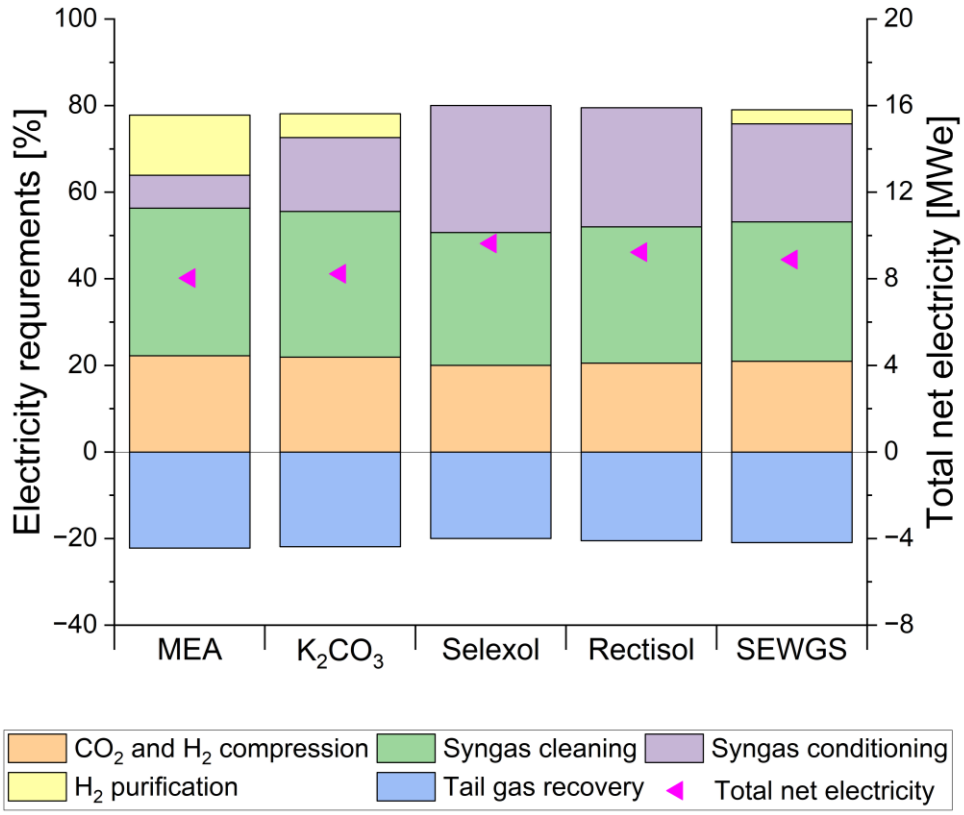

Figure 6.6 – Breakdown of contributions of electricity requirements in the Waste-to-H_2+CCS plant with the different technologies investigated for CO_2 removal.

It is worth mentioning that the comparison has been done on the same basis of carbon capture rate of 90%, however, each technology presents different challenges when increasing the capture rate.

Regarding scalability to higher capture rates, each technology presents distinct characteristics, despite all scenarios presented here having the same capture rate at 90%. Chemical solvents show a non-linear increase in energy consumption and solvent requirements being limited by the solubility of

CO_2 and sizing of the columns, while physical technologies demonstrate a rather linear increase in energy requirements for solvent regeneration. SEWGS exhibits minimal energy penalty for increased capture rates, mainly related to steam requirements for purging and rinsing cycles. Furthermore, SEWGS can deliver H_2 at the design purity, making additional H_2 purification redundant and potentially improving overall plant efficiency by combining WGS, carbon capture, and H_2 purification in one unit.

This comprehensive analysis demonstrates that while all technologies can achieve the desired capture rates, their selection should consider the balance between energy efficiency, operational complexity, and potential for integration within the broader process.

6.7 Environmental reflection on H_2 production from waste

As discussed in Section 1.4, the production of H_2 integrated with CCS offers substantial environmental benefits, particularly when using biomass and waste feedstocks due to their biogenic CO_2 content. Biogenic carbon sources in waste include food, wood, paper, textiles, and bio-plastics. These biogenic carbon emissions have lower climate change impacts compared to fossil emissions because the released carbon is partially balanced by its uptake during biomass growth [245,246]. The proportion of biogenic carbon in waste therefore becomes a critical factor in determining the environmental performance of waste management systems with CCS, as sequestering biogenic carbon effectively reduces atmospheric carbon levels. Such technologies that sequester more carbon than they release over their lifecycle are classified as "negative emission technologies" [247]. Both biomass and RDF-based processes qualify as BECCS technologies, enabling crucial negative emissions.

Figure 6.7 presents a preliminary environmental assessment using Life cycle assessment (LCA) methodology, comparing climate change impacts across different carbon capture technologies for the Waste-to-H_2 plant, normalized to 1 ton of H_2 produced. The analysis includes a base case without carbon capture, where H_2 is purified via PSA, energy is recovered from tail gas in a gas engine, and flue gas is released to the atmosphere.

In the assessment, positive climate change impacts represent direct and indirect greenhouse gas emissions. Direct emissions are released on-site, e.g. from gas engines. Indirect emissions are associated with the supply chain and end-of-life treatment (where applicable) of chemicals and energy in UK. The climate change impacts that are negative in sign represent avoided greenhouse gas emissions associated with the displacement of natural gas and electricity. The total climate change impact is also reported on the graph, calculated as the sum of direct and indirect emissions.

As expected, carbon capture technologies based on physical absorption (i.e. Selexol, Rectisol and SEWGS) outperform chemical absorption. Direct and indirect carbon emissions, represented by the positive contributions in Figure 6.7, for physical technologies range from 4044 kg CO_2-eq. for SEWGS

to 4825 and 5359 kg CO_2-eq. per ton of H_2 for Selexol and Rectisol, respectively. They are significantly higher for chemical technologies, totalling 8111 and 8717 kg CO_2-eq. for MEA and K_2CO_3. The emissions from the carbon capture phase are dominated by the consumption of thermal energy that is required to regenerate the solvent, representing nearly two-thirds of all carbon emissions. The remaining emissions originate from the purification of the H_2-rich stream and from the compression of the captured CO_2 stream. The energy penalties associated with solvent regeneration have a significant impact on the environmental performance of the process, resulting in overall direct emissions being higher than the base case without CCS, rendering the integration of chemical an unfavourable solution to be avoided.

However, when considering avoided emissions, particularly from the permanent sequestration of biogenic CO_2 from waste, the environmental benefits become clear. While fossil CO_2 from waste plastics remains carbon-neutral, those associated with the biogenic nature of carbon contribute to negative emissions when captured. The avoided emissions and CO_2 credits are comparable across all capture technologies and often exceed the sum of direct and indirect emissions. This crucial finding demonstrates the process's potential to not only deliver low-carbon hydrogen but also achieve negative emissions, particularly with MEA and physical absorption technologies.

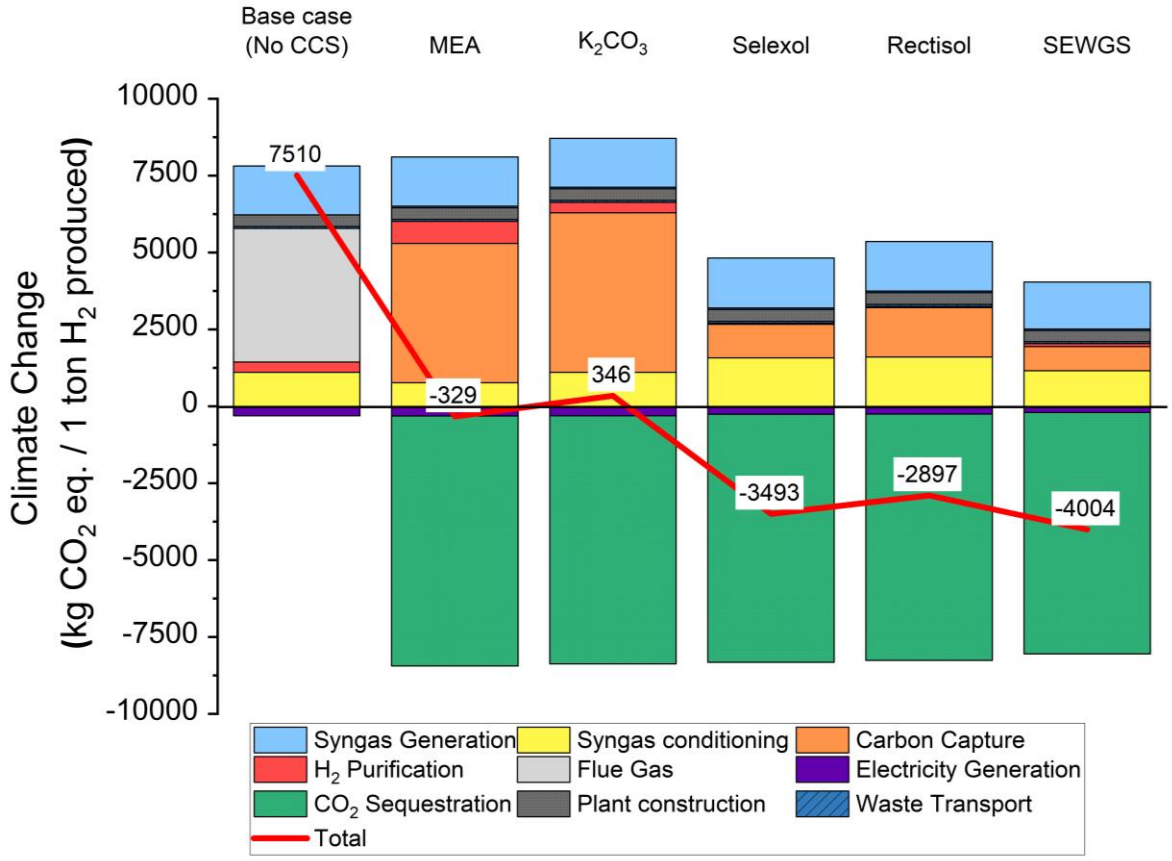

Figure 6.7 – Comparison of climate change impacts for alternative carbon capture technologies.

Waste-to-H_2 integrated with CCS, particularly when using physical solvents, demonstrates significant potential for achieving carbon-negative emissions, which are crucial for offsetting emissions from hard-to-abate sectors such as heavy transport and aviation. The environmental benefits extend beyond direct emissions reduction, including the avoided impacts from conventional H2 production routes. For comparison, blue hydrogen produced via methane reforming with CCS generates significant emissions: 2,248 $kgCO_2eq$. per ton of H_2 for autothermal reforming and 2,510 $kgCO_2eq$. per ton of H_2 for steam methane reforming. Even green hydrogen from electrolysis produces approximately 1,670 $kgCO_2eq$. per ton of H_2. Both these conventional technologies show substantially higher environmental impacts compared to waste-derived H_2 when biogenic CO_2 credits are considered.

The results can be interpreted in a broader context and compared with conventional waste management technologies. A techno-environmental assessment of a conventional WtE plant retrofitted with CCS capabilities is provided in Appendix E. To ensure a fair comparison, the functional unit for both systems has been normalized to 1 ton of waste treated. Despite the higher energy penalties associated with operating the carbon capture unit, waste gasification for hydrogen production still outperforms the WtE-CCS plant. Additional details are available in Appendix E.

As shown in Figure 6.8, the analysis of process efficiencies for fuel cell-grade H_2 production from waste gasification demonstrates that physical capture technologies offer superior performance in both energy efficiency and climate change mitigation. Among these, SEWGS emerges as the leading technology across all evaluated metrics. For commercially mature technologies, Selexol presents the optimal solution for carbon capture. However, despite these clear advantages, the implementation of physical absorption technologies requires careful consideration of technical and safety aspects due to their high operating pressure requirements. These considerations warrant further investigation before large-scale deployment.

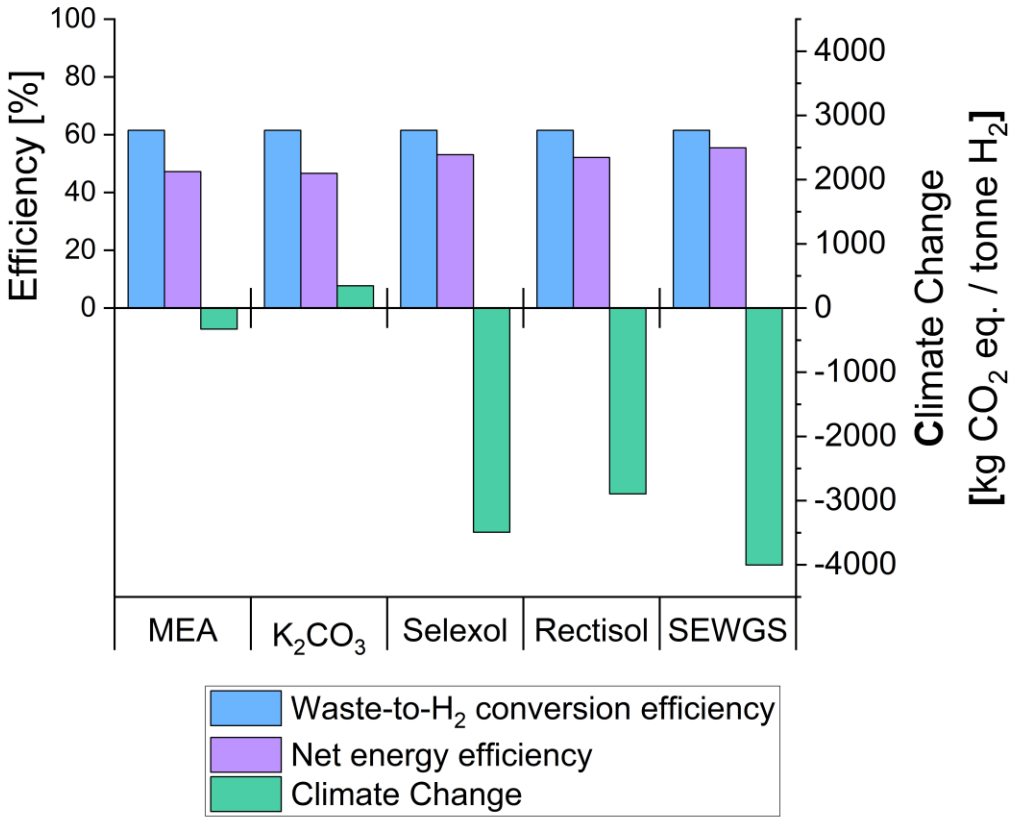

Figure 6.8 – Overall plant technical and environmental efficiencies for the different carbon capture technologies

6.8 Concluding remarks

This chapter aimed to address the growing need for sustainable hydrogen production by investigating the techno-environmental implications of waste-to-hydrogen production integrated with carbon capture and storage technologies. Full plant process simulations were developed using Aspen Plus to produce mass and energy balances. The simulations were directly informed by the detailed modelling of the fluidized bed gasifier presented in Chapter 4, particularly regarding feedstock-to-syngas conversion and syngas composition. The simulation results enabled the calculation of chemical requirements, such as O_2 for tar reforming, steam for WGS reactors, and solvent for CO_2 separation. Furthermore, the results of the simulations provided relevant information regarding energy requirements, in terms of electricity and heat for different utilities.

The performance of the H_2 production plant has been investigated for different feedstocks, end-uses, H_2 purity requirements, and pre-combustion carbon capture technologies, with an estimation of the net carbon sequestration potential. The main conclusions are as follows:

- In the feedstock comparison, plastic waste demonstrated slightly higher overall efficiency, 49% against around 47% for the other feedstocks, and required approximately 30% less utilities and materials compared to biomass and mixed waste. However, biomass and waste feedstocks enabled 20-30% higher CO_2 sequestration potential per ton of H_2 produced, highlighting their superior environmental benefits. For instance, all feedstocks allowed for sequestration of up to 0.82 ton of CO_2 per ton of H_2 produced, however biomass and waste show higher waste-to-H_2 conversion.
- Regarding end-use applications, refining processes (requiring 95% H_2 purity) showed the highest conversion efficiency, however all scenarios attained around 50% of net energy efficiency. While refining demonstrated optimal process performance, applications in fuel cells and heating offered greater potential for decarbonization of the energy sector. Notably, increasing CO_2 capture rates from 90% to 95% improved PSA hydrogen recovery up to 10%, despite a 10% increase in energy penalty for capturing more CO_2.
- Carbon capture technology selection significantly impacted environmental performance. With the current UK gas grid and electricity mix composition, physical absorption technologies achieved 40-50% lower climate change direct and indirect impact compared to chemical absorption methods. This advantage stems from pressure-swing solvent regeneration in physical technologies, avoiding the natural gas combustion required for thermal regeneration in chemical systems. At commercial scale (65 MWth input), awaste-to-H_2 plant could achieve net negative emissions of 12-14 ton CO_2-eq./h using physical CCS technologies, compared to 7.6-8.6 ton CO_2-eq./h with chemical CCS technologies, before accounting for H_2 product and electricity credits.
- Among the evaluated technologies, SEWGS, though at a lower Technology Readiness Level (TRL), demonstrated the best environmental performance with 15-28% lower CO_2 emissions compared to conventional physical absorption methods. For commercially available options, Selexol emerged as the optimal technology, offering the best balance of technical maturity and environmental performance.

Chapter 7. Conclusions and future works

This Chapter summarizes the results obtained in the Thesis. These results highlight the importance of investigating fluidized bed gasification technologies to produce H_2 from waste. Emphasis is placed on the findings from the development and investigation of the 1D kinetic model developed, including feedstock-specific considerations, development of reactor design and most-suited operating conditions for H_2 production form waste. This model has proven to be sensitive to the main operational challenges of such reactors, first and foremost the problem of tars, crucial for a comprehensive assessment of the process. The model successfully identified the role of the main operating parameters, and the performance of fluidized bed gasifiers treating different feedstocks. The advantages, potential exploitation, as well as limitations, of this work are highlighted. Ultimately, future activities representing a possible continuation of the work presented in this Thesis are discussed.

7.1 Conclusions

This work investigated H_2 production from waste, with a particular focus on the gasification stage in large-scale bubbling fluidized bed reactors. Understanding the effect of operating conditions on the overall process, including the benefits and challenges associated with different gasification agents and feedstocks, is crucial for supporting reactor design and deployment of WtH_2 technologies at a large scale. The development of an accurate and operationally straightforward 1D kinetic model enabled a comprehensive and systematic investigation while avoiding significant costs and technical challenges associated with experimental studies. The research encompassed biomass, plastics (synthetic polyolefin materials), and their blends to understand the behaviour of main waste feedstock constituents during conversion in fluidized bed reactors. The investigation extended to the complete waste-to-hydrogen plant through process simulations to evaluate technical feasibility and environmental opportunities.

This thesis addressed the following objectives:

1. To develop a model to predict the operation of waste gasification in large-scale fluidized beds, extensively validated with real plant data The model is to be developed with a flexible and modular approach, making it easy to be adapted depending on reactor design requirements.

2. To develop an empirical semi-kinetic devolatilization pattern release to overcome the common assumption of instantaneous reaction. This approach has to account for the complex interplay of mixing and segregation behaviour with volatlies release that characterize reacting particles in fluidized beds.
3. To accurately predict tar formation and behaviour by including a broad spectrum of heavy hydrocarbon species. The model should be particularly accurate and detailed with respect to the freeboard and the complex pathway of reaction kinetics that can occur.
4. To identify the most suited operating conditions for different configurations, including different types of feedstocks and gasification agents. Particular emphasis is given to the two extremes represented by the most conventional, air, and the most promising, steam-O_2.
5. To develop a full-plant process simulation, informed by the detailed kinetic model, to investigate the technical feasibility and environmental benefits of a Waste-to-H_2 plant.

The key findings can be summarized as follows:

1. A 1D fluidization model was developed and described in Chapter 3. The model effectively represents fluidized bed reactor characteristics through a comprehensive set of well-suited semi-empirical correlations for bubbling bed fluid dynamics, achieving superior accuracy compared to existing FM in literature. The modular structure, built with hierarchical sub-models and sub-routines, enables prediction of gasifier operations across various conditions and helps investigate different bubbling fluidized bed designs (e.g. changing bed inventory, height, and diameter) through simple input data updates. The model builds upon the conventional two-phase fluidization theory, with modifications introduced for enhanced accuracy and flexibility. The model provides detailed concentration profiles of all species across all phases and temperature distribution throughout the bed. A notable advancement over existing fluidization models lies in the comprehensive energy balance calculations, which include heat released or absorbed by chemical reactions, inter-phase heat exchange, and heat transfer induced by the mixing of bed particles. A novel approach was developed to account for complex gas phase mixing induced by bubble bursting in the splashing zone. This represents a significant improvement over existing FMs, which either disregard freeboard modelling entirely or assume unrealistic perfectly mixed plug flow conditions. The model underwent extensive validation against experimental data from large-scale fluidized bed gasifiers across diverse feedstocks and operating conditions. Computational

time is up to 300 seconds, with results typically within experimental error margins and maximum deviations of approximately 10%.

2. An effective approach has been applied to represent the species released during the devolatilization, detailed in Chapter 3. The conventional two-phase theory was modified by introducing a third phase to include gases released during fuel devolatilization. The volatiles release pattern was derived from empirical observations of fuel particle reaction and mixing behaviour in fluidized beds, while the feedstock-specific product distribution of species was based on literature data at relevant reactor scales. Experimental observations revealed distinct particle behaviours: biomass particles are characterized by marked segregation toward the top of the bed, consistent with buoyant body behaviour, Plastic fuels, instead, demonstrated enhanced mixing with the bed inventory due to particle softening and melting prior to devolatilization. The devolatilization modelling approach achieves an optimal balance between accuracy and model complexity through indirect phenomenological representation of the devolatilization stage. The method demonstrates superior performance compared to existing approaches in the literature, which typically assume either instantaneous devolatilization or assume arbitrary release patterns. Incorporating an endogenous bubbles phase enhances model accuracy in representing reactor fluid dynamics, axial species evolution, and overall performance predictions.
3. During the development of the model development, particular attention was paid to tar species representation. The heterogeneous nature of tars and heavy hydrocarbons was captured including phenol, toluene, naphthalene, and a gravimetric compound. This approach differentiates the model from existing literature, which are often not sensitive to tar presence and composition, limiting their utility in investigating the problems associated with gasification processes. A separate detailed kinetic model was implemented for the reactor freeboard, acknowledging the significance of secondary tar reactions in this zone due to extended residence times and favourable conditions (temperature and reactant concentrations). This detailed approach enabled a comprehensive analysis of tar composition and behaviour throughout the freeboard length, providing insights regarding correlations between operating conditions and tar content variations. The model predictions indicated higher tar content for plastic and plastic-rich blends across both air gasification (Chapter 4) and steam-oxygen gasification (Chapter 5). Steam-oxygen gasification produced a better-quality syngas, with tar concentrations ranging from 2-4 g_{Tar}/Nm^3 compared to 7-3 g_{Tar}/Nm^3 for air gasification.

Despite more favourable results with biomass in steam-oxygen conditions, predicted tar levels remained excessive across all operating conditions, highlighting the need for secondary tar reforming stages when processing waste-derived feedstocks.

4. The model enabled comprehensive investigation of operating parameter effects across multiple performance metrics. The analysis focused on identifying optimal operating conditions for different feedstocks under both conventional air gasification and steam-oxygen gasification conditions. Air gasification, despite operational simplicity, produces syngas significantly diluted by nitrogen (approximately 50% on dry basis) with heating values ranging from 4-7 MJ/Nm³. This quality limitation renders the syngas unsuitable for further processing into sustainable fuels without a complex and energy-intensive separation stage. The ER emerged as the most influential operating parameter across all feedstocks, with optimal performance in the range of 0.24-0.28, aligning with theoretical predictions. Steam-oxygen gasification demonstrated better results for hydrogen production, achieving H_2 concentrations between 15-20% for plastics and up to 30% for biomass, and overall lower tar content. The primary advantage of steam over nitrogen lies mainly in the easier downstream separation. The model identified an optimal steam-to-carbon ratio of approximately 1.5, effectively balancing temperature moderation and reforming reaction promotion. Biomass-rich fuels represent the most ideal feedstock, showing optimal performance of high H_2 concentration with reduced tar content.
5. In Chapter 6, the full plant simulations confirm waste-to-hydrogen as a promising pathway for sustainable pure H_2 production. The analysis revealed significant energy penalties associated with tar reforming and carbon capture and storage units, resulting in overall plant efficiency of 49% for plastic-rich waste processing and 47% for waste woody biomass. The analysis explored various hydrogen markets with distinct purity requirements. From technological and efficiency perspectives, H_2 production for the refining industry combined with 95% CO_2 capture and storage emerged as the optimal solution with the highest energy efficiency. However, a comprehensive economic assessment remains necessary to definitively identify the most viable option. The analysis of pre-combustion CO_2 capture technologies indicated physical capture methods as the preferable option due to lower energy penalties. These methods, however, require high operating pressures that introduce safety and technological challenges. A preliminary environmental assessment validated the potential of waste-to-hydrogen processes to achieve negative emissions when combined with the physical separation of CO_2, crucial for supporting the decarbonization of the energy sector and net-zero objectives.

7.2 Recommendations and future work

Before presenting considerations on improvements and future research directions, this section discusses further potential applications of the developed kinetic model and identifies critical areas for plant optimization. This analysis informs future research priorities and current limitations in the investigative approaches:

1. The kinetic model presented in Chapter 3 features a modular structure that can be easily adapted to different reactor geometries. The model incorporates a comprehensive set of semi-empirical correlations for fluidized bed behaviour, enabling accurate fluid dynamic representation across different bed materials and fluidizing gases. However, the development-design mode requires iterative changes in geometry and feeding rates, making the optimization process labour-intensive.
2. The adopted volatile release pattern effectively represents the distinct behaviours of biomass and plastic, fractions usually present in waste feedstocks. This approach offers simplicity and straightforward implementation when developing more complex models. However, the model does not account for potential synergistic effects resulting from biomass-plastic interactions within the fuel particles in the fluidized bed. A significant limitation stems from the reliance on literature data for chemical species released during devolatilization, which introduces constraints based on data availability.
3. The detailed representation of heavy hydrocarbon behaviour and composition enabled a comprehensive analysis of operating parameters for syngas purity improvement. The model, in its current form, can investigate additional tar reduction strategies, such as secondary air injection in the splashing zone or freeboard. Implementation of other approaches, including catalytic bed inventory or freeboard filters, would require substantial, but feasible, model modifications. Despite strong predictive capabilities, the model exhibits limitations in the number and type of chemical species included in the fluidized bed calculations and the scope of reaction kinetics developed. These constraints affect the accuracy of freeboard predictions in the detailed kinetic model.
4. The full-plant process simulation identified both challenges and opportunities in waste-to-hydrogen plants, highlighting energy-intensive areas requiring further development. The investigation revealed tar reforming and final hydrogen purification as critical areas for improvement, both requiring dedicated process development through kinetic studies and experimental investigation. The model demonstrates versatility for studying various process configurations and end products, as syngas-based plants share similar layouts and units. For

example, adapting to waste-to-bioSNG processes requires straightforward modification of the water-gas shift unit and addition of catalytic reactors for converting H_2-CO stream to CH_4. Abundant literature data exists for methanation reactor kinetics and design. Similar modifications apply to methanol and heavier synthetic fuel production, though the latter introduces additional complexity.

7.2.1 Future improvement

From a modelling perspective, future research could be focused on the following pathways:

1. Developing comprehensive model for gas release from devolatilization. This effort requires expanding volatile release patterns across diverse feedstocks through collaboration with experimental researchers, including various biomass types, plastics, refuse-derived fuel, and mixed plastic waste.
2. Enhancing the devolatilization product distribution modelling through data collection from a broader range of feedstocks or empirical correlations in the case of unknown feedstocks. A relevant example would be implementing the model proposed by Neves et al for pyrolysis of biomass [147]. A possible improvement of this model would involve incorporating an energy balance for the overall devolatilization reaction based on fuel heating value. This approach would replace the current assumption made by the authors regarding tar heating values and provide more accurate thermodynamic representation process.
3. Expanding the fluidized bed model capabilities at representing tars by including additional aromatic and polycyclic compounds (such as pyrene, acetylene, indene, guaiacol, etc.), along with their associated reaction kinetics. This expansion would complement and extend the existing kinetic framework
4. The model highlighted the need for an additional stage for syngas cleaning and tar reforming. Plasma reactors represent a promising technology, though the feasibility and effectiveness remain unproven at large scale. To advance plasma technology, researchers must investigate reaction kinetics in detail to identify optimal operating conditions and methods to reduce parasitic power loads. The freeboard modelling approach could serve to develop kinetic models for plasma reactors. This development would need to incorporate the reaction kinetics of radicals and electrically charged species induced by plasma power, which drive effective tar cracking. Experimental validation studies would strengthen this modelling approach.
5. Additional model development opportunities emerge from challenges identified by plant operators when processing heterogeneous, low-value waste feedstocks. The fluidized bed model could incorporate ash behaviour and investigate the dynamic of agglomerates

formation and how these affects reactor fluid dynamics. Further development could address the impact of corrosive compounds such as sulphur, chlorine, and ammonia on reactor performance and material integrity.

6. The plant layout requires a comprehensive economic assessment to evaluate the real practical feasibility. The simulation would benefit from a more detailed modelling approach to include reaction kinetics and sizing of all the units in the plant to strengthen technical assessments and improve economic evaluation accuracy.

This research advances technologies to process low-value waste materials with high potential, while addressing climate change through carbon-negative hydrogen production. These contributions support solutions to two global challenges facing current and future generations.

References

[1] U.S. Energy Information Administration, International Energy Outlook 2019, 2019. https://www.eia.gov/outlooks/ieo/pdf/ieo2019.PDF (accessed January 3, 2025).

[2] S. Iannello, S. Morrin, M. Materazzi, Fluidised Bed Reactors for the Thermochemical Conversion of Biomass and Waste, KONA Powder and Particle Journal 37 (2020) 114–131. https://doi.org/10.14356/KONA.2020016.

[3] International Energy Agency, World Energy Outlook 2024, 2024. https://www.iea.org/reports/world-energy-outlook-2024 (accessed January 3, 2025).

[4] M. Fridahl, M. Lehtveer, Bioenergy with carbon capture and storage (BECCS): Global potential, investment preferences, and deployment barriers, Energy Res Soc Sci 42 (2018) 155–165. https://doi.org/10.1016/j.erss.2018.03.019.

[5] International Energy Agency, Net Zero by 2050 - A Roadmap for the Global Energy Sector, 2021. https://www.iea.org/reports/net-zero-by-2050 (accessed January 3, 2025).

[6] Statista, Municipal solid waste generation 2050 | Statista, (n.d.). https://www.statista.com/statistics/916625/global-generation-of-municipal-solid-waste-forecast/ (accessed January 3, 2025).

[7] The World Bank, Trends in Solid Waste Management, (n.d.). https://datatopics.worldbank.org/what-a-waste/trends_in_solid_waste_management.html (accessed January 3, 2025).

[8] Committee on Climate Change Bioenergy, (2011).

[9] M. Materazzi, P. Lettieri, L. Mazzei, R. Taylor, C. Chapman, Thermodynamic modelling and evaluation of a two-stage thermal process for waste gasification, Fuel 108 (2013) 356–369. https://doi.org/10.1016/j.fuel.2013.02.037.

[10] E.R. Teixeira, A. Camões, F.G. Branco, Valorisation of wood fly ash on concrete, Resour Conserv Recycl 145 (2019) 292–310. https://doi.org/10.1016/j.resconrec.2019.02.028.

[11] E.E. Kwon, S. Kim, J. Lee, Pyrolysis of waste feedstocks in CO2 for effective energy recovery and waste treatment, Journal of CO2 Utilization 31 (2019) 173–180. https://doi.org/10.1016/J.JCOU.2019.03.015.

[12] M.-S. Safdari, E. Amini, D.R. Weise, T.H. Fletcher, Heating rate and temperature effects on pyrolysis products from live wildland fuels, Fuel 242 (2019) 295–304. https://doi.org/10.1016/j.fuel.2019.01.040.

[13] B.B. Uzoejinwa, X. He, S. Wang, A. El-Fatah Abomohra, Y. Hu, Q. Wang, Co-pyrolysis of biomass and waste plastics as a thermochemical conversion technology for high-grade biofuel production: Recent progress and future directions elsewhere worldwide, Energy Convers Manag 163 (2018) 468–492. https://doi.org/10.1016/j.enconman.2018.02.004.

[14] L. Zhou, Y. Wang, Q. Huang, J. Cai, Thermogravimetric characteristics and kinetic of plastic and biomass blends co-pyrolysis, Fuel Processing Technology 87 (2006) 963–969. https://doi.org/10.1016/j.fuproc.2006.07.002.

[15] M. Sharifzadeh, M. Sadeqzadeh, M. Guo, T.N. Borhani, N.V.S.N. Murthy Konda, M.C. Garcia, L. Wang, J. Hallett, N. Shah, The multi-scale challenges of biomass fast pyrolysis and bio-oil upgrading: Review of the state of art and future research directions, Prog Energy Combust Sci 71 (2019) 1–80. https://doi.org/10.1016/j.pecs.2018.10.006.

[16] G. Perkins, T. Bhaskar, M. Konarova, Process development status of fast pyrolysis technologies for the manufacture of renewable transport fuels from biomass, Renewable and Sustainable Energy Reviews 90 (2018) 292–315. https://doi.org/10.1016/j.rser.2018.03.048.

[17] M. Materazzi, P. Lettieri, R. Taylor, C. Chapman, Performance analysis of RDF gasification in a two stage fluidized bed – plasma process, Waste Management 47 (2016) 256–266. https://doi.org/10.1016/j.wasman.2015.06.016.

[18] S. Safarian, R. Unnþórsson, C. Richter, A review of biomass gasification modelling, Renewable and Sustainable Energy Reviews 110 (2019) 378–391. https://doi.org/10.1016/J.RSER.2019.05.003.

[19] K.J. Whitty, H.R. Zhang, E.G. Eddings, Emissions from Syngas Combustion, Combustion Science and Technology 180 (2008) 1117–1136. https://doi.org/10.1080/00102200801963326.

[20] J. Karl, T. Pröll, Steam gasification of biomass in dual fluidized bed gasifiers: A review, Renewable and Sustainable Energy Reviews 98 (2018) 64–78. https://doi.org/10.1016/j.rser.2018.09.010.

[21] N. Mazaheri, A.H. Akbarzadeh, E. Madadian, M. Lefsrud, Systematic review of research guidelines for numerical simulation of biomass gasification for bioenergy production, Energy Convers Manag 183 (2019) 671–688. https://doi.org/10.1016/j.enconman.2018.12.097.

[22] P. Basu, Biomass Gasification Design Handbook, 2010. https://doi.org/10.1016/B978-0-12-374988-8.00005-2.

[23] S. Chopra, A.K. Jain, A Review of Fixed Bed Gasification Systems for Biomass, E-Journal - Internationale Kommission Für Agrartechnik 9 (2007).

[24] P. Basu, P. Kaushal, Modeling of Pyrolysis and Gasification of Biomass in Fluidized Beds: A Review, Chemical Product and Process Modeling 4 (2009). https://doi.org/10.2202/1934-2659.1338.

[25] P. Basu, Biomass Gasification, Pyrolysis and Torrefaction: Practical Design and Theory, 2013. https://doi.org/10.1016/C2011-0-07564-6.

[26] J.K. Ratnadhariya, S.A. Channiwala, Three zone equilibrium and kinetic free modeling of biomass gasifier – a novel approach, Renew Energy 34 (2009) 1050–1058. https://doi.org/10.1016/J.RENENE.2008.08.001.

[27] BEIS, Advanced Gasification Technologies – Review and Benchmarking Methodology for Techno-Economic Assessment of Advanced Gasification, (2021).

[28] European Biogas Association, Gasification Diversification of biomass processing and waste utilisation, 2024. www.europeanbiogas.eu (accessed January 3, 2025).

[29] I. Staffell, D. Scamman, A. Velazquez Abad, P. Balcombe, P.E. Dodds, P. Ekins, N. Shah, K.R. Ward, The role of hydrogen and fuel cells in the global energy system, Energy Environ Sci 12 (2019) 463–491. https://doi.org/10.1039/c8ee01157e.

[30] Committee on Climate Change, The Sixth Carbon Budget. The UK's path to Net Zero, (2020) 209.

[31] M. Materazzi, R. Taylor, M. Cairns-Terry, Production of biohydrogen from gasification of waste fuels: Pilot plant results and deployment prospects, Waste Management 94 (2019) 95–106. https://doi.org/10.1016/j.wasman.2019.05.038.

[32] J.D. Holladay, J. Hu, D.L. King, Y. Wang, An overview of hydrogen production technologies, Catal Today 139 (2009) 244–260. https://doi.org/10.1016/j.cattod.2008.08.039.

[33] N.Z. Muradov, T.N. Veziroğlu, From hydrocarbon to hydrogen-carbon to hydrogen economy, Int J Hydrogen Energy 30 (2005) 225–237. https://doi.org/10.1016/j.ijhydene.2004.03.033.

[34] A. Ursúa, L.M. Gandía, P. Sanchis, Hydrogen production from water electrolysis: Current status and future trends, in: Proceedings of the IEEE, Institute of Electrical and Electronics Engineers Inc., 2012: pp. 410–426. https://doi.org/10.1109/JPROC.2011.2156750.

[35] S. Shiva Kumar, V. Himabindu, Hydrogen production by PEM water electrolysis – A review, Mater Sci Energy Technol 2 (2019) 442–454. https://doi.org/10.1016/J.MSET.2019.03.002.

[36] R. Bhandari, C.A. Trudewind, P. Zapp, Life Cycle Assessment of Hydrogen Production via Electrolysis-A Review Contribution to Journal of Cleaner Production, 2013.

[37] C. Antonini, K. Treyer, A. Streb, M. van der Spek, C. Bauer, M. Mazzotti, Hydrogen production from natural gas and biomethane with carbon capture and storage - A techno-environmental analysis, Sustain Energy Fuels 4 (2020) 2967–2986. https://doi.org/10.1039/d0se00222d.

[38] S. Chari, A. Sebastiani, A. Paulillo, M. Materazzi, The Environmental Performance of Mixed Plastic Waste Gasification with Carbon Capture and Storage to Produce Hydrogen in the U.K, ACS Sustain Chem Eng (2023). https://doi.org/10.1021/acssuschemeng.2c05978.

[39] M. Materazzi, S. Chari, S. Bajwa, A. Sebastiani, Waste-To-Hydrogen: Challenges and Opportunities in the Uk Scenario, Detritus 23 (2023) 65–75. https://doi.org/10.31025/2611-4135/2023.18274.

[40] G. Amaya-Santos, S. Chari, A. Sebastiani, F. Grimaldi, P. Lettieri, M. Materazzi, Biohydrogen: A life cycle assessment and comparison with alternative low-carbon production routes in UK, J Clean Prod 319 (2021) 128886. https://doi.org/10.1016/j.jclepro.2021.128886.

[41] C. Antonini, K. Treyer, E. Moioli, C. Bauer, T.J. Schildhauer, M. Mazzotti, Hydrogen from wood gasification with CCS-a techno-environmental analysis of production and use as transport fuel, Sustain Energy Fuels 5 (2021) 2602–2621. https://doi.org/10.1039/d0se01637c.

[42] M. Materazzi, S. Chari, A. Sebastiani, P. Lettieri, A. Paulillo, Waste-to-energy and waste-to-hydrogen with CCS: Methodological assessment of pathways to carbon-negative waste treatment from an LCA perspective, Waste Management 173 (2024) 184–199. https://doi.org/10.1016/J.WASMAN.2023.11.020.

[43] U. Arena, Process and technological aspects of municipal solid waste gasification. A review, Waste Management 32 (2012) 625–639. https://doi.org/10.1016/j.wasman.2011.09.025.

[44] E. Savuto, A. Di Carlo, K. Gallucci, A. Di Giuliano, S. Rapagnà, Steam gasification of lignite and solid recovered fuel (SRF) in a bench scale fluidized bed gasifier, Waste Management 114 (2020) 341–350. https://doi.org/10.1016/j.wasman.2020.07.016.

[45] D. Krause, P. Herdel, J. Ströhle, B. Epple, HTW^{TM}-gasification of high volatile bituminous coal in a 500 kWth pilot plant, Fuel 250 (2019) 306–314. https://doi.org/10.1016/j.fuel.2019.04.014.

[46] H. Thunman, M. Seemann, The GoBiGas plant, Substitute Natural Gas from Waste: Technical Assessment and Industrial Applications of Biochemical and Thermochemical Processes (2019) 455–474. https://doi.org/10.1016/B978-0-12-815554-7.00017-9.

[47] H. Thunman, M. Seemann, T. Berdugo Vilches, J. Maric, D. Pallares, H. Ström, G. Berndes, P. Knutsson, A. Larsson, C. Breitholtz, O. Santos, Advanced biofuel production via gasification – lessons learned from 200 man-years of research activity with Chalmers' research gasifier and the GoBiGas demonstration plant, Energy Sci Eng (2018). https://doi.org/10.1002/ese3.188.

[48] C. Courson, K. Gallucci, Gas cleaning for waste applications (syngas cleaning for catalytic synthetic natural gas synthesis), in: Substitute Natural Gas from Waste, Elsevier, 2019: pp. 161–220. https://doi.org/10.1016/B978-0-12-815554-7.00008-8.

[49] M. Materazzi, R. Taylor, P. Cozens, C. Manson-Whitton, Production of BioSNG from waste derived syngas: Pilot plant operation and preliminary assessment, Waste Management (2018). https://doi.org/10.1016/j.wasman.2018.08.031.

[50] B. Rehling, H. Hofbauer, R. Rauch, C. Aichernig, BioSNG-process simulation and comparison with first results from a 1-MW demonstration plant, Biomass Convers Biorefin 1 (2011) 111–119. https://doi.org/10.1007/s13399-011-0013-3.

[51] M. Materazzi, P.U. Foscolo, The role of waste and renewable gas to decarbonize the energy sector, in: Substitute Natural Gas from Waste: Technical Assessment and Industrial Applications of Biochemical and Thermochemical Processes, 2019. https://doi.org/10.1016/B978-0-12-815554-7.00001-5.

[52] H. Hofbauer, M. Materazzi, Waste gasification processes for SNG production, in: M. Materazzi, P.U. Foscolo (Eds.), Substitute Natural Gas from Waste: Technical Assessment and Industrial Applications of Biochemical and Thermochemical Processes, Academic Press, 2019: pp. 105–160. https://doi.org/10.1016/B978-0-12-815554-7.00007-6.

[53] O. Senneca, Kinetics of pyrolysis, combustion and gasification of three biomass fuels, Fuel Processing Technology 88 (2007) 87–97. https://doi.org/10.1016/J.FUPROC.2006.09.002.

[54] S. Weihrich, X. Xing, X. Zhang, Co-pyrolysis and HTC refined biomass-biosolid-mixes: combustion performance and residues, International Journal of Energy and Environmental Engineering 13 (2022) 657–669. https://doi.org/10.1007/S40095-021-00453-6/TABLES/5.

[55] Global Plastics Outlook, Global Plastics Outlook (2022). https://doi.org/10.1787/DE747AEF-EN.

[56] V. Lahtela, M. Hyvärinen, T. Kärki, Composition of Plastic Fractions in Waste Streams: Toward More Efficient Recycling and Utilization, Polymers 2019, Vol. 11, Page 69 11 (2019) 69. https://doi.org/10.3390/POLYM11010069.

[57] S.M. Al-Salem, P. Lettieri, J. Baeyens, The valorization of plastic solid waste (PSW) by primary to quaternary routes: From re-use to energy and chemicals, Prog Energy Combust Sci 36 (2010) 103–129. https://doi.org/10.1016/J.PECS.2009.09.001.

[58] P. Salatino, R. Solimene, Mixing and segregation in fluidized bed thermochemical conversion of biomass, Powder Technol 316 (2017) 29–40. https://doi.org/10.1016/J.POWTEC.2016.11.058.

[59] S. Iannello, P.U. Foscolo, M. Materazzi, Investigation of single particle devolatilization in fluidized bed reactors by X-ray imaging techniques, Chemical Engineering Journal 431 (2022) 133807. https://doi.org/10.1016/J.CEJ.2021.133807.

[60] S. Iannello, Z. Bond, A. Sebastiani, M. Errigo, M. Materazzi, Axial segregation behaviour of a reacting biomass particle in fluidized bed reactors: experimental results and model validation, Fuel 338 (2023) 127234. https://doi.org/10.1016/J.FUEL.2022.127234.

[61] A. Gómez-Barea, B. Leckner, Modeling of biomass gasification in fluidized bed, Prog Energy Combust Sci 36 (2010) 444–509. https://doi.org/10.1016/J.PECS.2009.12.002.

[62] R. Chirone, L. Massimilla, P. Salatino, Comminution of carbons in fluidized bed combustion, Prog Energy Combust Sci 17 (1991) 297–326. https://doi.org/10.1016/0360-1285(91)90006-9.

[63] V. Wilk, J.C. Schmid, H. Hofbauer, Influence of fuel feeding positions on gasification in dual fluidized bed gasifiers, Biomass Bioenergy 54 (2013) 46–58. https://doi.org/10.1016/j.biombioe.2013.03.018.

[64] G. Bruni, R. Solimene, A. Marzocchella, P. Salatino, J.G. Yates, P. Lettieri, M. Fiorentino, Self-segregation of high-volatile fuel particles during devolatilization in a fluidized bed reactor, Powder Technol 128 (2002) 11–21. https://doi.org/10.1016/S0032-5910(02)00149-3.

[65] A. Sebastiani, D. Macrì, K. Gallucci, M. Materazzi, Steam - oxygen gasification of refuse derived fuel in fluidized beds: Modelling and pilot plant testing, Fuel Processing Technology 216 (2021) 106783. https://doi.org/10.1016/j.fuproc.2021.106783.

[66] U. Arena, F. Di Gregorio, Fluidized bed gasification of industrial solid recovered fuels, Waste Management 50 (2016) 86–92. https://doi.org/https://doi.org/10.1016/j.wasman.2016.02.011.

[67] C. Li, K. Suzuki, Tar property, analysis, reforming mechanism and model for biomass gasification—An overview, Renewable and Sustainable Energy Reviews 13 (2009) 594–604. https://doi.org/10.1016/J.RSER.2008.01.009.

[68] M. Materazzi, Clean Energy from Waste - Fundamental Investigations on Ashes and Tar Behaviours in a Two Stage Fluid Bed-Plasma Process for Waste Gasification, 2017.

[69] T.A. Milne, R.J. Evans, Biomass gasifier “Tars”: their natura, formation and conversion, Developments in Thermochemical Biomass Conversion (1997) 803–816. https://doi.org/10.1007/978-94-009-1559-6_64.

[70] A. Kumar, D.D. Jones, M.A. Hanna, Thermochemical Biomass Gasification: A Review of the Current Status of the Technology, Energies 2009, Vol. 2, Pages 556-581 2 (2009) 556–581. https://doi.org/10.3390/EN20300556.

[71] I. Petersen, J. Werther, Experimental investigation and modeling of gasification of sewage sludge in the circulating fluidized bed, Chemical Engineering and Processing: Process Intensification 44 (2005) 717–736. https://doi.org/10.1016/J.CEP.2004.09.001.

[72] R. Khalil, G. Várhegyi, S. Jäschke, M.G. Grønli, J. Hustad, CO2 gasification of biomass chars: A kinetic study, Energy and Fuels 23 (2009) 94–100. https://doi.org/10.1021/EF800739M/ASSET/IMAGES/LARGE/EF-2008-00739M_0005.JPEG.

[73] P.U. Foscolo, A. Germanà, N. Jand, S. Rapagnà, Design and cold model testing of a biomass gasifier consisting of two interconnected fluidized beds, Powder Technol 173 (2007) 179–188. https://doi.org/10.1016/J.POWTEC.2007.01.008.

[74] G. Schuster, G. Löffler, K. Weigl, H. Hofbauer, Biomass steam gasification – an extensive parametric modeling study, Bioresour Technol 77 (2001) 71–79. https://doi.org/10.1016/S0960-8524(00)00115-2.

[75] J. Gil, J. Corella, M.P. Aznar, M.A. Caballero, Biomass gasification in atmospheric and bubbling fluidized bed: Effect of the type of gasifying agent on the product distribution, Biomass Bioenergy 17 (1999) 389–403. https://doi.org/10.1016/S0961-9534(99)00055-0.

[76] T.Y. Ahmed, M.M. Ahmad, S. Yusup, A. Inayat, Z. Khan, Mathematical and computational approaches for design of biomass gasification for hydrogen production: A review, Renewable and Sustainable Energy Reviews 16 (2012) 2304–2315. https://doi.org/10.1016/J.RSER.2012.01.035.

[77] Y. Yoshida, K. Dowaki, Y. Matsumura, R. Matsuhashi, D. Li, H. Ishitani, H. Komiyama, Comprehensive comparison of efficiency and CO2 emissions between biomass energy conversion technologies—position of supercritical water gasification in biomass technologies, Biomass Bioenergy 25 (2003) 257–272. https://doi.org/10.1016/S0961-9534(03)00016-3.

[78] D. Kunii, O. Levenspiel, Fluidization Engineering, 1991. https://doi.org/10.1016/b978-0-7506-9121-5.50001-x.

[79] F. Alobaid, N. Almohammed, M. Massoudi Farid, J. May, P. Rößger, A. Richter, B. Epple, Progress in CFD Simulations of Fluidized Beds for Chemical and Energy Process Engineering, Prog Energy Combust Sci 91 (2022) 100930. https://doi.org/10.1016/J.PECS.2021.100930.

[80] H. Cui, J.R. Grace, Fluidization of biomass particles: A review of experimental multiphase flow aspects, Chem Eng Sci 62 (2007) 45–55. https://doi.org/10.1016/J.CES.2006.08.006.

[81] Y. Zhang, B. Jin, W. Zhong, Experimental investigation on mixing and segregation behavior of biomass particle in fluidized bed, Chemical Engineering and Processing: Process Intensification 48 (2009) 745–754. https://doi.org/10.1016/J.CEP.2008.09.004.

[82] F. Scala, Fluidized Bed Technologies for Near-Zero Emission Combustion and Gasification | ScienceDirect, Woodhead Publishing, 2013. https://www.sciencedirect.com/book/9780857095411/fluidized-bed-technologies-for-near-zero-emission-combustion-and-gasification (accessed January 4, 2025).

[83] A.C. Rees, J.F. Davidson, J.S. Dennis, A.N. Hayhurst, The rise of a buoyant sphere in a gas-fluidized bed, Chem Eng Sci 60 (2005) 1143–1153. https://doi.org/10.1016/J.CES.2004.09.045.

[84] A.C. Rees, J.F. Davidson, J.S. Dennis, A.N. Hayhurst, The Rise of Buoyant Fuel-Particles in a Slugging Gas-Fluidized Combustor, Chemical Engineering Research and Design 84 (2006) 319–327. https://doi.org/10.1205/CHERD05043.

[85] S. Iannello, A. Sebastiani, M. Errigo, M. Materazzi, The behaviour of plastic particles during pyrolysis in bubbling fluidized bed reactors: Incipient agglomeration and axial segregation, Powder Technol 441 (2024) 119846. https://doi.org/10.1016/J.POWTEC.2024.119846.

[86] A. Vitale, A.A. Papa, S. Iannello, E. Ciro, A. Hatunoglu, V. Corradetti, N. Rovelli, P.U. Foscolo, A. Di Carlo, Devolatilization of Polypropylene Particles in Fluidized Bed, Energies (Basel) 16 (2023) 6324. https://doi.org/10.3390/EN16176324/S1.

[87] F. Scala, P. Salatino, Modelling fluidized bed combustion of high-volatile solid fuels, Chem Eng Sci 57 (2002) 1175–1196. https://doi.org/10.1016/S0009-2509(02)00004-0.

[88] S. Tebianian, R. Solimene, P. Salatino, Flow structures and mixing patterns in the freeboard of gas-fluidized bed reactors, Ind Eng Chem Res 53 (2014) 9296–9302. https://doi.org/10.1021/ie403337c.

[89] R. Solimene, A. Marzocchella, R. Ragucci, P. Salatino, Laser diagnostics of hydrodynamics and gas-mixing induced by bubble bursting at the surface of gas-fluidized beds, Chem Eng Sci 62 (2007) 94–108. https://doi.org/10.1016/J.CES.2006.08.007.

[90] M. Horio, A. Taki, Y.S. Hsieh, I. Muchi, Elutriation and Particle Transport Through the Freeboard of a Gas-Solid Fluidized Bed, in: Fluidization, Springer US, Boston, MA, 1980: pp. 509–518. https://doi.org/10.1007/978-1-4684-1045-7_54.

[91] S.T. Pemberton, J.F. Davidson, Turbulence in the freeboard of a gas-fluidised bed. The significance of ghost bubbles, Chem Eng Sci 39 (1984) 829–840. https://doi.org/10.1016/0009-2509(84)85052-6.

[92] R. Solimene, A. Marzocchella, R. Ragucci, P. Salatino, Flow structures and gas-mixing induced by bubble bursting at the surface of an incipiently gas-fluidized bed, Ind Eng Chem Res 43 (2004) 5738–5753. https://doi.org/10.1021/IE049729X/ASSET/IMAGES/MEDIUM/IE049729XE00010.GIF.

[93] R. Solimene, P. Salatino, A. Marzocchella, R. Ragucci, Flow Structures and Gas-Mixing Induced by Bubble Bursting at the Surface of an Incipiently Gas-Fluidized Bed, Ind Eng Chem Res (2006) 5738–5753.

[94] X.T. Li, J.R. Grace, C.J. Lim, A.P. Watkinson, H.P. Chen, J.R. Kim, Biomass gasification in a circulating fluidized bed, Biomass Bioenergy 26 (2004) 171–193. https://doi.org/10.1016/S0961-9534(03)00084-9.

[95] H. Enwald, E. Peirano, A.E. Almstedt, Eulerian two-phase flow theory applied to fluidization, International Journal of Multiphase Flow 22 (1996) 21–66. https://doi.org/10.1016/S0301-9322(96)90004-X.

[96] S. Gerber, F. Behrendt, M. Oevermann, An Eulerian modeling approach of wood gasification in a bubbling fluidized bed reactor using char as bed material, Fuel 89 (2010) 2903–2917. https://doi.org/10.1016/J.FUEL.2010.03.034.

[97] Y. Wang, L. Yan, CFD modeling of a fluidized bed sewage sludge gasifier for syngas, Asia-Pacific Journal of Chemical Engineering 3 (2008) 161–170. https://doi.org/10.1002/APJ.128.

[98] T.M. Ismail, M. Abd El-Salam, E. Monteiro, A. Rouboa, Fluid dynamics model on fluidized bed gasifier using agro-industrial biomass as fuel, Waste Management 73 (2018) 476–486. https://doi.org/10.1016/J.WASMAN.2017.06.018.

[99] E. Monteiro, T.M. Ismail, A. Ramos, M. Abd El-Salam, P.S.D. Brito, A. Rouboa, Assessment of the miscanthus gasification in a semi-industrial gasifier using a CFD model, Appl Therm Eng 123 (2017) 448–457. https://doi.org/10.1016/J.APPLTHERMALENG.2017.05.128.

[100] T.M. Ismail, M. Abd El-Salam, E. Monteiro, A. Rouboa, Eulerian – Eulerian CFD model on fluidized bed gasifier using coffee husks as fuel, Appl Therm Eng 106 (2016) 1391–1402. https://doi.org/10.1016/J.APPLTHERMALENG.2016.06.102.

[101] N. Couto, V. Silva, A. Rouboa, Municipal solid waste gasification in semi-industrial conditions using air-CO2 mixtures, Energy 104 (2016) 42–52. https://doi.org/10.1016/J.ENERGY.2016.03.088.

[102] N. Couto, V. Silva, E. Monteiro, S. Teixeira, R. Chacartegui, K. Bouziane, P.S.D. Brito, A. Rouboa, Numerical and experimental analysis of municipal solid wastes gasification process, Appl Therm Eng 78 (2015) 185–195. https://doi.org/10.1016/J.APPLTHERMALENG.2014.12.036.

[103] N.D. Couto, V.B. Silva, E. Monteiro, A. Rouboa, Assessment of municipal solid wastes gasification in a semi-industrial gasifier using syngas quality indices, Energy 93 (2015) 864–873. https://doi.org/10.1016/J.ENERGY.2015.09.064.

[104] N. Couto, V. Silva, E. Monteiro, P. Brito, A. Rouboa, Using an Eulerian-granular 2-D multiphase CFD model to simulate oxygen air enriched gasification of agroindustrial residues, Renew Energy 77 (2015) 174–181. https://doi.org/10.1016/J.RENENE.2014.11.089.

[105] V. Silva, E. Monteiro, N. Couto, P. Brito, A. Rouboa, Analysis of syngas quality from Portuguese biomasses: An experimental and numerical study, Energy and Fuels 28 (2014) 5766–5777. https://doi.org/10.1021/EF500570T/ASSET/IMAGES/LARGE/EF-2014-00570T_0011.JPEG.

[106] N. Couto, V. Silva, E. Monteiro, P.S.D. Brito, A. Rouboa, Experimental and Numerical Analysis of Coffee Husks Biomass Gasification in a Fluidized Bed Reactor, Energy Procedia 36 (2013) 591–595. https://doi.org/10.1016/J.EGYPRO.2013.07.067.

[107] O. Onel, A.M. Niziolek, F.M.F. Hasan, C.A. Floudas, Municipal solid waste to liquid transportation fuels – Part I: Mathematical modeling of a municipal solid waste gasifier, Comput Chem Eng 71 (2014) 636–647. https://doi.org/10.1016/J.COMPCHEMENG.2014.03.008.

[108] X.T. Li, J.R. Grace, C.J. Lim, A.P. Watkinson, H.P. Chen, J.R. Kim, Biomass gasification in a circulating fluidized bed, Biomass Bioenergy 26 (2004) 171–193. https://doi.org/10.1016/S0961-9534(03)00084-9.

[109] C. Higman, M. Van der Burgt, Gasification, Gasification (2008) 1–435. https://doi.org/10.1016/B978-0-7506-8528-3.X0001-6.

[110] P. Mathieu, R. Dubuisson, Performance analysis of a biomass gasifier, Energy Convers Manag 43 (2002) 1291–1299. https://doi.org/10.1016/S0196-8904(02)00015-8.

[111] C.M. Kinoshita, Y. Wang, P.K. Takahashi, Chemical Equilibrium Computations for Gasification of Biomass to Produce Methanol, Energy Sources 13 (1991) 361–368. https://doi.org/10.1080/00908319108908994.

[112] V. Marcantonio, L. Di Paola, M. De Falco, M. Capocelli, Modeling of Biomass Gasification: From Thermodynamics to Process Simulations, Energies 2023, Vol. 16, Page 7042 16 (2023) 7042. https://doi.org/10.3390/EN16207042.

[113] S. Rupesh, C. Muraleedharan, P. Arun, ASPEN plus modelling of air–steam gasification of biomass with sorbent enabled CO2 capture, Resource-Efficient Technologies 2 (2016) 94–103. https://doi.org/10.1016/J.REFFIT.2016.07.002.

[114] L.P.R. Pala, Q. Wang, G. Kolb, V. Hessel, Steam gasification of biomass with subsequent syngas adjustment using shift reaction for syngas production: An Aspen Plus model, Renew Energy 101 (2017) 484–492. https://doi.org/10.1016/J.RENENE.2016.08.069.

[115] S.A. Kalogirou, Artificial neural networks in renewable energy systems applications: a review, Renewable and Sustainable Energy Reviews 5 (2001) 373–401. https://doi.org/10.1016/S1364-0321(01)00006-5.

[116] M. Baratieri, P. Baggio, L. Fiori, M. Grigiante, Biomass as an energy source: Thermodynamic constraints on the performance of the conversion process, Bioresour Technol 99 (2008) 7063–7073. https://doi.org/10.1016/J.BIORTECH.2008.01.006.

[117] B. Guo, D. Li, C. Cheng, Z.A. Lü, Y. Shen, Simulation of biomass gasification with a hybrid neural network model, Bioresour Technol 76 (2001) 77–83. https://doi.org/10.1016/S0960-8524(00)00106-1.

[118] S. van Wyk, Development of a novel physics-informed machine learning model for advanced thermochemical waste conversion, Chemical Engineering Journal Advances 21 (2025) 100699. https://doi.org/10.1016/J.CEJA.2024.100699.

[119] S. Iannello, D. Macrì, M. Materazzi, A comprehensive assessment of endogenous bubbles properties in fluidized bed reactors via X-ray imaging, Powder Technol 413 (2023) 118013. https://doi.org/10.1016/J.POWTEC.2022.118013.

[120] R.D. Toomey, H.F. Johnstone, Gaseous Fluidization of Solid Particles, Chem. Engr. Prog. (1952) 220–226.

[121] J.F. Davidson, D. Harrison, Fluidised particles, 1963.

[122] M.B. Nikoo, N. Mahinpey, Simulation of biomass gasification in fluidized bed reactor using ASPEN PLUS, Biomass Bioenergy 32 (2008) 1245–1254. https://doi.org/10.1016/J.BIOMBIOE.2008.02.020.

[123] R. Radmanesh, J. Cnaouki, C. Guy, Biomass gasification in a bubbling fluidized bed reactor: Experiments and modeling, AIChE Journal 52 (2006) 4258–4272. https://doi.org/10.1002/AIC.11020.

[124] S.S. Sadaka, A.E. Ghaly, M.A. Sabbah, Two-phase biomass air-steam gasification model for fluidized bed reactors: Part III—model validation, Biomass Bioenergy 22 (2002) 479–487. https://doi.org/10.1016/S0961-9534(02)00025-9.

[125] S.S. Sadaka, A.E. Ghaly, M.A. Sabbah, Two phase biomass air-steam gasification model for fluidized bed reactors: Part II—model sensitivity, Biomass Bioenergy 22 (2002) 463–477. https://doi.org/10.1016/S0961-9534(02)00024-7.

[126] S.S. Sadaka, A.E. Ghaly, M.A. Sabbah, Two phase biomass air-steam gasification model for fluidized bed reactors: Part I—model development, Biomass Bioenergy 22 (2002) 439–462. https://doi.org/10.1016/S0961-9534(02)00023-5.

[127] S.S. Sadaka, A.E. Ghaly, M.A. Sabbah, Two phase biomass air-steam gasification model for fluidized bed reactors: Part I—model development, Biomass Bioenergy 22 (2002) 439–462. https://doi.org/10.1016/S0961-9534(02)00023-5.

[128] D. Fiaschi, M. Michelini, A two-phase one-dimensional biomass gasification kinetics model, Biomass Bioenergy 21 (2001) 121–132. https://doi.org/10.1016/S0961-9534(01)00018-6.

[129] J. -F Bilodeau, N. Thérien, P. Proulx, S. Czernik, E. Chornet, A mathematical model of fluidized bed biomass gasification, Can J Chem Eng 71 (1993) 549–557. https://doi.org/10.1002/CJCE.5450710407.

[130] H. Jiang, R.V. Morey, A numerical model of a fluidized bed biomass gasifier, Biomass Bioenergy 3 (1992) 431–447. https://doi.org/10.1016/0961-9534(92)90039-S.

[131] F.G. Van den Aarsen, Fluidised bed wood gasifier performance and modeling, (1985).

[132] P. Raman, W.P. Walawender, L.T. Fan, C.C. Chang, Mathematical model for the fluid-bed gasification of biomass materials. Application to feedlot manure, Ind. Eng. Chem. Process Des. Dev.; (United States) 20:4 (1981) 686–692. https://doi.org/10.1021/I200015A019.

[133] J. Corella, A. Sanz, Modeling circulating fluidized bed biomass gasifiers. A pseudo-rigorous model for stationary state, Fuel Processing Technology 86 (2005) 1021–1053. https://doi.org/10.1016/J.FUPROC.2004.11.013.

[134] A. Sanz, J. Corella, Modeling circulating fluidized bed biomass gasifiers. Results from a pseudo-rigorous 1-dimensional model for stationary state, Fuel Processing Technology 87 (2006) 247–258. https://doi.org/10.1016/J.FUPROC.2005.08.003.

[135] I. Petersen, J. Werther, Three-dimensional modeling of a circulating fluidized bed gasifier for sewage sludge, Chem Eng Sci 60 (2005) 4469–4484. https://doi.org/10.1016/J.CES.2005.02.058.

[136] K.D. Panopoulos, L.E. Fryda, J. Karl, S. Poulou, E. Kakaras, High temperature solid oxide fuel cell integrated with novel allothermal biomass gasification: Part I: Modelling and feasibility study, J Power Sources 159 (2006) 570–585. https://doi.org/10.1016/J.JPOWSOUR.2005.12.024.

[137] T.D.B. Nguyen, S.I. Ngo, Y. Il Lim, J.W. Lee, U. Do Lee, B.H. Song, Three-stage steady-state model for biomass gasification in a dual circulating fluidized-bed, Energy Convers Manag 54 (2012) 100–112. https://doi.org/10.1016/J.ENCONMAN.2011.09.019.

[138] I. Adeyemi, I. Janajreh, Modeling of the entrained flow gasification: Kinetics-based ASPEN Plus model, Renew Energy 82 (2015) 77–84. https://doi.org/10.1016/J.RENENE.2014.10.073.

[139] P. Kaushal, J. Abedi, N. Mahinpey, A comprehensive mathematical model for biomass gasification in a bubbling fluidized bed reactor, Fuel 89 (2010) 3650–3661. https://doi.org/10.1016/j.fuel.2010.07.036.

[140] M.S. Eikeland, R.K. Thapa, Stepwise analysis of gasification reactions with Aspen Plus and CPFD, International Journal of Energy Production and Management 2 (2017) 70–80. https://doi.org/10.2495/EQ-V2-N1-70-80.

[141] C.E. Agu, C. Pfeifer, M. Eikeland, L.A. Tokheim, B.M.E. Moldestad, Detailed One-Dimensional Model for Steam-Biomass Gasification in a Bubbling Fluidized Bed, Energy and Fuels (2019). https://doi.org/10.1021/acs.energyfuels.9b01340.

[142] A. Pitkäoja, J. Ritvanen, Steam-oxygen blown circulating fluidised bed gasification for synthetic biofuel production: Pilot-scale reactor modelling, model-based reactor scale-up and analysis for power-biomass-to-liquid processes, Biomass Bioenergy 193 (2025) 107540. https://doi.org/10.1016/J.BIOMBIOE.2024.107540.

[143] Y. Zhang, M. Ashizawa, S. Kajitani, K. Miura, Proposal of a semi-empirical kinetic model to reconcile with gasification reactivity profiles of biomass chars, Fuel 87 (2008) 475–481. https://doi.org/10.1016/J.FUEL.2007.04.026.

[144] F. Scala, Attrition during steam gasification of lignite char in a fluidized bed reactor, Fuel Processing Technology 141 (2016) 38–43. https://doi.org/10.1016/j.fuproc.2015.03.031.

[145] F. Scala, R. Chirone, P. Salatino, 6 - Attrition phenomena relevant to fluidized bed combustion and gasification systems, in: F. Scala (Ed.), Fluidized Bed Technologies for Near-Zero Emission Combustion and Gasification, Woodhead Publishing, 2013: pp. 254–315. https://doi.org/https://doi.org/10.1533/9780857098801.1.254.

[146] U. Arena, R. Chirone, P. Salatino, The fate of fixed carbon during the fluidized-bed combustion of a coal and two waste-derived fuels, Symposium (International) on Combustion 26 (1996) 3243–3251. https://doi.org/10.1016/S0082-0784(96)80170-6.

[147] D. Neves, H. Thunman, A. Matos, L. Tarelho, A. Gómez-Barea, Characterization and prediction of biomass pyrolysis products, Prog Energy Combust Sci 37 (2011) 611–630. https://doi.org/10.1016/j.pecs.2011.01.001.

[148] A. Gómez-Barea, B. Leckner, Estimation of gas composition and char conversion in a fluidized bed biomass gasifier, Fuel 107 (2013) 419–431. https://doi.org/10.1016/J.FUEL.2012.09.084.

[149] A. Gomez-Barea, B. Leckner, Modeling of biomass gasification in fluidized bed, 36 (2010) 444–509. https://doi.org/10.1016/j.pecs.2009.12.002.

[150] V. Claude, J.G. Mahy, S. Douven, S.L. Pirard, C. Courson, S.D. Lambert, Ni- and Fe-doped γ-Al2O3 or olivine as primary catalyst for toluene reforming, Mater Today Chem 14 (2019) 100197. https://doi.org/10.1016/j.mtchem.2019.100197.

[151] A. Gomez-Barea, S. Nilsson, F.V. Barrero, M. Campoy, Devolatilization of wood and wastes in fluidized bed, Fuel Processing Technology 91 (2010) 1624–1633. https://doi.org/10.1016/j.fuproc.2010.06.011.

[152] G.B. de D. Ribeiro, F.R.S. Batista, M.A. de Magalhães, S.R. Valverde, A. de C.O. Carneiro, D.H. Amaral, Techno-economic feasibility analysis of a eucalyptus-based power plant using woodchips, Biomass Bioenergy 153 (2021) 106218. https://doi.org/10.1016/J.BIOMBIOE.2021.106218.

[153] A. Heidari, R. Stahl, H. Younesi, A. Rashidi, N. Troeger, A.A. Ghoreyshi, Effect of process conditions on product yield and composition of fast pyrolysis of Eucalyptus grandis in fluidized bed reactor, Journal of Industrial and Engineering Chemistry 20 (2014) 2594–2602. https://doi.org/10.1016/J.JIEC.2013.10.046.

[154] W. Kaminsky, Chemical recycling of plastics by fluidized bed pyrolysis, Fuel Communications 8 (2021) 100023. https://doi.org/10.1016/J.JFUECO.2021.100023.

[155] W. Kaminsky, J.S. Kim, Pyrolysis of mixed plastics into aromatics, J Anal Appl Pyrolysis 51 (1999) 127–134. https://doi.org/10.1016/S0165-2370(99)00012-1.

[156] W.-C. Yang, Handbook of fluidization and fluid-particle systems, 2008. https://doi.org/10.1016/s1672-2515(07)60126-2.

[157] U. Arena, R. Chirone, M. D'Amore, M. Miccio, P. Salatino, Some issues in modelling bubbling and circulating fluidized-bed coal combustors, Powder Technol 82 (1995) 301–316. https://doi.org/10.1016/0032-5910(94)02933-F.

[158] S. Iannello, S. Morrin, M. Materazzi, Fluidised Bed Reactors for the Thermochemical Conversion of Biomass and Waste, KONA Powder and Particle Journal (2020). https://doi.org/10.14356/kona.2020016.

[159] R.H. Perry, D.W. Green, J.O. Maloney, Perry's Chemical Engineer's Handbook, 8th ed., McGraw-Hill Education, 2007. https://doi.org/10.1036/0071422943.

[160] R.H. Perry, D.W. Green, J.O. Maloney, Perry's Chemical Engineer's Handbook, 8th ed., McGraw-Hill Education, 2007. https://doi.org/10.1036/0071422943.

[161] R.C. Darton, R.D. LaNauze, J.F. Davidson, D. Harrison, Bubble Growth Due To Coalescence in Fluidised Beds., Trans Inst Chem Eng 55 (1977) 274–280.

[162] E.N. Fuller, P.D. Schettler, J.C. Giddings, A NEW METHOD FOR PREDICTION OF BINARY GAS-PHASE DIFFUSION, (n.d.). https://doi.org/10.1021/ie50677a007.

[163] T.A. Davidson, Report of Investigations 9456 - A simple and accurate method for calculatlng viscosity of gaseous mixtures, Report of Investigations. UNITED STATES DEPARTMENT OF THE INTERIOR (1993) 1–12.

[164] W.-C. Yang, Handbook of fluidization and fluid-particle systems, 2008. https://doi.org/10.1016/s1672-2515(07)60126-2.

[165] S. Iannello, P.U. Foscolo, M. Materazzi, Investigation of single particle devolatilization in fluidized bed reactors by X-ray imaging techniques, Chemical Engineering Journal 431 (2022) 133807. https://doi.org/10.1016/j.cej.2021.133807.

[166] G. Amaya-Santos, S. Chari, A. Sebastiani, F. Grimaldi, P. Lettieri, M. Materazzi, Biohydrogen: A life cycle assessment and comparison with alternative low-carbon production routes in UK, J Clean Prod 319 (2021) 128886. https://doi.org/10.1016/j.jclepro.2021.128886.

[167] M. Materazzi, R. Taylor, Plasma-Assisted Gasification for Waste-to-Fuels Applications, Ind Eng Chem Res 58 (2019) 15902–15913. https://doi.org/10.1021/acs.iecr.9b01239.

[168] S. Iannello, S. Morrin, M. Materazzi, Fluidised Bed Reactors for the Thermochemical Conversion of Biomass and Waste, KONA Powder and Particle Journal (2020). https://doi.org/10.14356/kona.2020016.

[169] A. Sebastiani, D. Macrì, K. Gallucci, M. Materazzi, Steam - oxygen gasification of refuse derived fuel in fluidized beds : Modelling and pilot plant testing, Fuel Processing Technology 216 (2021) 106783. https://doi.org/10.1016/j.fuproc.2021.106783.

[170] G. Bagheri, E. Ranzi, M. Pelucchi, A. Parente, A. Frassoldati, T. Faravelli, Comprehensive kinetic study of combustion technologies for low environmental impact: MILD and OXY-fuel combustion of methane, Combust Flame 212 (2020) 142–155. https://doi.org/10.1016/J.COMBUSTFLAME.2019.10.014.

[171] E. Ranzi, A. Frassoldati, A. Stagni, M. Pelucchi, A. Cuoci, T. Faravelli, Reduced Kinetic Schemes of Complex Reaction Systems: Fossil and Biomass-Derived Transportation Fuels, Int J Chem Kinet 46 (2014) 512–542. https://doi.org/10.1002/KIN.20867.

[172] E. Ranzi, A. Frassoldati, R. Grana, A. Cuoci, T. Faravelli, A.P. Kelley, C.K. Law, Hierarchical and comparative kinetic modeling of laminar flame speeds of hydrocarbon and oxygenated fuels, Prog Energy Combust Sci 38 (2012) 468–501. https://doi.org/10.1016/J.PECS.2012.03.004.

[173] E. Ranzi, C. Cavallotti, A. Cuoci, A. Frassoldati, M. Pelucchi, T. Faravelli, New reaction classes in the kinetic modeling of low temperature oxidation of n-alkanes, Combust Flame 162 (2015) 1679–1691. https://doi.org/10.1016/J.COMBUSTFLAME.2014.11.030.

[174] I. Petersen, J. Werther, Experimental investigation and modeling of gasification of sewage sludge in the circulating fluidized bed, Chemical Engineering and Processing: Process Intensification 44 (2005) 717–736. https://doi.org/10.1016/j.cep.2004.09.001.

[175] Y. Wang, C.M. Kinoshita, KINETIC MODEL OF BIOMASS GASIFICATION, 51 (1993) 19–25.

[176] F. Marias, R. Demarthon, A. Bloas, J.P. Robert-Arnouil, F. Nebbad, Design of a High Temperature Reactor Fed by a Plasma Torch for Tar Conversion: Comparison Between CFD Modelling and Experimental Results, Waste Biomass Valorization 6 (2014) 97–108. https://doi.org/10.1007/s12649-014-9331-6.

[177] P. Morf, P. Hasler, T. Nussbaumer, Mechanisms and kinetics of homogeneous secondary reactions of tar from continuous pyrolysis of wood chips, Fuel 81 (2002) 843–853. https://doi.org/10.1016/S0016-2361(01)00216-2.

[178] D. Tokmurzin, J.Y. Nam, S.J. Park, S.J. Yoon, T.Y. Mun, S.M. Yoon, J.H. Moon, J.G. Lee, D.H. Lee, H.W. Ra, M.W. Seo, Three-Dimensional CFD simulation of waste plastic (SRF) gasification in a bubbling fluidized bed with detailed kinetic chemical model, Energy Convers Manag 267 (2022) 115925. https://doi.org/10.1016/J.ENCONMAN.2022.115925.

[179] F. Marias, R. Demarthon, A. Bloas, J.P. Robert-Arnouil, F. Nebbad, Design of a High Temperature Reactor Fed by a Plasma Torch for Tar Conversion: Comparison Between CFD Modelling and Experimental Results, Waste Biomass Valorization 6 (2015) 97–108. https://doi.org/10.1007/S12649-014-9331-6/TABLES/5.

[180] D.W. Green, M.Z. Southard, Perry's Chemical Engineers' Handbook, 9th Edition, 9th editio, McGraw-Hill Education, New York, N.Y, 2019.

[181] Engineering ToolBox, (2005). Benzene Gas - Specific Heat. [online] Available at: https://www.engineeringtoolbox.com/benzene-d_983.html, (n.d.).

[182] G.M. Barrow, A.L. McClellan, A.L. McClellan, The Thermodynamic Properties of Naphthalene, J Am Chem Soc 73 (1951) 573–575. https://doi.org/10.1021/ja01146a020.

[183] M. Materazzi, P. Lettieri, L. Mazzei, R. Taylor, C. Chapman, Fate and behavior of inorganic constituents of RDF in a two stage fluid bed-plasma gasification plant, Fuel 150 (2015). https://doi.org/10.1016/j.fuel.2015.02.059.

[184] M. Materazzi, R. Taylor, P. Cozens, C. Manson-Whitton, Production of BioSNG from waste derived syngas: Pilot plant operation and preliminary assessment, Waste Management (2018). https://doi.org/10.1016/j.wasman.2018.08.031.

[185] R. Taylor, R. Ray, C. Chapman, Advanced thermal treatment of auto shredder residue and refuse derived fuel, Fuel 106 (2013) 401–409. https://doi.org/10.1016/J.FUEL.2012.11.071.

[186] T.M. Knowlton, Fluidized bed reactor design and scale-up, in: F. Scala (Ed.), Fluidized Bed Technologies for Near-Zero Emission Combustion and Gasification, Woodhead Publishing, 2013: pp. 481–523. https://doi.org/10.1533/9780857098801.2.481.

[187] F. Parrillo, F. Ardolino, G. Calì, A. Pettinau, M. Materazzi, A. Sebastiani, U. Arena, Plastic waste gasification using oxygen-enriched air and steam: Experimental and model results from a large pilot-scale reactor, Waste Management 183 (2024) 53–62. https://doi.org/10.1016/J.WASMAN.2024.04.045.

[188] F. Parrillo, F. Ardolino, G. Calì, D. Marotto, A. Pettinau, U. Arena, Fluidized bed gasification of eucalyptus chips: Axial profiles of syngas composition in a pilot scale reactor, Energy 219 (2021) 119604. https://doi.org/10.1016/J.ENERGY.2020.119604.

[189] F. Parrillo, F. Ardolino, C. Boccia, G. Calì, D. Marotto, A. Pettinau, U. Arena, Co-gasification of plastics waste and biomass in a pilot scale fluidized bed reactor, Energy 273 (2023) 127220. https://doi.org/10.1016/J.ENERGY.2023.127220.

[190] A. Sebastiani, F. Parrillo, F. Ardolino, U. Arena, S. Iannello, M. Materazzi, Modelling of oxygen-steam gasification of waste feedstock in industrial fluidized bed reactors, Chemical Engineering Journal 506 (2025) 159763. https://doi.org/10.1016/J.CEJ.2025.159763.

[191] I.Blu, Products, (2022). https://www.iblu.it/en/products.html (accessed October 18, 2024).

[192] H. Knoef, Handbook biomass gasification, (2005).

[193] U. Arena, L. Zaccariello, M.L. Mastellone, Fluidized bed gasification of waste-derived fuels, Waste Management 30 (2010) 1212–1219. https://doi.org/10.1016/j.wasman.2010.01.038.

[194] U. Arena, L. Zaccariello, M.L. Mastellone, Gasification of Natural and Waste Biomass in a Pilot Scale Fluidized Bed Reactor, Combustion Science and Technology 182 (2010) 625–639. https://doi.org/10.1080/00102200903467689.

[195] S. Hamel, W. Krumm, Mathematical modelling and simulation of bubbling fluidised bed gasifiers, Powder Technol 120 (2001) 105–112. https://doi.org/10.1016/S0032-5910(01)00356-4.

[196] F. Ardolino, C. Lodato, T.F. Astrup, U. Arena, Energy recovery from plastic and biomass waste by means of fluidized bed gasification: A life cycle inventory model, Energy 165 (2018) 299–314. https://doi.org/10.1016/j.energy.2018.09.158.

[197] F. Parrillo, F. Ardolino, C. Boccia, G. Calì, A. Pettinau, U. Arena, Mixed plastic waste gasification in a large pilot scale fluidized bed reactor operated with oxygen enriched air and steam, Energy&Fuels (in Press) (2024).

[198] F. Parrillo, C. Boccia, G. Ruoppolo, M. Commodo, F. Berruti, U. Arena, Steam reforming of tar in hot syngas cleaning by different catalysts: Removal efficiency and coke layer characterization, Can J Chem Eng 101 (2023) 97–109. https://doi.org/10.1002/CJCE.24535.

[199] S. Ciuta, D. Tsiamis, M.J. Castaldi, Field Scale Developments, Gasification of Waste Materials: Technologies for Generating Energy, Gas, and Chemicals from Municipal Solid Waste, Biomass, Nonrecycled Plastics, Sludges, and Wet Solid Wastes (2018) 65–91. https://doi.org/10.1016/B978-0-12-812716-2.00004-2.

[200] U. Arena, Fluidized bed gasification, in: F. Scala (Ed.), Fluidized Bed Technologies for Near-Zero Emission Combustion and Gasification, Woodhead Publishing, 2013: p. iv. https://doi.org/10.1016/B978-0-85709-541-1.50025-X.

[201] S.W. Han, D. Tokmurzin, J.J. Lee, S.J. Park, H.W. Ra, S.J. Yoon, T.-Y. Mun, S.M. Yoon, J.H. Moon, J.G. Lee, Y.-M. Kim, Y.W. Rhee, M.W. Seo, Gasification characteristics of waste plastics (SRF) in a bubbling fluidized bed: Use of activated carbon and olivine for tar removal and the effect of steam/carbon ratio, Fuel 314 (2022) 123102. https://doi.org/10.1016/j.fuel.2021.123102.

[202] F. Pinto, C. Franco, R.N. André, M. Miranda, I. Gulyurtlu, I. Cabrita, Co-gasification study of biomass mixed with plastic wastes, Fuel 81 (2002) 291–297. https://doi.org/10.1016/S0016-2361(01)00164-8.

[203] U. Arena, L. Zaccariello, M.L. Mastellone, Fluidized bed gasification of waste-derived fuels, Waste Management 30 (2010) 1212–1219. https://doi.org/10.1016/j.wasman.2010.01.038.

[204] M. Materazzi, R. Taylor, Plasma-Assisted Gasification for Waste-to-Fuels Applications, Ind Eng Chem Res (2019). https://doi.org/10.1021/acs.iecr.9b01239.

[205] A. Erkiaga, G. Lopez, M. Amutio, J. Bilbao, M. Olazar, Syngas from steam gasification of polyethylene in a conical spouted bed reactor, Fuel 109 (2013) 461–469. https://doi.org/10.1016/j.fuel.2013.03.022.

[206] S. Li, I. Cañete Vela, M. Järvinen, M. Seemann, Polyethylene terephthalate (PET) recycling via steam gasification – The effect of operating conditions on gas and tar composition, Waste Management 130 (2021) 117–126. https://doi.org/10.1016/J.WASMAN.2021.05.023.

[207] A. Arregi, M. Amutio, G. Lopez, J. Bilbao, M. Olazar, Evaluation of thermochemical routes for hydrogen production from biomass: A review, Energy Convers Manag 165 (2018) 696–719. https://doi.org/10.1016/j.enconman.2018.03.089.

[208] NETL, Seventh Edition Fuel Cell Handbook, Pittsburgh, PA, and Morgantown, WV, 2004. https://doi.org/10.2172/834188.

[209] C. Tagliaferri, S. Evangelisti, F. Acconcia, T. Domenech, P. Ekins, D. Barletta, P. Lettieri, Life cycle assessment of future electric and hybrid vehicles: A cradle-to-grave systems engineering approach, Chemical Engineering Research and Design 112 (2016) 298–309. https://doi.org/10.1016/J.CHERD.2016.07.003.

[210] M. Materazzi, R. Taylor, Plasma-Assisted Gasification for Waste-to-Fuels Applications, Ind Eng Chem Res 58 (2019). https://doi.org/10.1021/acs.iecr.9b01239.

[211] S. Sharma, S. Basu, N.P. Shetti, T.M. Aminabhavi, Waste-to-energy nexus for circular economy and environmental protection: Recent trends in hydrogen energy, Science of the Total Environment 713 (2020) 136633. https://doi.org/10.1016/j.scitotenv.2020.136633.

[212] L. Devi, K.J. Ptasinski, F.J.J.G. Janssen, A review of the primary measures for tar elimination in biomass gasification processes, Biomass Bioenergy 24 (2003) 125–140. https://doi.org/10.1016/S0961-9534(02)00102-2.

[213] R.W.R. Zwart, Gas cleaning downstream biomass gasification, Petten, 2009.

[214] Y. Wang, D.F. Ruiz Diaz, K.S. Chen, Z. Wang, X.C. Adroher, Materials, technological status, and fundamentals of PEM fuel cells – A review, Materials Today 32 (2020) 178–203. https://doi.org/10.1016/j.mattod.2019.06.005.

[215] V.F. Valdés-López, T. Mason, P.R. Shearing, D.J.L. Brett, Carbon monoxide poisoning and mitigation strategies for polymer electrolyte membrane fuel cells – A review, Prog Energy Combust Sci 79 (2020) 100842. https://doi.org/10.1016/j.pecs.2020.100842.

[216] D. Jansen, M. Gazzani, G. Manzolini, E. Van Dijk, M. Carbo, Pre-combustion CO2 capture, International Journal of Greenhouse Gas Control 40 (2015) 167–187. https://doi.org/10.1016/j.ijggc.2015.05.028.

[217] B.M. Besancon, V. Hasanov, R. Imbault-Lastapis, R. Benesch, M. Barrio, M.J. Mølnvik, Hydrogen quality from decarbonized fossil fuels to fuel cells, Int J Hydrogen Energy 34 (2009) 2350–2360. https://doi.org/10.1016/J.IJHYDENE.2008.12.071.

[218] M. Materazzi, S. Chari, A. Sebastiani, WASTE-TO-HYDROGEN : CHALLENGES AND OPPORTUNITIES IN THE UK SCENARIO, (2022).

[219] R.K. Sinnott, Coulson & Richardson's Chemical Engineering Design, (1999).

[220] W.L. Theo, J.S. Lim, H. Hashim, A.A. Mustaffa, W.S. Ho, Review of pre-combustion capture and ionic liquid in carbon capture and storage, Appl Energy 183 (2016) 1633–1663. https://doi.org/10.1016/j.apenergy.2016.09.103.

[221] S.H. Park, K.B. Lee, J.C. Hyun, S.H. Kim, Correlation and prediction of the solubility of carbon dioxide in aqueous alkanolamine and mixed alkanolamine solutions, Ind Eng Chem Res 41 (2002) 1658–1665. https://doi.org/10.1021/ie010252o.

[222] M.K. Mondal, H.K. Balsora, P. Varshney, Progress and trends in CO2 capture/separation technologies: A review, Energy 46 (2012) 431–441. https://doi.org/10.1016/j.energy.2012.08.006.

[223] S.H. Park, S.J. Lee, J.W. Lee, S.N. Chun, J. Bin Lee, The quantitative evaluation of two-stage pre-combustion CO2 capture processes using the physical solvents with various design parameters, Energy 81 (2015) 47–55. https://doi.org/10.1016/j.energy.2014.10.055.

[224] W.H. Chen, S.M. Chen, C.I. Hung, Carbon dioxide capture by single droplet using Selexol, Rectisol and water as absorbents: A theoretical approach, Appl Energy 111 (2013) 731–741. https://doi.org/10.1016/j.apenergy.2013.05.051.

[225] R. Sadegh-Vaziri, M. Amovic, R. Ljunggren, K. Engvall, A Medium-scale 50 MWfuel biomass gasification based Bio-SNG plant: A developed gas cleaning process, Energies (Basel) 8 (2015) 5287–5302. https://doi.org/10.3390/EN8065287.

[226] J. De Winter, Process simulation of SEWGS technology for applications in the steel industry, (2014) 133. https://daim.idi.ntnu.no/masteroppgaver/010/10912/masteroppgave.pdf.

[227] D. Jansen, E. Van Selow, P. Cobden, G. Manzolini, E. Macchi, M. Gazzani, R. Blom, P.P. Henriksen, R. Beavis, A. Wright, SEWGS technology is now ready for scale-up!, Energy Procedia 37 (2013) 2265–2273. https://doi.org/10.1016/j.egypro.2013.06.107.

[228] G. Manzolini, E. Macchi, M. Gazzani, CO2 capture in natural gas combined cycle with SEWGS. Part B: Economic assessment, International Journal of Greenhouse Gas Control 12 (2013) 502–509. https://doi.org/10.1016/j.ijggc.2012.06.021.

[229] B. Malsegna, A. Sebastiani, J.G. da Gama Paz-Dias, F. Di Luca, A. Di Giuliano, K. Gallucci, M. Materazzi, Simulation of a sorption-enhanced water gas-shift pilot technology for pure hydrogen production from a waste gasification plant, Fuel Processing Technology 254 (2024) 108032. https://doi.org/10.1016/J.FUPROC.2024.108032.

[230] C.T. Chou, F.H. Chen, Y.J. Huang, H.S. Yang, Carbon dioxide capture and hydrogen purification from synthesis gas by pressure swing adsorption, Chem Eng Trans 32 (2013) 1855–1860. https://doi.org/10.3303/CET1332310.

[231] S. Sircar, T.C. Golden, Purification of hydrogen by pressure swing adsorption, Sep Sci Technol 35 (2000) 667–687. https://doi.org/10.1081/SS-100100183.

[232] D.F.B. Lima, F.A. Zanella, M.K. Lenzi, P.M. Ndiaye, D.F.B. Lima, F.A. Zanella, M.K. Lenzi, P.M. Ndiaye, Modeling and Simulation of Water Gas Shift Reactor: An Industrial Case, Petrochemicals (2012). https://doi.org/10.5772/37181.

[233] M. Kamaraj, K.K. Ramachandran, J. Aravind, Biohydrogen production from waste materials: benefits and challenges, International Journal of Environmental Science and Technology 17 (2020) 559–576. https://doi.org/10.1007/S13762-019-02577-Z/FIGURES/5.

[234] C. Manson-Whitton, Biohydrogen: Production of hydrogen by gasification of waste, (2017) 130. https://gogreengas.com/wp-content/uploads/2015/11/Biohydrogen-Cadent-Project-Report-FINAL-3.pdf.

[235] M. Voldsund, K. Jordal, R. Anantharaman, Hydrogen production with CO2 capture, Int J Hydrogen Energy 41 (2016) 4969–4992. https://doi.org/10.1016/j.ijhydene.2016.01.009.

[236] J.J. Alves, G.P. Towler, Analysis of Refinery Hydrogen Distribution Systems, Ind Eng Chem Res 41 (2002) 5759–5769. https://doi.org/10.1021/ie010558v.

[237] J.H. Gary, J.H. Handwerk, M.J. Kaiser, D. Geddes, Petroleum Refining : Technology and Economics, Fifth Edition, Petroleum Refining (2007). https://doi.org/10.4324/9780203907924.

[238] International Organization for Standardization, ISO 14687:2019 - Hydrogen fuel quality — Product specification, (n.d.). https://www.iso.org/standard/69539.html (accessed January 6, 2025).

[239] J.H. Gary, G.E. Handwerk, Petroleum Refining : Technology and Economics, 2001.

[240] J.J. Alves, G.P. Towler, Analysis of refinery hydrogen distribution systems, Ind Eng Chem Res 41 (2002) 5759–5769. https://doi.org/10.1021/IE010558V/ASSET/IMAGES/LARGE/IE010558VF00013.JPEG.

[241] J.A. Ritter, A.D. Ebner, State-of-the-Art Adsorption and Membrane Separation Processes for Hydrogen Production in the Chemical and Petrochemical Industries, Sep Sci Technol 42 (2007) 1123–1193. https://doi.org/10.1080/01496390701242194.

[242] Max. Appl, Ammonia : principles and industrial practice, (1999) 301.

[243] S. Rönsch, J. Köchermann, J. Schneider, S. Matthischke, Global Reaction Kinetics of CO and CO2 Methanation for Dynamic Process Modeling, Chem Eng Technol 39 (2016) 208–218. https://doi.org/10.1002/CEAT.201500327.

[244] A. Padurean, C.C. Cormos, P.S. Agachi, Pre-combustion carbon dioxide capture by gas-liquid absorption for Integrated Gasification Combined Cycle power plants, International Journal of Greenhouse Gas Control 7 (2012) 1–11. https://doi.org/10.1016/j.ijggc.2011.12.007.

[245] F. Cherubini, G.P. Peters, T. Berntsen, A.H. Strømman, E. Hertwich, CO2 emissions from biomass combustion for bioenergy: Atmospheric decay and contribution to global warming, GCB Bioenergy 3 (2011) 413–426. https://doi.org/10.1111/j.1757-1707.2011.01102.x.

[246] F. Cherubini, S. Bargigli, S. Ulgiati, Life cycle assessment (LCA) of waste management strategies: Landfilling, sorting plant and incineration, Energy (2009). https://doi.org/10.1016/j.energy.2008.08.023.

[247] V. Masson-Delmotte, P. Zhai, A. Pirani, S.L. Connors, C. Péan, S. Berger, N. Caud, Y. Chen, L. Goldfarb, M.I. Gomis, M. Huang, K. Leitzell, E. Lonnoy, J.B.R. Matthews, T.K. Maycock, T. Waterfield, O. Yelekçi, R. Yu, B. Zhou, (eds.), Climate Change 2021: The Physical Science Basis. Contribution of Working Group I to the Sixth Assessment Report of the Intergovernmental Panel on Climate Change, Cambridge University Press, 2021.

[248] M. Errigo, A. Sebastiani, S. Iannello, M. Materazzi, P. Lettieri, Application of imaging techniques for the characterization of lumps behaviour in gas–solid fluidized-bed reactors, Fuel 349 (2023) 128634. https://doi.org/10.1016/j.fuel.2023.128634.

[249] A. Welfle, P. Thornley, M. Röder, A review of the role of bioenergy modelling in renewable energy research & policy development, Biomass Bioenergy 136 (2020). https://doi.org/10.1016/j.biombioe.2020.105542.

[250] P. Lettieri, L. Yassin, S.J.R. Simons, Advanced thermal treatment of composite wastes for energy recovery, in: Management, Recycling and Reuse of Waste Composites, 2009. https://doi.org/10.1533/9781845697662.2.152.

[251] L. Lombardi, E. Carnevale, A. Corti, A review of technologies and performances of thermal treatment systems for energy recovery from waste, Waste Management (2015). https://doi.org/10.1016/j.wasman.2014.11.010.

[252] H. Hofbauer, M. Materazzi, Waste gasification processes for SNG production, in: Substitute Natural Gas from Waste, Elsevier, 2019: pp. 105–160. https://doi.org/10.1016/B978-0-12-815554-7.00007-6.

[253] P. Salatino, R. Solimene, Mixing and segregation in fluidized bed thermochemical conversion of biomass, Powder Technol 316 (2017) 29–40. https://doi.org/10.1016/j.powtec.2016.11.058.

[254] S. Iannello, P.U. Foscolo, M. Materazzi, Investigation of single particle devolatilization in fluidized bed reactors by X-ray imaging techniques, Chemical Engineering Journal 431 (2022) 133807. https://doi.org/10.1016/j.cej.2021.133807.

[255] L. Garcia, M.L. Salvador, J. Arauzo, R. Bilbao, CO2 as a gasifying agent for gas production from pine sawdust at low temperatures using a Ni/Al coprecipitated catalyst, Fuel Processing Technology 69 (2001) 157–174. https://doi.org/10.1016/S0378-3820(00)00138-7.

[256] H.C. Butterman, M.J. Castaldi, CO2 as a carbon neutral fuel source via enhanced biomass gasification, Environ Sci Technol 43 (2009) 9030–9037. https://doi.org/10.1021/es901509n.

[257] A.M. Mauerhofer, J. Fuchs, S. Müller, F. Benedikt, J.C. Schmid, H. Hofbauer, CO2 gasification in a dual fluidized bed reactor system: Impact on the product gas composition, Fuel 253 (2019) 1605–1616. https://doi.org/10.1016/J.FUEL.2019.04.168.

[258] I. Ahmed, A.K. Gupta, Characteristics of cardboard and paper gasification with CO2, Appl Energy 86 (2009) 2626–2634. https://doi.org/10.1016/J.APENERGY.2009.04.002.

[259] R.B. Bates, A.F. Ghoniem, W.S. Jablonski, D.L. Carpenter, C. Altantzis, A. Garg, J.L. Barton, R. Chen, R.P. Field, Steam-air blown bubbling fluidized bed biomass gasification (BFBBG): Multi-scale models and experimental validation, AIChE Journal 63 (2017) 1543–1565. https://doi.org/10.1002/aic.15666.

[260] H.C. Butterman, M.J. Castaldi, CO2 as a carbon neutral fuel source via enhanced biomass gasification, Environ Sci Technol 43 (2009) 9030–9037. https://doi.org/10.1021/es901509n.

[261] Y. Oki, J. Inumaru, S. Hara, M. Kobayashi, H. Watanabe, S. Umemoto, H. Makino, Development of oxy-fuel IGCC system with CO2 recirculation for CO2 capture, Energy Procedia 4 (2011) 1066–1073. https://doi.org/10.1016/J.EGYPRO.2011.01.156.

[262] M. Chester, D. Stupples, M. Lees, A Comparison of the Physical and Chemical Composition of Uk Waste Streams Based on Hypothetical Compound Structure, White Rose Research Papers (2008) 10–12.

[263] H. Zhou, A. Meng, Y. Long, Q. Li, Y. Zhang, Classification and comparison of municipal solid waste based on thermochemical characteristics, J Air Waste Manage Assoc 64 (2014) 597–616. https://doi.org/10.1080/10962247.2013.873094.

[264] H. Zhong, X. Mao, A.C. Rousso, C.L. Patrick, C. Yan, W. Xu, Q. Chen, G. Wysocki, Y. Ju, Kinetic study of plasma-assisted n-dodecane/O2/N2 pyrolysis and oxidation in a nanosecond-pulsed discharge, Proceedings of the Combustion Institute 38 (2021) 6521–6531. https://doi.org/10.1016/j.proci.2020.06.016.

[265] X. Mao, A. Rousso, Q. Chen, Y. Ju, Numerical modeling of ignition enhancement of CH 4 /O 2 /He mixtures using a hybrid repetitive nanosecond and DC discharge, Proceedings of the Combustion Institute 37 (2019) 5545–5552. https://doi.org/10.1016/j.proci.2018.05.106.

[266] X. Mao, Q. Chen, A.C. Rousso, T.Y. Chen, Y. Ju, Effects of controlled non-equilibrium excitation on H2/O2/He ignition using a hybrid repetitive nanosecond and DC discharge, Combust Flame 206 (2019) 522–535. https://doi.org/10.1016/J.COMBUSTFLAME.2019.05.027.

[267] M.S. Benilov, G. V. Naidis, Modeling of hydrogen-rich gas production by plasma reforming of hydrocarbon fuels, Int J Hydrogen Energy 31 (2006) 769–774. https://doi.org/10.1016/j.ijhydene.2005.06.018.

[268] J.A.M. R.J. Kee, F.M. Rupley, E. Meeks, CHEMKIN-II: A FORTRAN CHEMICAL KINETICS PACKAGE FOR THE ANALYSIS OF GAS-PHASE CHEMICAL KINETICS, 15 (1989) 1–23.

[269] J.A.M. R.J. Kee, F.M. Rupley, E. Meeks, CHEMKIN-III A Fortran Chemical Kinetics Package for the Analysis of Gas-phase Chemical and Plasma Kinetics, (1996) 166. https://www.ansys.com/products/fluids/ansys-chemkin-pro.

[270] L. Cai, H. Pitsch, S.Y. Mohamed, V. Raman, J. Bugler, H. Curran, S.M. Sarathy, Optimized reaction mechanism rate rules for ignition of normal alkanes, Combust Flame 173 (2016) 468–482. https://doi.org/10.1016/J.COMBUSTFLAME.2016.04.022.

[271] S. Kaza, L. Yao, P. Bhada-Tata, F. Van Woerden, What a waste 2.0. A global snapshot of solid waste management to 2050., 2018.

[272] CCC, Deep-Decarbonisation Pathways for UK Industry (Element Energy), Climate Change Committee 44 (2020).

[273] Climate Change Committee, The Sixth Carbon Budget. The UK' s path to Net Zero, 2020.

[274] J. Rockström, O. Gaffney, J. Rogelj, M. Meinshausen, N. Nakicenovic, H.J. Schellnhuber, A roadmap for rapid decarbonization, Science (1979) 355 (2017) 1269–1271. https://doi.org/10.1126/science.aah3443.

[275] IPCC, Climate Change 2022 - Mitigation of Climate Change. Contribution of Working Group III to the Sixth Assessment Report of the Intergovernmental Panel on Climate Change, 2022.

[276] T.F. Astrup, D. Tonini, R. Turconi, A. Boldrin, Life cycle assessment of thermal Waste-to-Energy technologies: Review and recommendations, Waste Management 37 (2015) 104–115. https://doi.org/10.1016/j.wasman.2014.06.011.

[277] A. Laurent, I. Bakas, J. Clavreul, A. Bernstad, M. Niero, E. Gentil, M.Z. Hauschild, T.H. Christensen, Review of LCA studies of solid waste management systems - Part I: Lessons learned and perspectives, Waste Management 34 (2014) 573–588. https://doi.org/10.1016/j.wasman.2013.10.045.

[278] B. Dastjerdi, V. Strezov, M.A. Rajaeifar, R. Kumar, M. Behnia, A systematic review on life cycle assessment of different waste to energy valorization technologies, J Clean Prod 290 (2021) 125747. https://doi.org/10.1016/j.jclepro.2020.125747.

[279] M.K. Chandel, G. Kwok, R.B. Jackson, L.F. Pratson, The potential of waste-to-energy in reducing GHG emissions, Carbon Manag 3 (2012) 133–144. https://doi.org/10.4155/cmt.12.11.

[280] C. Lausselet, F. Cherubini, G.D. Oreggioni, G. del Alamo Serrano, M. Becidan, X. Hu, P.K. Rørstad, A.H. Strømman, Norwegian Waste-to-Energy: Climate change, circular economy and carbon capture and storage, Resour Conserv Recycl 126 (2017) 50–61. https://doi.org/10.1016/j.resconrec.2017.07.025.

[281] Y. Tang, F. You, Multicriteria Environmental and Economic Analysis of Municipal Solid Waste Incineration Power Plant with Carbon Capture and Separation from the Life-Cycle Perspective, ACS Sustain Chem Eng 6 (2018) 937–956. https://doi.org/10.1021/acssuschemeng.7b03283.

[282] V. Bisinella, T. Hulgaard, C. Riber, A. Damgaard, T.H. Christensen, Environmental assessment of carbon capture and storage (CCS) as a post-treatment technology in waste incineration, Waste Management 128 (2021) 99–113. https://doi.org/10.1016/j.wasman.2021.04.046.

[283] V. Bisinella, J. Nedenskov, C. Riber, T. Hulgaard, T.H. Christensen, Environmental assessment of amending the Amager Bakke incineration plant in Copenhagen with carbon capture and storage, Waste Management and Research 40 (2022) 79–95. https://doi.org/10.1177/0734242X211048125.

[284] H. Birgisdóttir, G. Bhander, M.Z. Hauschild, T.H. Christensen, Life cycle assessment of disposal of residues from municipal solid waste incineration: Recycling of bottom ash in road construction or landfilling in Denmark evaluated in the ROAD-RES model, Waste Management 27 (2007) 75–84. https://doi.org/10.1016/j.wasman.2007.02.016.

[285] M. Wang, A. Lawal, P. Stephenson, J. Sidders, C. Ramshaw, Post-combustion CO2 capture with chemical absorption: A state-of-the-art review, Chemical Engineering Research and Design 89 (2011) 1609–1624. https://doi.org/10.1016/j.cherd.2010.11.005.

[286] A. Kothandaraman, Carbon Dioxide Capture by Chemical Absorption: A Solvent Comparison Study, 9 (2010) 159–176.

[287] IPCC, Carbon dioxide capture and storage, 2005. https://doi.org/10.1016/bs.ache.2021.10.005.

[288] B. Wetenhall, J.M. Race, M.J. Downie, The Effect of CO2 Purity on the Development of Pipeline Networks for Carbon Capture and Storage Schemes, International Journal of Greenhouse Gas Control 30 (2014) 197–211. https://doi.org/10.1016/j.ijggc.2014.09.016.

[289] J. Parikh, S.A. Channiwala, G.K. Ghosal, A correlation for calculating HHV from proximate analysis of solid fuels, Fuel 84 (2005) 487–494. https://doi.org/10.1016/j.fuel.2004.10.010.

[290] H. Zhou, A. Meng, Y. Long, Q. Li, Y. Zhang, Classification and comparison of municipal solid waste based on thermochemical characteristics, J Air Waste Manage Assoc 64 (2014) 597–616. https://doi.org/10.1080/10962247.2013.873094.

[291] G. Wernet, C. Bauer, B. Steubing, J. Reinhard, E. Moreno-Ruiz, B. Weidema, The ecoinvent database version 3 (part I): overview and methodology, International Journal of Life Cycle Assessment 21 (2016) 1218–1230. https://doi.org/10.1007/s11367-016-1087-8.

[292] JRC, Product Environmental Footprint Category Rules Guidance. Version 6.3, 2018.

[293] K. Sipilä, Cogeneration, biomass, waste to energy and industrial waste heat for district heating, Advanced District Heating and Cooling (DHC) Systems (2015) 45–73. https://doi.org/10.1016/B978-1-78242-374-4.00003-3.

[294] T. Fruergaard, T.H. Christensen, T. Astrup, Energy recovery from waste incineration: Assessing the importance of district heating networks, Waste Management 30 (2010) 1264–1272. https://doi.org/10.1016/j.wasman.2010.03.026.

[295] A. Zsebik, J. Sitku G., Heat exchanger connection in substations-a tool of decreasing return temperature in district heating networks, Energy Engineering: Journal of the Association of Energy Engineering 98 (2001) 20-28+31. https://doi.org/10.1092/FYL2-FF8N-6B6C-A57R.

[296] B. Rezaie, M.A. Rosen, District heating and cooling: Review of technology and potential enhancements, Appl Energy 93 (2012) 2–10. https://doi.org/10.1016/j.apenergy.2011.04.020.

[297] D. Kearns, H. Liu, C. Consoli, Technology Readiness and Costs of CCS, Global CCS Insitute (2021) 50.

[298] D.T. Kearns, Waste-to-Energy with CCS: A pathway to carbon-negative power generation, Global CCS Institute (2019) 1–11.

[299] Statista, United Kingdom Emission Trading System (UK-ETS) carbon pricing in 2022, (n.d.).

[300] H.K. Jeswani, A. Azapagic, Assessing the environmental sustainability of energy recovery from municipal solid waste in the UK, Waste Management 50 (2016) 346–363. https://doi.org/10.1016/j.wasman.2016.02.010.

[301] S. Mühle, I. Balsam, C.R. Cheeseman, Comparison of carbon emissions associated with municipal solid waste management in Germany and the UK, Resour Conserv Recycl 54 (2010) 793–801. https://doi.org/10.1016/j.resconrec.2009.12.009.

APPENDIX A. Lab scale reactor: UCL

The experimental apparatus consists of a cylindrical vessel with 146 mm inner diameter and 1000 mm height. The reactor is made of Inconel and is operated at atmospheric pressure and temperature around 750°C. Temperature is mostly controlled by oxygen inlet and an external heater, which provides the heat necessary to compensate for the heat losses in the system. The vessel contains Geldart group B quartz sand (particle density 2650 kg/m^3 and average particle size 250 µm) with a fixed bed height of 15 cm. The gasification agent is pre-heated up to 450°C and sent into the reactor through a windbox and stainless steel distributor plate in order to uniform the flow stream. A disengaging section of 500mm height is placed above the reactor as a freeboard extension and to prevent particles elutriation. In the disengaging section, the finest solid particles in the product gas are captured and collected in a filter. The product gas stream leaves the reactor and flows into a cold trap, in which the gas stream is cooled down to ambient temperature and separated from most of the condensable compounds. A gas stream of 1 L/min is sampled and passed through an on-line gas analyzer (Rapidox 7100 Multigas Analyzer, Cambridge Sensotech). The analyzer measures the volume fractions of CO, CO_2, H_2, and light hydrocarbons (HC). Figure A.1 shows a simple scheme of the whole experimental apparatus.

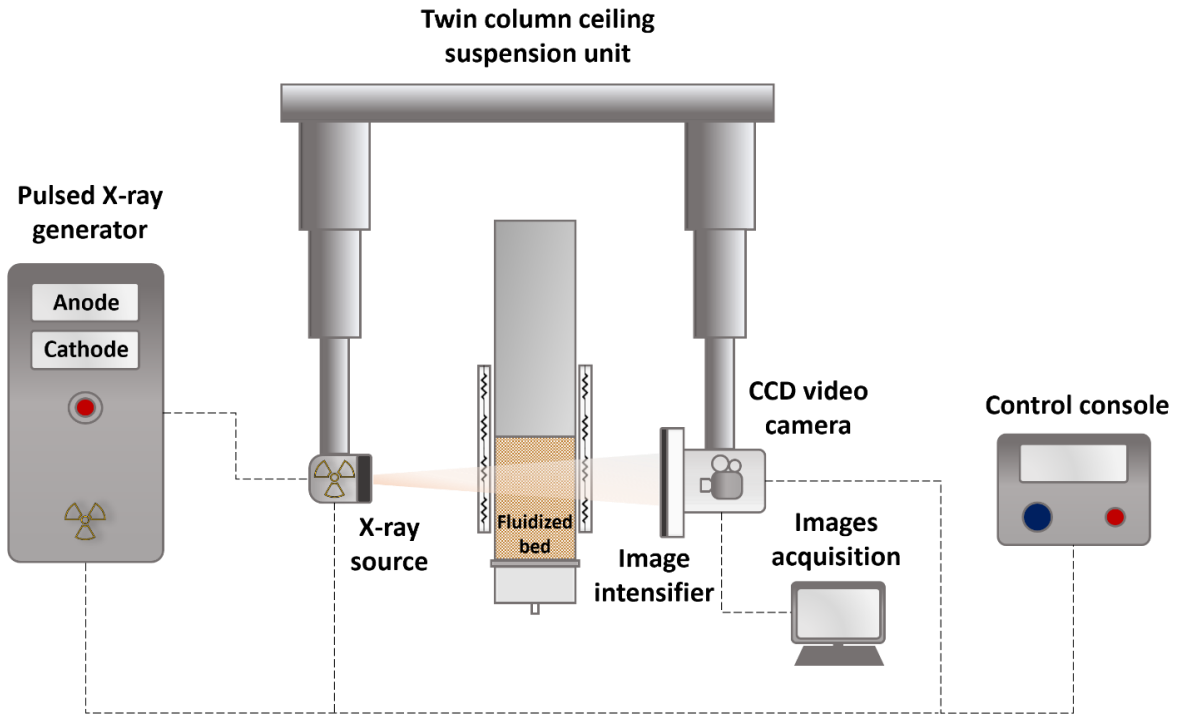

Figure A.1 – Schematic representation of the X-Ray experimental set-up. Adapted from [248]

The particle tracking and fluidization behaviour is investigated by means of the X-ray facility shown in Figure A.2. The X-ray radiography system used in this work is composed of three elements: the X-ray source, a twin column ceiling suspension unit and the detection system (image intensifier). The X-ray source and detector are positioned overhead, allowing flexibility in adjusting the object-to-intensifier distance (OID) and the source-to-intensifier distance (SID), as well as accommodating larger vessels for imaging purposes. The X-ray generator is located in an adjacent room and is composed of a cathode and an anode, contained within an evacuated tube lined with lead. The cathode is made up of filaments, from which electrons are emitted through thermionic emission. The anode serves as the destination for the electrons accelerated from the cathode. Anodes can be rotated using induction motors to distribute the heat load across a wider surface, enabling the utilization of higher power loads. The X-rays are pulsed by modulating the current to the cathode, resulting in a minimum pulse duration of 200 µs at a frequency of 36 frames per second (fps). The system can be operated with a maximum current of 450 mA and a voltage up to 150 kV. The X-ray settings can be changed using a control console. Figure A.2 shows a more detailed schematization of the entire X-ray facility

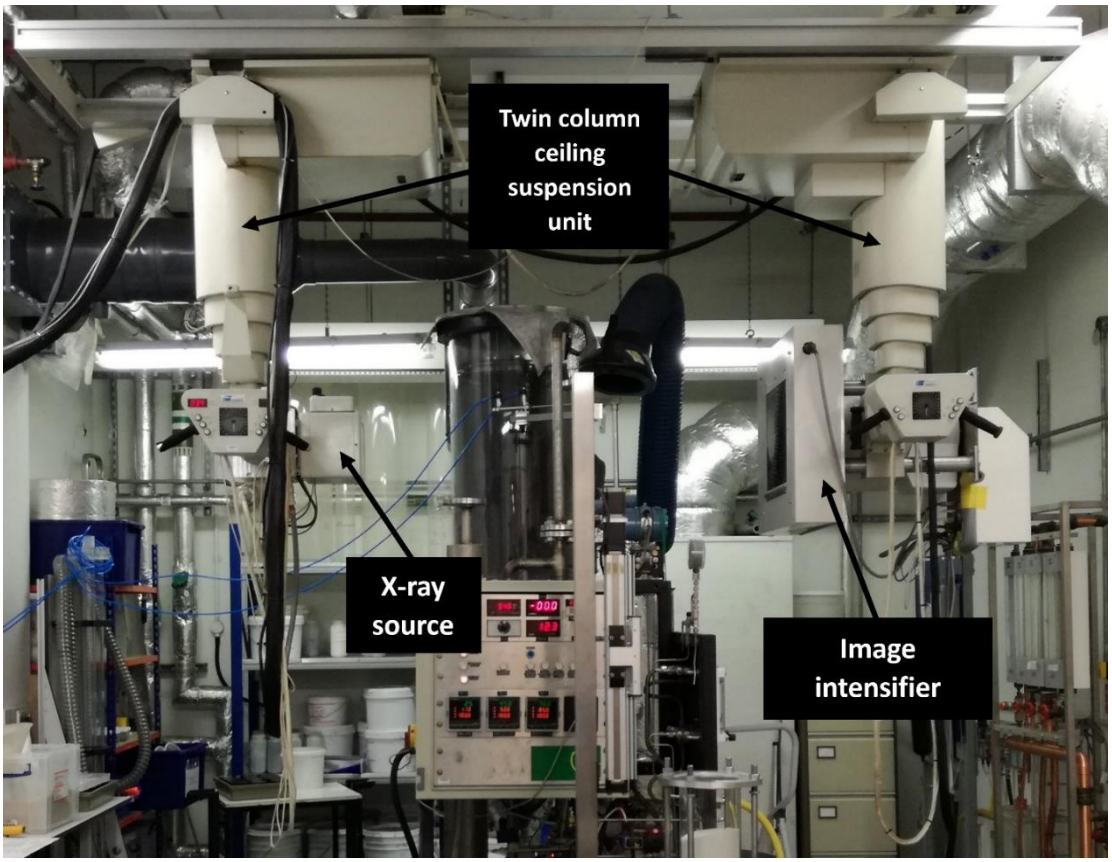

Figure A.2 – X-ray facility.

APPENDIX B. Oxy-gasification of biomass waste in lab-scale fluidized bed: Steam VS CO_2

The work presented in this section aims to investigate the effect of different gasification agents on the performance of waste gasification in a lab-scale bubbling fluidized bed. In particular, the influence of CO_2 against steam on syngas quality is studied in a lab-scale fluidized bed for autothermal (oxygen-based) gasification, with on-line gas analysis and temperature measurements. The results are used to inform a one-dimensional kinetic model for waste gasification, which is then used to investigate the scale-up of the process from lab to demo scale. Experimental results show that the use of CO_2 as a gasification agent produces an increase in CO/H_2 ratio, with the maximum variation observed being +/- 40% relative to the complete switch from steam to CO_2 in oxi-gasification. The model results are in good agreement with the experimental and literature values.

This appendix has been published in the conference paper:

Sebastiani A., Iannello S., Chari S., Macri' D., Materazzi M. (2022) Steam-CO_2/Oxygen gasification of biomass waste in lab-scale fluidized bed. Fluidized bed conversion conference. The 24th fluidized bed conversion conference.

B.1. Introduction

The landmark 2015 Paris Agreement, confirmed by the UN Climate Change Conference in Glasgow (COP26), agreed to hold the increase in the global average temperature to well below 2°C above the pre-industrial level. To keep global warming well below 2 °C, current greenhouse gas (GHG) emissions must be halved by mid-century and must then continue to decline [4]. This will require rapid changes in energy systems. The interest is converging towards a combined solution represented by the use of residual biomass and waste as a renewable source in bioenergy systems [249]. This represents a key component for mitigation strategies to reduce the carbon footprint of the energy sector.

Amongst all the available options, gasification represents the most promising technology in terms of waste reduction potential, energy efficiency, and the number of possible applications [250,251]. It involves partial oxidation of the fuel at high temperature (700-900 ºC) to generate a gas rich in hydrogen and carbon monoxide (syngas) with a net calorific value of 4-10 MJ/Nm^3. Autothermal

gasification can be accomplished through several reactors configuration including bubbling fluidized bed reactors, which are particularly suitable to waste operation due to their flexibility with respect to feedstock and operating conditions, favorable mixing features, and enhanced heat and mass transfer [168,252,253]. Nevertheless, there are still unsolved challenges when operating with highly volatile and heterogeneous feedstocks, such as biomass and waste [169,254]. Extensive research has been done to understand the effect of steam, air, oxygen and their combinations on the process. Steam is usually used as a gasification agent to promote tars reforming and act as temperature control to balance the exothermicity of combustion reactions. Furthermore, having steam in the produced syngas entails easier separation by condensation. Although it is an easily accessible utility, steam generation is energy-intensive for the process.

One promising option to reduce the CO_2 emissions of a bioenergy plant is represented by capturing the generated CO_2 (in pre-combustion asset) and reusing some of this within the process. Thus, the carbon cycle could be effectively closed and arising CO_2 reused within different processes. This has been investigated also for gasification, replacing steam with CO_2. The role of CO_2 as a gasification agent has been explored in a limited number of studies [255–258], and often not in autothermal reactors. CO_2 is not a popular gasification agent because the reaction of CO_2 with carbon (the Boudouard reaction) is highly endothermic and, hence, highly energy-intensive. Furthermore, separating CO_2 from the produced syngas entails more complex unit operations that are usually energy-consuming [255,256,259]. However, since the stream of CO_2 does not require additional heat of vaporization during the preheating stage, its usage as a gasification medium represents a lower energy-intensive solution than steam [260]. A wide range of H_2/CO ratios in the syngas can be achieved to suit different applications while not significantly affecting the process efficiency. Using CO_2 as a gasification agent can result in higher fractions of reactive char, which affects tar reforming and syngas cleaning [256]. Oki et al. [261] developed a novel gasification technology in which coal is gasified in an entrained flow gasifier using a mixture of O_2 and recycled flue gas rich in CO_2. The higher concentration of CO_2 in the gasifier resulted in increased gasification efficiency. Thermal efficiency around 40% is expected for the proposed oxy-fuel integrated gasification combined cycle (IGCC) even after capturing CO_2.

The aim of this work is to investigate the effect of different gasification agents on the performance of waste gasification in an oxygen-powered bubbling fluidized bed. In particular, the influence of CO_2, alone or in combination with steam, is studied in a lab-scale fluidized bed for autothermal gasification, with on-line gas analysis and temperature measurements. This is done by investigating the degradation of feedstock particles to resemble a typical waste composition in a bubbling fluidized bed reactor operated at gasification conditions [9,166,262].

B.2. Methodology

B.2.1. Experimental apparatus

The experimental apparatus consists of a cylindrical vessel with 146 mm inner diameter and 1000 mm height. The reactor is made of Inconel and is operated at atmospheric pressure and temperature around 750°C. Temperature is mostly controlled by oxygen inlet and an external heater, which provides the heat necessary to compensate for the heat losses in the system. The vessel contains Geldart group B quartz sand (particle density 2650 kg/m^3 and average particle size 250 µm) with a fixed bed height of 15 cm. Figure B.3 shows a simple scheme of the whole experimental apparatus.

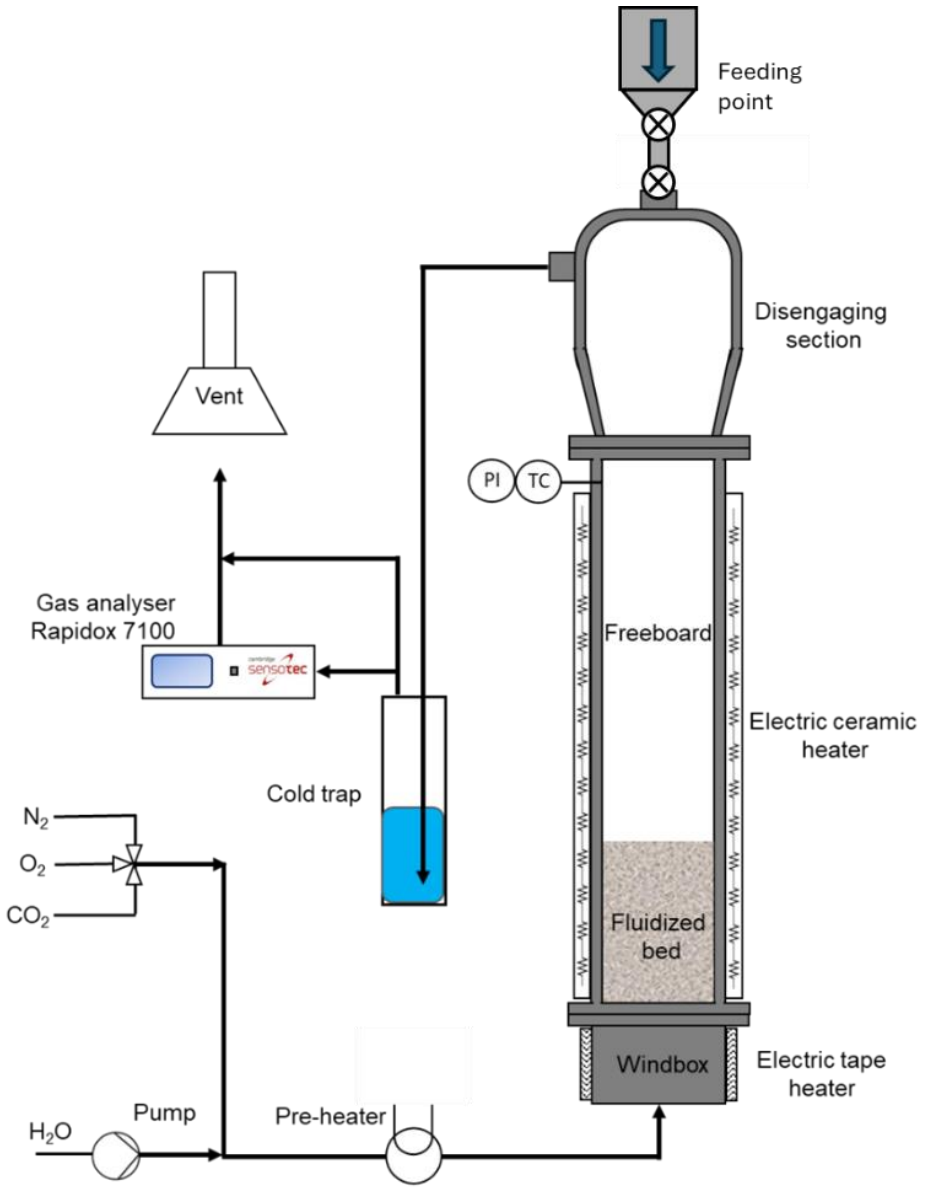

Figure B.3 – Schematic representation of the fluidized bed gasifier experimental set-up

The gasification agent is pre-heated up to 450°C and sent into the reactor through a windbox and stainless-steel distributor plate in order to uniform the flow stream. A disengaging section of 500mm height is placed above the reactor as a freeboard extension and to prevent particles elutriation. In the disengaging section, the finest solid particles in the product gas are captured and collected in a filter. The product gas stream leaves the reactor and flows into a cold trap, in which the gas stream is cooled down to ambient temperature and separated from most of the condensable compounds. A gas slip-stream of 1 L/min is sampled and passed through an on-line gas analyzer (Rapidox 7100 Multigas Analyzer, Cambridge Sensotech). The analyzer measures the volume fractions of CO, CO_2, H_2, and light hydrocarbons (HC).

An on-bed gravimetric feeder has been purposely designed to feed a precise amount of fuel particles to the reactor. The feeder capacity is 10L, feeding up to 10g of fuel pellets. Figure B.4 shows

An image of the two-valve gravimetric feeder designed.

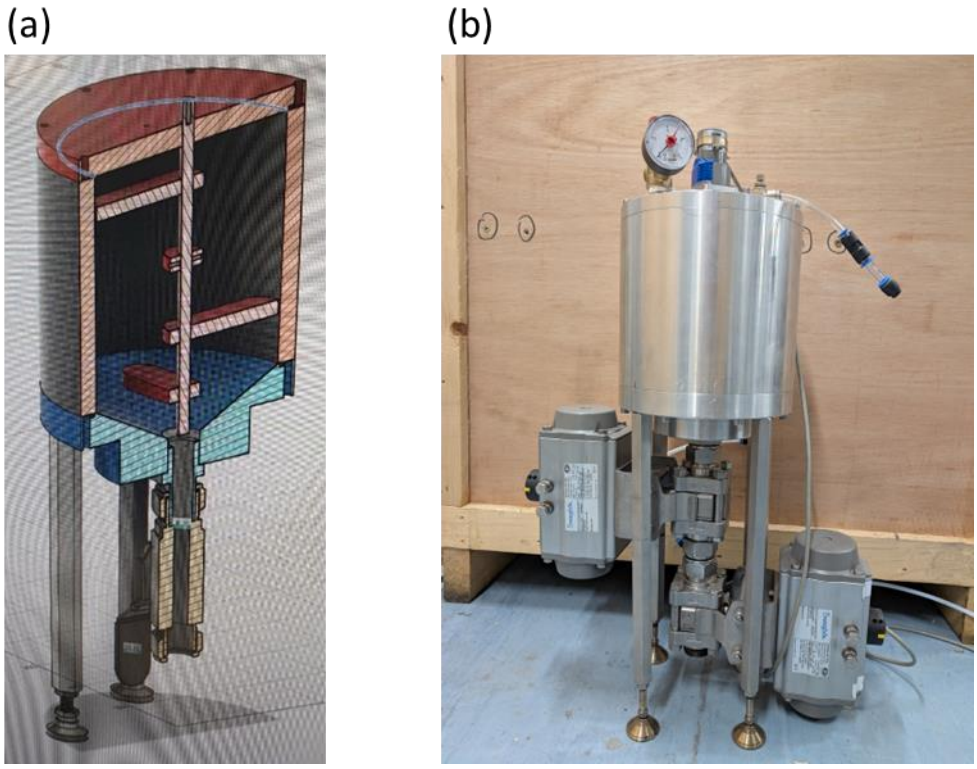

Figure B.4 – Gravimetric feeder (a) rendering of the design, (b) photo of the equipment.

B.2.2. Materials

Experiments were carried out using beech wood and polypropylene particles in a mass ratio of approximately 65:35 to represent the average ratio between biomass- and fossil-based components in waste [262,263]. Particles sizes varied in the range of 3-8 mm (Figure B-0.5).

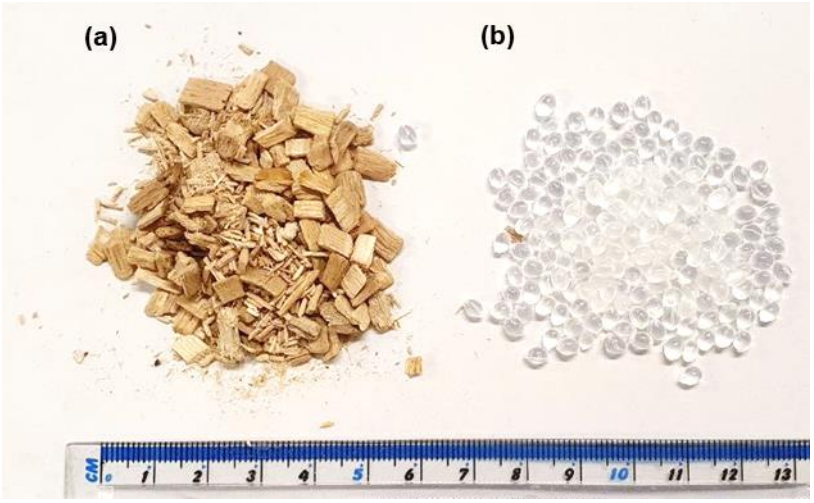

Figure B-0.5 – Samples of feedstock material, crushed beech wood (a), and polypropylene particles (b).

Typical physical and chemical properties of the materials investigated are listed in Table B.1. Feedstock particles are fed into the reactor from a port on the top of the disengaging section, allowing for an overbed feeding with a feeding rate of approximately 150 g/h.

Table B.1 – Typical physical and chemical properties of beech wood and polypropylene [131,164,166,167].

Property	Wood (Biomass)	Polyolefins (Plastic)
Density (kg/m^3)	774	697
Proximate analysis (wt. %)	As received	Dry basis
Fixed Carbon	15.7	0.07
Volatile matter	74.8	99.55
Ash	0.7	0.39
Total moisture	8.8	-
Ultimate analysis (wt. %)	Dry basis	Dry ash-free
Carbon	41.76	85.82
Hydrogen	5.05	13.65
Oxygen	23.39	-
Nitrogen	3.02	0.43
Sulphur	0.13	0.09
Energy content	Dry basis	Dry basis
Heating value (MJ/kg)	15.0	45.25

In the present study, CO_2 and steam were used alone or in combination as reforming and fluidization agents, co-fed with pure oxygen at the base of the reactor. Experimental tests were operated using different molar ratios between steam and CO_2 in the fluidizing gas, while keeping the other parameters constant, including the superficial velocity inside the reactor. The oxygen flow rate is set according to suitable equivalent ratio (ER), typically in the range 0.25-0.35 [52,168,169]. The steam flowrate is fixed to reach an H_2O/Carbon mass ratio of about 1.2, which is representative of the operating conditions of industrial oxy-steam gasification plants [166,167,169]. The CO_2 flowrate is determined on a molar basis according to the steam flowrate to be replaced. This ensures that at all

conditions explored in this work, the fluid dynamic behavior of the bed is maintained constant (in bubbling mode). The experimental tests were carried varying the volume ratio of CO_2 in the CO_2–H_2O mixture between 0% (steam only), 50%, and 100% (CO_2 only). The total volume flowrate is kept constant. A stream of nitrogen is added to guarantee bubbling conditions of the bed, with a superficial gas velocity 3 times higher than minimum fluidization velocity. This was needed to compensate for the low gas throughput of the system, limited by the reduced feeding capacity of the feeder in the lab apparatus. The experimental conditions used for the tests are reported in Table B.2.

Table B.2 – Experimental conditions.

Test	Steam/CO_2 molar ratio	Water flowrate (ml/h)	CO_2 flowrate (NL/min)	O_2 flowrate (NL/min)	N_2 flowrate (NL/min)	Feeding rate (g/h)	Bed temperature (°C)
A	100/0	80.6	0	0.6	25	110-130	720-750
B	50/50	40.3	1	0.6	25	110-130	720-750
C	0/100	0	2	0.6	25	110-130	720-750

B.2.3. Model

The results are used to inform a one-dimensional kinetic model for waste gasification developed in the MATLAB® environment (MathWorks Inc., Version 2020a). Within the model, the whole gasifier is divided into two different sections: the bottom zone, which represents the bubbling fluidized bed, and the top of the reactor, which represents the freeboard section. The freeboard is modelled as a homogeneous plug flow reactor (PFR), while the bed zone is described according to the two-phase theory. It is assumed that there are no variations of temperature and concentrations in the radial direction; therefore, the model is one-dimensional and predicts changes only in the axial direction. The height of the bed has been divided into a series of compartments of suitable finite volume where the set of differential equations of mass and energy balances are solved. The model incorporates the fluid dynamics of a fluidized bed with the reaction network of gasification, for which reaction kinetics have been selected from the literature. A more detailed description of the model can be found elsewhere [169].

B.3. Results and discussion

Figure B.6 shows the steady-state molar gas composition with the different Steam/CO_2 ratios examined. The concentrations are recalculated on dry and N_2-free basis and reported as molar percentage. The values predicted by the model are also reported, with a slight deviation between the calculated and experimental data. The gas composition and dry gas yield obtained when only steam and oxygen are used (Figure B.6(a)) well agree with literature data [257].

The most evident effect of the total switch to CO_2-O_2 gasification was, as expected, a significant increase in CO_2 in the product syngas. Unlike steam, CO_2 is not removed from the condensation at the outlet of the gasifier; therefore, a higher quantity of gas throughput was generated. A decrease in hydrogen and an increase in CO were also observed as a consequence of the reverse water gas shift reaction promoted by the higher amount of CO_2. This is likely due to a modification of the water gas shift equilibrium with the replacement of H_2O with CO_2 in the fluidizing gas. In contrast to pure steam gasification, where an H_2–rich product gas is generated, a CO–rich product gas when CO_2 is used instead. The H_2/CO ratio, which represents an important factor for different downstream synthesis processes, decreased when a higher content of CO_2 was used in the gasification agent mixture, as can be seen in Table B.3.

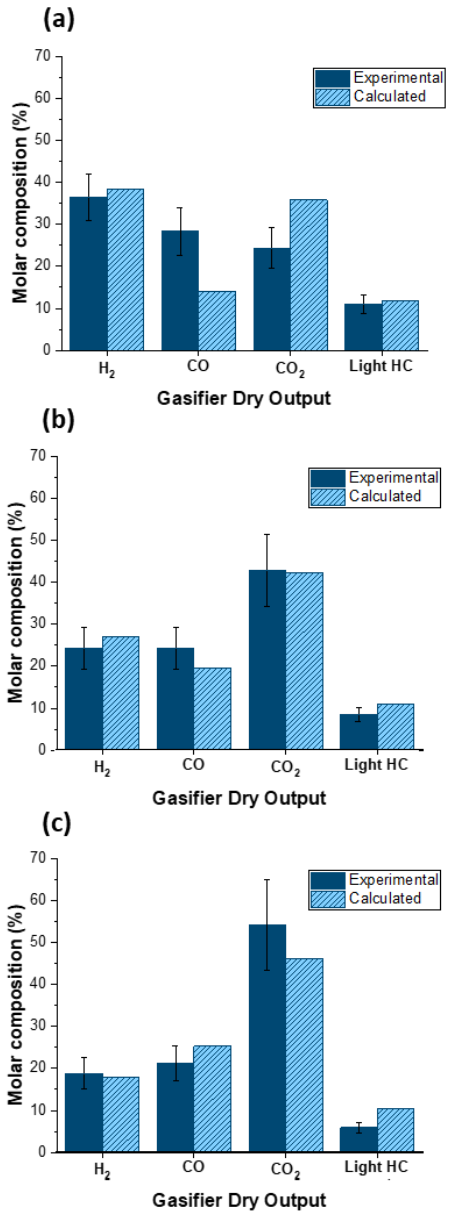

Figure B.6 – Comparison of dry N_2-free outlet gas composition between experimental results and values calculated by the model. (a) Test A (Only steam used as gasification agent), (b) Test B (50% steam and 50%CO_2), (c) Test C (CO_2 only).

The decreasing trend of the H_2/CO ratio can be explained by the decreased formation of H_2 and increased formation of CO. Similarly, the LHV of the syngas, shows a declining trend as a combined result of the lower H_2 content and dilution of the product gas by CO_2. However, the increase in CO_2 ratio resulted in higher carbon conversion efficiency, suggesting the possibility to recover carbon from the inlet CO_2.

Table B.3 – H_2/CO ratio and LHV depending on the Steam/CO_2 ratios analysed.

Test	H_2/CO		LHV (MJ/Nm^3)		Carbon Conversion (%)
	Experimental	Model	Experimental	Model	Model
A	1.3	2.7	11.4	10.1	65
B	1	1.3	8.8	9.4	70
C	0.8	0.7	6.8	8.9	73

Light hydrocarbons values show a decreasing trend in the experimental data, as result of dry reforming reaction ($C_\alpha H_\beta + \alpha CO_2 \rightarrow 2\alpha CO + \beta/2\, H_2$) [257]. Since the dry reforming reactions were not implemented within the reaction network of the model, this would explain the discrepancy between the experimental and calculated values. The decrease in light hydrocarbons concentration can also be attributed to the dilution effect caused by the CO_2. The effect of the gasification agent (i.e. either steam, CO_2, or a mixture) has been further investigated through the model, as shown in Figure B.7. Heavy and light hydrocarbons content in the syngas is mildly affected by the change of fluidizing gas, in particular, the concentration of hydrocarbons decreases due to the reforming reactions promoted by the steam. The model results for tar species are in contrast with what is reported in the literature [257]. This is due to the absence of dry-reforming reactions among the reaction considered, representing a limit of the model. Nonetheless, in both cases (i.e. either using steam or CO_2), the tar content released when treating low-quality feedstocks like waste-derived fuel is too high to allow for the syngas use, requiring additional stages for gas cleaning and tar reforming [68].

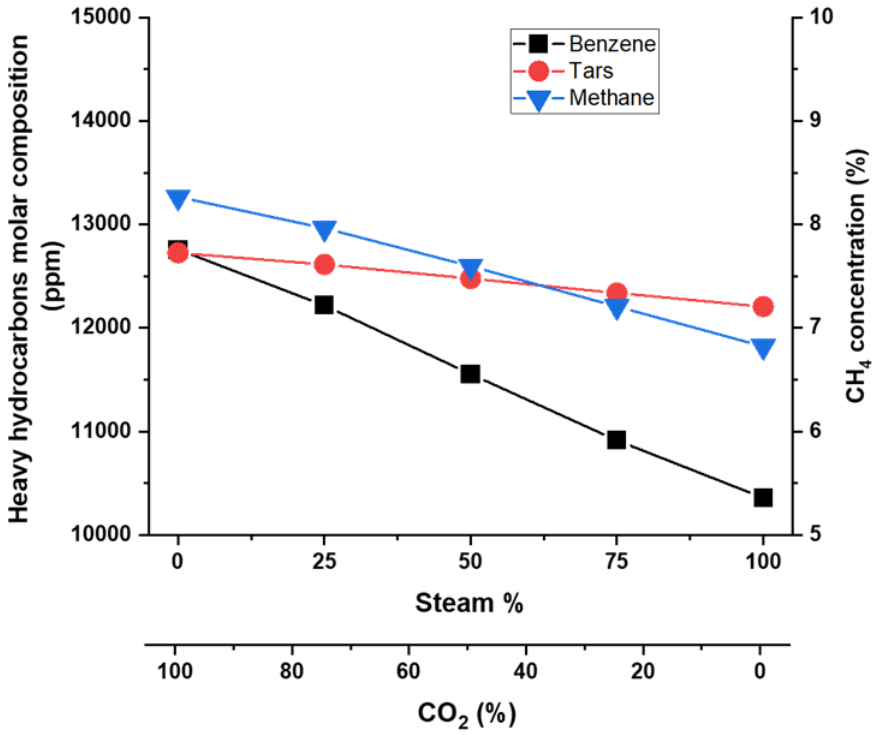

Figure B.7 – Model prediction of dry N_2-free results for the hydrocarbons content in the produced syngas as a function of the gasification agent composition

B.4. Conclusions

The objective of the present work was to investigate the influence of CO_2 as a gasification agent when used in substitution or combination with steam in an autothermal steam-oxygen fluidized bed reactor. A waste-reproducing feedstock was tested in a lab-scale gasifier, and the experimental results are consistent with the kinetic one-dimensional model predictions. The major effect of replacing steam with CO_2 is the increase of CO_2 in the syngas. The use of CO_2 produced an increase of CO with respect to H_2 according to the water gas shift reaction; nonetheless, the overall performance of the process was not found to be significantly affected by the switch of gasifying agents. The undesirable decrease in H_2 content could entail a reduction in the heating value of the syngas once that produced steam is condensed. However, this is counterbalanced by an increase in total gas throughput. Hydrocarbons content in the syngas is seemingly unaffected by the change of fluidizing gas. As CO_2 in autothermal processes is always generated, this would not necessarily entail a complication in the downstream separation processes, but would rather simplify the separation process as a result of a higher CO_2 partial pressure in the syngas. This suggests that the feasible use of CO_2 for co-gasification depends on the final use of the produced syngas and whether a carbon capture facility is already in place.

This study also presents a sustainable optimization strategy for CO_2 utilization and energy reduction when a carbon capture facility is already included within the plant. On one side, it would allow for the recovery of carbon, thus contributing to a reduced global warming impact. On the other side, the investigated process requires a reduced quantity of steam to operate the gasifier. This work confirmed the importance of investigating novel strategies to reduce the energy requirements of bioenergy processes, reducing the carbon intensity, promoting the successful growth and deployment of waste gasification that, at present, appears to be one of the most effective strategies for greenhouse gases emission reduction.

APPENDIX C. Aspen plus flowsheets

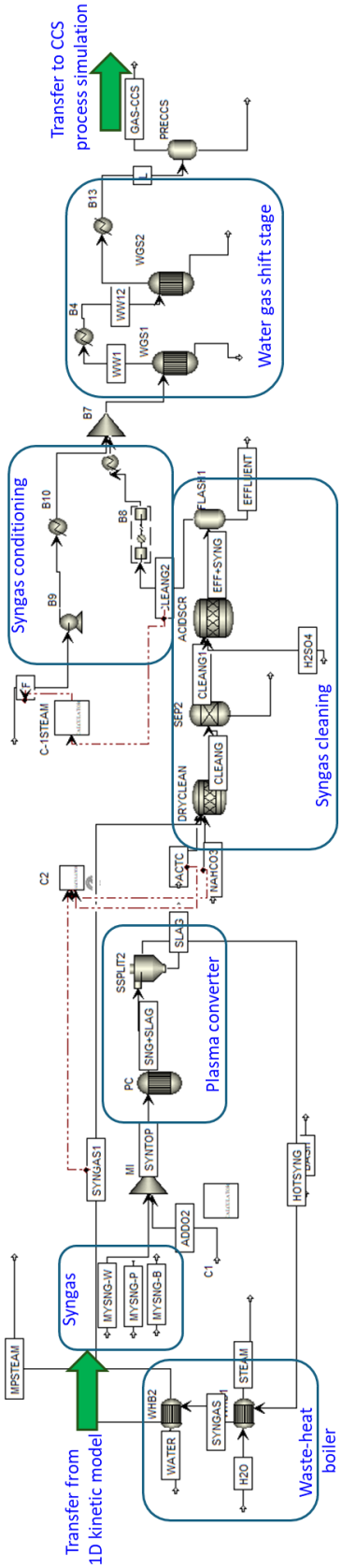

Figure C.8 – Aspen Plus flowsheet of the Gasification and syngas cleaning process simulation.

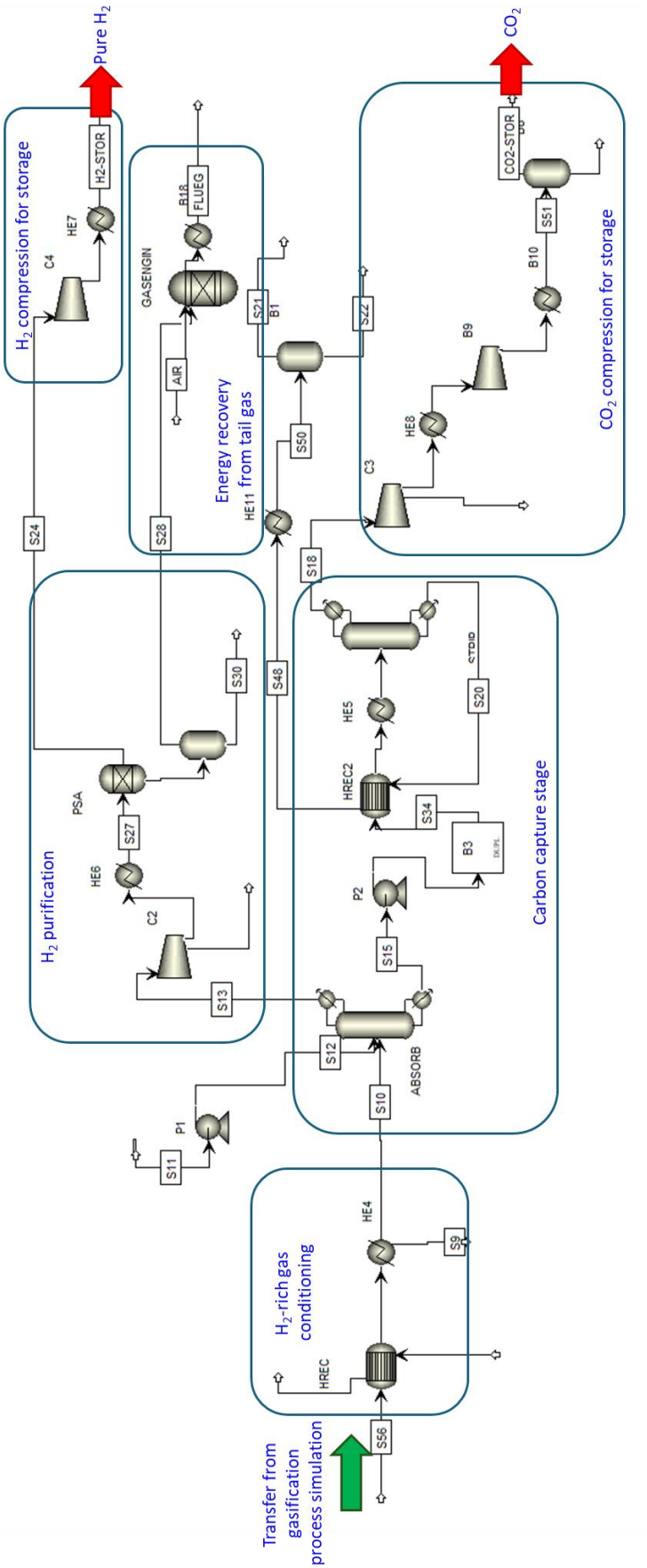

Figure C.9 – Aspen Plus flowsheet of the Carbon capture and storage and H_2 purification process simulation

APPENDIX D. Preliminary investigation of temperature induced tar reforming: a theoretical model

This Appendix includes a preliminary assessment of Plasma technology for Tar reforming. This is the principle of the two-stage gasification process of low-falue waste materials developed by industrial partner ABSL.

The work presented in this appendix has been produced as part of the project "Development of Biomass Gasification Tar Reformation and Ash Removal", awarded by BEIS for the "Hydrogen BECCS Innovation Programme".

D.1. Introduction

D.1.1. The ABSL gasification process

Advanced Biofuel solutions (ABSL) developed a two-stage process which combines fluid bed gasification with plasma technology. The fact that the final stage of the thermal process uses plasma as an energy source instead of the energy content of the syngas makes the system more suitable for low-energy fuels, such as household and industrial wastes that often cannot sustain their own gasification without additional fuel. ABSL operates a demo plant in Swindon (UK), which can treat up to 1,000 kg/h of waste to generate clean syngas that is further converted into bioSNG and biohydrogen.

The gasifier is a bubbling fluidized bed operated in a temperature range between 650° and 800 °C, with the actual operating conditions depending on fuel characteristics and desired reaction profiles. The gasifier contains a bed of sand particles and is fluidized with a supply of steam and oxygen whose flow is controlled to maintain the bed temperature and the required degree of fluidization. The gasifier's main function is to decompose the waste and to separate the combustibles and small ash particles from larger inert and metallic particles. The organic components of the feedstock (i.e., carbon and hydrogen-based material, including food waste, yard waste, paper, plastic, rubber, textiles, etc.)

are converted into a fuel gas, which flows upward in the reactor. The fuel gas is in a ‘‘raw” state, containing combustion gases (H_2O, CO_2), tar, fine char, fly ash, and hydrocarbons, in addition to carbon monoxide (CO) and hydrogen (H_2) typically found in a gasification synthesis gas. The percentage of these components in the fuel gas depends on the broader range of feedstock types and C/O ratio used. At the same time, dense inorganic materials (i.e., glass, metals, bones, and stones) drop by gravity to the bottom of the reactor. These materials are removed from the bottom of the reactor, along with some of the sand medium that is used as the fluidized bed of the gasifier.

Fuel gas and carbonaceous particles, both produced in the gasifier, are upgraded together in the second stage of the process: a single carbon electrode plasma furnace at temperatures between 1100–1200 °C. Unlike some other gasification technologies, there is no need for intermediate fuel gas clean-up between the gasifier and the ash-melting plasma converter. An addition of secondary oxygen feed assists in the breakdown of long-chain hydrocarbons and ensures full conversion of carbonaceous residuals to a syngas virtually free of condensable liquids and tars. The gas flow pattern is intended to produce a slow cyclonic action to promote the separation of particulates from the syngas and also to maximize the residence time in the converter. The fine ash particles are collected on the walls, where they are vitrified and proceed slowly down through the furnace. This molten (i.e., vitrified) slag flows slowly down the furnace walls and is continuously discharged at the bottom of the furnace. As the slag is discharged, it is immediately cooled in a water bath. This quenching process results in the slag being pulverized into a glassy, granulate material, which is marketed as a construction material.

The plasma power is controlled, along with the secondary oxygen inlet, to provide a uniform syngas temperature and destruction of the residual tars and chars contained within the crude syngas. The refined syngas is then cooled and cleaned from other contaminants (sulphur chlorine, etc.) before it can be used for hydrogen production and separation.

D.1.2. Problem statement

Thermal plasma technologies can be used in combination with fluidized bed gasification thanks to their capability of converting the tars and breaking down other contaminants (thiophenes, etc.) to facilitate removal by well-established processes. Differently from other purely thermal technologies, the chemical reactivity and quenching rate of plasmas is far greater. This is due to temperatures which exceed those under combustion and the formation of chemically active species (CAS) – free radicals, ions, and excited molecules. As a result, any organic molecules, exposed to the intensive radiation, break down into simpler elements (e.g., H_2, CO, N_2, H_2S, etc.), with solid inorganic components (ashes, metals, silicates) fusing to form a molten slag, which vitrifies on cooling.

In order to promote tar cracking and improve the flow-ability of the ash melt, most thermal plasma reforming processes are operated at elevated temperatures, in excess of 1200 °C. In a conventional electric arc, the energy of all species (electrons, ions, etc.) is approximately equal and the gas is locally heated to very high temperatures (>10,000 °C). However, at a certain distance from the discharge, the temperature drops significantly and the addition of oxygen is required to maintain the gas phase at elevated temperatures. The combustion reactions between oxygen and syngas and the resulting very high gas temperatures lead to waste of energy in gas heating and can lead to several inefficiencies and operational problems. Furthermore, the high capital and operating costs of conventional directly-transferred plasmas, as well as the cost of the maintenance of the refractory lining of the reformer and the rapid consumption of electrodes would suggest important benefits of operating the system at lower temperatures.

Most research in the field of plasma processing has focused on the decomposition of tar analogue compounds in a carrier gas. However, product gas from gasifiers contains various different gases (CO_2, H_2, N_2, CO and CH_4), all of which may influence the performance of the plasma system. Therefore, it is very important to investigate the effect of key individual species (especially those containing oxygen, such as steam and CO_2, which will contribute to the formation of CAS in absence of molecular oxygen) to study the contribution towards the product distribution and tar decomposition.

The use of plasma as a potential reforming and catalytic agent has been investigated, exploiting our previous work on tars reforming in direct-transferred electric torches. In particular, the main objective will be that of discerning the role of temperature (controlled by secondary oxygen injection) from that of plasma in generating key CAS species, which are crucial for tar reforming. This has been done by developing a kinetic model to identify the role of oxygen, temperature, and residence time in tar reforming. N-dodecane was selected as the tar analogue compound, due to its simple structure, relatively high thermal stability and low boiling point. Its simple structure aids understanding of the mechanism involved in the cracking of tar under thermal plasma conditions at relatively low temperatures and ambient pressure.

D.2. Model description

The tar reforming mechanism used in this work is based on the detailed kinetic model developed by Zhong et al. [264] which was assessed against experimental data issued from studies that have been conducted in flames, shock tubes, perfectly stirred and plug flow reactors all under a wide range of temperatures, pressures, and stoichiometries [264–267]. Predictive capabilities of the model were found to be at least fair and often good to excellent for the consumption of the reactants (primary

tars, steam, and oxygen, mostly), the formation of the main reforming products, and the formation and depletion of major tars intermediates including radicals.

All model calculations were performed with CHEMKIN code, a combustion kinetics solver embedded in the ANSYS software package [268,269]. A zero-dimensional open plasma-assisted combustion model of n-dodecane (selected as tar's representative component) is developed to calculate the composition of species and temperature at the outlet of a perfectly stirred reactor. The code computes the species profiles for continuous fully mixed laminar flame, using the cold mass flow rate through the converter, feed gas composition, pressure, and an estimated solution profile as input. The program can also compute the temperature profile. However, heat losses to the converter and the external environment are unknown; therefore, adiabatic conditions are assumed as the first approximation for the operation of the plasma converter.

The combustion mechanism is reduced from the model proposed by Cai et al. [270] and consists of 198 species, including permanent gases (i.e. H_2, CO, CO_2, N_2), steam, a wide range of hydrocarbons (from C1 to C12, in alkanes, alkenes, oxygenated and cyclic compounds), as well as the electronically excited species. The reaction mechanism entails 1128 reactions, with partial and total combustion reactions, reforming reactions, water gas shift, and all other relevant reactions [264]. N-dodecane is assumed to be the species representing tars, therefore the overall mechanism is triggered by its consumption. Figure D.10 shows the reaction pathway of n-dodecane (primary tars) that is dissociated to produce lighter hydrocarbons directly or fuel radicals, as well as H_2 by H-abstraction reaction. The fuel radicals are consumed to produce H_2 and C1–C3 hydrocarbons. The n-dodecane consumption by radicals OH and O becomes the dominant pathway for fuel consumption. The O radical produced promotes the H-abstraction reaction of n-dodecane to form $C_{12}H_{25}$ and OH, which further accelerates the fuel consumption, triggering the cycle of reactions involving free radicals until complete consumption.

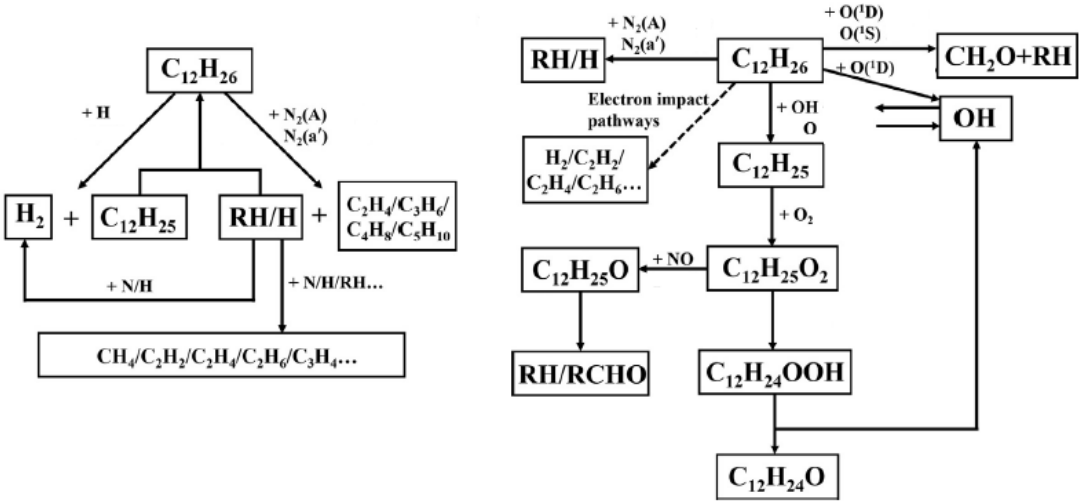

Figure D.10 – Path flux of fuel in the partial-combustion simulations. (R is the fuel radical). Adapted from [264].

In order to partially validate the kinetic model and the choice of the reaction pathways, a compatibility test with thermodynamic constraints (according to Gibbs free energy minimization) was also performed. This was performed on Aspen Plus considering the same species of the kinetic model (i.e. H_2, CO, CO_2, N_2, H_2O, C1-12 hydrocarbons) excluding the radicals. The simulations are run adiabatically and predict the outlet composition and temperature at thermodynamic equilibrium.

D.2.1. Inlet conditions

Syngas flowrate and composition at the inlet of the modelled plasma converter are reported in Table D.4. Since N-dodecane has been assumed as the tar-representing species, the molar fraction was calculated to have a tar content of 10 g/Nm^3, which is compatible with fluidized bed gasifier products reported in the literature. Oxygen is added to the tar-laden syngas prior to entering the plasma reactor to increase the operating temperature to above 1100 °C. The high temperature is required in the Swindon plant to crack tar species and keep the slag melt in liquid form. In order to saturate the degrees of freedom for the kinetic model, either the residence time or the volume of the reactor was required as model input. The reactor is considered to be a shallow cylindrical vessel, for which a simplified geometry is reported in Figure D.11. A scaled down version of the Swindon plasma converter was designed and manufactured at UCL. The lab-scale reactor's volume is approximately 1.5 L, which corresponds to a residence time of about 1.7s at the inlet conditions.

Table D.4 – Inlet syngas conditions before plasma conversion.

Species	Mole Flows (kmol/h)	Mole Composition (%)
CO_2	0.0050	13.78
H_2	0.0128	35.16
CO	0.0095	26.09
H_2O	0.0075	20.63
AR	0	0
N_2	0.0007	1.98
CH_4	0.00018	0.50
O_2	0.0006	1.73
$C_{12}H_{26}$	4.2 E-05	0.115
Total	0.0364	100
Temperature (°C)	800	
Pressure (bar)	1	

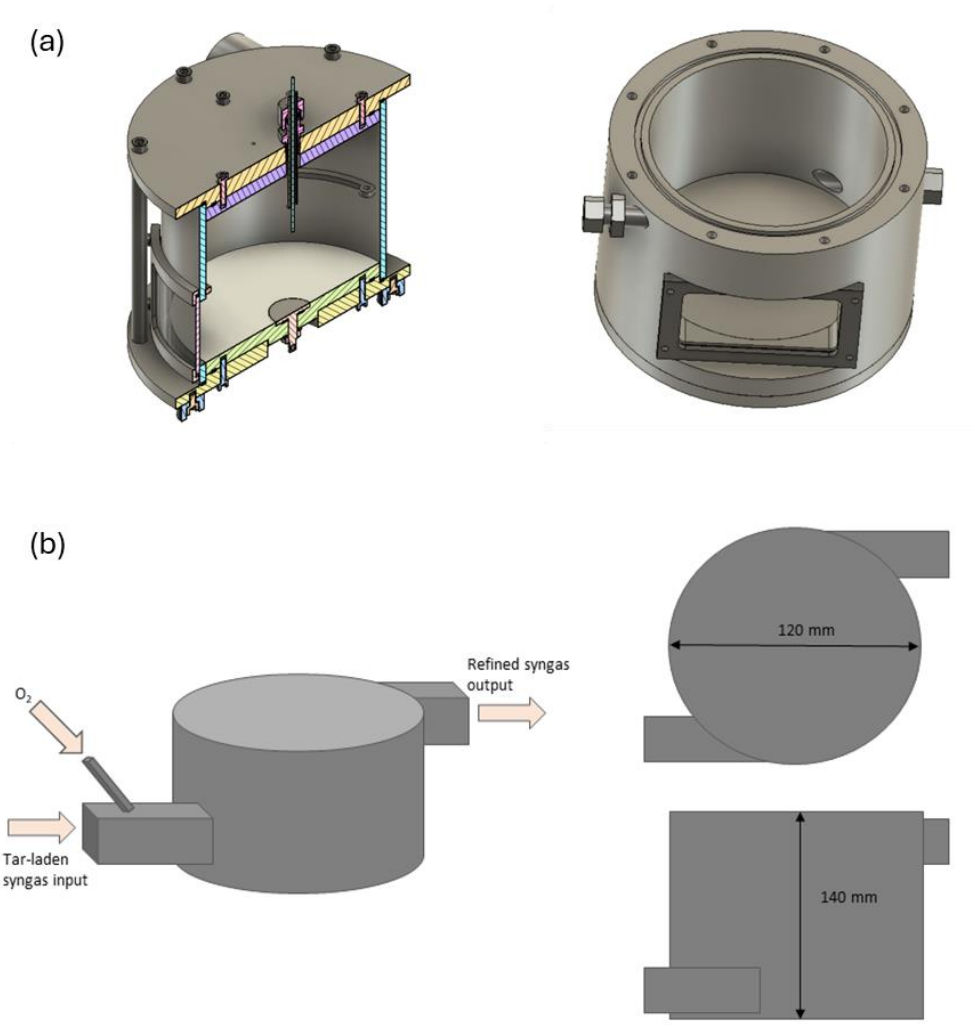

Figure D.11 – UCL lab-scale plasma reactor design (a) and geometry (b), replicating ABSL's plasma converter.

D.3. Model results and discussion

Both Kinetic and equilibrium models were first run at the same inlet conditions, considering a residence time of 1.7 s, which is similar to that used in the Swindon plant. The results of the simulations are reported in Figure D.12 and Figure D.13,showing the outlet gas composition for the permanent gases (Figure D.12) and the hydrocarbon species (Figure D.13) grouped according to the number of Carbon atoms in the molecule. As regards the permanent gases, the results predicted by both models are close to each other, with a deviation of about 3% for most species. This suggests that a simple equilibrium model can be suitable to predict the syngas composition at elevated temperatures and residence times. However, the equilibrium model overestimates the consumption of total hydrocarbon species, with a predicted composition of around 0.002% vol., which is well below the one predicted by the kinetic model, 1.19% vol. Specifically, according to the kinetic model results, the amount of tars in the refined outlet syngas is 1.2 mg/Nm^3, with the content of light hydrocarbons (C2-

C5) being 3.4 g/Nm^3. The Gibbs equilibrium estimation, instead, shows the amount of tars and light hydrocarbons being 0 and 1.4×10-^{9} g/Nm^3 repectively. This has an impact also on the other species (e.g. overestimation of H_2) and suggests that an equilibrium model is not reliable for predicting the evolution of hydrocarbon species in the reactor. Therefore, a kinetic model is deemed essential to assess tar reformation.

The different predicting capabilities of the two model are more evident in Figure D.13 that show the composition of hydrocarbons at the inlet and outlet of the reactor for both models. According to the equilibrium model, primary tars are completely cracked into light hydrocarbons such as CH_4, C_2H_4, and C_2H_6 only. The kinetic model, however, shows how tars are only partially converted into light hydrocarbons (C1-C5), while a fraction of heavier compounds (>C6) is still present in the syngas. Despite being very low, these heavier compounds can still pose a significant risk to the process. Discrepancies between the values predicted by the kinetic model and experimental evidence from the Swindon plant is attributed to the difference in temperature between plant operation (~1100-1200 °C) and the one predicted by the model (991 °C), the latter being generated by oxygen addition alone. In order to verify this, a simulation with the same syngas inlet composition, but allowing to reach an outlet temperature of 1120°C was performed. Notably, the results of this simulation predict a tar content in the outlet syngas of 0.006 mg/Nm^3 and 0.23 g/Nm^3 for the light hydrocarbons, which in in line with experimental evidence [17,210].

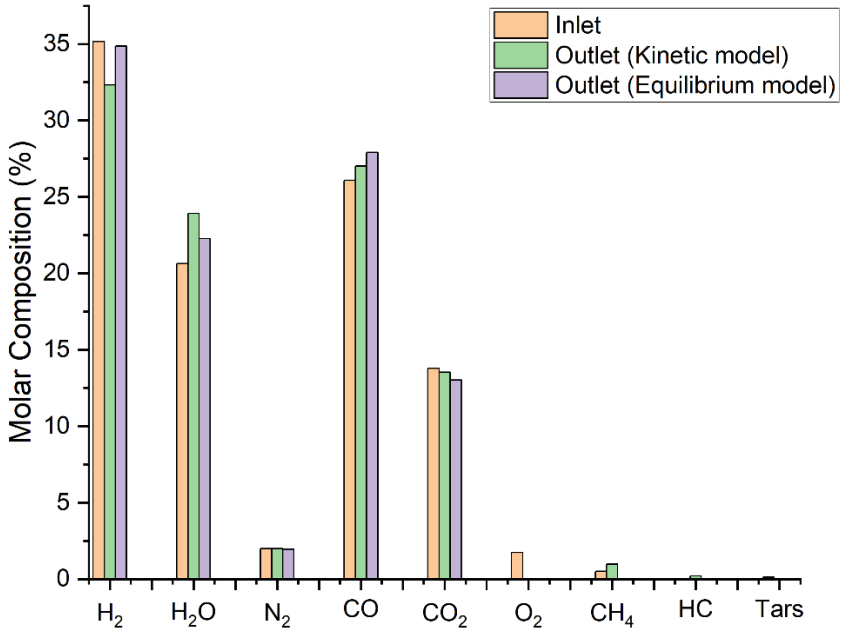

Figure D.12 – Molar composition of the gas at the inlet (orange bars) and outlet of the reactor (green and violet). HC represents light hydrocarbons (C2-C5).

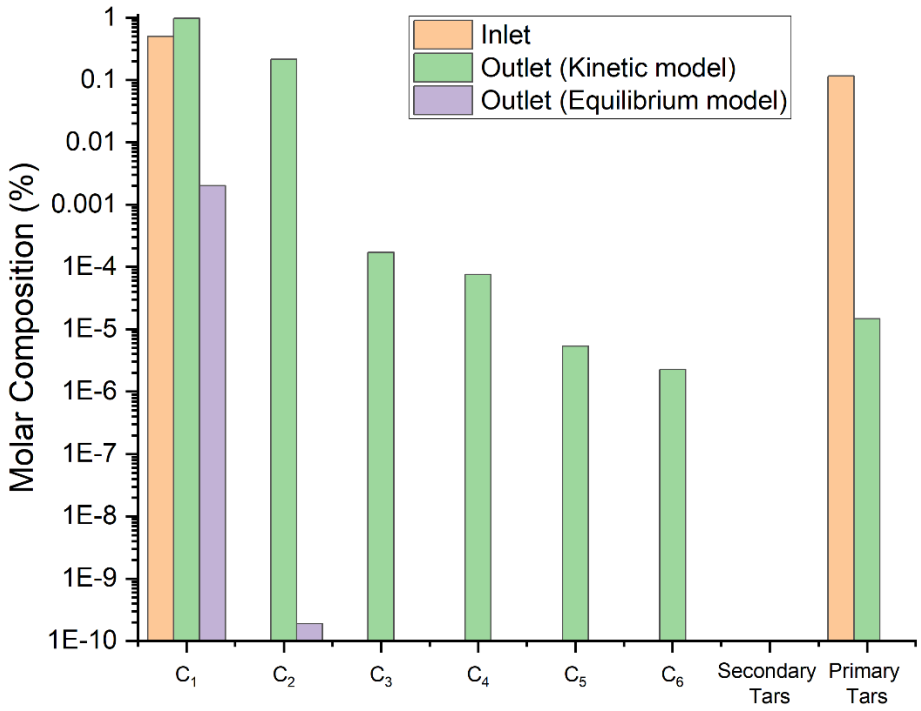

Figure D.13 – Molar composition of the hydrocarbons at the inlet (orange) and oultet of the reactor. Primary tars represent C12, secondary tars represent C7+

D.3.1 Effect of temperature/oxygen injection

The effect of secondary oxygen injected at the inlet of the plasma reactor has been investigated using both kinetic and equilibrium models. The first obvious consequence of the increase in O_2 is the increase in the temperature inside the reactor (Figure D.16), and therefore, that of the outlet gas. This is the result of the higher heat released by the combustion of hydrocarbons and other syngas species. However, the expected increase in combustion reaction is not followed by a proportional increase in the fully-oxidised species (CO_2 and H_2O). Figure D.14 shows, instead, a decrease in CO_2 with the increase in O2. This can be the result of the mildly exothermic water gas shift: on one side the reaction rate is enhanced, but hydrogen production becomes less favorable thermodynamically and the reaction is shifted towards the consumption of H_2 and CO_2 in favour of CO and H_2O. This is confirmed by the trend in Figure D.16 for all the species. When comparing the results predicted by the kinetic and equilibrium model, it is evident how the latter overestimates the performance of the process with generally higher H_2 concentration. Despite the discrepancies, the trends for each gas species appear to converge to similar values. This can be the result of the higher temperature that enhances the reaction rates, suggesting that the equilibrium model can work reliably only when operating the reactor at sufficiently high temperatures (>1100 °C).

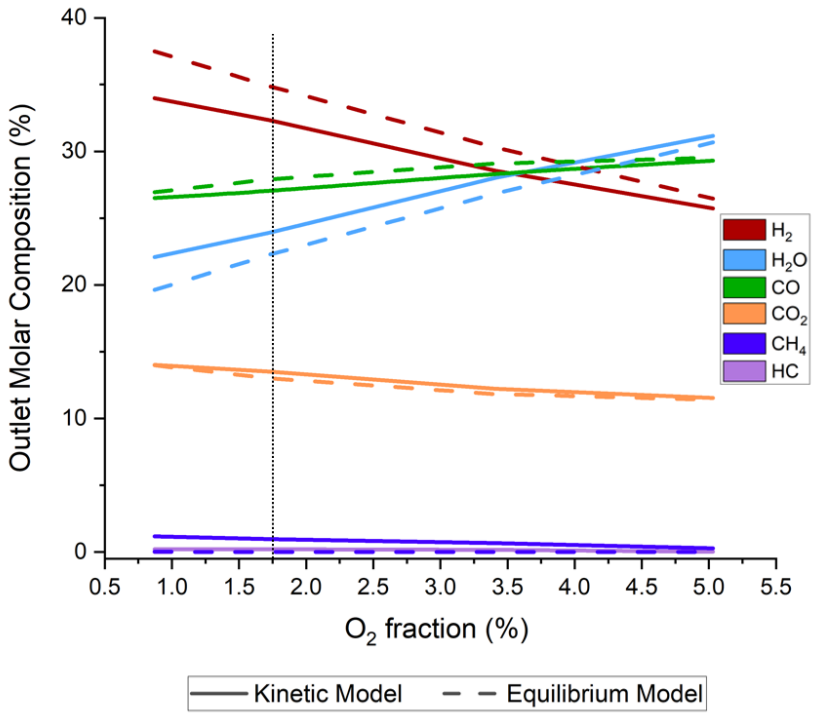

Figure D.14 – Outlet molar composition of permanent gases as a function of the fraction of the O_2 added to the inlet syngas. HC represents light hydrocarbons (C2-C5). The vertical dotted line represents the inlet conditions, O_2 1.7% τ 1.7s.

Figure D.15 shows how the hydrocarbon species are affected by the increase in O_2 and, therefore, the increase in combustion reactions. As expected, the concentration of all hydrocarbon species (including tars) decrease, with the heavier fractions approaching complete conversion with 5% O_2 addition. Similarly to Figure D.13, the equilibrium model shows lack of accuracy for the heavy fractions (primary and secondary tars), for which the concentration is zero for all O_2%.

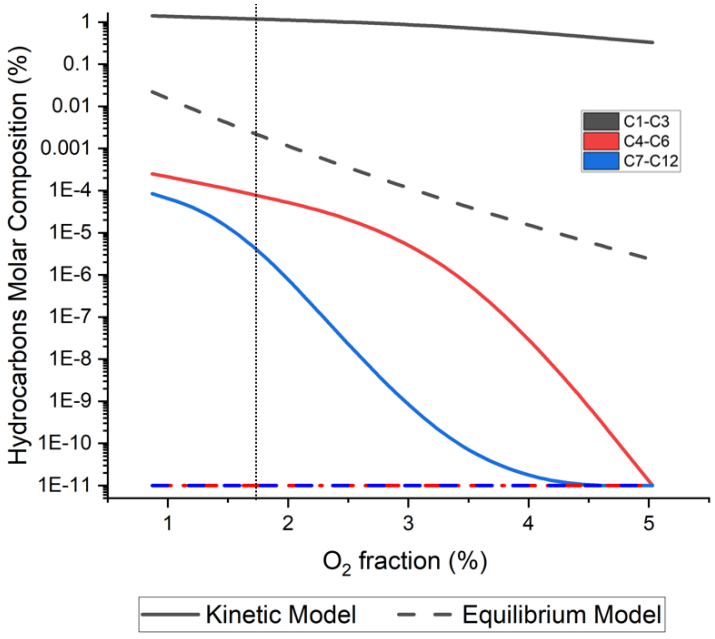

Figure D.15 – Molar composition of the hydrocarbons at the outlet of the reactor as a function of the O_2 added to the inlet syngas. The vertical dotted line represents the inlet conditions, O_2 1.7% τ 1.7s.

Despite showing an almost complete abatement of the heavy fractions, increasing the amount of O_2 injected appears to be unfeasible due to temperatures higher than 1300 °C. This temperature increase would be at least 10-20% higher when operating the plasma. This would pose problems for material resistance as well as increase the energy losses, therefore lowering the performance of the process.

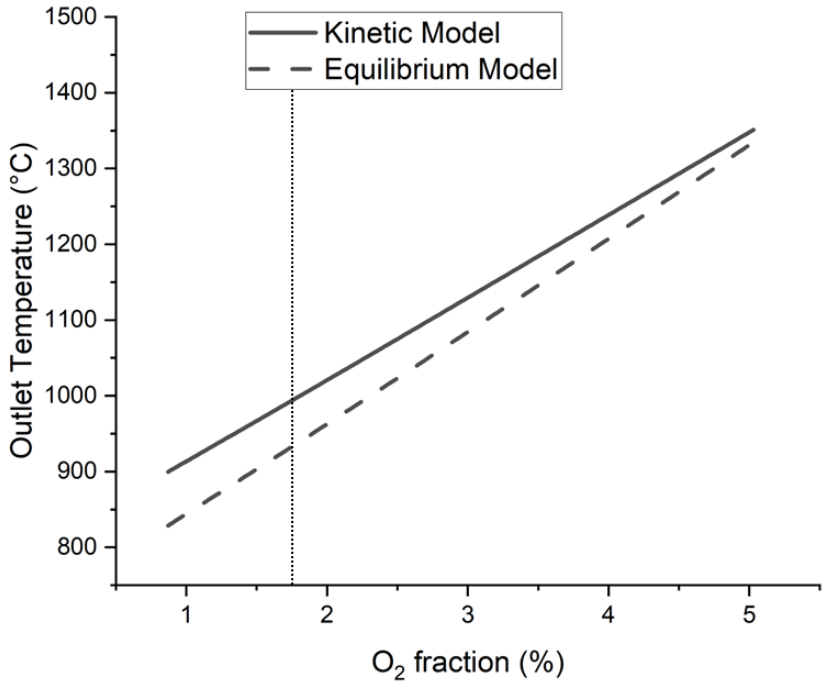

Figure D.16 – Temperature of the outlet gas stream as a function of the O_2 added to the inlet syngas. The vertical dotted line represents the inlet conditions, O_2 1.7% τ 1.7s.

D.3.2. Effect of residence time

The effect of changing the residence time of the gas inside the converter has been investigated further with the kinetic model, varying this between 0.5 and 6 seconds. Interestingly, the residence time (controlled by changing in gas flowrate or volume of the reactor) appears not to be a very impactful parameter of the process at the examined conditions. Concentration profiles of the permanent gases are reported in Figure D.17. The composition of the outlet gas appears to be substantially unaffected by the increase in residence time. This can be explained by the high combustion reaction rates that occur almost instantaneously, while the reforming reactions that are driven by equilibrium require longer times to settle. Figure D.17 suggests that the same performance can be achieved with lower residence time and, therefore, a smaller reactor (or higher syngas throughput) could be possible if considering the permanent species only. Conversely, Figure D.18 and Figure D.19 highlight how the optimal residence time for tars conversion appears to be around 2s.

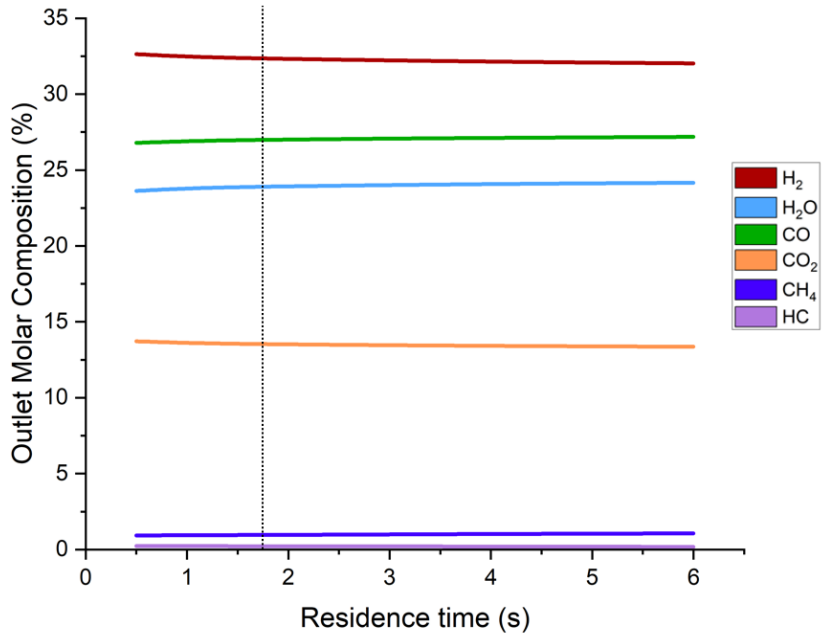

Figure D.17 – Outlet molar composition of the permanent gases as a function of the residence time. The vertical dotted line represents the inlet conditions, O_2 1.7% τ 1.7s.

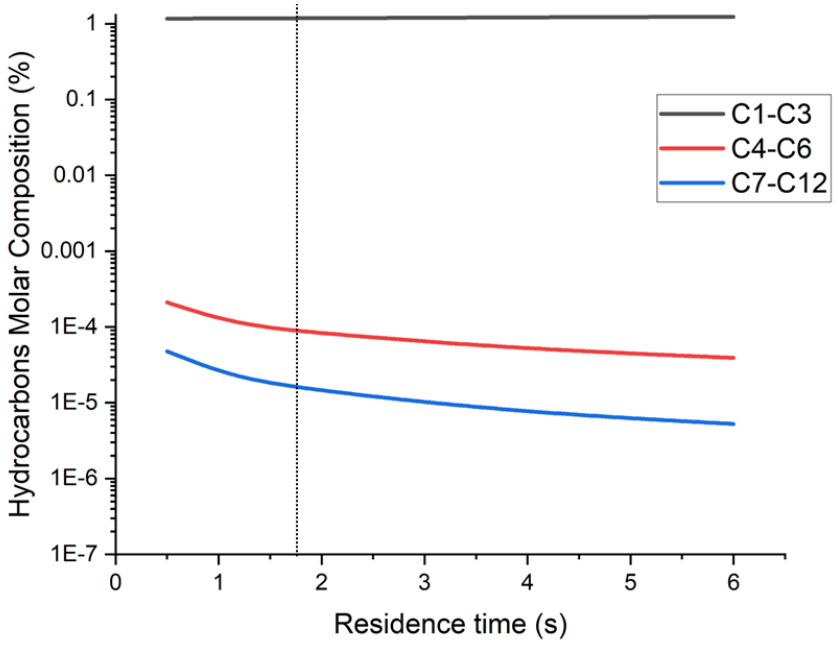

Figure D.18 – Molar composition of the hydrocarbons of the hydrocarbons at the outlet of the reactor as a function of the residence time. The vertical dotted line represents the inlet conditions, O_2 1.7% τ 1.7s.

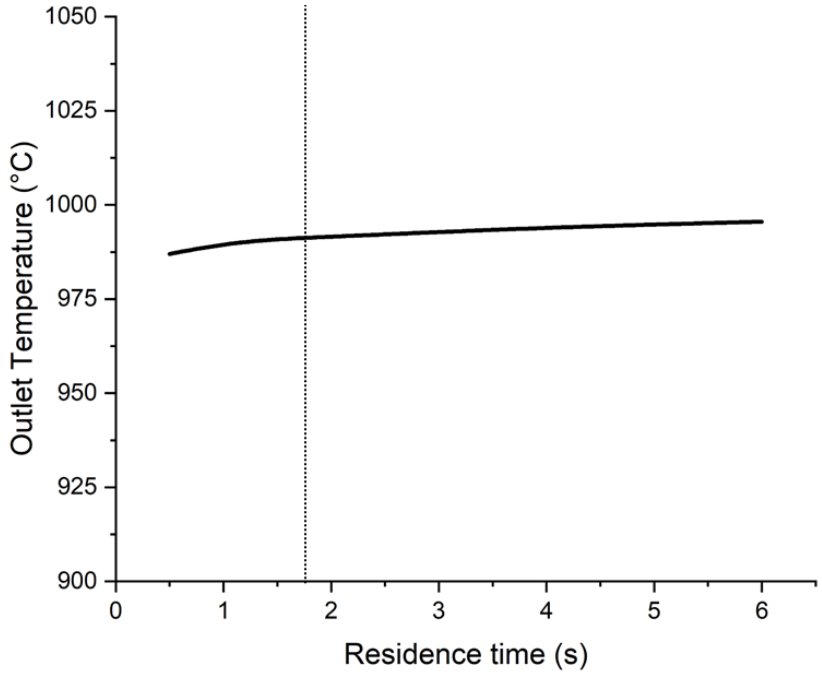

Figure D.19 – Temperature of the outlet gas stream as a function of the residence time. The vertical dotted line represents the inlet conditions, O_2 1.7% τ 1.7s.

D.4. Conclusions

A kinetic model for tar conversion has been developed to identify the role of oxygen, temperature, and residence time in tar reforming (with no plasma-induced effect). In addition, a second model based on equilibrium has been developed to substantiate the kinetic model predictions against thermodynamic constraints.

Key findings resulting from the models are as follow:

- The additional injection of O_2 to unrefined syngas leads to an increase in temperature that promotes the formation of chemically charged species and the reforming of tar species. Hydrocarbons content appear to be substantially affected by O_2 and temperature, and a tar-free syngas can be obtained with 5% vol. O_2 content in the inlet syngas.
- Increasing O_2, however, results in high operating temperature (>1300C), which poses serious operating issues for material resistance and energy losses, jeopardizing the efficiency of the process. Furthermore, increasing O_2 lowers H_2 yield.
- The high tar reforming efficiency resulting from the increase in operating temperature is attributed to the higher content of radicals and chemically charged species promoted by oxygen flames. This suggests that the same conversion efficiency can be obtained when

the radicals and chemically active species are produced by an external source (e.g. plasma), but with a higher energy efficiency, i.e. with less heat being generated.

- Residence time appears not to affect considerably the process at the examined conditions, suggesting that shorter residence times can be possibly adopted.

APPENDIX E. Retrofitting waste-to-energy with carbon capture and storage: a techno-economic and environmental assessment

Waste incineration facilities are the prevailing technology for disposing of non-recyclable or unsorted fractions of municipal solid waste: waste is combusted and, in the case of Waste-to-Energy (WtE) plants, the resulting energy can be used to generate electricity and excess heat recovered. This work aims at understanding the technical, environmental, and economic values of retrofitting an existing WtE facility equipped with a carbon capture and storage (CCS) facility. The study is based on advanced process simulation using Aspen Plus and Life Cycle Assessment (LCA) to understand integration challenges and the impact of several variables (e.g. waste composition, carbon capture rate) on the techno-environmental performance of the plant. The results show that for the WtE-CCS system to operate self-sufficiently, substantial energy penalties are required with the reduction of the heat and electricity export to power the CCS. The significant additional economic penalty makes CCS unfavourable, considering the current lack of negative emissions market mechanisms and incentives in the UK. The LCA results show that CCS contributes to reducing the overall climate change impact of WtE from 68 to -816 $kgCO_2$ eq per ton of MSW treated. The biogenic nature of the waste feedstock plays a key role in determining the environmental performance of WtE plants with and without carbon capture.

This appendix has been published in the conference paper:

Sebastiani, A., Paulillo, A., Lettieri, P., & Materazzi, M. (2023). Retrofitting waste-to-energy with Carbon Capture and Storage in the UK: a techno-economic and environmental assessment. *European Biomass Conference and Exhibition Proceedings*, 628–634.

E.1. Introduction

The growth of the global population, changes in people's lifestyles, and industrial development are all contributing factors to a significant increase in consumption levels and, consequently, the production of solid waste. This trend is expected to continue in the future. This increase is primarily

driven by low-income countries, with waste management relying mostly on landfills, and only a small portion is incinerated using environmentally friendly technologies [271].

While recycling is the preferred environmental solution for waste management, incineration, especially through modern efficient Waste-to-Energy (WtE) plants, is expected to maintain an important role, and potentially increase over time. This trend would result in the increase of carbon emissions from the WtE sector from 2020 to 2050 [272], which conflicts with net-zero targets if carbon emissions are not abated, such as by deploying carbon capture and storage (CCS) or utilization technologies [273].

Capturing and permanently storing CO_2 from WtE plants can have substantial climate benefits, which are mainly associated with the biogenic nature of the municipal solid waste (MSW) because it leads to a net reduction in CO_2 content in the atmosphere. Consequently, WtE equipped with CCS has the potential to contribute with negative emissions as part of the bioenergy with carbon capture and storage (BECCS) technologies. These technologies, together with direct air capture (DAC), are expected to play a crucial role in addressing climate change in the future [274,275].

Extensive research in the literature has thoroughly examined the techno-economic and environmental impact of various waste management technologies, including incinerators with and without energy recovery [276–280]. Nevertheless, there have been limited research efforts focusing on the implementation of CCS in WtE plants, especially when it comes to retrofitting existing facilities [281–283]. Studies using Life Cycle Assessment (LCA) have shown that advanced WtE plants that prioritize the generation of electricity and/or heat offer significant environmental advantages. These plants replace the electricity and heat generated by traditional fossil carbon-intensive sources.

In this study, a holistic approach has been adopted to address and study the techno-economic and environmental implications of integrating CCS capabilities into a WtE plant, to identify challenges and opportunities for decarbonizing the energy sector in the UK scenario. To achieve this, a comprehensive process simulation of the WtE facility was developed using Aspen Plus considering both scenarios with and without carbon capture. A cradle-to-gate LCA was then performed to quantify and compare the environmental performance of the system. These two tools together can also be used to assess the economic and social costs and benefits of large-scale implementation. Different scenarios of carbon capture rates and feedstock were considered to investigate the effect of these key parameters on the technical and environmental sustainability of the WtE-CCS plant.

E.2. Methods

E.2.1. Process description

Conventional WtE plants rely on burning the combustible fraction of waste feedstocks like MSW or wood waste (WW). This process generates a high-temperature flue gas that is used to produce electricity through a steam cycle and heat. Prior to being released into the atmosphere, the flue gas is treated to eliminate contaminants and harmful species. Figure E.20 shows a schematic block flow diagram of the WtE plant coupled with CCS capability.

The incineration process also produces a solid residue in the form of bottom ashes, which is mainly associated with the incombustible fraction of waste. Typically, these residues undergo a processing stage to recover both ferrous and non-ferrous metals, whilst the remaining portion can be repurposed, such as being utilized as a substitute for gravel in pavement construction [284].

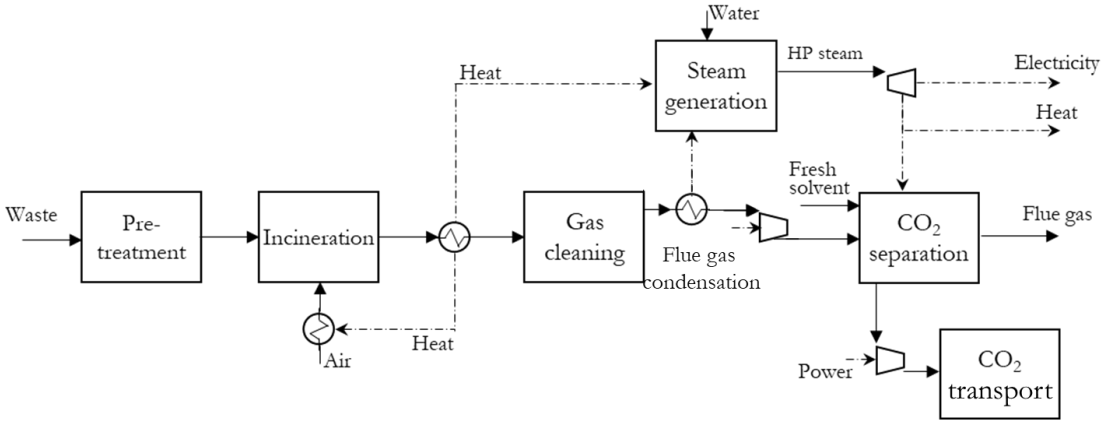

Figure E.20 – Schematic of the steps modelled to simulate the operation of Waste-to-Energy retrofitted with CCS.

After cleaning, the flue gas contains 11% CO_2 and is typically released into the atmosphere, thereby contributing to climate change. One possible solution to mitigate the impact is to separate and capture CO_2 from the flue gas prior to being vented.

Amine-based technologies are the most commonly adopted for post-combustion capture applications [285–287]; in this work, monoethanolamine (MEA) in an aqueous solution of 30% wt was used as an absorption solvent in the carbon capture unit.

When retrofitting a WtE with CCS, a flue gas condensation unit is usually required to better integrate the two plants. This unit takes the high-temperature flue gas from WtE and reduces its moisture content (from ~14% to about 4%) via condensation with heat recovery.

In this work, a commercial scale WtE plant was modelled to treat approximately 28 ton/h of MSW, corresponding to 75MW_{HHV} based on the waste calorific value. The energy throughput has been kept constant when investigating a different scenario in which the feedstock is wood waste. In the latter

case, the WtE process would treat approximately 25 ton/h of WW, equal to 75 MW_{HHV}. The differences in amount of waste fed into the incinerator are attributed to the higher heating value of the wood waste having a lower content of inert material compared to MSW.

The capture unit yields a CO_2 removal of 85% and 95% and a high-purity CO_2 stream (>99%), which is then compressed and refrigerated for transportation purposes [288]. CO_2 is first compressed at a pressure of 60 bar and transported via truck to a UK carbon cluster hub, where it is then injected into the geological storage site via pipeline, in supercritical conditions, at a pressure of 120 bar.

E.2.2. Waste characterization

The heterogeneous nature of MSW, both in terms of composition and origin, determines the heating value of the waste and, consequently, can impact the operation and the energy throughput of the WtE plant. Amaya-Santos and Chari et al. [166] reported a typical composition of MSW in the UK, which is also illustrated in Figure E.21.

Proximate and ultimate analyses were assigned to each component present in the waste (paper, cardboard, dense plastic, etc.) based on literature data [262,289,290]. Then, the proximate and ultimate analyses for the waste feedstock were calculated as a weighted average of each fraction and used in the process simulations.

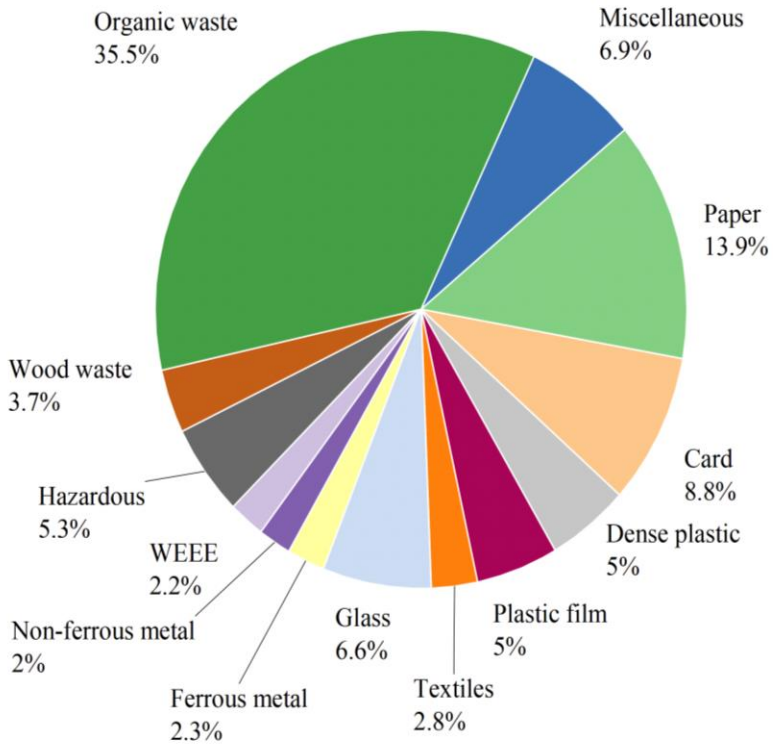

Figure E.21 – Average MSW feedstock composition, adapted from [19].

The proximate and ultimate analyses obtained and used in the models are reported in Table E.5, together with other useful parameters, such as the biogenic content and heating value.

Table E.5 – Waste Characterization [19,23].

	MSW	WW
Proximate analysis [% wt dry]		
Volatile matter	68.5	85.2
Fixed carbon	8.5	14.3
Ash	23	0.5
Ultimate analysis [%wt dry]		
C	40.78	50.65
H	5.64	5.73
O	28.91	42.78
N	1.14	0.28
Cl	0.23	0.01
S	0.25	0.01
Ash	23	0.54
Other		
Moisture [%wt]	17	26
Calorific value [MJ/kg]	9.5	10.4
Biogenic carbon [%]	64	98

E.2.3. Life Cycle Assessment

The LCA Methodology was used to assess the carbon and environmental performance of the WtE plant with and without CCS capabilities. This approach allows identifying the environmental advantages and disadvantages of CO_2 capture by comparing the performance of CCS with the baseline case without carbon capture, while the main contributors of the impact are identified through detailed hot-spot analyses.

The functional unit of this analysis is 1 tonne of waste treated. The system boundaries encompass the entire life cycle, from the origin of waste to its final disposal, including waste treatment in a WtE plant, as well as the capture, transportation, and storage of CO_2. The LCA study relies on mass and energy balances obtained from the Aspen models, complemented with data from the ecoinvent database, cut-off system model, version 3.8 [291].

The circular footprint formula [292] was adopted to allocate the environmental impacts to the function of waste management. This formula follows a “crediting” approach to account for the environmental benefits of substituting electricity from the grid mix and heat from natural gas. For the recovered products (i.e. metals and ashes) the formula allocates the benefits between the “producer” and the “user”. The extent of the benefit distribution is determined by the ratio between the demand and supply of recyclable materials in the market.

Figure E.22 shows a schematic representation of the system boundaries, divided into Background and Foreground systems.

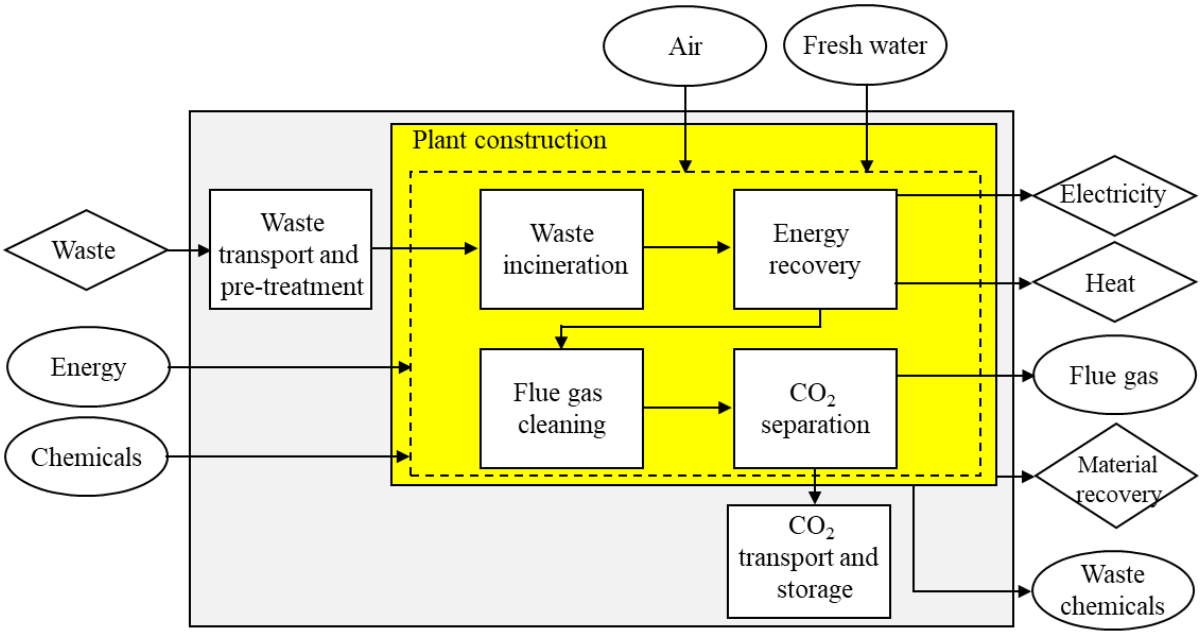

Figure E.22 – Schematic representation of the LCA system boundaries.

E.3. Results and Discussion

E.3.1. Techno-economic assessment

E.3.1.1. Process simulation

The results of the process simulation are reported in Table E.6 in the form of mass and energy balance together with key performance indicators.

The base case of the WtE plant without carbon capture exports approximately 14.4MW of electricity and 14.75MW of thermal energy when treating about 231 kiloton of MSW per year. The ratio between heat and electricity is in line with literature data [293–295]. Retrofitting the WtE with CCS results in additional electric and thermal energy requirements which reduce the overall efficiency of the plant. The heat demand is mainly due to the regeneration of the MEA solution and supplied to the reboiler. Electricity is instead needed for the initial compression of the flue gas to be sent into the adsorption unit, for solvent circulation, and for the final CO_2 compression and storage.

Notably, about 5MW of additional heat can be recovered from the flue gas condensation unit that interconnects the WtE and CCS, and used for district heating [294,296].

The results indicate that, depending on the carbon capture rate (CCR), the carbon capture (CC) unit requires almost 4 MJ of heat for solvent regeneration and around 0.6 MJ of electricity per ton of CO_2 captured. The overall energy intensity of the CC increases with increasing the amount of carbon captured and the amount of flue gas to be treated.

Table E.6 – Summary Mass and Energy balance for the WtE treating MSW and the WtE-CCS for the different capture rates examined.

	MSW		
Capture rate	**No CCS**	**85%**	**95%**
Feedstock	28.4 ton/h 75MW	28.4 ton/h 75MW	28.4 ton/h 75MW
Air	160 ton/h	160 ton/h	160 ton/h
CO_2 captured	n.a	27.3 ton/h	30.5 ton/h
Flue gas	181 ton/h	142 ton/h	139 ton/h
Make up solvent	n.a.	0.1 ton/h	0.1 ton/h
Net Electricity exported	13.8 MW	6.3 MW	5 MW
Net Heat exported	14.2 MW	4.7 MW	4.7 MW
CC reboiler duty	n.a.	3.82 MJ/kgCO_2	3.96 MJ/kgCO_2
CHP efficiency	37.3%	14.6%	12.9%

The thermal energy required by CCS (29MW and 34MW depending on the capture rate) cannot be satisfied with the excess heat available in the WtE plant. Therefore, in order for the WtE-CCS system to operate self-sufficiently, ~10 MW of steam is diverted from the turbine to provide for the thermal energy required by the CCS. This corresponds to an electricity sacrifice of about 3.4MW and 4.4MW for 85% and 95% CCR respectively, hindering the overall performance of the plant.

A similar trend is found in the case reported in Table E.7 when WW is the feedstock for WtE, requiring a higher energy sacrifice due to the higher amount of flue gas and CO_2 being generated.

This is a direct of two effects: on one side the lower fraction of inerts results in more flue gas being generated, on the other side the higher fraction of carbon in the waste ends up in more CO_2 in the flue gas. The higher heat required by the CC unit (~37MW) is partly counterbalanced by the overall higher amount of electricity produced by the WtE plant when operating with WW, resulting in an electricity sacrifice of about 5MW.

Flue gas stack emissions for the scenarios investigated are reported in Table E.8. The flue gas has a high content of CO_2 and Steam, around 12% and 14% respectively, as the product of complete

combustion, and O_2 due to the excess air required for complete combustion. The product stream is highly diluted by the inert N_2 present in the air used as the oxidizing agent.

Table E.7 – Summary Mass and Energy balance for the WtE treating WW as feedstock and the WtE-CCS with 95% capture rate.

	WW	
Capture rate	**No CCS**	**95% CCR**
Feedstock	25.98 ton/h 75MW	25.98 ton/h 75MW
Air	160 ton/h	160 ton/h
CO_2 captured	n.a.	34 ton/h
Flue gas	185.7 ton/h	139 ton/h
Make up solvent	n.a.	0.1 ton/h
Net Electricity exported	14.4 MW	4.7 MW
Net Heat exported	14.75 MW	4.8 MW
CC reboiler duty	n.a.	3.96 MJ/kgCO_2
CHP efficiency	38.9%	12.6%

Table E.8 – Flue gas stack emissions for the different cases investigated.

	MSW			**WW**	
Capture rate	**No CCS**	**85%**	**95%**	**No CCS**	**95%**
Flowrate (ton/h)	181	142	139	186	139
Composition					
H_2O [%]	13.9	4.3	4.3	14.3	4.3
CO_2 [%]	11.5	2.2	0.7	12.6	0.8
N_2 [%]	69.6	87.2	88.6	68.1	88.4
O_2 [%]	5	6.3	6.4	5	6.5
CO [ppm]	7.4	9.3	9.5	10.4	13.5
NOx [ppm]	148	185	188	158	205

E.3.1.2. Economic considerations

The economic impact of adding CCS to an existing 230ktpa WtE plant has been investigated by means of the Aspen Plus economic analysis tool. The main results are summarized in Table E.9 together with the economic assumptions that have been used in this indicative techno-economic assessment.

Table E.9 – Key economic assumptions and costs for the WtE-CCS facility.

Assumptions	
Plant availability	8109 h/year
CO_2 generation	1.13 $tonCO_2$/tonMSW
Waste throughput	28.4 ton/h
CC heat requirement	3.96 MJ/$kgCO_2$
CCR	95%, 85%
Biogenic content	64%
Cost results	
Gate fees	80 £/tonMSW
Power price (2030)	60 £/MW
Heat price (2030)	11 £/MW
Carbon price (2023)	76.9 £/$tonCO_2$
Total WtE	44 £/tonMSW
Total CCS	85 £/$tonCO_2$

The assumed power price and carbon price relationship have been derived using a Plexos model of the UK power market [297,298].

Figure E.23 refers to a projected case in which carbon credits and carbon taxation regulation would exist, assuming the present carbon price (average of the first half of 2023 in UK) of £76.9/ton of CO_2 emitted or removed [299]. Using the assumptions from Table E.9, with the hypothesis that all non-biogenic CO_2 emitted attracts a carbon tax, and stored biogenic carbon attracts a credit, a simple picture of revenue streams for a typical WtE-CCS plant can be built as reported in Figure E.23.

The largest costs are those associated with the operation of the CCS and WtE facilities. Gate fees, followed by power exported and carbon credits, which are all related to plant throughput and CCR, are key for the economic sustainability of the WtE and WtE with CCS plant. However, currently, WtE plants do not pay a carbon tax and no credit is available to WtE plants with CCS for storing or using biogenic CO_2. Nonetheless, with a carbon price of £76.9/$tonCO_2$, retrofitting a WtE plant with CCS of the scale investigated in the work represents an unfavourable and financially unreasonable option.

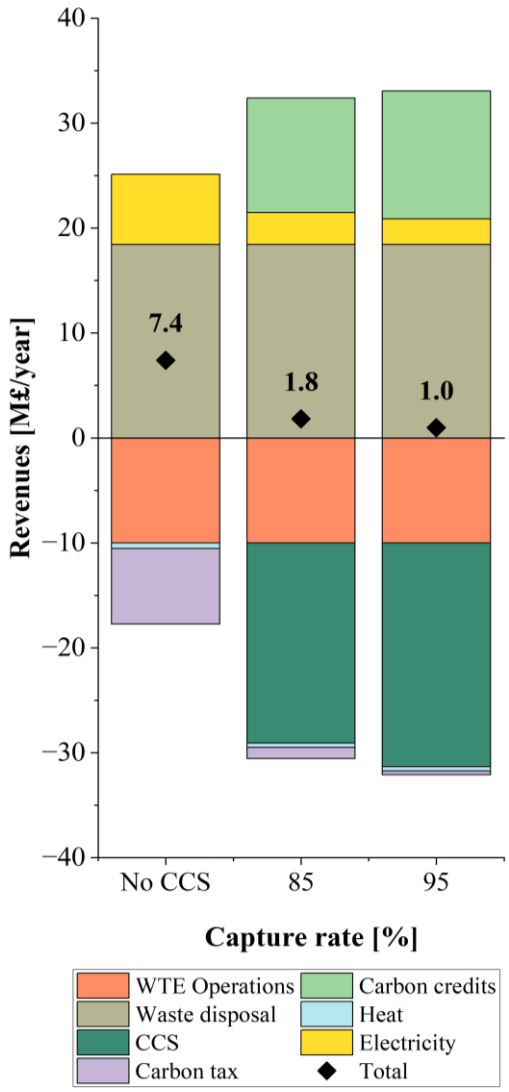

Figure E.23 – Revenue streams of the WtE plant with and without CCS at different CCRs.

A reduced penalty would be generated by reducing the cost associated with solvent regeneration in the CCS plant and transport infrastructure, or by increasing the share of biogenic carbon in the waste if a carbon incentive mechanism is established.

E.3.2. Environmental Assessment

E.3.3.1. Carbon capture rate

The climate performance of the WtE plant with and without CCS is reported in Figure E.24. The results show that the WtE plant alone contributes to climate change with net carbon emissions equal to 86 kg CO_2-eq. per tonne of MSW combusted, including credits for metal and bottom ashes recovery. Conversely, capturing CO_2 from the flue gas mitigates the climate change impact of the WtE-CCS plant contributing with net negative climate impacts. The climate change impact is in the range of -720 kg CO_2-eq./tonMSW up to -816 kg CO_2-eq./tonMSW for CCRs of 85% and 95%. As expected, the 95%

capture rate would be the most favourable from a climate standpoint, despite the reduced credits for energy export.

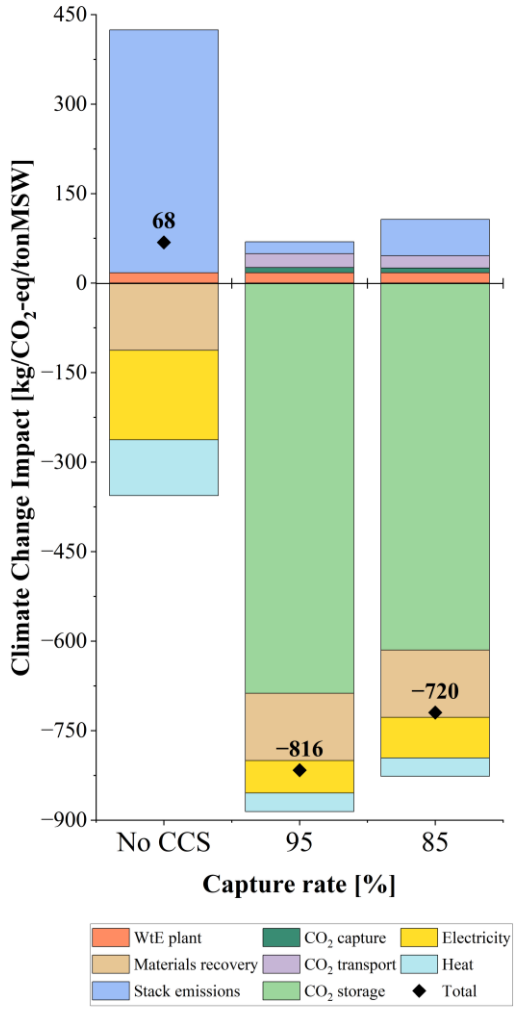

Figure E.24 – Climate change impacts for the WtE with different carbon capture scenarios.

Without CCS, the main contributor to climate change impacts is the direct emissions of fossil CO_2 with the flue gas. Credits for electricity and heat export, and materials recovery, only provide partial compensation for stack emissions.

The process of capturing CO_2 offers two primary advantages: firstly, it reduces emissions of fossil carbon in the flue gas and vented, and secondly, it sequesters biogenic CO_2, thereby contributing to climate change mitigation by removing CO_2 from the natural carbon cycle and lowering its concentration in the atmosphere. Increasing the capture rate improves climate performance. Despite potentially resulting in lower exports of heat and electricity, capturing CO_2 remains environmentally beneficial. The results are in line with literature data [300,301].

E.3.3.2. Waste composition

The impact of the waste composition on the climate performance of a WtE plant with and without carbon capture is shown in Figure E.25. In particular, the baseline scenario of the WtE treating MSW as feedstock is compared with the scenario of WW being the primary feedstock of the process.

The analysis shows that increasing the biogenic fraction results in a notable decrease in climate change impacts, regardless of whether CO_2 is captured or not. When WW is used, the WtE plant would become a "carbon negative" technology, with an overall climate change impact of -237 kg CO_2- eq/tonWW. This is due to the biogenic nature of the carbon emitted that does not contribute to a net overall increase in CO_2 concentration in the atmosphere. This is justified by the counterbalancing effect played by the amount of CO_2 captured in a reasonable timeframe by the wood whilst growing.

In general, the effect of waste composition on climate performance is predominantly influenced by three key parameters: the biogenic fraction and calorific value of the waste, as well as the quantity of recoverable material after incineration. In the WW scenario, the waste has both a higher biogenic fraction and higher calorific value, however, no credits for metals and bottom ashes have been considered for wood.

The advantages of a higher proportion of biogenic carbon outweigh the missing credits for material recovery and the decrease in electricity and heat export due to the higher energy requirements for CCS, compared to the MSW case. Furthermore, despite the amount of WW treated being lower than in the MSW case, it generates a higher amount of flue gas and more CO_2 is captured: 276 ktpa compared to 248 ktpa in the case of MSW. This results in higher credits for the WW scenario, despite the impact of the difference in biogenic content.

This analysis suggests that using WW would be a preferable option to bolster the environmental performance of the process. However, this might not hold true when considering the economic implication of using biomass instead of waste, with the loss of revenues associated with the gate fees. However, a similar outcome of the WW scenario could be achieved by changing the MSW composition.

An increase in the biogenic fraction of carbon in MSW can be obtained by upgrading the MSW supply chain upstream, reducing the plastics content or increasing that of bioplastics. This suggests that the climate performance of WtE plants will improve over the long term as waste collection and separation methods become more efficient and the global consumption of single-use plastic decreases.

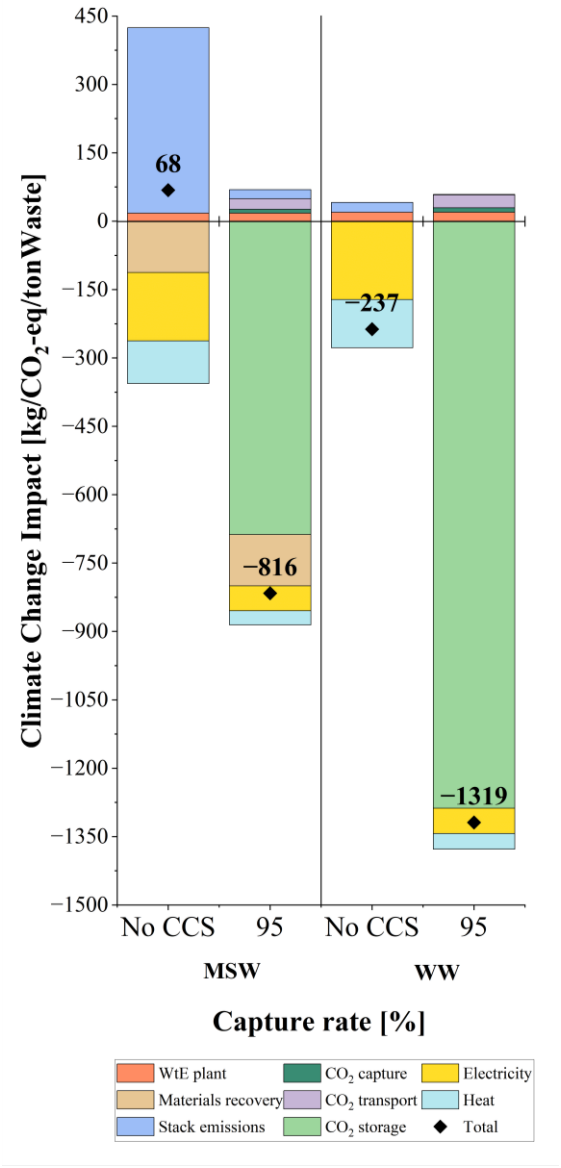

Figure E.25 – Climate change impact for waste composition scenarios for a WtE plant with and without CC.

The environmental performance of the WtE-CCS plant can be compared to those of a WtH2 assessed in Chapter 6. The total climate change impact of the WtH2 plant, considering MEA solvent with a capture rate of 90%, was calculated to be -329 kg CO_2 eq/ton H_2. For a fair comparison, both systems are evaluated using a consistent functional unit of 1 ton of waste treated. LCA results are significantly affected by the allocation approach [42], especially for WtH2 systems where H_2 applications are not yet widespread. This creates significant uncertainty in selecting the appropriate substituted products or technologies [42]. In this work, the credit for H_2 production in the WtH2 process is based on the displacement of an equivalent amount of H_2 produced via conventional steam methane reforming. By considering a climate credit of 10.9 kg CO_2-eq/kg H_2 for the H_2 produced, the overall climate change impact of the WtH2-CCS becomes -952 kg CO_2-eq/ton waste. This result is

significantly higher compared to the WtE-CCS plant, which contributes -768 kg CO_2-eq/ton waste at the same 90% capture rate.

The climate performance of WtH2 and WtE is primarily driven by the sequestration of biogenic carbon, which amounts to ~−580 kg CO_2-eq and is equal for WtE and WtH2, assuming the same waste input and carbon capture rate. In addition, WtH2 also benefits from significant credits from avoided burdens linked to H_2 production, which was assumed to be displacing natural gas in the gas grid (i.e. for heating). WtH2 has higher direct and indirect emissions than WtE, but these are more than offset by the credits for H_2, thus making WtH2 preferable to WtE from a climate perspective.

E.4. Conclusions

In this study, the techno-economic and environmental implications of decarbonising Waste to Energy (WtE) plants were investigated by means of detailed process simulations on Aspen Plus, used to then inform a comprehensive LCA study, which also relies on inventory data.

The integration of CCS with the WtE plant shows that energy sacrifice is deemed necessary to operate the plant self-sufficiently. The CC unit requires about 3.9 MJ of heat and 0.6 MJ of electricity per ton of CO_2 captured, depending on the capture rate. These resulting energy penalties affect the overall plant CHP efficiency, reducing from 37% to 13% due to the lower energy export.

Capturing carbon significantly reduces climate change impacts compared to the case when CO_2 is not captured, from 68 kg CO_2-eq. to -720/-816 kg CO_2-eq. per tonne of MSW.

The scenario analysis indicates that the composition of the waste feedstock can affect largely the environmental performance of WtE, both with and without carbon capture. The main key parameters associated with the waste composition are the biogenic fraction, which determines the extent of carbon credits, and the calorific value, which affects the size and the functional unit of the study. Despite wood waste showing the best environmental performance, its use as feedstock might either not be an economically viable option or involve major issues with the sourcing and supply chain. Benefits similar to the use of WW can be achieved by reducing the plastic component in MSW via enhanced separation upstream or in the pre-treatment stage.

Overall, economics is the biggest limitation to deploying carbon capture in any sector due to additional operational costs; but it is particularly challenging in the WtE sector due to additional costs linked to transport. Therefore, carbon taxation, and in particular tax credits for biogenic carbon removals, are key to the economic feasibility of capturing carbon. The economic estimation shows that at current market conditions, a WtE plant with carbon capture may at best break even or provide limited revenues.